

San Joaquin River Restoration Program

Thermal Conditions in Riverine Pools from the Eastside Bypass/Reach 4 to Reach 5

Nathaniel L. Butler^{1,2}

November 2013

U.S. Department of Interior
Bureau of Reclamation
San Joaquin River Restoration Program
Sacramento, CA 95825

¹ U.S. Department of Interior
Bureau of Reclamation
San Joaquin River Restoration Program
Program Office, MP-170
2800 Cottage Way
Sacramento, CA 95825

² University of California, Berkeley
Davis Hall
Berkeley, CA 94720

Table of Contents

26.0 Thermal Conditions in Riverine Pools from the Eastside Bypass/Reach 4 to Reach 5	26-2
26.1 Introduction / Background	26-2
26.2 Methods.....	26-4
26.2.1 Summer Thermal Refugia Survey	26-4
26.2.2 Piezometer and Water Temperature Array Instrumentation	26-9
26.3 Results.....	26-15
26.3.1 Summer Thermal Refugia Survey	26-15
26.3.2 Piezometer and Water Temperature Array Instrumentation	26-27
26.4 Discussion.....	26-41
26.4.1 Availability and Persistence of Thermal Stratification in the Eastside Bypass, Reach 4B2, and Reach 5 of the San Joaquin River system.....	26-41
26.4.2 Influence of Surface Water Flow and Pool Geometry on Thermal Stratification	26-42
26.4.3 Influence of Subsurface-Surface Water Interactions on Thermal Stratification in Pools	26-48
26.4.4 Air Temperature Correlations with Pool Water Temperature	26-52
26.4.5 Thermal Refugia in the Eastside Bypass, Reach 4B2, and Reach 5.....	26-58
26.5 Conclusions.....	26-63
26.6 Acknowledgements.....	26-64
26.7 References.....	26-65
26.8 Appendix.....	26-72
26.8.1 Fall Instrumentation Individual Site Analysis	26-72

26.0 Thermal Conditions in Riverine Pools from the Eastside Bypass/Reach 4 to Reach 5

26.1 Introduction / Background

As part of the San Joaquin River Restoration Program's ongoing efforts to reintroduce Chinook salmon (*Oncorhynchus tshawytscha*) to the San Joaquin River, this study was conducted to determine the availability, distribution, and variability of cold-water thermal refugia in the Eastside Bypass, Reach 4B2 and Reach 5. One concern for Chinook reintroduction is that sufficient cold water habitat exists in the San Joaquin River system for Chinook survival and migration. Water temperature is a critical water quality parameter for Chinook salmon and is identified as a potentially limiting factor/stressor in the San Joaquin River system (SJRRP FMWG, 2010). Recent modeling of water temperature in the San Joaquin River indicates water temperature will exceed critical thresholds for Chinook salmon between April and October (SJRRP WMWG, 2008a - c). Historically, Chinook in the San Joaquin River system experienced some of the warmest water temperatures of any Chinook population (Stillwater, 2003). In 1875 and 1877 California Fisheries Commission reports, Chinook were documented migrating up the San Joaquin River in July and August when average ambient surface water temperatures reached 80°F (CFC 1875; CFC, 1877; Yoshiyama et al., 1996). To explain Chinook migrating when water temperature exceeded published Chinook thermal tolerances, it was hypothesized historic Chinook populations utilized cold-water thermal refugia to survive high water temperatures (McBain and Trush Inc., 2002).

Water temperature is critical for Chinook salmon because their survival, abundance, and distribution are negatively impacted by high water temperatures. When water temperatures exceed the physiological optimums for Chinook, high metabolic demands suppress growth, increase susceptibility to disease, and lead to increased mortality (Fry, 1971; Torgersen et al., 1999; Sullivan et al., 2000; Madej et al., 2006). Thermal barriers due to high water temperatures limit the abundance, distribution, and migration of salmon by rendering suitable upstream habitat inaccessible (Matthews and Zimmerman, 1990; Meisner, 1990; Ebersole et al., 2001; SJRRP FMWG, 2009). When ambient stream water temperatures exceed salmonid temperature tolerances, salmon seek out cooler water including areas of thermal refugia (Li et al., 1993; Nielsen et al., 1994; Matthews and Berg, 1997; Ebersole et al., 2003).

Cold-water thermal refugia occurs where local stream water temperature is sufficiently cooler than ambient stream water temperature that it can be used by fish to behaviorally thermoregulate (Nielsen et al., 1994; Torgersen et al., 1999; Ebersole et al., 2003). It is

created when a source of cold water couples with low mixing conditions to form vertical temperature gradients and thermal stratification in the surface water (Nielsen et al., 1994). Two processes that form vertical water temperature gradients in rivers are differential heating of the water column and upwelling cool subsurface flow. Differential heating of the water column occurs when heat exchange causes water near the stream surface to warm more than water near the streambed. In differential heating, thermal stratification preserves cool water temperatures near the streambed as the surface water near the air-water interface warms during the day. Vertical water temperature gradients and thermal stratification also form when a cold water source enters the river from upwelling cool groundwater, by hyporheic exchange, or from a combination of the two (Nielsen et al., 1994; Keller et al., 1995; Matthews and Berg, 1997; Ebersole et al., 2003). While groundwater is subsurface water with long residence times, hyporheic exchange is subsurface water with short residence times that is a mixture of surface stream water and groundwater (White, 1993). Groundwater and hyporheic water have different properties, but both are subsurface water flows that move through the streambed. In this report, subsurface flow will be used to describe all water entering the surface water through the streambed unless the source of the flow is clearly identified as groundwater or hyporheic.

Low mixing conditions needed for the formation of vertical temperature gradients occur when water velocity is sufficiently low in a river (Nielsen et al., 1994). Deep pools frequently have low water velocities that promote thermal stratification. Pool geomorphology including the length, width, depth, curvature, and entrance and exit slopes determines the distribution of water velocity in a pool (Thompson et al., 1998; Sawyer et al., 2010; Thompson and McCarrick, 2010; MacVicar and Rennie, 2012). Backwater channels, slackwater channels, large woody debris, or other geomorphology and structures that reduce water velocities can cause low mixing conditions favorable to the formation of thermal refugia (Bilby, 1984; Ozaki, 1988; Nielsen et al., 1994; Keller et al., 1995; Ebersole et al., 2003).

Vertical water temperature gradients or thermal stratification enables salmonids to select cooler water temperatures when ambient surface water temperatures exceed thermal tolerances (Gibson, 1966; Keller and Hofstra, 1983; Nielsen et al., 1994; Matthews and Berg, 1997; Ebersole et al., 2001, Ebersole et al., 2003). Salmonids occupy thermal refugia primarily during the hottest parts of the day when ambient surface water temperatures approach the lethal limit (Frissell et al., 1996; Matthews and Berg, 1997; Ebersole et al., 2003). Studies found that their preferred cold water refugia were thermally stratified pools (Keller and Hofstra, 1983; Nielsen et al., 1994; Matthews and Berg, 1997; Tate et al., 2007), though Frissell et al. (1996) and Ebersole et al. (2003) observed salmonids occupying cold water patches along bars and riffles. Salmonids were observed traveling up to 25 meters to take advantage of cold water refuge, though it is believed they will travel much greater distances (Li et al., 1993; Nielsen et al., 1994; Ebersole et al., 2001). If there is more demand for thermal refugia than available area, salmonids may be forced to migrate significant distances or perish (Ebersole et al., 2001). Thermal refugia longitudinally connects suitable habitat by enabling migration through reaches with water temperature above salmonid temperature tolerances (Ebersole et al., 2003). Salmonids migrate through thermally impaired reaches by alternating between migrating when ambient stream temperatures are cool and holding in thermal refugia

during high stream temperatures (Ebersole et al., 2001). While thermal stratification and thermal refugia are recognized as important habitat for salmon survival, historical documentation in the San Joaquin River system is scarce with no recent data records of vertical temperature profiles existing for the Eastside Bypass, Reach 4B2, or Reach 5 (McBain and Trush, Inc., 2002).

26.2 Methods

To assess the availability, quality, and distribution of thermal refugia, water temperature was measured from July through November 2012 in Reach 4B2 and Reach 5 of the San Joaquin River and in the Eastside Bypass from the Merced National Wildlife Refuge to its confluence with the San Joaquin River. These three reaches were studied because modeling indicated water temperature would exceed temperature tolerances for Chinook in these three reaches during this timeframe (SJRRP WMWG, 2008a - c; SJRRP FMWG, 2010). The two components of this investigation were a summer thermal refugia survey and a detailed instrumentation of six sites exhibiting thermal stratification. The summer thermal refugia survey of pools was conducted to quantify the vertical water temperature profiles in pools and to determine how prevalent thermal stratification is along the three selected reaches of the San Joaquin River system. Six pool-riffle-pool sites with thermal refugia identified in the thermal refugia survey were then instrumented to measure the variation of vertical temperature gradients in pools, its relationship to upwelling subsurface flow, and pool volume of thermal refugia habitat below Chinook temperature thresholds.

26.2.1 Summer Thermal Refugia Survey

26.2.1.1 Site Characteristics and Survey Site Selection

The San Joaquin River Restoration Program area extends approximately 153 miles along the San Joaquin River from Friant Dam at the upstream end to the river's confluence with the Merced River at the downstream end and includes the network of flood bypass channels that run along the river (Figure 1). This study focuses on three reaches that form the lower portion of the restoration area: Reach 4B2, Reach 5, and the Eastside Bypass. During summer and fall 2012, no San Joaquin River flow passed Sack Dam so flows in these reaches were a combination of agricultural returns, incoming tributary flow, water deliveries, and upwelling groundwater. The proportions from different water sources were not determined. Between 2008 and 2010, LIDAR and bathymetric data was collected along the San Joaquin River and the Eastside Bypass that was used to generate San Joaquin River digital terrain models (SJRRP, 2010). Using the San Joaquin River digital terrain model (SJR DTM), pool sites in the three study reaches with the best thermal refugia potential were identified. Streambed elevation, pool depth, pool shape, and geomorphology were used as criteria to select the pools to survey (Figure 2).

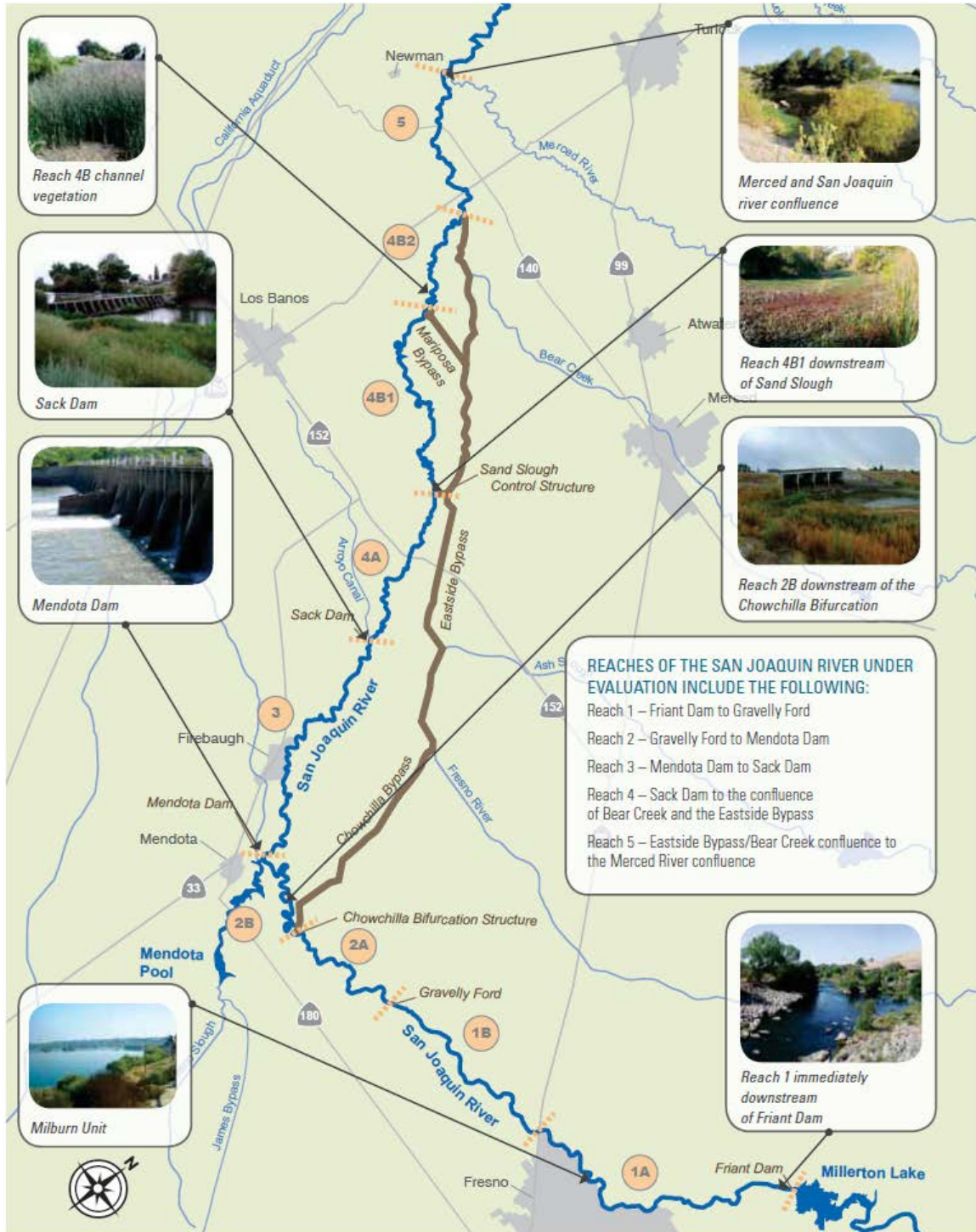


Figure 1: Map of San Joaquin River Restoration Program Area.

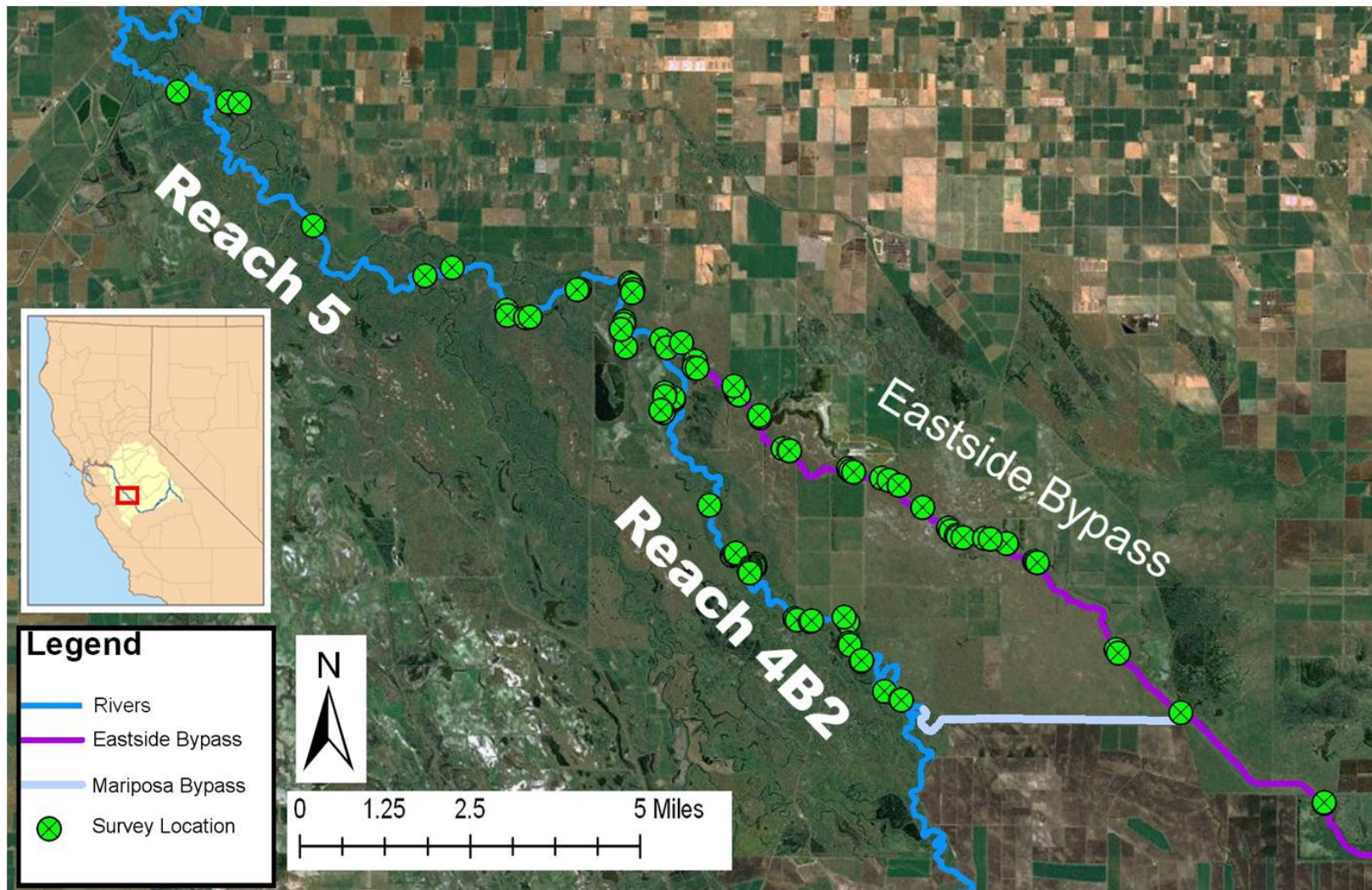


Figure 2: Map of study area showing summer survey measurement sites.

Multiple measurement locations were chosen in pool-riffle-pool sequence sites to measure water temperature variations created by upwelling subsurface flow. Streambed and water surface elevation differences create pressure variations that cause exchange between subsurface and surface water (Harvey and Bencala, 1993; Harvey et al., 1996; Woessner, 2000; Poole and Berman, 2001; Conant, 2004; Poole et al., 2008). In pool-riffle-pool sequences, high pressure gradients at the end of pools force water into the subsurface that reemerges at downstream pool entrances where low pressure gradients occur (Conant, 2004; Packman et al., 2004; Tonina and Buffington, 2007; Hannah et al., 2009; Hatch et al., 2010). Spatial variations in the subsurface hydraulic conductivity create a multi-scale network of subsurface flow paths (Woessner, 2000; Poole et al., 2008). Variability in subsurface flow path lengths results in subsurface-surface water exchange that varies laterally and longitudinally along the streambed in rivers (Tonina and Buffington, 2007; Hatch et al., 2010). Variations in upwelling subsurface flow produce variations in vertical water temperature gradients between the deepest points in pools (Matthews and Berg, 1997). Pools in the San Joaquin River system with more than one deepest point had multiple measurement locations to quantify spatial variations in vertical water temperature gradients.

26.2.1.2 Survey Data Collection

Water temperature and conductivity profiles were measured in 55 riverine pool sites during July 2012 to assess the abundance and degree of thermal refugia in Reach 4B2 and Reach 5 of the San Joaquin River and in the Eastside Bypass from the Merced National Wildlife Refuge to its confluence with the San Joaquin River. Water temperature and conductivity with depth were measured by an In-Situ Troll 9000 lowered from a canoe or boat. At each location, the canoe or boat was maneuvered into the GPS position identified during site selection taking care to minimally disturb the vertical temperature gradient of the surface water. Once in position, the In-Situ Troll 9000 was slowly lowered and raised through the pool water column to record the surface water temperature and conductivity. Locations and sites were added and removed from the initial list of pools when field conditions differed from the San Joaquin River digital terrain model. Pool locations were added when field observations identified a deep pool that was not found in the bathymetric data, streambed elevation changes indicated potential subsurface upwelling into a pool, or sheltering from sediment bars, large woody debris, or meandering indicated low mixing conditions that promoted thermally stratified pools. Pools were subtracted when no pool was located at the GPS coordinates, pool depth was too shallow to measure, the pool was fully disconnected from the river at the existing water level, or the pool was inaccessible by canoe or boat.

26.2.1.3 Survey Data Analysis

Collected water temperature and water conductivity data were analyzed to quantify the degree of thermal refugia and the potential source of upwelling cold water at each location. Degree of thermal refugia was assessed by several parameters: the maximum water temperature, minimum water temperature, change in water temperature with depth, and total depth of the pool. The change in water temperature between the top and the bottom of the pool (ΔT) was calculated to identify the level of thermal stratification present at each location. To distinguish between stable, persistent thermal stratification and water temperature variations caused by the measurement process, only pools with ΔT

greater than 3°F were considered thermally stratified for this study. To evaluate whether thermally stratified pools contained thermal refugia, the maximum and minimum water temperatures for each location were compared with Chinook water temperature tolerances (SJRRP FMWG, 2010). While maximum water temperatures were expected to exceed the Chinook habitat target temperature of 63°F for July based on water temperature modeling of the San Joaquin River system, minimum water temperature were used to indicate whether thermal refugia existed at measurement locations.

Specific conductance (SC) data was analyzed to classify the potential source of upwelling cold water in each pool location. Changes in SC between the top and bottom of the pool (Δ SC) was calculated from the water conductivity data and compared with the shape of the SC gradient to inform whether subsurface flow upwelling into the pool was from hyporheic or groundwater sources. The different SC characteristics of groundwater and hyporheic flow were used by Soulsby et al. (2007) to identify the source of upwelling subsurface flow in upland streams. Generally, groundwater has higher SC than surface water, while hyporheic flow has lower SC that approaches the SC of surface water. Specific conductance in hyporheic flow has a wide range, because hyporheic flow is a mixture of surface water and groundwater (White, 1993; Woessner, 2000; Poole and Berman, 2001). Hyporheic flow tends to have SC similar to surface water because it has shorter residence times in the subsurface than groundwater (Conant, 2004; Malcolm et al., 2005; Soulsby et al., 2007; Nelson and Reed, 2012). In the San Joaquin River system, general trends in the SC of surface water and groundwater must be used cautiously because agricultural returns have significantly altered the SC of both the surface water and groundwater (McBain and Trush, Inc., 2002). When pool SC near the streambed was greater than the average surface water SC, it was assumed groundwater upwelled into the pool. Upwelling hyporheic flow was assumed to be the cold water source when pools exhibited thermal stratification but had a small Δ SC and pool bottom SC was similar to average surface water SC.

Distances between pools with thermal refugia were calculated to determine the longitudinal connectivity of the cold water habitat along the three reaches. The distances between GPS positions for each measurement location were calculated using the San Joaquin River system digital terrain model. To evaluate the distance Chinook would travel to access different levels of thermal refugia, three temperature thresholds were applied to the pools. Pools with minimum water temperature between 65°F and 68°F were grouped into the “critical” temperature threshold. All the pools with minimum water temperature greater than 68°F and less than or equal to 75°F were classified as “sub-lethal.” The pools with minimum water temperature greater than 75°F were classified as “lethal” since prolonged exposure to water temperatures above 75°F is considered lethal to fall-run and spring-run migrating adult Chinook salmon (Moyle et al., 1995; Ward et al., 2006; Rich, 2007; SJRRP FMWG, 2010). Distances were calculated between the pools in each of the three classifications to identify how raising or lowering temperature thresholds decreased or increased distances Chinook would travel to access cold-water habitat.

26.2.2 Piezometer and Water Temperature Array Instrumentation

26.2.2.1 Array Site Selection

Based on the results of the thermal survey analysis, six pool sites with thermal refugia were identified for further study with piezometers and water temperature sensor arrays. All pool sites were named with the letters abbreviating the name of the waterway the pool was located in and the numbers identified the approximate waterway mile marker associated with the pool. For example, SJR 193 was located in the San Joaquin River, one hundred ninety-three miles downstream of the confluence of the Middle Fork San Joaquin River and the South Fork San Joaquin River. For reference, Friant Dam is located 71 miles downstream of the confluence of the Middle Fork San Joaquin River and the South Fork San Joaquin River. Three sites with thermal stratification between 8°F to 11°F and minimum water temperatures around 76°F were selected for instrumentation in the San Joaquin River: SJR 193, SJR 199, and SJR 204 (Figure 3).

The three sites were distributed from the upstream end of Reach 4B2 to middle of Reach 5 to evaluate the longitudinal variability along with the site specific variability of thermal refugia. Sites were chosen to represent a range of pool geomorphologies to investigate how thermal stratification varied with different pool shapes. Sites were also chosen to represent three different upwelling conditions in the San Joaquin River. Analysis of the survey conductivity data suggested SJR 193 had hyporheic flow, SJR 199 had groundwater flow, and SJR 204 had hyporheic in the upstream off-channel pool and groundwater in the downstream main channel pool.

Three sites distributed along the Eastside Bypass were selected for array instrumentation to evaluate the site specific and longitudinal variability of thermal refugia in the Eastside Bypass: ESB 22, ESB 29, and ESB 33 (Figure 3). The three Eastside Bypass pools chosen were those with the best available thermal refugia with thermal stratification ranging from 12°F to 19°F and minimum water temperatures ranging from 66°F to 74°F. The geomorphology of the pools in the Eastside Bypass differed from the San Joaquin River with pools usually separated by long shallow runs creating many isolated pools. ESB 22 and ESB 33 were both isolated pools with over 0.5 miles of long shallow runs upstream and downstream. ESB 29 had pool-riffle-pool morphology, but when it was instrumented the upstream and downstream pools were disconnected and there was no surface flow through the pools. These three sites represented the range of morphologies encountered in the Eastside Bypass. While the majority of Eastside Bypass sites had no change in conductivity with depth, these three sites had conductivity increase with depth. Data collected at the Eastside Bypass and San Joaquin River sites enabled evaluation of the range of conditions present along the Reach 4B2 and Reach 5 of the San Joaquin River and the Eastside Bypass.

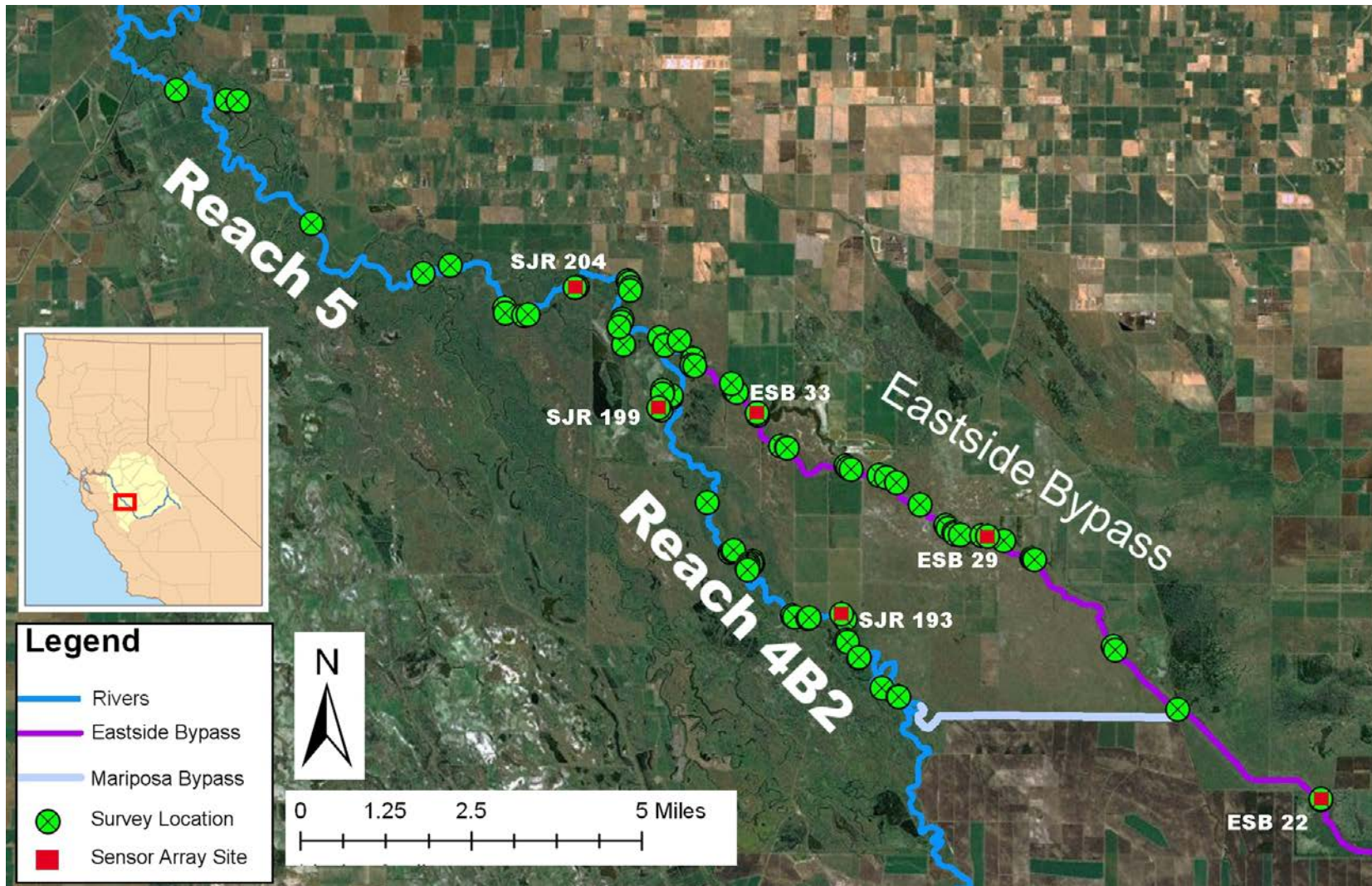


Figure 3: Map of San Joaquin River system sites instrumented with sensor arrays

26.2.2.2 Array Data Collection

Piezometer and water temperature sensor arrays were built and installed at each site to monitor water temperature and level. Streambed piezometers were constructed from 1.25 inch schedule-40 PVC pipe, 1.25 inch or 2 inch steel drive points, and brass screens using a design modified from Hatch et al., 2006. Screened sections were constructed for each piezometer by drilling 15/64" holes in the PVC pipe 6 inches above the steel drive point coupling and gluing a 60 mesh brass screen inside the pipe (Figure 4). This enabled the field installation of a sensor inside the piezometer to sample the subsurface water without sediment filling the screened section of the piezometer. Additional sections of PVC pipe were constructed that could be attached in the field with PVC couplings to extend the piezometer length based on pool water depth.



Figure 4: Screened bottom sections of sensor array piezometers

Several different piezometer and water temperature sensor array setups were developed and deployed at the pool sites depending on pool conditions. Four types of sensors were used for the water temperature sensor arrays to monitor the water temperature, water level, and water electro-conductivity in the pools (Table 1). Water temperature sensor arrays were constructed by attaching sensors at regular intervals to the exterior of a piezometer to sample the surface water conditions (Figure 5).

Table 1: Sensor specifications

Sensor Type	Temperature Accuracy	Temperature Resolution	Water level accuracy	Conductivity accuracy	Conductivity Resolution
Solinst Levellogger Gold	$\pm 0.09^{\circ}\text{F}$	0.005°F	0.05% FS	n/a	n/a
Solinst Levellogger Edge	$\pm 0.09^{\circ}\text{F}$	0.005°F	0.05% FS	n/a	n/a
Solinst LTC Levellogger Junior	$\pm 0.18^{\circ}\text{F}$	0.18°F	0.1% FS	$20\ \mu\text{S}/\text{cm}$	$1\ \mu\text{S}/\text{cm}$
Onset HOBO U22-001	$\pm 0.38^{\circ}\text{F}$	0.04°F	n/a	n/a	n/a

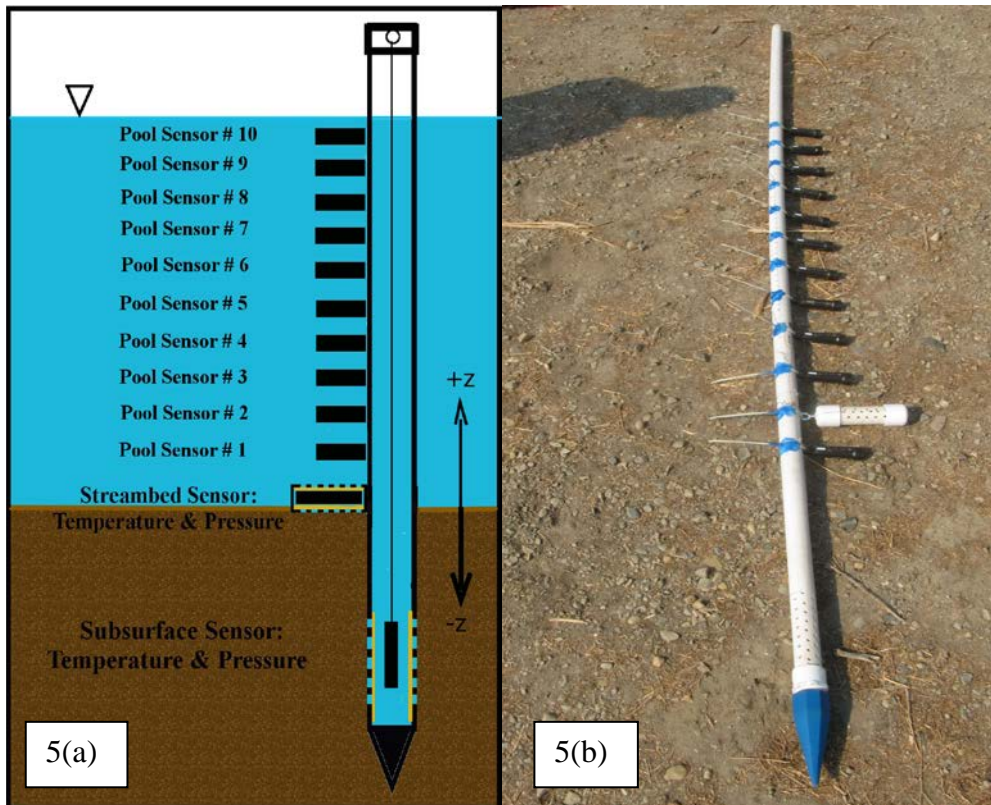


Figure 5: (a) Side view cut-away schematic of water temperature sensor array (b) Water temperature sensors array prepared for installation at SJR 193

At each site, at least one piezometer was constructed to be a water temperature sensor array. To record the vertical surface water temperature in the pools, six to ten Onset HOBO U22-001 sensors were attached with zip-ties to the exterior of piezometers. Onset HOBO U22-001 sensors were approximately equally spaced throughout the water column in each pool. Water depth in each pool was different, so the spacing between the Onset HOBO U22-001 sensors varied between sites with deeper pool sites having sensors spaced further apart. At SJR 193, SJR 204, and ESB 33, an additional Onset HOBO U22-001 sensor was attached to the exterior of the piezometer below the streambed level to measure subsurface water temperature. One Solinst Levellogger Edge, Gold, or Junior LTC sensor was suspended at the bottom of each piezometer and hung by a nylon string from an eyebolt screwed into the piezometer cap to record water conditions at the depth

the piezometer was driven into the subsurface. An additional Solinst Levellogger Edge, Gold, or Junior LTC sensor was housed in a perforated PVC pod and zip-tied to the exterior of a piezometer in each pool. The PVC sensor pod was positioned at the streambed-surface water interface to measure surface water conditions at the streambed including the pool water level (Figure 6).

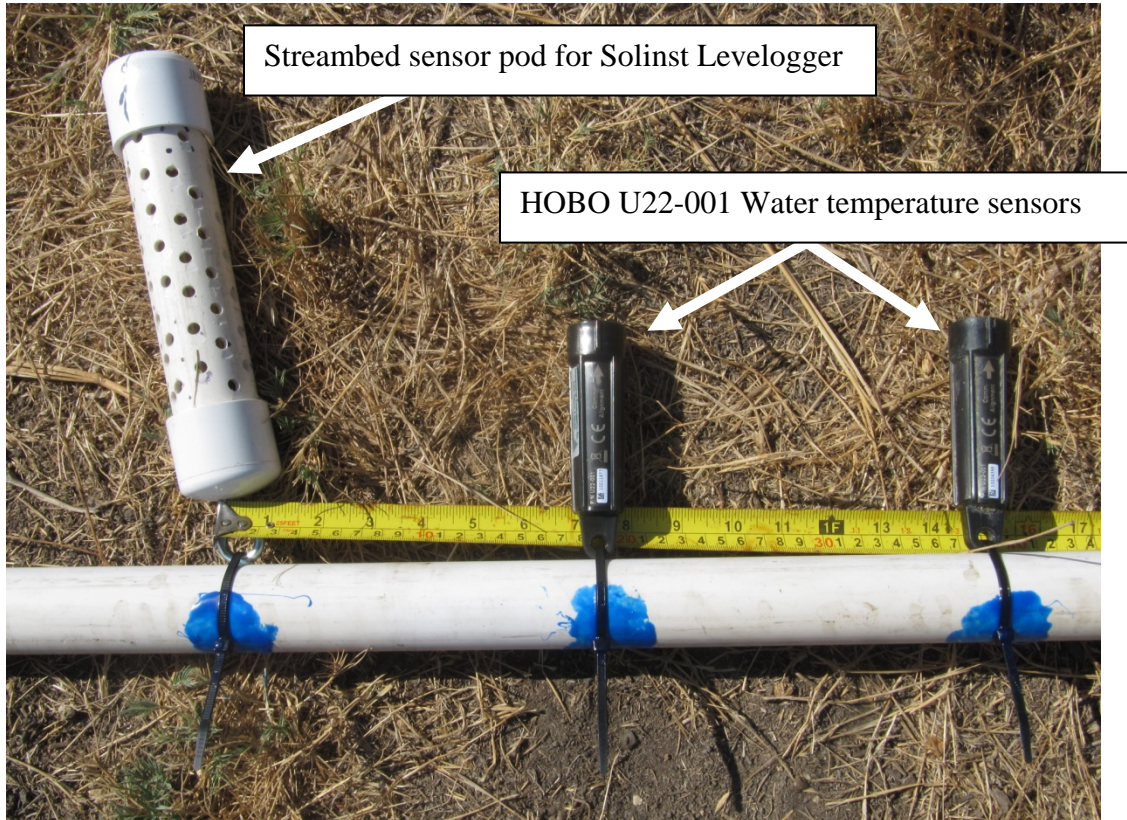


Figure 6: Water temperature sensor array with streambed sensor pod and water temperature sensors attached.

Solinst Levellogger Junior LTC sensors were used only in sensor arrays deployed in ESB 33 to measure specific conductance in addition to water level and temperature. Resolution, accuracy, and cross-calibration of all sensors were tested prior to being deployed. Water temperature sensors were tested in room temperature air, a constant temperature ice bath, and at least one warming cycle from the ice bath to room temperature air. Any sensors that failed to perform within the specifications of the sensor were rejected and not used during the study. Data was recorded at 15 minute intervals for each two to three week deployment since all temperature sensors had characteristic response times in water of 5 minutes or less.

Piezometer and water temperature sensor arrays were driven into the streambed from 1 to 7 feet using a steel drive rod and hammer at the six pool sites in the San Joaquin River and Eastside Bypass. At each measurement location, shallow and deep piezometers were installed to quantify trends in subsurface water flow direction and subsurface water temperature with depth (Figure 7).

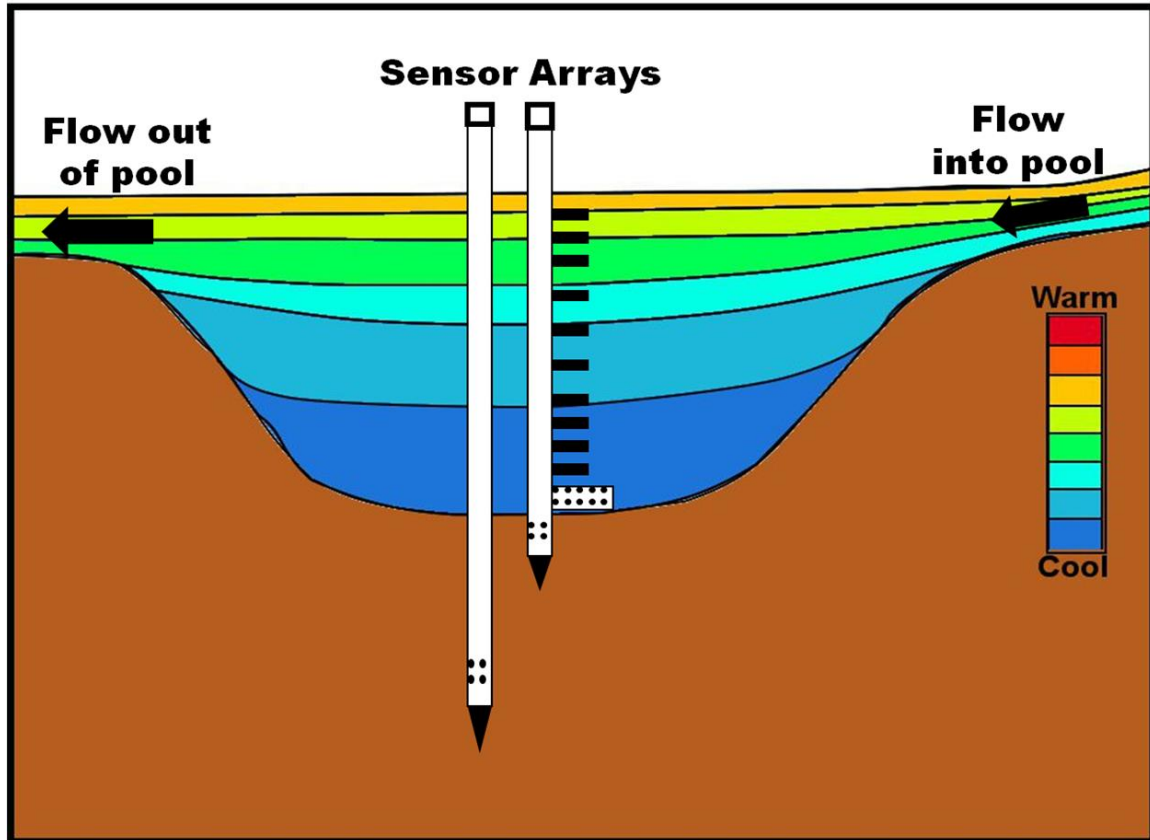


Figure 7: Schematic side-view of piezometer and water temperature sensor array installation in San Joaquin River system pools.

Piezometers and water temperature sensors arrays were deployed for two to three weeks at each site. Piezometers and sensor arrays were inspected after removal to verify the depth they had been driven into the subsurface and sensor placement relative to the streambed. Correction factors were applied to sensor placements whenever the intended driven depth varied from the actual driven depth.

26.2.2.3 Array Data Analysis

Data from each site was analyzed to identify water temperature trends in the pools and the factors that influenced the thermal conditions in these reaches of the San Joaquin River system. Analysis first focused on assessing the level of thermal stratification present in pools. Water temperature data from the surface water was analyzed to determine the level of thermal stratification and thermal refugia present in each pool. Daily maximum and minimum levels of thermal stratification were calculated using the sensors nearest the air-water interface and the streambed. Variations in water temperature were analyzed for all sensors to evaluate water temperature trends with depth. Analysis also focused on determining a typical daily cycle of thermal stratification and uniformity across all pools instrumented. Subsurface water temperature data was analyzed to identify water temperature trends with depth below the streambed. Surface and subsurface water temperature was compared to evaluate the effects of surface-subsurface exchange on pool thermal stratification.

To evaluate the direction of subsurface flow and its effect on thermal stratification, hydraulic head was calculated from the water level data collected at each instrumentation location. Using the streambed at each location as the reference height, hydraulic head gradients were calculated between water level sensors. Locations were considered upwelling when streambed hydraulic head was less than subsurface hydraulic head. Downwelling occurred when streambed hydraulic head was greater than subsurface hydraulic head. Hydraulic head was only measured in the vertical direction at each instrumentation location, since most pools had only one set of sensors positioned at three different depths. Lateral and longitudinal variations in subsurface flow direction were not accounted for in this study. Periods when surface water level and hydraulic head varied were used to identify how changes in surface flows altered the thermal environment in both the surface and subsurface water. Variations in subsurface-surface water temperature combined with subsurface flow direction were used to evaluate the role of subsurface-surface water exchange in creating and maintaining thermal stratification measured in pools.

Regional meteorological data from the California Irrigation Management Information System (CIMIS) and San Joaquin River flow and stage data from the California Department of Water Resources California Data Exchange Center (CDEC) was compared with collected water temperature and water level data to determine the role of meteorological parameters and surface water flow on pool water temperature trends. Using pool water temperature data and estimates of the pool geometry from the San Joaquin River digital terrain model, the total pool heat was calculated. Trends in total pool heat were compared to trends in meteorological parameters to evaluate the regional influences on pool thermal stratification and thermal refugia.

26.3 Results

26.3.1 Summer Thermal Refugia Survey

26.3.1.1 Pool Water Temperature

Thermal stratification was measured in 82% of the pools surveyed in the Eastside Bypass, Reach 4B2, and Reach 5. Differences between surface and bottom water temperatures (dT_w) at the 77 locations in the 55 pools surveyed ranged from less than 1°F to greater than 20°F with an average dT_w of 7.6°F across all the locations measured (Table 2).

Table 2-A: Eastside Bypass 2012 summer survey data summary

Site Name	Bypass Mile	Date Measured	Time Measured	dTw (°F)	depth (ft)	ΔSC (microSiemens/cm)	Maximum Temperature (°F)	Minimum Temperature (°F)
ESB 22.42(2)	22.42	8/1/2012	3:08:58 PM	19.02	5.072	226.6	92.22	73.2
ESB 26.30	26.3	7/31/2012	12:07:57 PM	11.49	4.712	64	84.77	73.28
ESB 26.37	26.37	7/31/2012	11:58:18 AM	11.01	7.254	117	85.6	74.59
ESB 28.32	28.32	7/26/2012	11:59:19 AM	2.46	9.986	26	79.03	76.57
ESB 28.32(2)	28.32	7/26/2012	11:54:33 AM	3.65	3.675	50.9	80.32	76.67
ESB 28.32(3)	28.32	7/26/2012	11:39:52 AM	5	6.087	59	76.08	71.08
ESB 28.9	28.9	7/26/2012	11:10:47 AM	3.58	3.424	20	75.91	72.33
ESB 29.25	29.25	7/31/2012	1:06:44 PM	8.93	7.391	113.2	83.69	74.76
ESB 29.25(2)	29.25	7/31/2012	12:57:28 PM	13.26	11.417	227.5	83.45	70.19
ESB 29.25(3)	29.25	7/31/2012	12:53:08 PM	18.6	13.362	474.9	85.02	66.42
ESB 29.6(2)	29.6	7/31/2012	1:51:51 PM	11.98	6.049	56.4	87.22	75.24
ESB 29.7	29.7	7/31/2012	2:08:19 PM	13.6	5.077	400.6	89.57	75.97
ESB 29.88	29.88	7/31/2012	2:51:50 PM	11.79	2.391	135	89.28	77.49
ESB 29.88(2)	29.88	7/31/2012	2:23:57 PM	9.54	3.227	85.7	85.85	76.31
ESB 30.4	30.4	7/31/2012	3:18:32 PM	19.97	10.677	171.3	90.95	70.98
ESB 31.1	31.1	8/1/2012	11:18:33 AM	6.16	5.425	50.6	79.65	73.49
ESB 31.2	31.2	8/1/2012	11:24:15 AM	8.39	9.56	67	80.47	72.08
ESB 31.9	31.9	8/1/2012	11:59:06 AM	6.93	14.895	690.1	81.4	74.47
ESB 31.9(2)	31.9	8/1/2012	11:53:03 AM	6.08	7.28	217.7	81.89	75.81
ESB 31.9(3)	31.9	8/1/2012	11:35:24 AM	6.92	6.271	56.9	82.57	75.65
ESB 33.05	33.05	8/1/2012	12:46:18 PM	8.92	6.564	1125	84.86	75.94
ESB 33.05(2)	33.05	8/1/2012	12:38:45 PM	7.2	3.059	904	82.64	75.44
ESB 33.13	33.13	8/1/2012	12:53:32 PM	7.51	4.54	1272	84.26	76.75
ESB 33.8	33.8	8/1/2012	1:23:24 PM	11.78	10.883	441	85.38	73.6
ESB 34.3	34.3	7/13/2012	11:02:55 AM	0.63	2.371	11.54	83.51	81.34
ESB 34.43	34.43	7/13/2012	11:24:02 AM	9.25	4.393	315.81	83.98	74.73
ESB 35.15	35.15	7/13/2012	12:17:02 PM	12.38	3.554	1016.55	86.46	74.08
ESB 35.3	35.3	7/13/2012	12:43:18 PM	3.66	2.67	123.87	81.67	78.01
ESB 35.3(2)	35.3	7/13/2012	12:35:19 PM	6.97	3.915	287.71	83.35	76.38

Table 2-B: Reach 4B2 of the San Joaquin River 2012 summer survey data summary

Site Name	River Mile	Date Measured	Time Measured	dTw (°F)	depth (ft)	ΔSC (microSiemens/cm)	Maximum Temperature (°F)	Minimum Temperature (°F)
SJR 190.14	190.14	7/19/2012	1:32:24 PM	8.91	8.358	91.33	82.65	73.74
SJR 190.14(0)	190.14	7/19/2012	1:25:42 PM	9.63	3.758	118.37	83.13	73.5
SJR 190.14(2)	190.14	7/19/2012	1:41:51 PM	4.33	5.448	64.19	78.81	74.48
SJR 191.89	191.89	7/19/2012	12:35:49 PM	6.39	4.036	133.7	80.62	74.23
SJR 192.48	192.48	7/19/2012	11:47:02 AM	2.48	3.173	27.76	78.66	76.18
SJR 192.48(2)	192.48	7/19/2012	12:03:57 PM	3.3	2.31	188.6	78.87	75.57
SJR 192.48 opt4new	192.58	7/19/2012	12:15:13 PM	3.98	3.804	989.09	79.48	75.5
SJR 192.6	192.6	7/19/2012	2:35:09 PM	8.27	4.179	62.3	83.08	74.81
SJR 192.8	192.8	7/19/2012	2:43:58 PM	10.41	3.174	96.27	84.76	74.35
SJR 192.9	192.9	7/19/2012	2:55:45 PM	4.77	7.263	30.58	81.53	76.76
SJR 193	193	7/19/2012	3:06:53 PM	2.94	5.467	44.39	80.68	77.74
SJR 193.24	193.24	7/19/2012	3:20:17 PM	0.53	7.132	3.8	81.35	80.82
SJR 193.27	193.24	7/19/2012	3:14:34 PM	8.97	3.261	107.34	85.49	76.52
SJR 193.29	193.29	7/19/2012	3:29:25 PM	7.82	4.878	75.27	83.92	76.1
SJR 193.85(2)	193.85	7/20/2012	11:58:59 AM	0.5	6.008	101.4	80.21	79.71
SJR 194.05	194.05	7/20/2012	12:36:39 PM	3.21	7.222	194.5	79.33	76.12
SJR 195.1	195.1	7/20/2012	1:31:49 PM	3.39	5.111	139.9	80.85	77.46
SJR 195.5	195.5	7/20/2012	1:50:35 PM	0.06	2.251	1	79.87	79.81
SJR 195.5(2)	195.5	7/20/2012	1:43:27 PM	3.31	6.082	27	81.35	78.04
SJR 195.7	195.7	7/20/2012	2:15:18 PM	5.91	5.016	167.3	82.57	76.66
SJR 195.95(2)	195.95	7/20/2012	2:36:31 PM	0.27	2.777	51	82.44	82.17
SJR 196.96	196.96	7/24/2012	11:25:19 AM	2.75	7.116	11	79.72	76.97
SJR 198.23	198.23	7/24/2012	12:51:12 PM	6.16	4.895	140.8	82.71	76.55
SJR 198.72	198.72	7/24/2012	1:18:52 PM	6.31	4.611	69	83.3	76.99
SJR 199.1	199.1	7/24/2012	1:34:00 PM	8.5	4.345	35	86.13	77.63
SJR 199.47	199.47	7/24/2012	2:05:10 PM	8.92	6.439	159.6	85.54	76.62
SJR 199.47(2)	199.47	7/24/2012	1:56:17 PM	9.48	3.92	221	84.52	75.04
SJR 199.75	199.75	7/24/2012	2:19:17 PM	10.62	5.791	51	85.26	74.64
SJR 200.1	200.1	7/24/2012	2:35:38 PM	8.2	6.403	130	84.82	76.62

Table 2-C: Reach 5 of the San Joaquin River 2012 summer survey data summary

Site Name	River Mile	Date Measured	Time Measured	dTw (°F)	depth (ft)	ΔSC (microSiemens/cm)	Maximum Temperature (°F)	Minimum Temperature (°F)
SJR 201.33	201.33	7/13/2012	12:58:35 PM	13.62	12.475	283.86	86.27	72.65
SJR 201.57	201.57	7/13/2012	1:08:23 PM	6.73	12.485	99.11	86.67	79.94
SJR 201.72	201.72	7/13/2012	1:20:11 PM	6.96	6.418	105.95	88.07	81.11
SJR 202.65	202.65	7/25/2012	12:26:18 PM	4.02	10.699	33	81.11	77.09
SJR 202.65 opt 2 mid	202.65	7/25/2012	12:16:28 PM	3.83	9.669	27	80.9	77.07
SJR 202.65(4)	202.65	7/25/2012	11:57:06 AM	3.6	8.077	115	79.92	76.32
SJR 203.2	203.2	7/25/2012	12:31:00 PM	2	3.5	Not recorded	83	81
SJR 203.3 opt 1	203.3	7/25/2012	12:34:39 PM	12.94	12.597	1441	83.41	70.47
SJR 203.3 opt 2	203.3	7/25/2012	1:16:14 PM	12.88	20.666	1682	81.61	68.73
SJR 203.8 (Hwy 165 Bridge)	203.8	7/25/2012	1:50:00 PM	7.5	5	Not recorded	84	76.5
SJR 204.6	204.6	7/25/2012	2:17:30 PM	8.85	13.514	145	84.91	76.06
SJR 204.6(2)	204.6	7/25/2012	2:03:05 PM	11.24	2.109	234	87.2	75.96
SJR 205.45	205.45	7/25/2012	2:52:44 PM	10.5	7.246	115	86.74	76.24
SJR 205.45(2)	205.45	7/25/2012	2:41:23 PM	8.16	7.95	79	85.39	77.23
SJR 205.95	205.95	7/25/2012	3:19:13 PM	10.43	14.245	197	85.55	75.12
SJR 205.95(2)	205.95	7/25/2012	3:08:59 PM	9.29	20.887	904	85.31	76.02
SJR 206.99	206.99	7/12/2012	1:57:59 PM	20.57	17.776	1015.21	87.86	67.29
SJR 211.42	211.42	7/12/2012	12:14:21 PM	3.35	7.027	255.77	82.28	78.93
SJR 215.45	215.45	7/12/2012	4:19:19 PM	0.12	7.409	6.17	86.99	86.87

Locations with dT_w greater than 3°F were classified as thermally stratified, while all other locations represented vertically mixed pools. Water temperature at the surface of pools near the air-water interface and the bottom of pools near the streambed ranged widely between reaches. The Eastside Bypass had both the greatest thermal stratification and the coolest pool bottom water temperatures (Table 3). Reaches with high thermal stratification didn't necessarily have the coolest surface water temperatures. Both the Eastside Bypass and Reach 5 had average dT_w greater than 9°F , but both also had maximum and average pool surface water temperatures greater than Reach 4B2. While Reach 4B2 had the warmest pool bottom water temperature, it also had the narrowest range of water temperatures and the coolest average surface water temperature.

Table 3: Variation in pool surface and bottom water temperature

Reach	Pool surface water temperature			Pool bottom water temperature		
	Max	Min	Avg	Max	Min	Avg
Eastside Bypass	92	76	84	83	66	75
Reach 4B2	86	79	82	82	74	77
Reach 5	88	80	85	87	67	76

Pools that were not thermally stratified tended to have the highest pool bottom water temperature. With one exception in Reach 5, pool bottom water temperatures exceeded 80°F only when pools had no thermal stratification.

Longitudinal trends in water temperature at the water surface in the Eastside Bypass, Reach 4B2, or Reach 5 could not be analyzed since the pool surface water temperature trends were a composite over a three week measurement period. Water temperature was measured over three weeks on nine different days and pool surface water temperature was influenced by both the time of day and day measured. Trends in surface water temperature were primarily due to daily warming of the surface water and variations in daily warming between days.

Pool bottom water temperature did not have a longitudinal trend in the Eastside Bypass, Reach 4B2, or Reach 5 of the San Joaquin River (Figure 8). Pool bottom water temperature was analyzed for longitudinal trends since thermal stratification reduced the influence of daily warming on pool bottom water temperatures. However, pools without thermal stratification had daily warming trends in pool bottom water temperature due to differences in measurement time. The apparent warming trend between SJR 211 and SJR 215 in Reach 5 occurred because both pools had 3°F or less thermal stratification and measurements were taken 4 hours apart. Overall, pool bottom water temperature varied between measurement locations, but did not consistently increase or decrease with river mile.

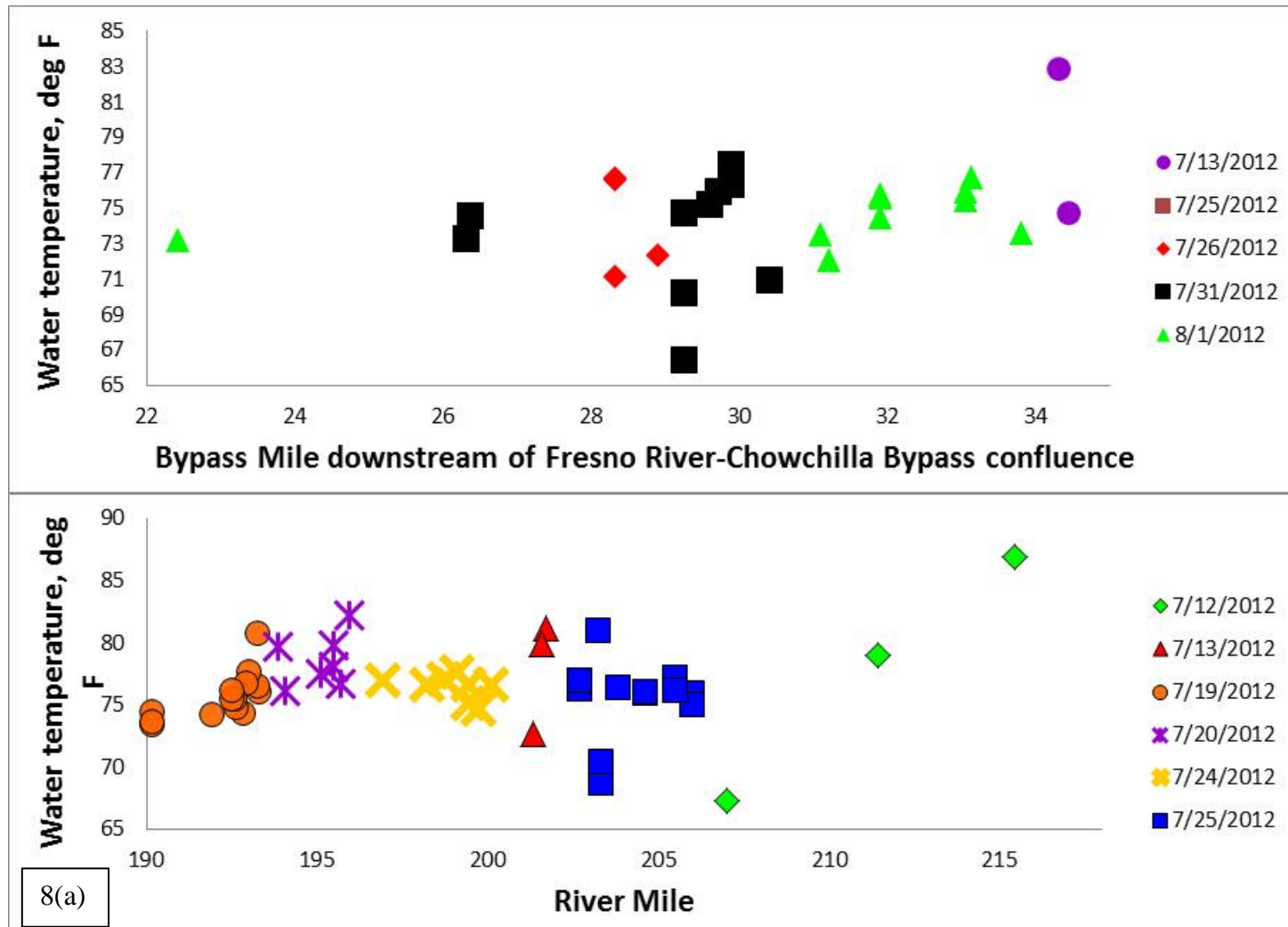


Figure 8: Longitudinal Profiles of Pool Bottom Water Temperature (a) There was no longitudinal trend in pool bottom water temperature in the Eastside Bypass (b) Pool bottom water temperature was greater in Reach 4B2 than in Reach 5 of the San Joaquin River.

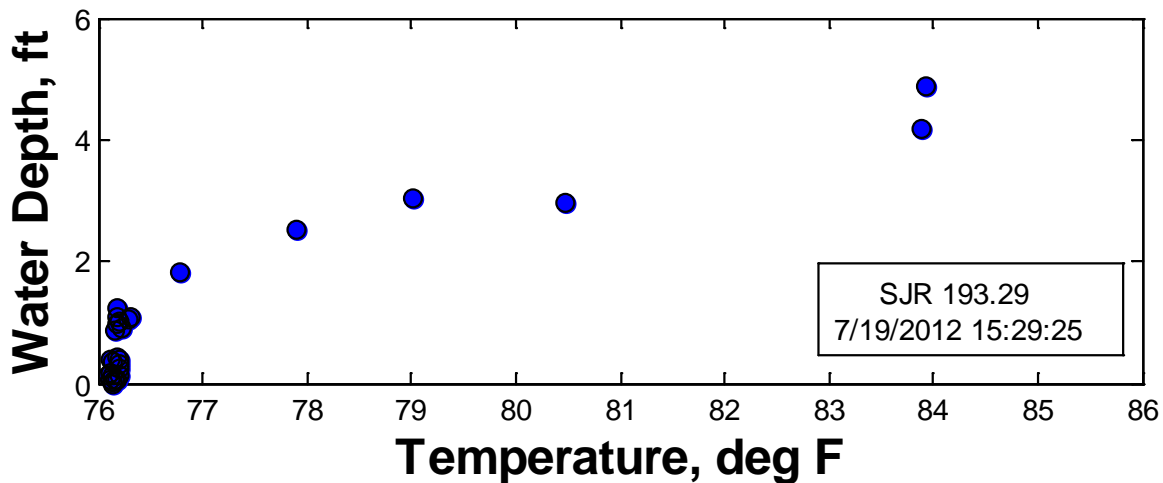
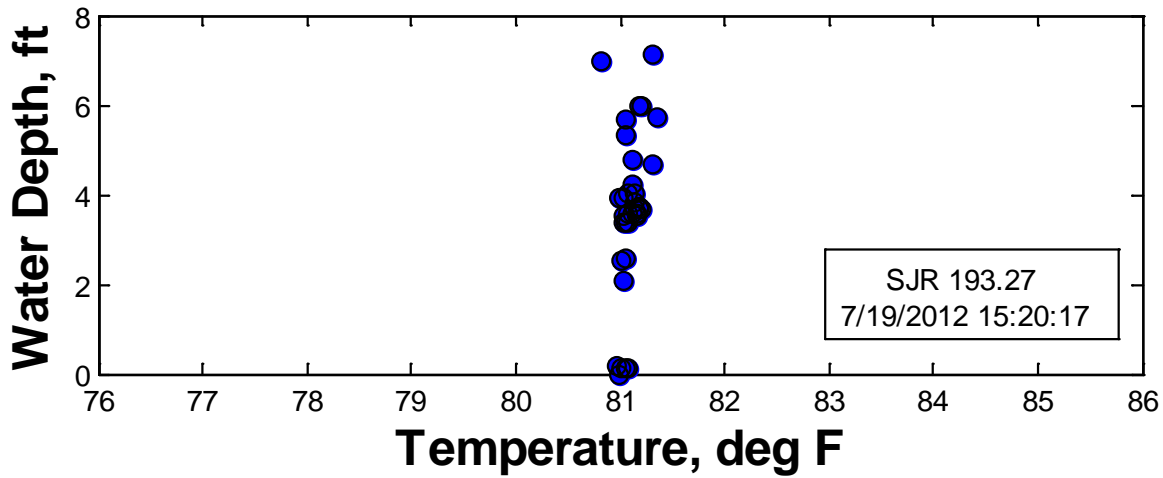
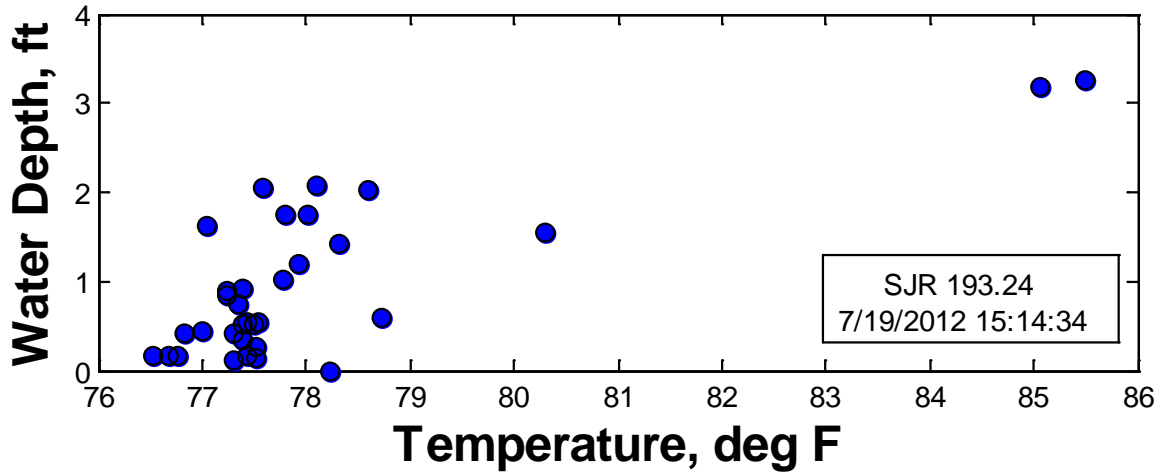


Figure 9: Thermal stratification was spatially variable in the San Joaquin River even under similar surface flow and meteorological conditions. In three sequential pools between SJR 193.24 – SJR 193.29, thermal stratification ranged from greater than 8°F to less than 1°F.

Thermal stratification was spatially variable with pools separated by less than 175 ft having completely different vertical water temperature profiles. Pools located at SJR 193.24, SJR 193.27, and SJR 193.29 had different vertical water temperature profiles even though they had similar surface flow, meteorological conditions, and canopy conditions (Figure 9). Both the upstream pool and the downstream pool had thermal stratification greater than 8°F. Water temperature was uniform with depth in the middle pool located between those two pools. Increases in pool depth did not correlate with vertical water temperature differences. The middle pool with no thermal stratification, SJR 193.27, was also the deepest pool. The upstream pool, SJR 193.24, was the shallowest, yet difference between pool surface and bottom water temperatures was 9°F. Pool volume, surface area, and geometry were different between the thermally stratified pools and the unstratified SJR 193.27 pool (Figure 10). Pool volume and surface area were greater in the thermally stratified pools.

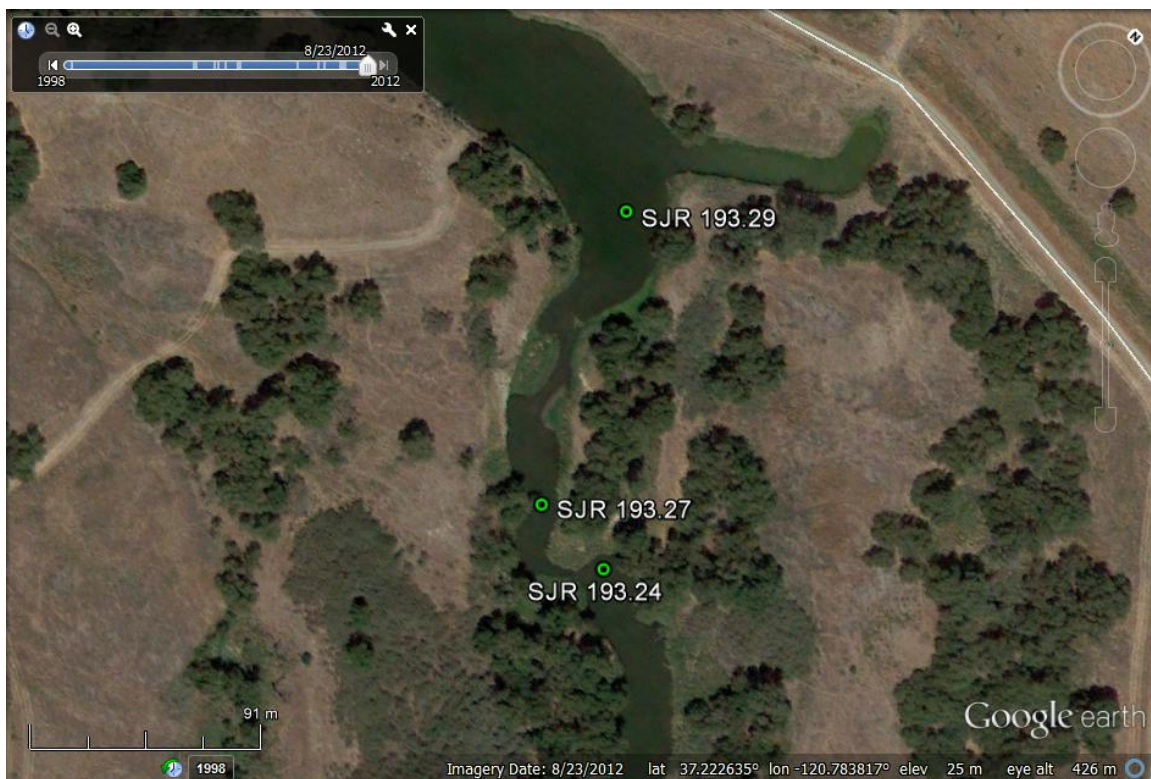


Figure 10: Aerial view of SJR 193 pools. SJR 193.27 was the deepest pool, but SJR 193.24 and SJR 193.29 had larger total volumes.

26.3.1.2 Water Specific Conductance

Water specific conductance (SC) in the Eastside Bypass, Reach 4B2, and Reach 5 indicated that vertical SC gradients existed in pools and frequently correlated with vertical water temperature gradients. Water temperature and SC did not consistently increase or decrease together. At 37% of the measurement locations, decreases in water temperature corresponded to decreases in SC (Figure 11). At 56% of the locations, SC and water temperature changed differently with depth (Figure 12). At the remaining 7% of locations, water temperature and SC were uniform with depth. Specific conductance

increased with depth in 26% of the locations measured. Differences between surface and bottom SC ranged from 1 $\mu\text{S}/\text{cm}$ to 1682 $\mu\text{S}/\text{cm}$ with an average of 254 $\mu\text{S}/\text{cm}$ across all locations measured. Specific conductance ranged from 3406 $\mu\text{S}/\text{cm}$ to 195 $\mu\text{S}/\text{cm}$ with an average SC of 1280 $\mu\text{S}/\text{cm}$ across all three reaches.

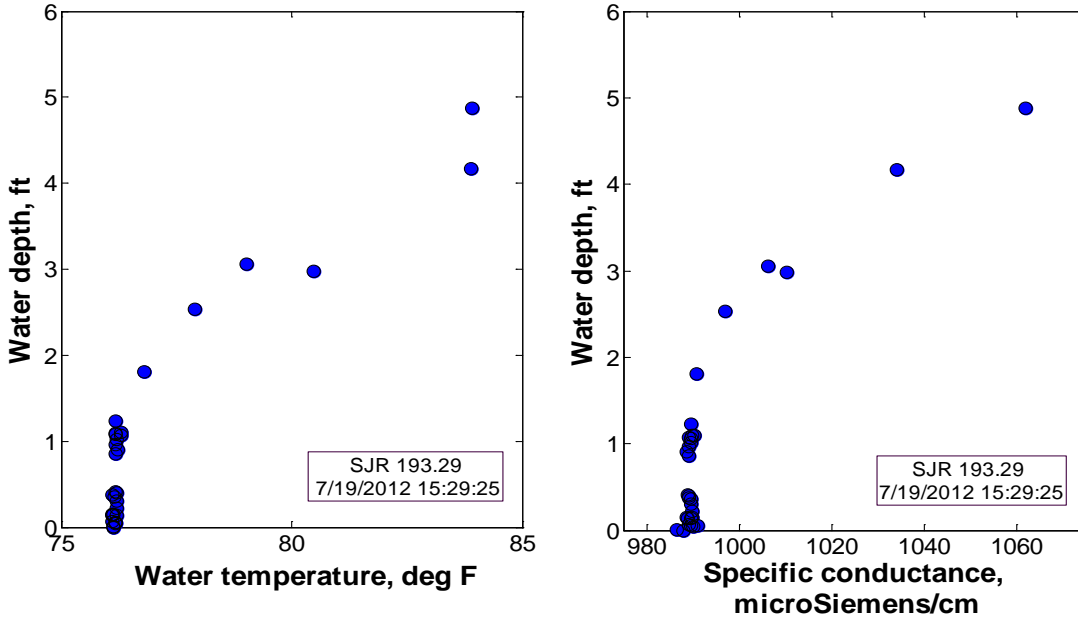


Figure 11: At SJR 193.29, decreases in water temperature with depth corresponded to decreases in water specific conductance with depth.

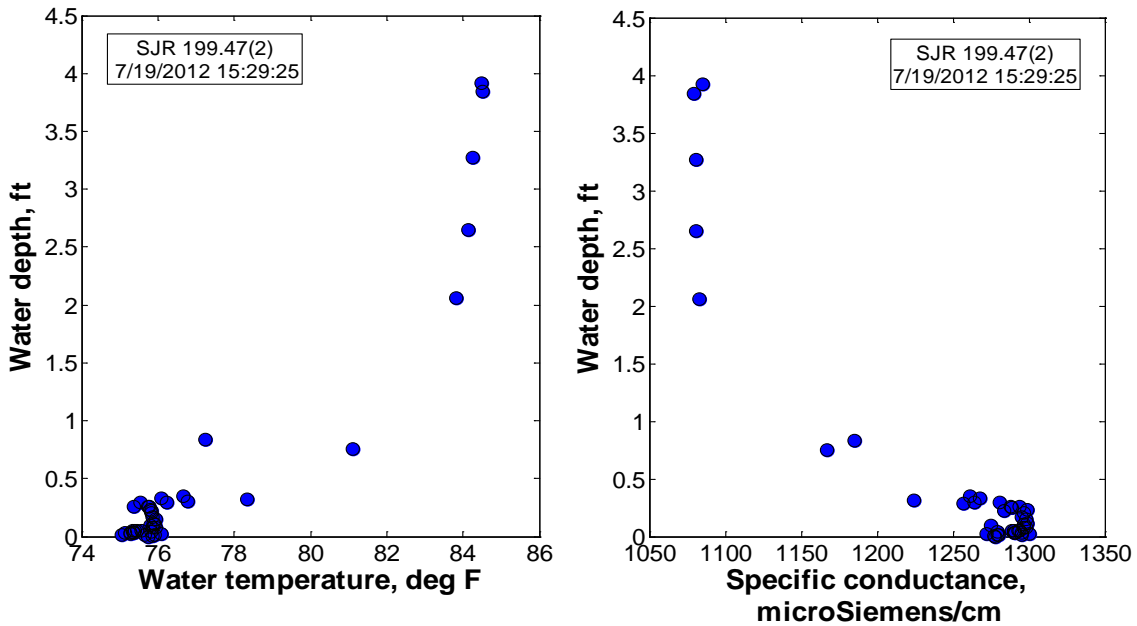


Figure 12: At SJR 199.47(2), water specific conductance increased with depth as water temperature decreased with depth.

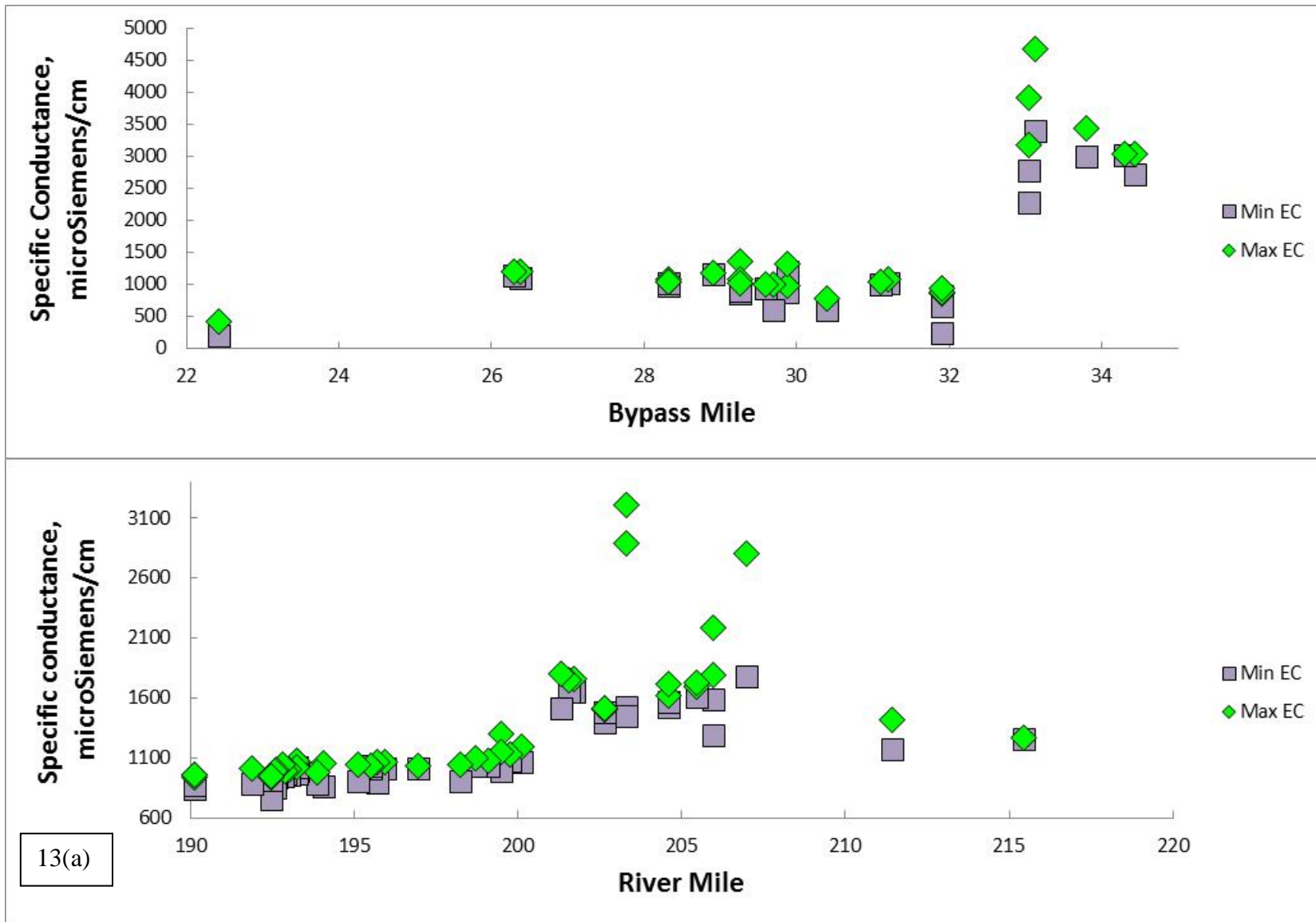


Figure 13: Longitudinal Profiles of Specific Conductance (a) Water specific conductance in the Eastside Bypass increased sharply after bypass mile 32 (b) Water Specific conductance in Reach 4B2 of the San Joaquin River gradually increased with distance downstream, increased sharply at its confluence with the Eastside Bypass, then decreased with distance downstream.

Specific conductance varied with distance along the waterway in both the Eastside Bypass and the San Joaquin River (Figure 13). In the Eastside Bypass, SC was initially between 422 $\mu\text{S}/\text{cm}$ and 195 $\mu\text{S}/\text{cm}$ in the Merced National Wildlife Refuge then increased to approximately 1000 $\mu\text{S}/\text{cm}$ between bypass mile 26 and 32. Between bypass mile 32 and 33 the SC sharply increased approximately 2000 $\mu\text{S}/\text{cm}$ and remained around 3000 $\mu\text{S}/\text{cm}$ until its confluence with the San Joaquin River. The source of the increase in SC was not identified. The last measurement location before the increase in SC was downstream of the confluence of the Eastside Bypass and Bear Creek. This indicated that Bear Creek was not a source of high SC water entering the Eastside Bypass. In the San Joaquin River, maximum SC gradually increased from 959 $\mu\text{S}/\text{cm}$ to 1300 $\mu\text{S}/\text{cm}$ in Reach 4B2. Specific conductance increased to approximately 1800 $\mu\text{S}/\text{cm}$ at the beginning of Reach 5 where the Eastside Bypass entered the San Joaquin River. Specific conductance in Reach 5 varied widely, but tended to decrease with distance downstream.

26.3.1.3 Distribution of Pool Habitat in the San Joaquin River System

Cold water habitat that contained thermal refugia was very infrequent in pools in the San Joaquin River system in July 2012. Pool locations were classified into three groups to determine cold water habitat potential. Pool locations with water temperature between 65°F and 68°F were “critical”; pool locations with water temperature between 68°F and 75°F were “sub-lethal”; and pool locations with water temperature greater than 75°F were “lethal.” Each pool location surveyed was considered a distinct cold water habitat location due to the variability of water temperature within individual pools. This means that a single river pool could have more than one region of cold water habitat especially if there are multiple deep points in the pool. No pools surveyed had cold water habitat below the lower “critical” water temperature threshold of 65°F (Table 4). The Eastside Bypass and Reach 5 each had one pool that was within the “critical” water temperature threshold, while Reach 4B2 had only pools with water temperature above 68°F. Water temperature was greater than 75°F in the majority of pools in all three reaches.

Table 4: Pool locations surveyed in the San Joaquin River system in July 2012

	Eastside Bypass	Reach 4B2	Reach 5
Total Pool Locations	29	29	19
Pool Locations / mile	2.3	2.6	1.3
“Critical” 65°F \leq T _{min} \leq 68°F	1	0	1
“Sub-lethal” 68°F < T _{min} \leq 75°F	14	7	3
“Lethal” T _{min} > 75°F	14	22	15

Distances between pools at different water temperature thresholds indicated that thermal barriers existed in Reach 4B2, Reach 5, and the Eastside Bypass during July. Reach 5

had the longest average distance between pools (Table 5), but Reach 4B2 had the longest maximum distance between pools at or below the “sub-lethal” temperature threshold (Table 6). Distances between “critical” pools could not be calculated because there were not two pools with minimum water temperature in the “critical” range in any of these reaches.

Table 5: Average distance between pools below temperature thresholds in July 2012

	Eastside Bypass	Reach 4B2	Reach 5
Pools with $T_{\min} \leq 68^{\circ}\text{F}$	-	-	-
Pools with $T_{\min} \leq 75^{\circ}\text{F}$	1.1 miles ¹	2.4 miles	2.8 miles
Pools with $T_{\min} \leq 80^{\circ}\text{F}$	0.7 miles ¹	0.5 miles	1.1 miles

Table 6: Maximum distance between “sub-lethal” threshold pools in July 2012

	Eastside Bypass	Reach 4B2	Reach 5
Pools with $T_{\min} \leq 75^{\circ}\text{F}$	4 miles ¹	7 miles	4 miles



Figure 14: Pools in the Eastside Bypass upstream of ESB 29.25 were isolated with no flow connecting them to downstream pools. Photo is looking upstream with thumb pointing in the downstream direction.

In addition to thermal barriers, the Eastside Bypass had physical barriers to movement between pool habitats. During July 2012, pool habitat was fragmented in the Eastside Bypass because pools upstream of bypass mile 29.25 were disconnected and had no flow between them (Figure 14). Six of the Eastside Bypass pools were upstream of bypass mile 29.25 and were isolated from other pool habitat in the system. Average distances

¹ Distance calculated based on only temperature thresholds

between pools below different temperature thresholds in the Eastside Bypass upstream of bypass mile 29.25 are only theoretical, while the maximum distance between Eastside Bypass pools at “sub-lethal” water temperatures was 7 miles when physical barriers were considered.

26.3.2 Piezometer and Water Temperature Array Instrumentation

26.3.2.1 Surface Water Temperature

Daily formation and breakdown of thermal stratification was measured in pools at all six sites instrumented in the Eastside Bypass, Reach 4B2, and Reach 5. Vertical water temperature was nearly uniform at the start of the day then water temperature near the air-water interface began increasing around 8 – 10 AM. Differences in water temperature with depth increased during the day and formed thermal stratification in the pool. Water temperature at the streambed, 0ft, varied the least during a day, but still showed diurnal variation. Thermal stratification peaked mid-afternoon then decreased as water temperature near the pool surface and bottom converged. Water temperature decreased throughout the night until the next day’s warming cycle began (Figure 15).

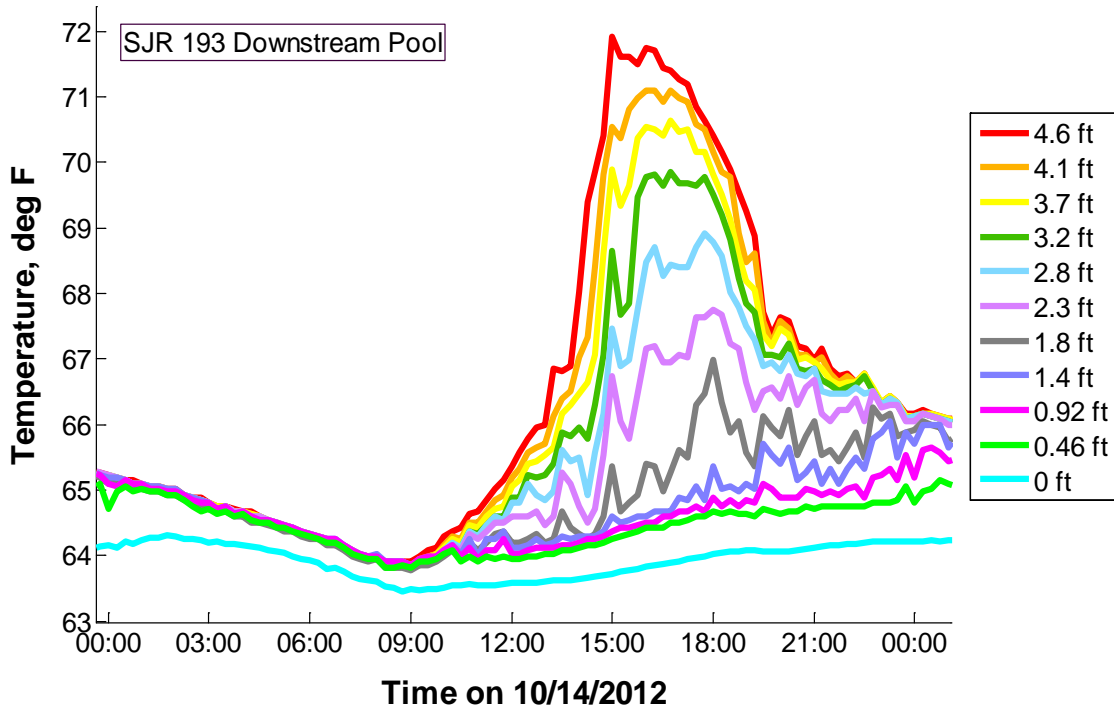


Figure 15: Water temperature data in the downstream SJR 193 pool highlights how surface water temperature in pools varied with depth during the day. Sensor heights are relative to the streambed so 0 ft is located at the streambed while 4.6 ft is located near the air-water interface.

Formation of vertical water temperature gradients in the San Joaquin River and Eastside Bypass system did not occur in all pools instrumented and was temporally and spatially variable. SJR 199 was selected for instrumentation because during July it exhibited thermal stratification in both its upstream and downstream pool (Figure 16)

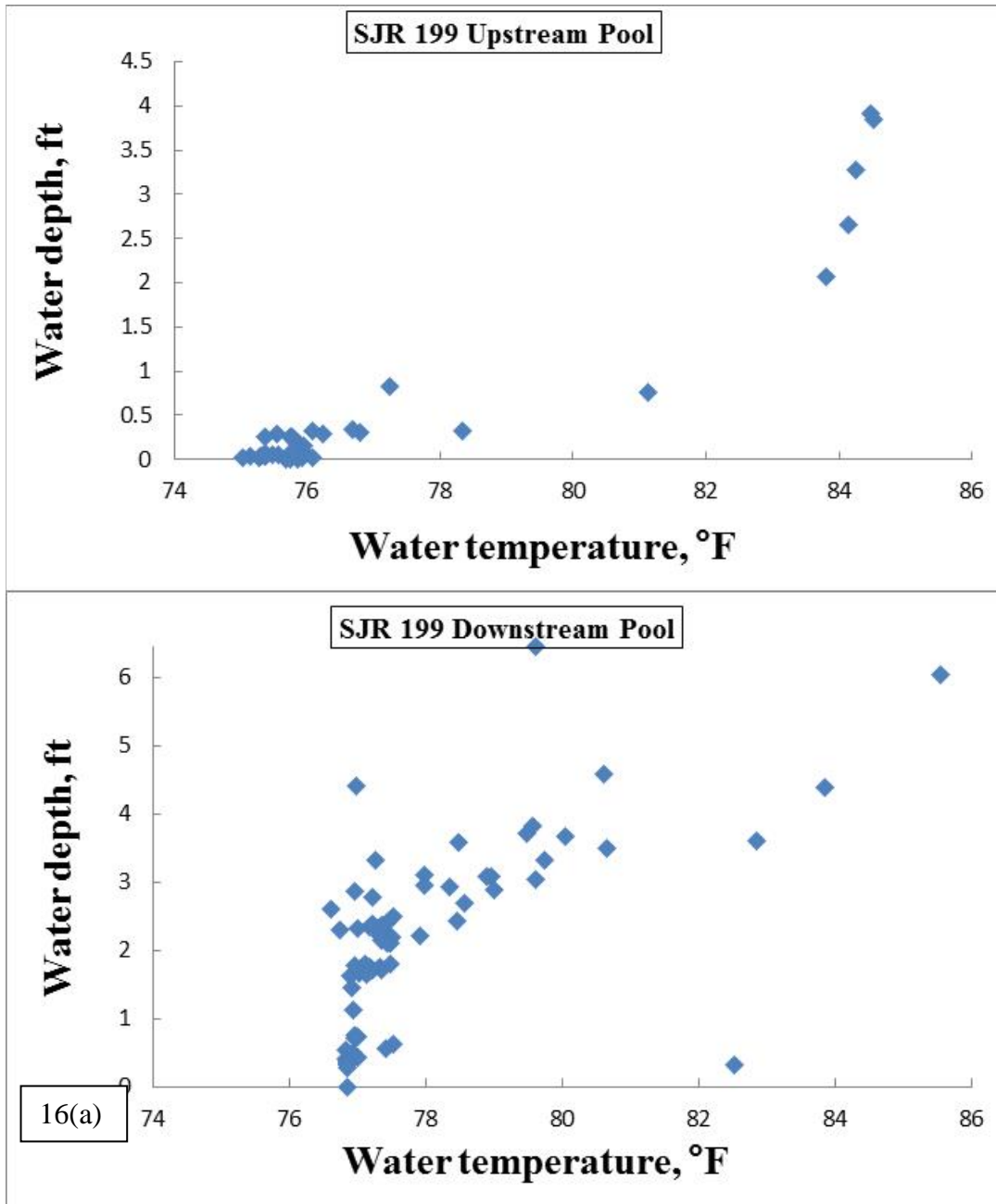


Figure 16: Comparison of thermal stratification at SJR 199 site pools from the July survey. (a) At the upstream SJR 199 pool, water temperature at the pool bottom was 9.5°F less than surface water temperature. (b) The downstream pool at SJR 199 was 2 feet deeper than the upstream pool, but had thermal stratification of 8.9°F.

During the instrumentation period from September 13 to October 6, thermal stratification was no longer present in either the upstream or the downstream SJR 199 pool. The upstream pool showed less than 1.1°F variation in water temperature with depth. At the SJR 199 pool, 260 feet downstream, the difference in vertical water temperature was measured between 2.9°F and 6.1°F (Figure 17). Although the upstream pool had shown

the greater thermal stratification during July, the downstream pool showed greater thermal stratification during the Sept/Oct instrumentation highlighting the temporal and spatial variation in vertical water temperature gradients.

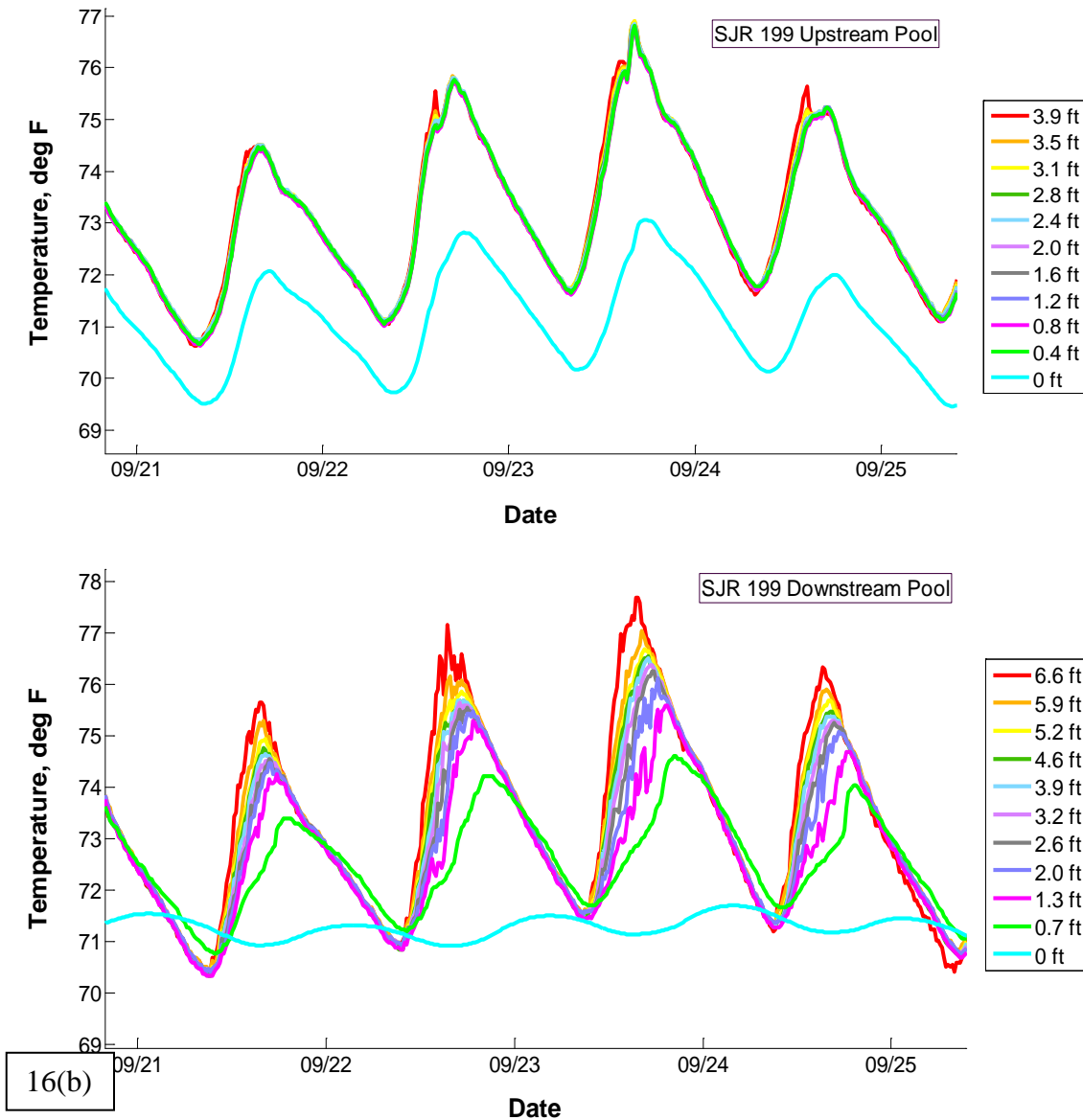


Figure 17: Thermal stratification in pools was spatially variable with different levels of stratification occurring in pools less than 275 feet apart. Note: The sensors located at 0 ft measured streambed subsurface water temperature not surface water temperature because they sank into the fine sediments at the streambed.

Temperature differences between the top and the bottom of pools varied daily over the course of the instrumentation. While each site had its own daily thermal characteristics, trends in water temperature variations were consistent across most sites. Water temperature variation near or at the streambed was less than the variation near the air-

water interface at the top of the pool. Across all sites, the average daily water temperature varied between 0.5°F and 3.1°F near the pool bottom, while average daily water temperature varied from 2.7°F to 10.3°F near the pool top. The variation in vertical water temperature between the top and bottom of pools resulted in average daily thermal stratification between 1.6°F and 10.1°F. Days with small thermal stratification were primarily due to small increases in water temperature near the air-water interface. Daily and weekly trends were regionally consistent with all sites exhibiting similar levels of thermal stratification for a given day (Figure 18).

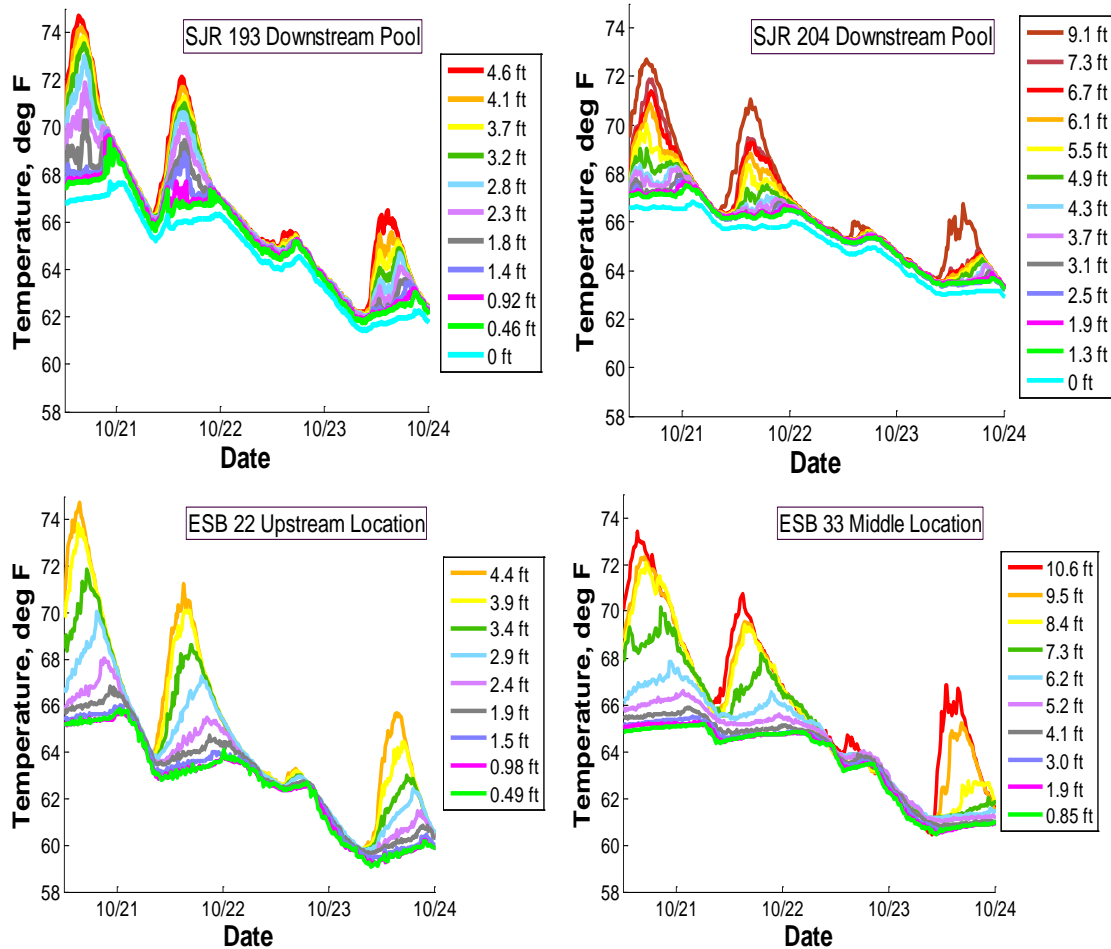


Figure 18: Daily water temperature trends were regionally consistent across pools in the San Joaquin River and the Eastside Bypass

26.3.2.2 Subsurface Water Temperature

While the range of subsurface water temperatures closely agreed with regional groundwater temperatures, temporal trends in subsurface water temperature were different. In 2011, monitoring wells were installed in Reach 4 at locations near the Eastside Bypass, the Mariposa Bypass, and the San Joaquin River upstream of the Mariposa Bypass. Monitoring wells were located between the furthest upstream pool site, ESB 22, and the next two downstream sites ESB 29 and SJR 193. Subsurface water temperature below pools ranged from 61°F to 72°F from September to November 2012 while groundwater temperature ranged from 63°F to 71°F. Groundwater temperature in three of the four monitoring wells showed no daily variations in water temperature while one well, MW-145, had a diurnal variation in groundwater temperature. Average subsurface water temperatures below pools decreased during the instrumentation and were similar to surface water temperature trends (Figure 19). Average regional groundwater temperature from the four monitoring wells increased between September and November and had no daily variation. Similarities in the daily variation and decreasing water temperature trend indicated surface water temperature influenced the subsurface water temperature. Increasing subsurface water temperature with depth indicated local groundwater temperature also influenced subsurface water temperature below pools.

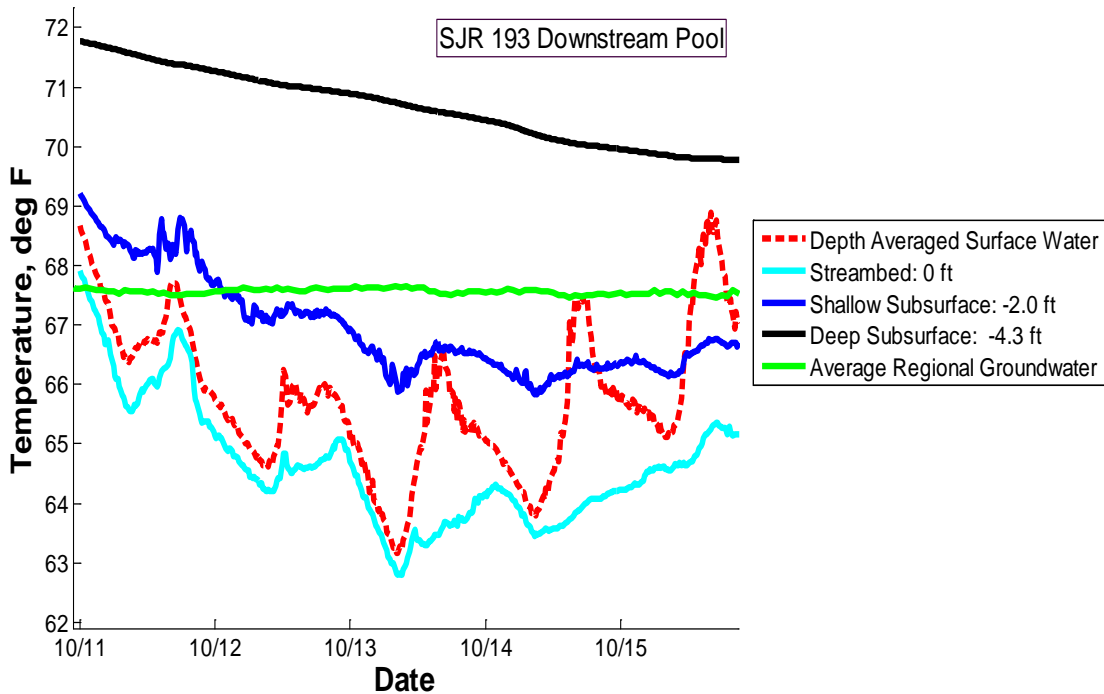


Figure 19: Patterns in subsurface water temperature below pools were more similar to depth averaged surface water temperature than average regional groundwater temperature. At the SJR 193 downstream pool, subsurface water temperatures ranged from greater than to less than the average regional groundwater temperature during October 2012.

Subsurface water temperature increased with depth below the streambed at four of the sites instrumented while two sites showed subsurface water temperature decreasing with depth. At each site, water temperature was measured in the subsurface at a “shallow” and a “deep” depth and compared with streambed water temperature to determine the trend in water temperature with depth. Trends in subsurface water temperature with depth did not correspond with specific hydraulic head trends (see Section 26.3.2.4 for discussion of hydraulic head). At SJR 193, SJR 204, ESB 22, and ESB 33, water temperature generally increased with depth below the streambed (Figure 20).

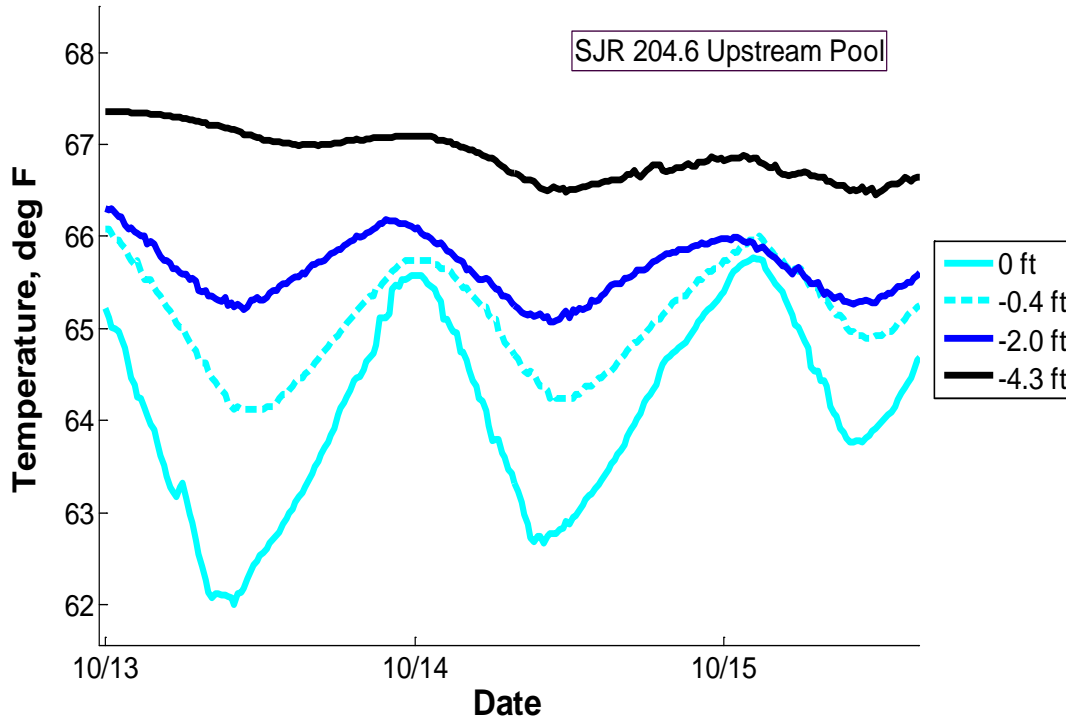


Figure 20: Subsurface water temperature increased with depth below the streambed at most sites in the San Joaquin River and the Eastside Bypass.

Diurnal variations in water temperature existed in the subsurface water temperature data. The amplitude of the daily variation in subsurface water temperature decreased with depth below the streambed. At the upstream SJR 204 pool, the average daily change in temperature ($dT_{\text{avg daily}}$) was 1.1°F at -2.0 ft and 0.5°F for the deepest sensor at -4.3 ft. The rate at which the amplitude decreased with depth below the streambed varied between sites. At ESB 22, $dT_{\text{avg daily}}$ was 0.7°F for the shallow sensor located 0.75 ft below the streambed and 0.2°F for the deepest sensor at -2.2 ft. At some sites, the amplitude of daily variation decreased so rapidly with depth below the streambed that there was no daily variation in subsurface water temperature in shallow or deep sensors (Figure 21). Weekly water temperature trends were still present in subsurface water temperature data even when daily variations were damped with depth.

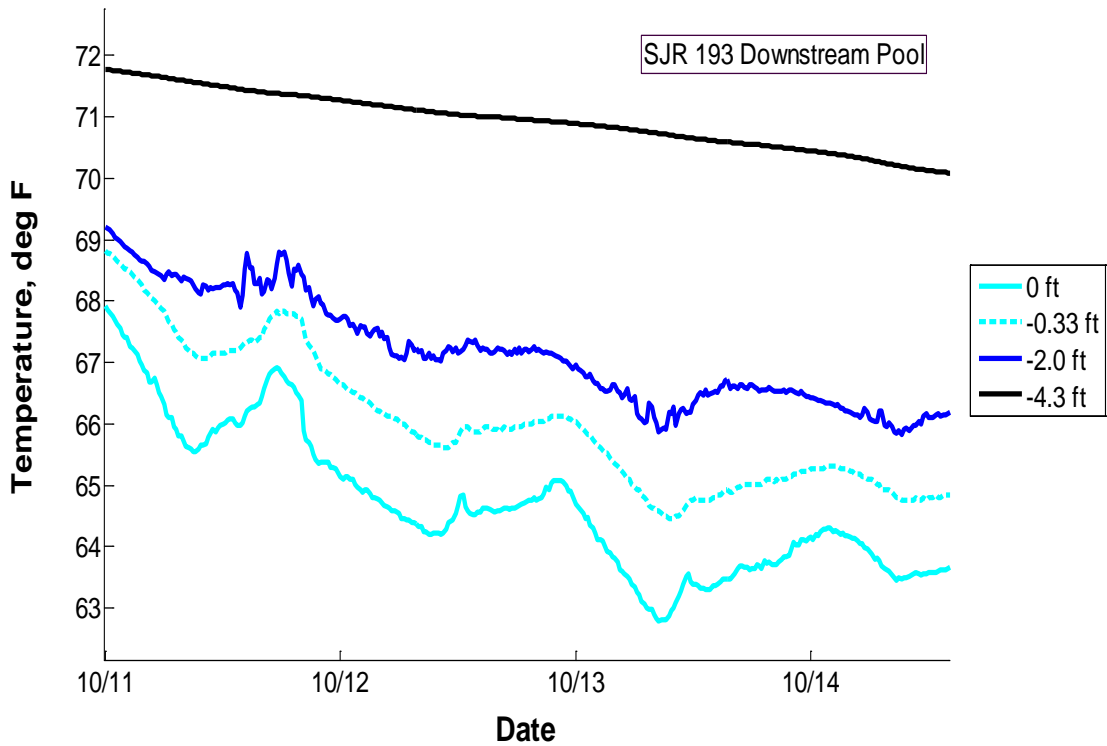


Figure 21: The amplitude of the daily variation in water temperature decreased with depth below the streambed at the downstream pool at SJR 193.

An increasing weekly trend in surface water temperature between 10/15 and 10/23 caused subsurface water temperature near the streambed to become warmer than deep subsurface water temperature at SJR 193, SJR 204, and ESB 22. During this period, increased surface water temperature and daily variation in surface water temperatures caused both the magnitude and amplitude of the near streambed subsurface water temperature to increase. Shallow and deep subsurface water temperature magnitude and amplitude generally did not increase as much as the near streambed subsurface water temperature. This caused the near streambed subsurface water temperature to exceed the deep subsurface water temperature at some sites during this period (Figure 22). After surface water temperature began decreasing on 10/23, the magnitude and amplitude of the near streambed subsurface water temperature decreased so subsurface water temperature consistently increased with depth.

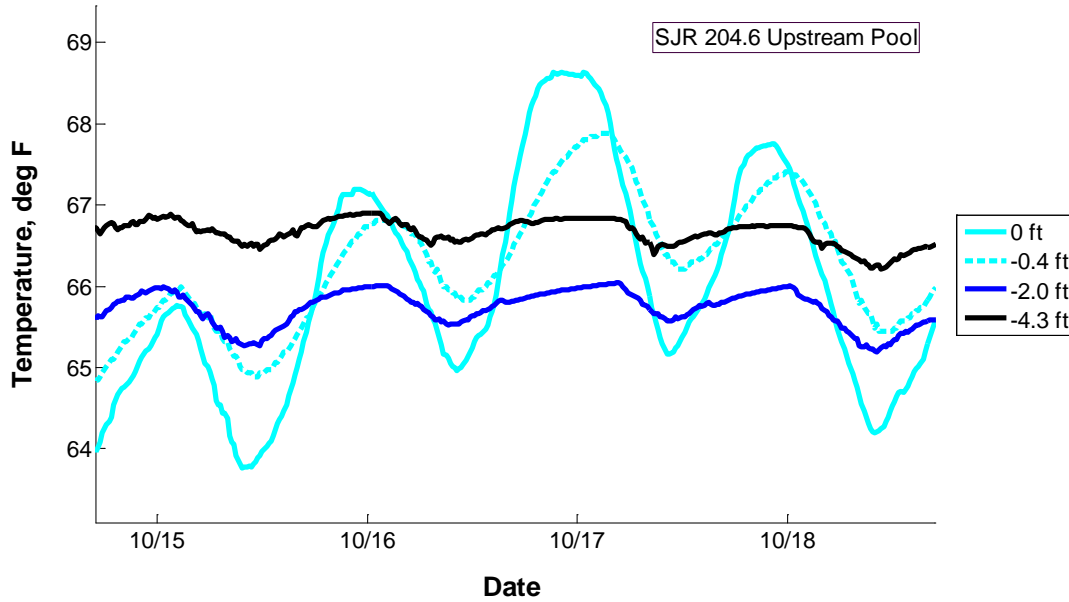


Figure 22: At the SJR 204 upstream pool, when streambed water temperature increased on 10/15, water temperature trends with depth were altered resulting in deep subsurface water being cooler than subsurface water temperature near the streambed.

Subsurface water temperature decreased with depth below the streambed at two instrumented sites. Both SJR 199 and ESB 29 showed decreases in subsurface water temperature with depth. The amplitude of daily variations in subsurface water temperature decreased below the downstream SJR 199 pool until there was no daily and minimal weekly variation in subsurface water temperature with depth (Figure 23).

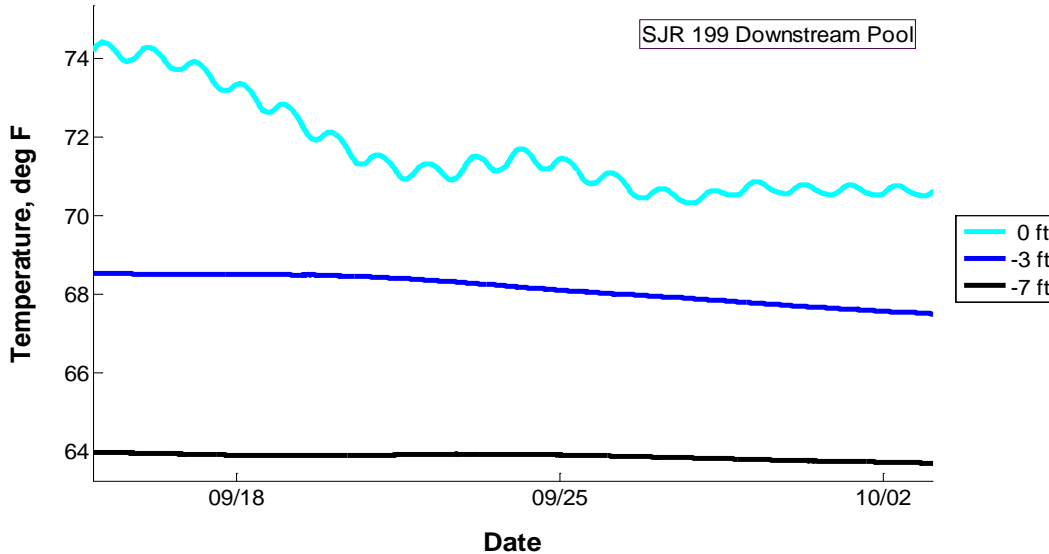


Figure 23: Subsurface water temperature decreased with depth below the streambed at the SJR 199 downstream pool.

26.3.2.3 Subsurface – Surface Water Temperature Comparison

Subsurface water temperature was frequently greater than surface water temperature in pools (Figure 24). While surface water temperature varied with depth during the day, daily heating and cooling cycles resulted in only water near the air-water interface exceeding subsurface water temperatures. Daily thermal stratification preserved colder water along the streambed where minimum water temperatures were consistently less than subsurface water temperatures in many sites.

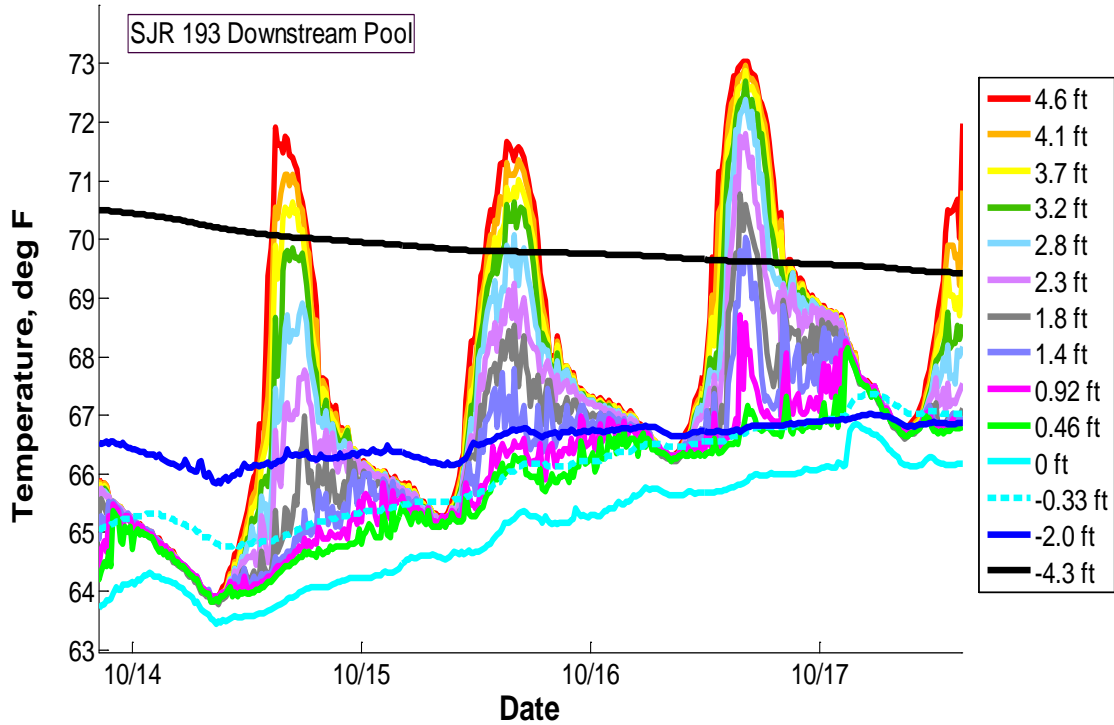


Figure 24: Subsurface water temperature was greater than pool surface water temperature throughout much of the day at SJR 193.

Surface water temperature was greater than subsurface water temperature in some pools. During mid-October, surface water temperature was warmer than in the subsurface water at SJR 204 and ESB 29. When surface water temperature increased due to a week long warming period, surface water temperature temporarily became greater than subsurface water temperature at SJR 204 (Figure 25). After the warming period ended, surface water temperature decreased and subsurface water temperature became greater than surface water temperature. While most sites had subsurface water temperature warmer than streambed water temperature, surface water temperature was consistently greater than subsurface water temperature at SJR 199. Subsurface water temperature at SJR 199 was between 68.9°F and 60.8°F during the instrumentation. This was within the temperature range measured in the subsurface at other sites and regional groundwater monitoring well sites so unusually cool subsurface water temperature was not responsible for the surface water being consistently warmer than subsurface water. Average surface water temperature greater than 73.4°F at SJR 199 was greater than surface water

temperature at other pool sites and was the reason for surface water being greater than subsurface water temperatures.

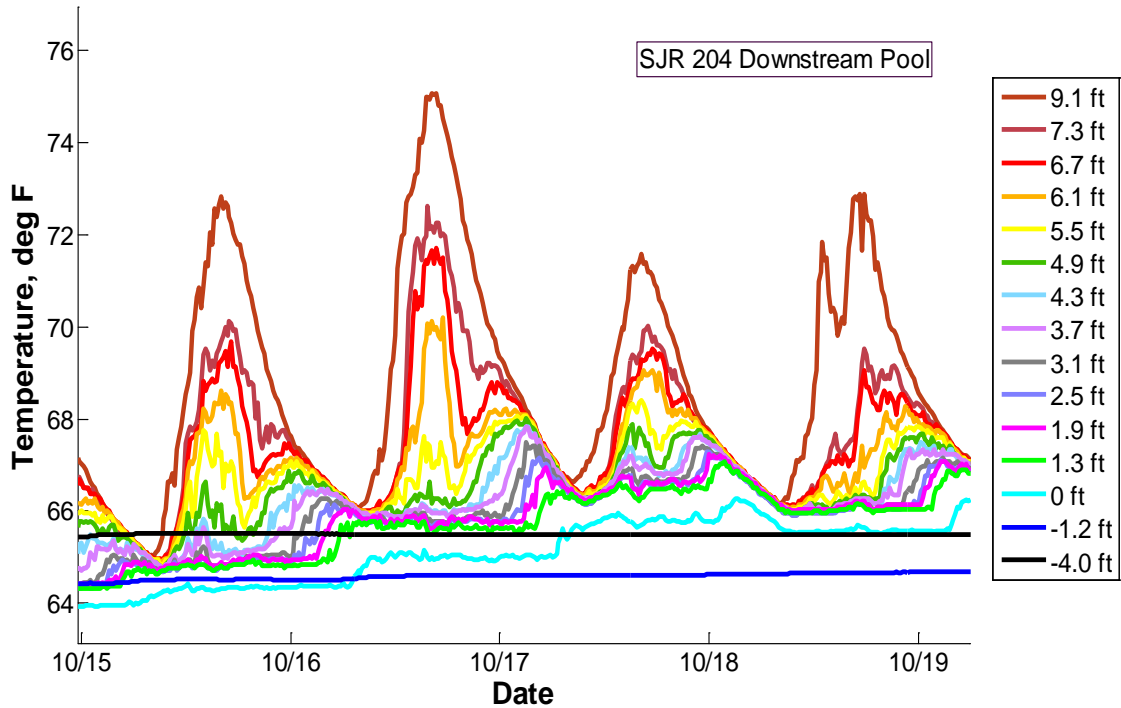


Figure 25: At the SJR 204 downstream pool, a warming trend between 10/16 and 10/22 resulted in the surface water temperature being greater than subsurface water temperature for six days.

26.3.2.4 Hydraulic Head

Hydraulic head gradients varied both between sites and within pools demonstrating a range of downwelling, upwelling, and neutral conditions in the San Joaquin River system. Five different hydraulic head gradient trends were measured in the thirteen locations instrumented at the six sites. Six locations had hydraulic head decreasing with depth, indicating downwelling of surface water into the subsurface, while two locations had hydraulic head increasing with depth, indicating upwelling subsurface flow. Hydraulic head at other measurement locations did not consistently increase or decrease with depth below the streambed. Water pressure sensors installed at the streambed, the “shallow” subsurface, and the “deep” subsurface enabled an evaluation of hydraulic head gradients in pools below each instrumentation site. While hydraulic head was assumed to determine the direction of subsurface flow, subsurface conditions that might inhibit or restrict flow were unknown. A confining layer at the surface (low hydraulic conductivity) and then a deeper area of sand (high hydraulic conductivity) could result in the appearance of an upwelling situation without actual subsurface flow entering the pool. Hydraulic conductivity of subsurface sediments was unknown below the pools and sediment cores were not taken at sites. Hydraulic head gradients below pools indicated directions of subsurface flow, but are not definitive without further geologic information.

Hydraulic head decreased with depth below the streambed at six locations so five of the ten distinct pools in the study were not gaining water from the subsurface. Consistent decreases in hydraulic head with depth were measured at the downstream pool at SJR 193, the downstream SJR 199 pool, both pools at ESB 29, and the middle and downstream locations in ESB 33. For the downstream pool at SJR 193, the hydraulic head at all depths responded to daily variations in the water level but maintained a consistent difference between the different depths (Figure 26). At many instrumented locations, the hydraulic head changed more between the shallow and deep sensors than between the shallow and streambed sensors even when the distance between sensors was considered. At the downstream pool at SJR 193, the average difference between hydraulic head at the streambed and the “shallow” sensor at -2.0 ft was less than 0.1 ft, while the average difference between hydraulic head at the “shallow” and “deep” sensor was 1.1 ft.

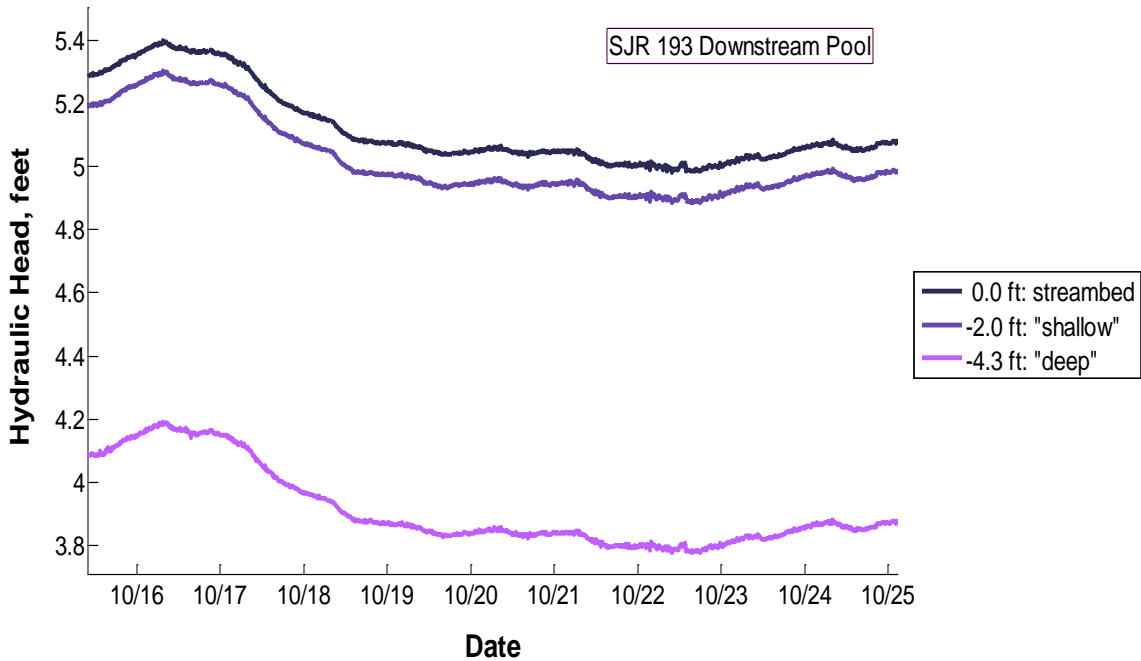


Figure 26: Hydraulic head below the downstream pool at SJR 193 decreased with depth indicating surface water in the pool flowed down into the subsurface

At two locations, streambed and “shallow” hydraulic head were the same within sensor accuracy then hydraulic head decreased between the “shallow” and “deep” sensors (Figure 27). Hydraulic head at both the upstream SJR 199 pool and the upstream location in ESB 33 was approximately equal at the streambed and the “shallow” sensor creating a neutral subsurface-surface water exchange condition.

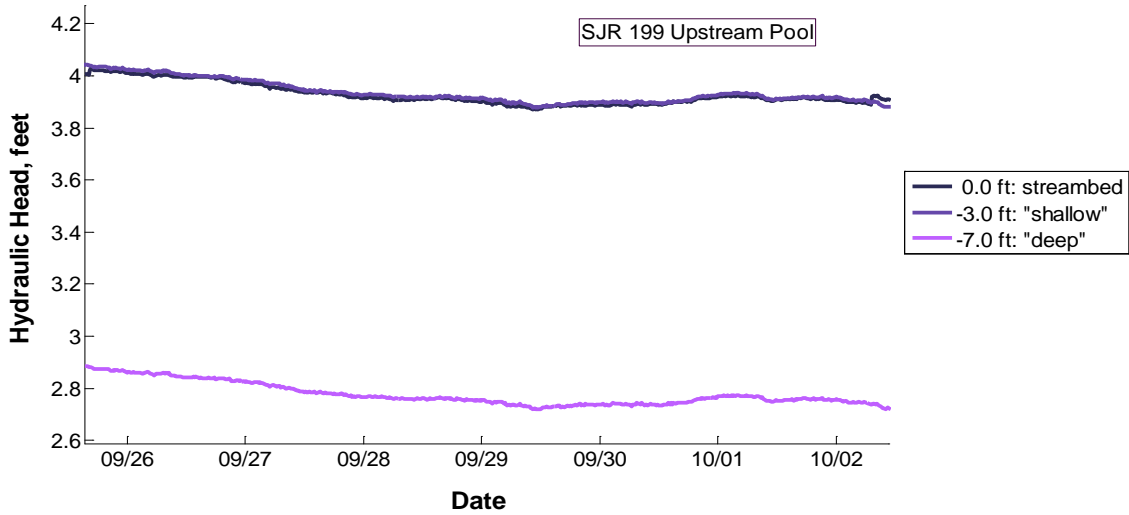


Figure 27: At SJR 199, hydraulic head trends below the upstream pool were variable. While streambed and shallow hydraulic head were equal, deep hydraulic head was less than both.

At the upstream pool location at SJR 193, variation in hydraulic head trends with depth resulted in a range of surface-subsurface exchange conditions during the instrumentation period (Figure 28). Changes in surface water level during the instrumentation corresponded with “shallow” hydraulic head at -2.1 ft becoming greater or less than streambed hydraulic head. Hydraulic head initially decreased with depth, but when the pool surface water level dropped from 10/16 and 10/19 the hydraulic head at -2.1 ft became greater than the hydraulic head at the streambed. When surface water level increased on 10/20, streambed hydraulic head increased more than “shallow” hydraulic head creating downwelling conditions again.

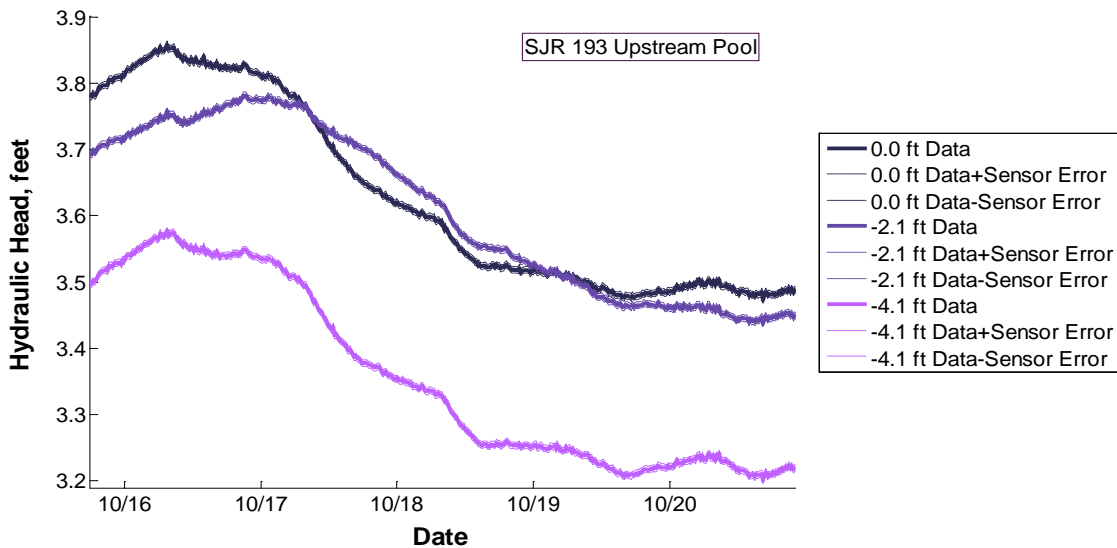


Figure 28: At the upstream pool in SJR 193, hydraulic head trends varied with depth when surface water levels changed producing upwelling, neutral, and downwelling subsurface flow conditions.

At two locations, hydraulic head trends were inconsistent with depth below the streambed. Hydraulic head initially increased with depth then decreased with depth indicating a perched higher hydraulic head region (Figure 29). At ESB 22, the “shallow” hydraulic head 0.8 ft below the streambed was 1.1 ft greater than the streambed hydraulic head and 1.0 ft greater than the “deep” hydraulic head 2.2 ft below the streambed. Changes in surface water level on 10/27 did not alter hydraulic head trends with depth.

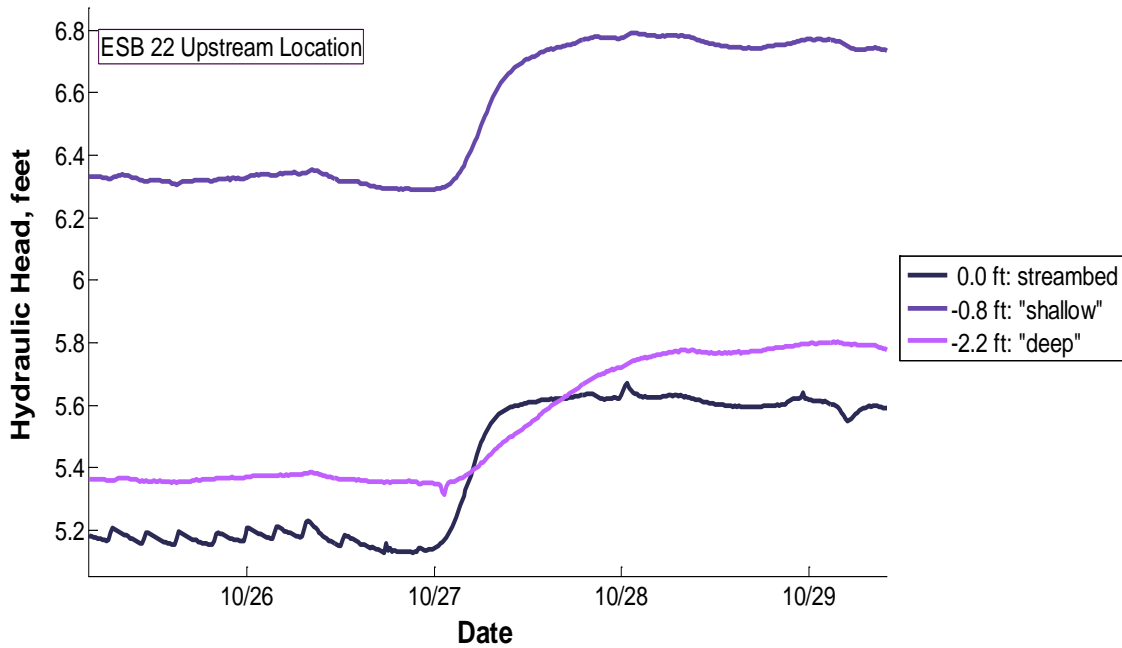


Figure 29: At the upstream location in ESB 22, hydraulic head did not have a consistent variation with depth.

Differences between the hydraulic head response times to surface water level changes suggested a low hydraulic conductivity sediment layer existed between the “shallow” and “deep” sensors. “Deep” hydraulic head took approximately 31 hours to re-equilibrate with streambed hydraulic head while “shallow” hydraulic head took only 21 hours to re-equilibrate. A lower hydraulic conductivity layer would inhibit subsurface flow, produce the longer response time between different sediment layers, and promote the formation of a perched higher hydraulic head region at the “shallow” sensor depth. Sediment cores would be required to test this hypothesis.

Hydraulic head increased with depth at the downstream pools at SJR 204 and ESB 22 indicating subsurface flow upwelled into these pools. At SJR 204, the hydraulic head increased an average of 0.49 ft between the streambed and -1.2 ft while it increased an average of 0.85 ft between -1.2 ft and -4.0 ft (Figure 30).

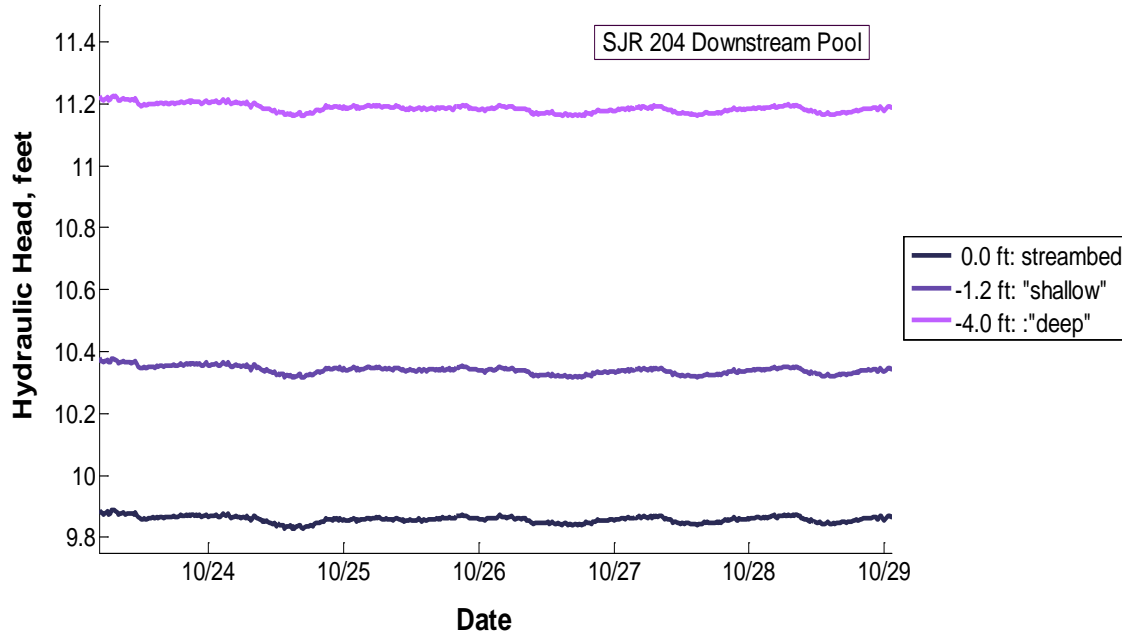


Figure 30: At the downstream SJR 204 pool, hydraulic head consistently increased with depth below the streambed.

In addition to variations between pools, hydraulic head trends with depth were variable within individual pools. Upstream and downstream hydraulic head instrumentations in ESB 22 indicated hydraulic head trends varied along the length of the pool. As previously discussed, hydraulic head trends were inconsistent with depth at the upstream location in ESB 22. At the downstream location in ESB 22, the hydraulic head increased with depth. The average difference in hydraulic head at the streambed and “shallow” sensor was 0.01 ft, while the hydraulic head increased an average of 0.36 ft between the “shallow” and “deep” sensors (Figure 31). While hydraulic head trends varied between the locations, the responses to changes in surface water level were consistent at both locations. On 10/27 when the pool surface water level increased, both upstream and downstream locations in ESB 22 showed subsurface hydraulic head responded slower than surface water level variations. However, “shallow” and “deep” hydraulic head at the upstream location showed different response curve slopes than the downstream location. At the downstream location, the response curve slopes were similar for the “shallow” and “deep” sensors suggesting both ESB 22 downstream piezometers were installed in sediment with similar hydraulic conductivity.

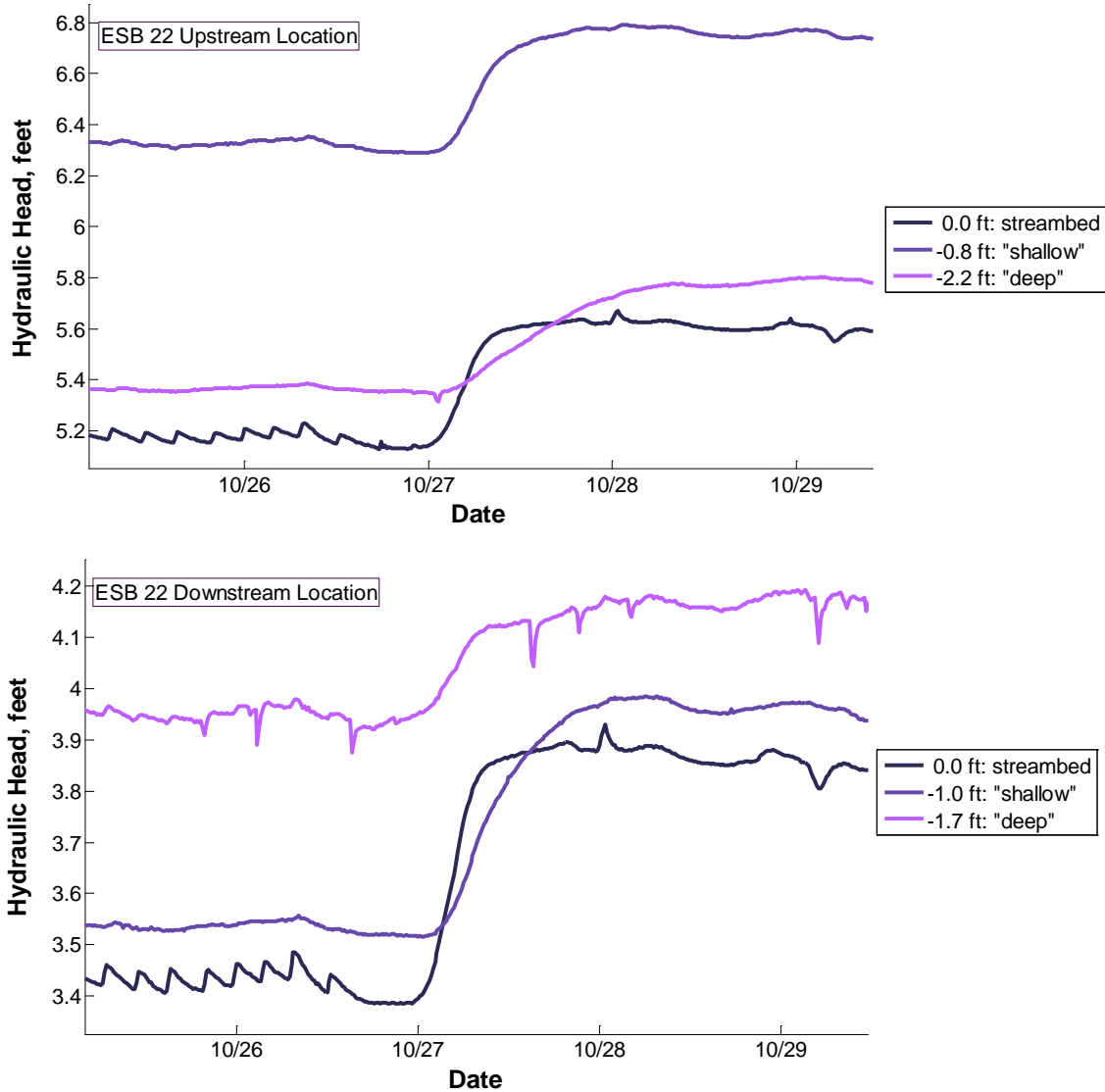


Figure 31: Comparison of hydraulic head at the upstream and downstream instrumented locations in ESB 22.

26.4 Discussion

26.4.1 Availability and Persistence of Thermal Stratification in the Eastside Bypass, Reach 4B2, and Reach 5 of the San Joaquin River system

Thermal stratification occurred in pools in the San Joaquin River system throughout summer and fall 2012, but spatial and temporal variations indicated thermal stratification was influenced by both local and regional drivers. Thermal stratification was frequently available in pools with 82% of pools surveyed during July 2012 showing thermal stratification from 3°F to 20°F. While the average pool thermal stratification was 7.6°F, the degree of thermal stratification was spatially variable with no trend in thermal

stratification with river mile in the Eastside Bypass, Reach 4B2, or Reach 5. Thermal stratification varied substantially between sequential pools during the summer survey suggesting that local variations in pool characteristics influenced whether pools thermally stratified. Thermal stratification in a three pool sequence between SJR 193.24 and SJR 193.29 ranged from 9°F to less than 0.5°F to 8°F (Figure 9). All three pools experienced similar surface water flow, weather conditions, and canopy cover, but showed different vertical water temperature profiles. This spatial variability indicated local conditions in the pools influenced the availability of thermal stratification.

Temporal variations in vertical water temperature profiles indicated there was also a regional influence on whether thermal stratification formed in pools. All pools with thermal stratification showed a daily formation and collapse of vertical water temperature gradients. Thermal stratification began between 8 A.M. and 10 A.M. as surface water temperatures increased faster than pool bottom water temperatures. It persisted until mid-afternoon when surface water temperature decreases caused convective mixing that collapsed vertical water temperature gradients. While the amount of thermal stratification varied between instrumented sites, the pattern of daily thermal stratification was regionally consistent across multiple pools (Figure 18). Days with thermal stratification in one pool corresponded to similar levels of thermal stratification in all other pools instrumented. When there was a sharp reduction in thermal stratification on 10/22, all pools instrumented in the Eastside Bypass and the San Joaquin River showed a similar decrease in thermal stratification. While local variations in pool characteristics influenced the availability of thermal stratification, regional conditions influenced the level of thermal stratification in pools.

In the following sections, local and regional influences on water temperature are investigated to determine how they influence thermal stratification in the San Joaquin River system. The conceptual model of thermal stratification states that both low mixing conditions and a cold water source are needed for the formation of thermal stratification and thermal refugia (Nielsen et al., 1994). Data gathered during the study is used to evaluate how several local and regional conditions affect either the mixing conditions or provide a cold water source that can produce thermal stratification.

26.4.2 Influence of Surface Water Flow and Pool Geometry on Thermal Stratification

Water temperature and hydraulic head data presented a conflicting picture of the influence of surface water flow, but indicated that surface water flow coupled with pool geometry influenced the formation of thermal stratification in pools. Surface water flow was measured in the San Joaquin River immediately upstream of SJR 204 by the California Department of Water Resources (DWR) at the Stevinson gauge (SJS) near the CA Highway 165 bridge. Between September and October 2012, surface flow ranged from 4.5 cfs to 24 cfs in the San Joaquin River at SJS, then peaked on November 3, 2012 when surface flow increased to 63 cfs. The proportion of flow at SJS that came from the Eastside Bypass or Reach 4B2 could not be calculated because the SJS gauge was downstream of the confluence of the Eastside Bypass with the San Joaquin River and there were no reliable flow gauges between SJS and the upstream study boundaries of the San Joaquin River and the Eastside Bypass. Changes in surface flow consistently

corresponded to changes in water level at the SJS gauge and at the SJR 204 site downstream (Figure 32). It was assumed that changes in water level at pool sites could be used to qualitatively evaluate how variations in surface flow effected thermal stratification when it was not possible to quantitatively determine the surface flow.

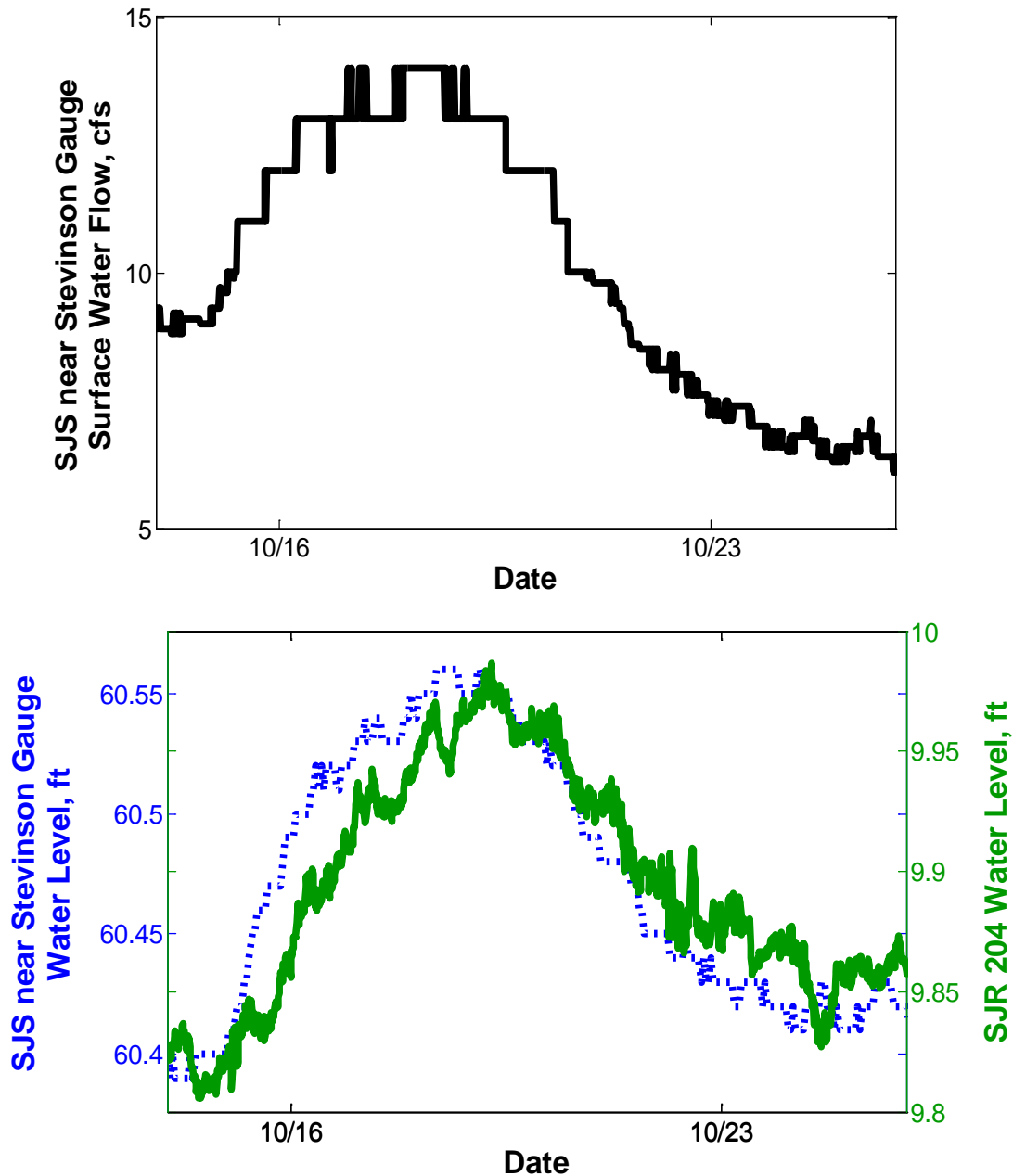


Figure 32: Changes in water level at SJR 204 corresponded to both changes in water level and surface flow at the upstream SJS near Stevinson gauge so it was assumed variations in water level in pool sites qualitatively indicated how surface flow in the pools varied.

Spatial variability in thermal stratification under similar flow during the summer survey at SJR 193 suggested that surface water flow alone did not determine whether pools thermally stratified. Different levels of thermal stratification under similar flow conditions were also measured during the fall instrumentation. While the upstream and downstream pools at SJR 199 had different degrees of thermal stratification (Figure 17), correlations between water level in the two pools indicated similar flow conditions existed (Figure 33).

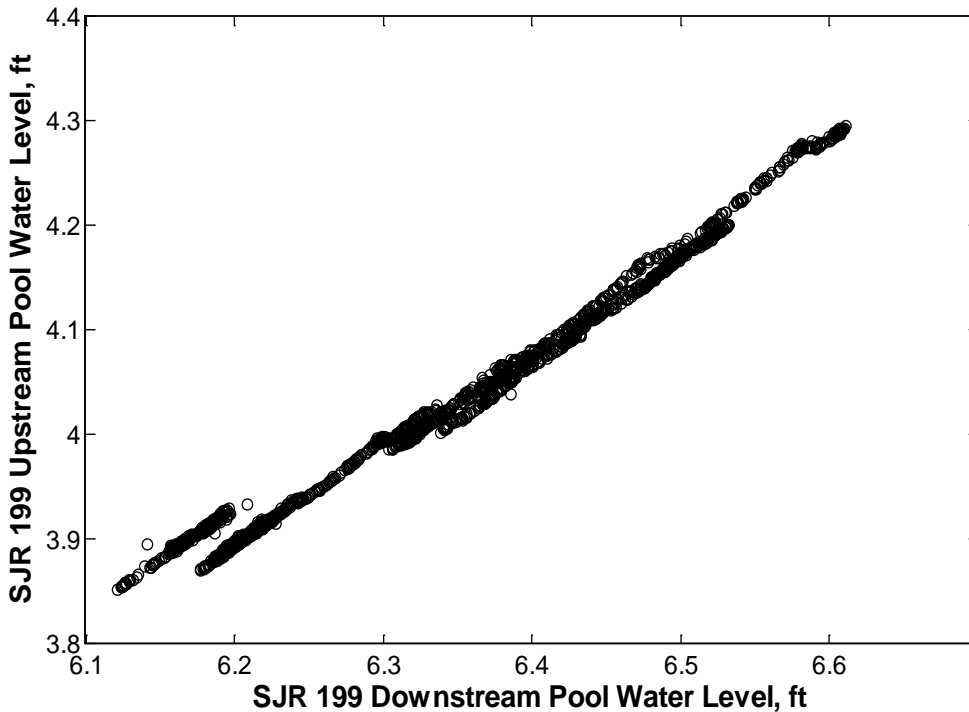


Figure 33: Variations in surface water level in the upstream and downstream SJR 199 pools were strongly correlated indicating flow conditions through the two pools were similar.

Changes in surface water flow did alter thermal stratification at the ESB 33 pool. When surface water flow increased on 11/02 at 6 P.M., the vertical water temperature profile collapsed into one uniform temperature with depth throughout the ESB 33 pool (Figure 34). At ESB 33, surface flow in the Eastside Bypass was observed to be less than 10 cfs during sensor installation on 10/16. Measured water level in the pool remained approximately constant until 11/02 when it increased 1.5 ft in 15 hours. Surface water flow downstream at the SJS gauge increased from approximately 10 cfs to 63 cfs between 11/02 and 11/03 which suggests the magnitude of surface water flow increase in the Eastside Bypass. Daily thermal stratification at ESB 33 ranged from 2°F to 16°F from 10/16 until surface water flow increased on 11/02. Afterwards, daily thermal stratification at ESB 33 became less than 0.1°F and remained that way until sensors were removed on 11/05.

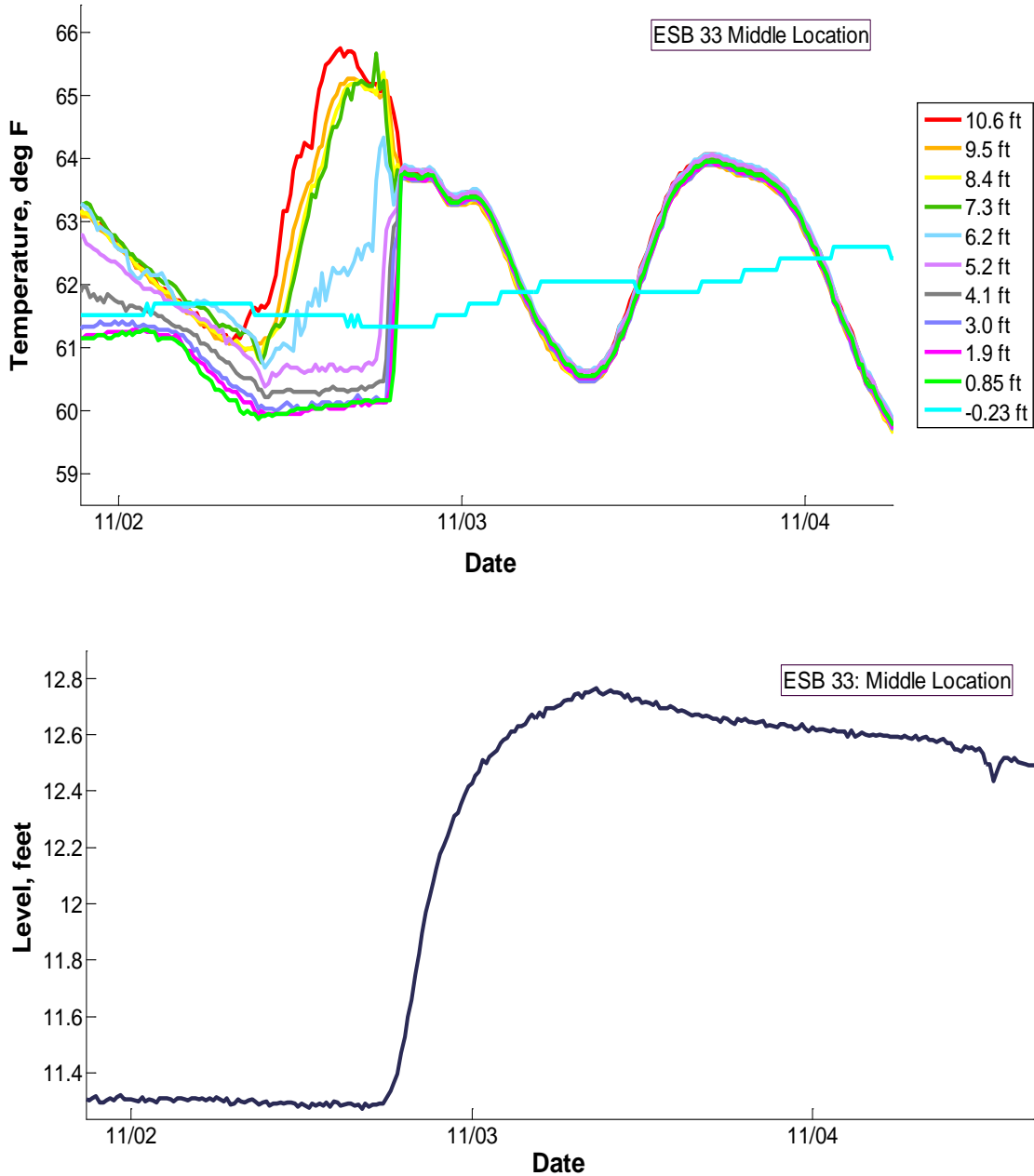


Figure 34: In the ESB 33 pool, the collapse of thermal stratification on 11/02/2012 occurred at the same time the water level increased indicating increased surface flow through the pool eliminated the thermal stratification.

Increases in water level did not always eliminate thermal stratification. Pools at ESB 29 continued to have thermal stratification after water level increased on 10/18 (Figure 35). Water level in the downstream pool at ESB 29 increased 0.98 ft between 10/18 and 10/21, but thermal stratification in the pool remained between 2°F and 11°F. These different relationships between thermal stratification and surface water flow at sites

throughout the study area indicated that surface water flow alone did not correlate with whether pools thermally stratified.

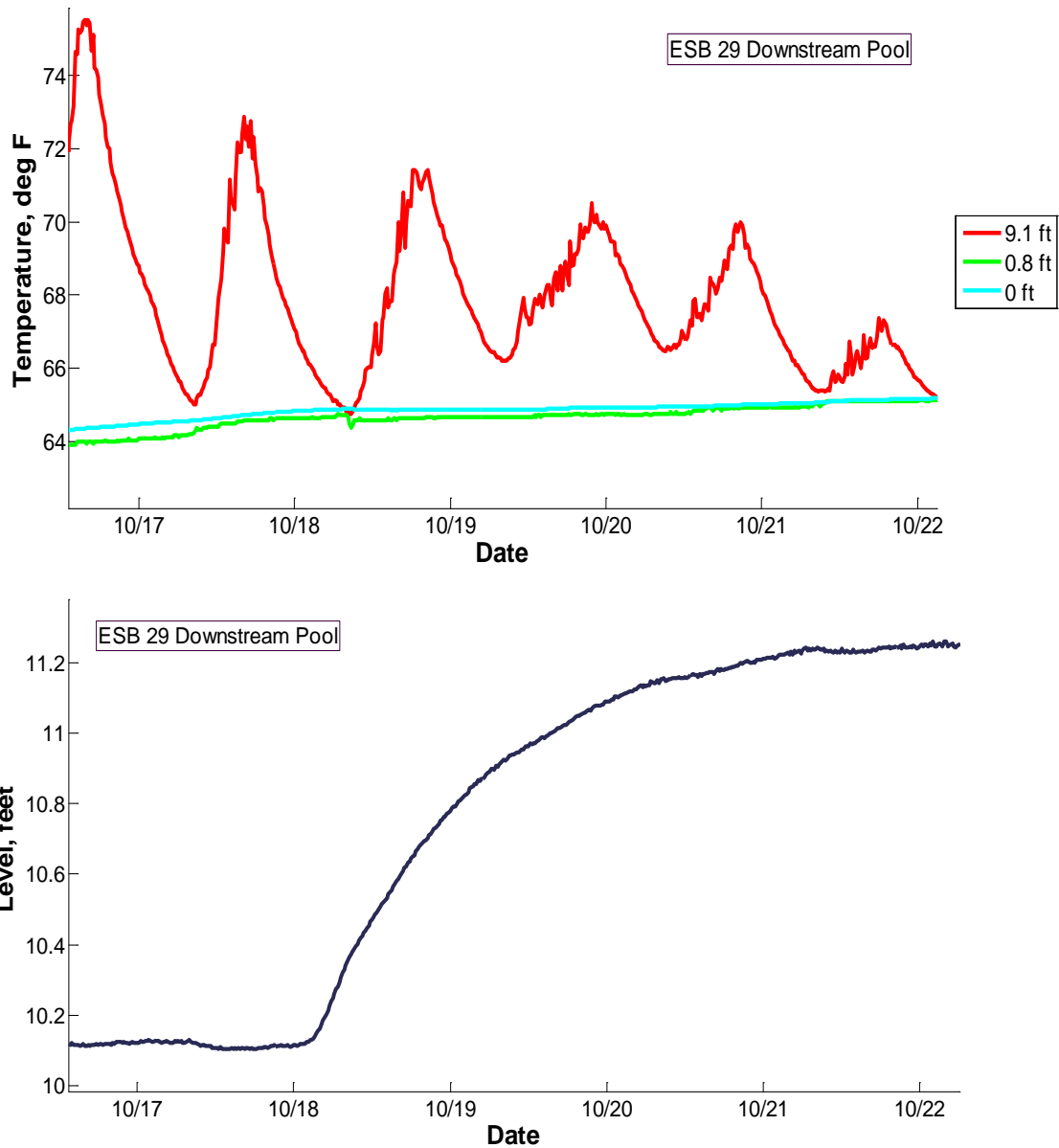


Figure 35: In the downstream pool at ESB 29, increases in water level on 10/18/2012 did not correspond to the collapse of thermal stratification.

It is hypothesized that the formation of thermal stratification in pools is influenced by the surface water velocity distribution that results from surface water flow interacting with pool geometry. Different stratification responses to surface water flow occur because variations in pool geometries create different surface water velocities and mixing conditions. In the thermal stratification conceptual model, low mixing conditions are necessary for the formation of thermal stratification. Rather than surface water flow, water velocity is the key parameter that determines mixing conditions in pools. In

laboratory studies of mixing in a thermally stratified flow, the rate of mixing between water at two different temperatures was proportional to water velocity (Gartrell, 1979). Increases in water velocity increased mixing and reduced thermal stratification. In laboratory studies of flow conditions that form pools, the pool length, width, depth, and entrance and exit slopes all contributed to flow convergence in a pool that altered the velocity profile through the pool (Thompson et al., 1998; Thompson and McCarrick, 2010; MacVicar and Rennie, 2012). Pool geometries resulted in variable water velocity distributions that altered mixing conditions both laterally and longitudinally throughout a pool (Sawyer et al., 2010). In a model of a Yuba River pool-riffle sequence, as surface flow increased, the water velocity distribution in pools changed as pool geometry interacted with the flow (Sawyer et al., 2010). Different pool geometries create different mixing conditions by altering the water velocity distribution.

Variations in thermal stratification in San Joaquin River system pools can be explained by the hypothesis that the water velocity distribution was more important to mixing conditions in pools than surface flow. At SJR 193, the thermally stratified SJR 193.24 and SJR 193.29 had larger volumes and were longer than the unstratified SJR 193.27 pool. Even though SJR 193.27 was deeper, mixing in the pool was greater because the incoming water velocity through the riffle had a greater influence on the shorter, smaller volume pool. At SJR 199, the upstream unstratified pool had a smaller volume and a shorter pool length than the downstream stratified pool. While both pools experienced the same surface water flow, the flow constriction combined with the shorter length of the upstream SJR 199 pool resulted in higher mixing and prevented the formation of thermal stratification in the upstream SJR 199 pool. Two possible explanations exist for why ESB 29 remained stratified when flow increased yet higher flow eliminated thermal stratification in ESB 33. First, the flow increase on 11/02 at ESB 33 was potentially greater than the flow increase on 10/18 at ESB 29 since the water level at ESB 33 increased 0.5 ft more than the water level at ESB 29. The increased water level and flow at the SJS gauge corresponding to the surface flow increase on 11/02 also suggested the 11/02 surface water flow increase was greater than the 10/18 flow increase. Second, pool width at ESB 33 increased less with length than pool width at ESB 29 so ESB 33 had a greater increase in surface water velocity with increased flow. Reinfeld and Williams (2011) found increases in surface water flow in the Shoalhaven River, New South Wales, Australia caused the depth of mixing in pools to increase. Pool thermal stratification collapsed when flow releases from the Tallowa Dam increased from 53 cfs to greater than 400 cfs (Reinfeld and Williams, 2011). In the San Joaquin River system, it is expected higher surface flows will cause complete mixing in many pools since surface flow increases from approximately 10 cfs to 63 cfs caused complete vertical mixing in ESB 33. Under restoration goal surface flows, thermal stratification in San Joaquin River system pools would be altered as the interaction of pool geometry with increased surface water flow would change the water velocity distribution and pool mixing conditions. Further measurements would be needed to confirm how the water velocity in pools responds to changes in surface water flow in the San Joaquin River.

26.4.3 Influence of Subsurface-Surface Water Interactions on Thermal Stratification in Pools

Subsurface exchange with surface water in pools did not promote thermal stratification or thermal refugia in San Joaquin River system pools during fall 2012 conditions. In the pools instrumented, either subsurface water temperature was greater than surface water temperature or hydraulic head indicated that the stream was losing in the pool. In many river systems subsurface flow either from hyporheic or groundwater sources provides a cold water source (Nielsen et al., 1994; Matthews and Berg, 1997; Johnson, 2004; Tompkins, 2005; Arrigoni et al., 2008; Burkholder et al., 2008; Acuna and Tockner, 2009). An upwelling source of cold water would promote the formation of stable thermal stratification and thermal refugia in pools (Nielsen et al., 1994). In the San Joaquin River system, subsurface water temperature was greater than surface water temperature and increased with depth below the streambed at SJR 193, SJR 204, ESB 22, and ESB 33 (Figure 36). While subsurface water temperature increased with depth, the range of subsurface water temperature below pools was consistent with regional groundwater temperature (Figure 19). Hydraulic head indicated SJR 204 and ESB 22 had subsurface flow upwell into pools. Upwelling subsurface flow that is warmer than surface water temperatures would create convective mixing in pools that would break down and reduce thermal stratification. Subsurface water temperature increased with depth at SJR 193 and ESB 33, but hydraulic head indicated surface water downwelled into the subsurface at these pools. Under downwelling conditions, warmer subsurface water temperature would not influence thermal stratification

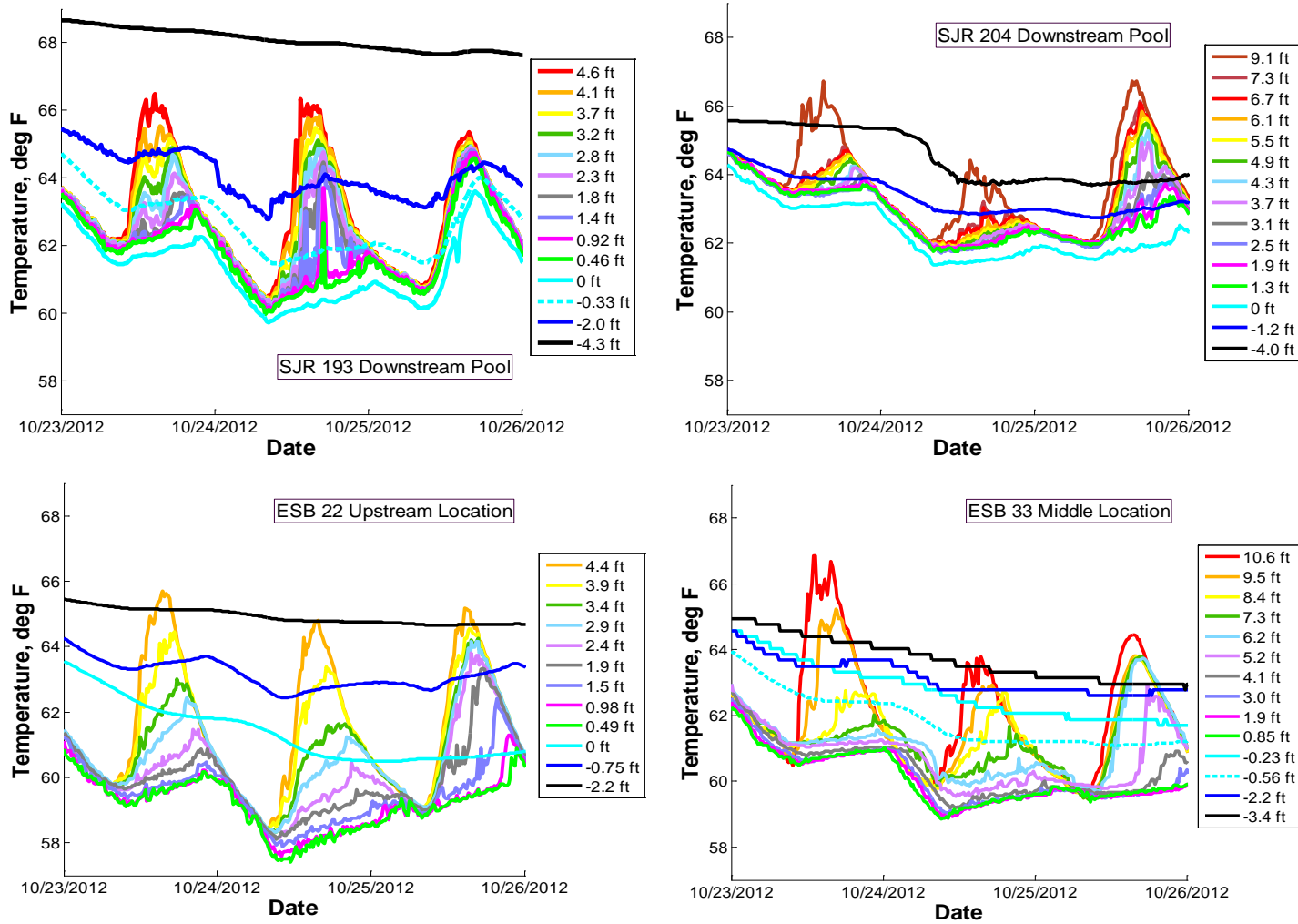


Figure 36: Subsurface water temperature increased with depth below the streambed and was greater than surface water temperatures during much of each day at four of the sites instrumented during fall 2012.

Subsurface water temperature decreased with depth at SJR 199 and ESB 29, but surface water temperature did not indicate subsurface-surface water exchange influenced thermal stratification at these sites. Additionally, hydraulic head indicated downwelling conditions in the pools prevented subsurface flow from upwelling cold water that would influence thermal stratification (Figure 37).

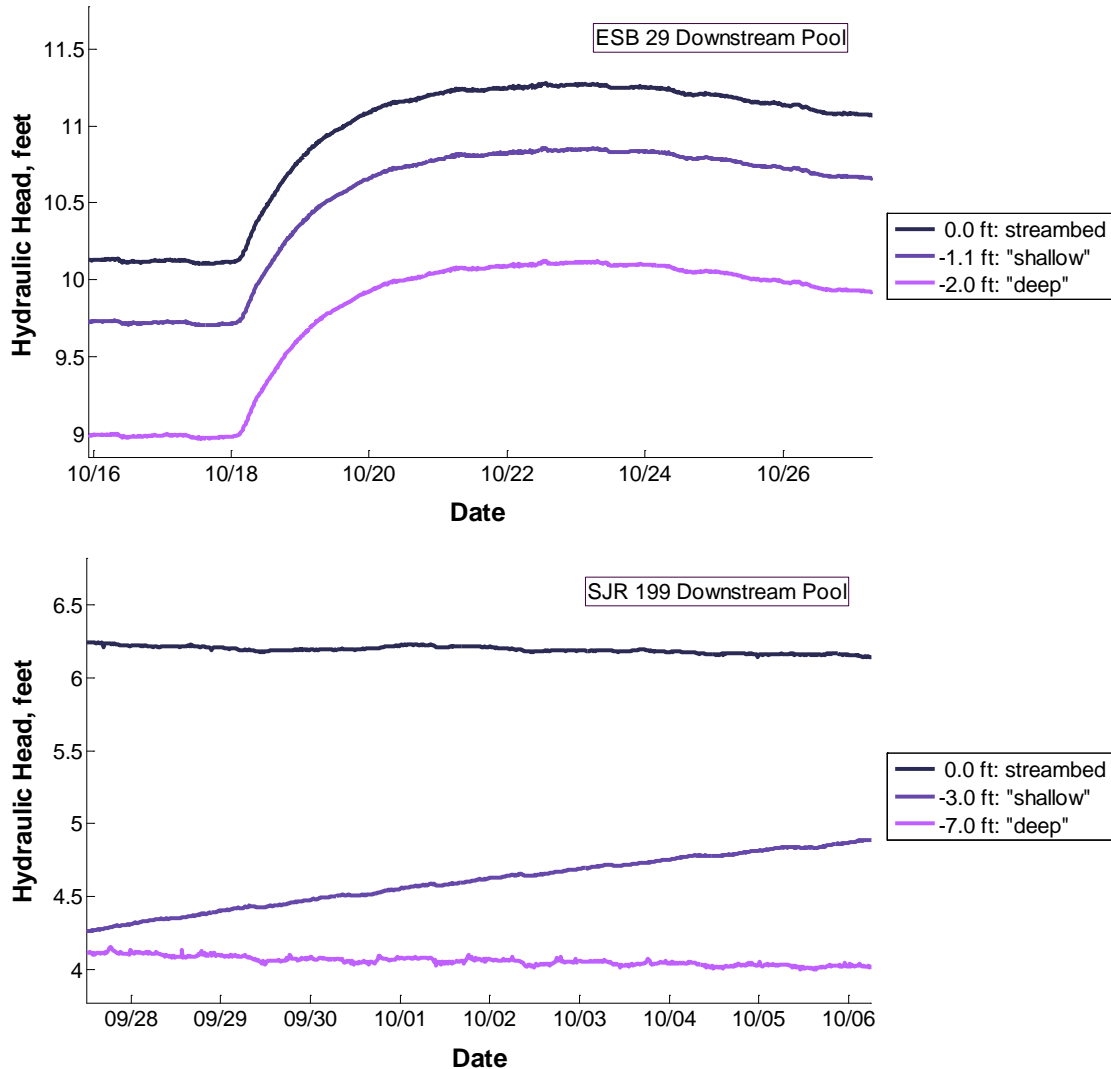


Figure 37: At both ESB 29 and SJR 199, hydraulic head decreased with depth below the streambed indicating that surface water was flowing downward into the subsurface. Note: Hydraulic head at SJR 199 -3.0 ft did not reach equilibrium during the 23 day instrumentation. The rate of change of hydraulic head at -3.0 ft decreased toward the end of the instrumentation indicating hydraulic head trends with depth would remain consistent once -3.0 ft did reach equilibrium.

While subsurface-surface water interactions did not promote thermal stratification during the fall instrumentation, it was hypothesized that seasonal variations in groundwater temperature would produce subsurface conditions that promote thermal stratification at other times of the year. Subsurface water temperature conditions below pools are a

product of heat exchange between surface water and groundwater below a stream (Constantz, 2008). In the San Joaquin River system, the subsurface water temperature trends occurred as surface water mixed with groundwater in the subsurface below pools. While heat exchange with surface water produced the diurnal variations in subsurface water temperature (Figure 19), heat exchange with groundwater temperature resulted in subsurface water temperature increasing with depth. Subsurface water temperature increased with depth below four of the pools instrumented because groundwater temperatures were generally warmer than average pool bottom surface water temperatures from October to November 2012 in Reach 4 (Figure 38). Regional groundwater temperature from monitoring wells located in Reach 4 varied seasonally between 2011 and 2013 and peaked between 1 – 4 months later than air temperature. In MW-140, seasonal groundwater temperature trends lagged behind seasonal air temperature trends with maximum groundwater temperature occurring in late November four months after maximum air temperatures peaked in July (Figure 39). A similar seasonal lag likely occurred in the groundwater influencing subsurface water temperature below pools. This seasonal variability suggests that subsurface water temperature would be less than surface water temperature during portions of the years, especially spring and early summer. Under these conditions, upwelling subsurface flow could promote the formation of thermal stratification and thermal refugia as surface water temperatures began to exceed salmon thermal tolerances. Further measurements would be required to confirm this.

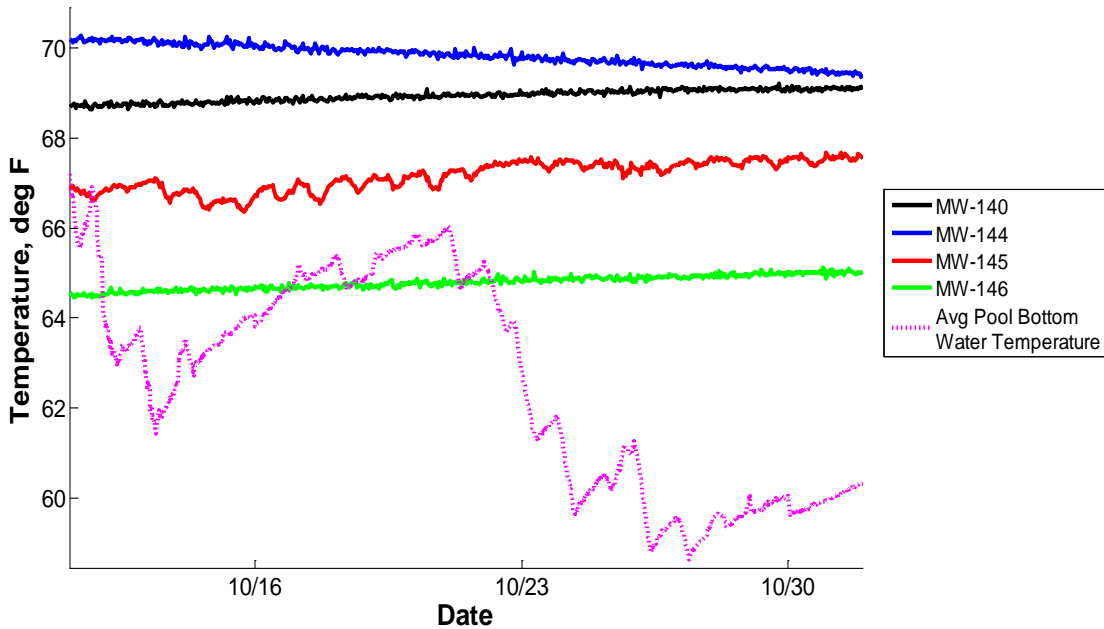


Figure 38: Regional groundwater temperature in four monitoring wells was greater than the average pool bottom surface water temperature. During October 2012, groundwater entering into pools would not have provided a cold water source to promote the formation of thermal stratification or thermal refugia.

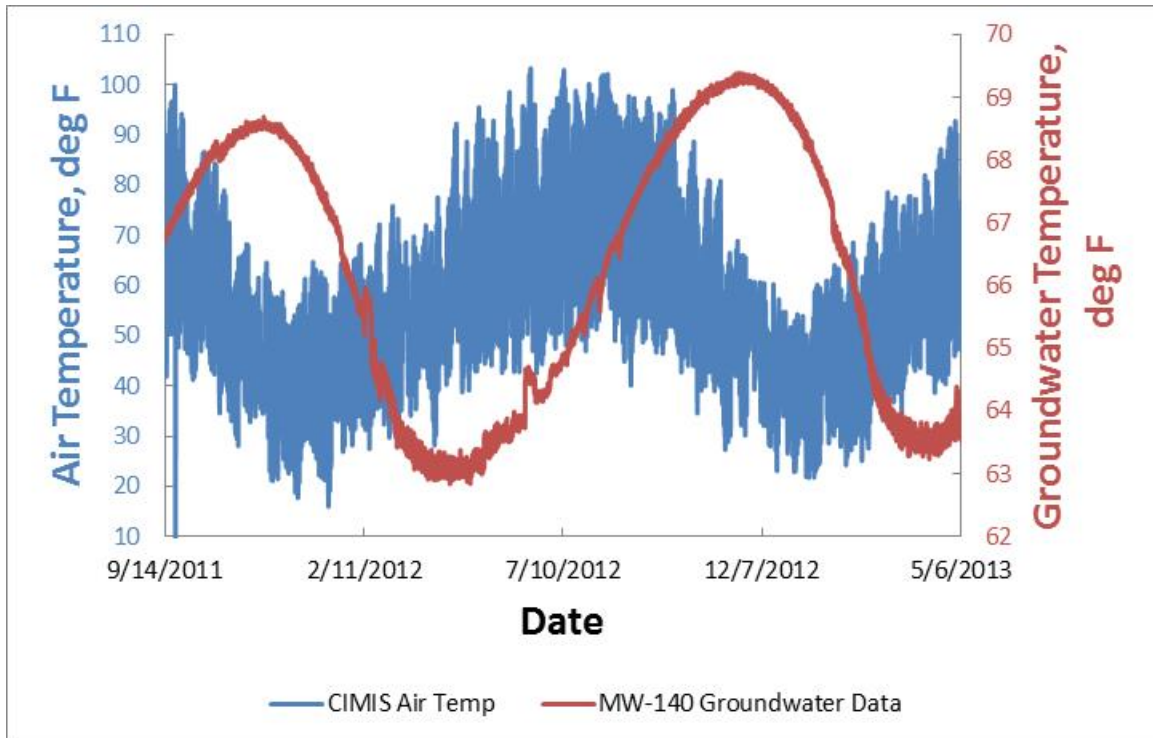


Figure 39: At MW-140, seasonal groundwater temperature trends lagged 4 months behind seasonal air temperature trends.

26.4.4 Air Temperature Correlations with Pool Water Temperature

Correlations between daily variations in thermal stratification and daily variations in air temperature indicated air temperature could be used to estimate maximum daily thermal stratification in pools. Various combinations of available regional meteorological parameters were tested against maximum daily thermal stratification. Air temperature, wind speed, wind direction, soil temperature, and solar radiation were all collected hourly by regional California Irrigation Management Information System (CIMIS) weather stations. CIMIS station regional air temperature and solar radiation data could be used to approximate local conditions at individual pools for air temperature and solar radiation. Air temperature and solar radiation data from the Los Banos, Kesterson, and Merced CIMIS stations were consistent over the entire region. CIMIS station wind speed, wind direction, and soil temperature data all showed variability and were not consistent between stations so these regional parameters could not be used to represent local pool conditions. Los Banos CIMIS station air temperature and solar radiation data was used for calculations because it was the nearest station with the most complete dataset.

While most meteorological parameters showed no correlation, the daily maximum change in air temperature (dT_{air}) correlated with the daily maximum thermal stratification (dT_{water}). Previous studies on the Modoc Plateau in northeastern California and south-central Oregon found similar results with thermal stratification in pool associated with air temperature (Tate et al., 2007). In the San Joaquin River system, the strength of the correlation between dT_{air} and dT_{water} varied between pools. At SJR 193, dT_{air} and dT_{water} showed a linear correlation with minimal scatter (Figure 40).

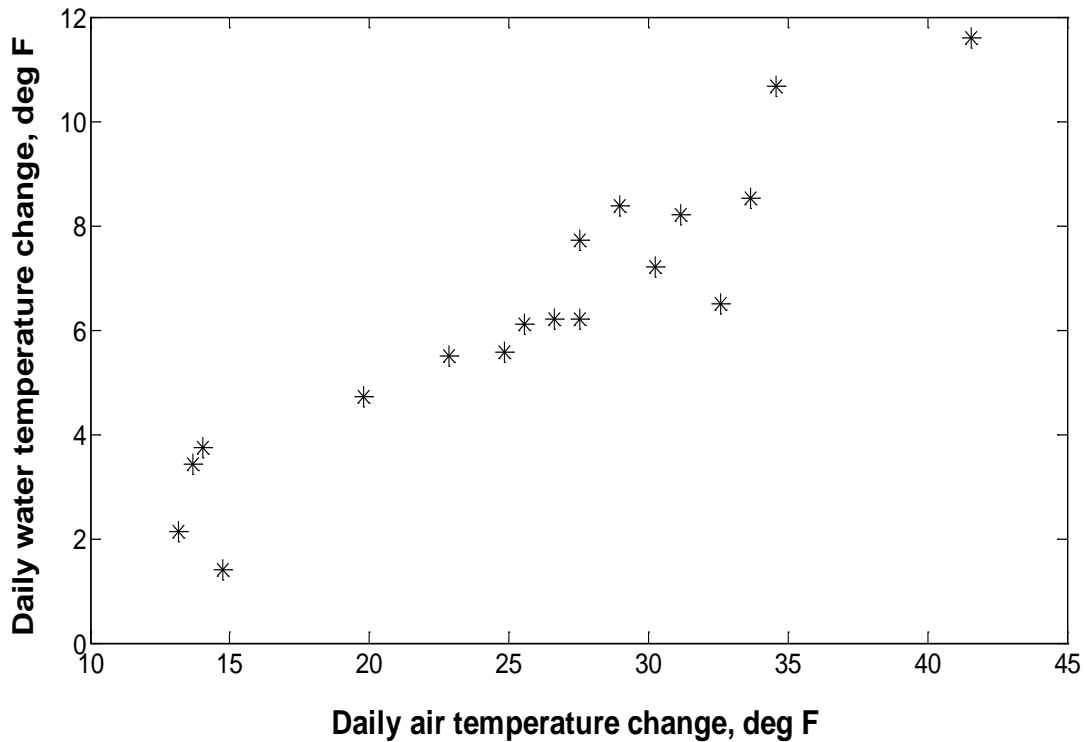


Figure 40: At SJR 193, daily maximum thermal stratification increased with increases in daily change in air temperature.

Other pool sites showed more variation in their correlations between regional dT_{air} and dT_{water} . At SJR 204, daily changes in air temperature were correlated with daily changes in thermal stratification, but more scatter in the relationship caused data points to occur further from the linear relationship seen at SJR 193 (Figure 41). At SJR 204, three days showed thermal stratification responding less to increases in daily air temperature variations, while two other days had thermal stratification increase more than normal with increases in daily air temperature. The cause of the scatter in the dT_{air} and dT_{water} relationship was not determined. One hypothesis for the scatter was that regional air temperature recorded by CIMIS stations did not approximate air temperature at the sites. Another hypothesis was that variations in local pool conditions influenced heat exchange on those days resulting different responses to variations in air temperature. Further data would be needed to test these hypotheses.

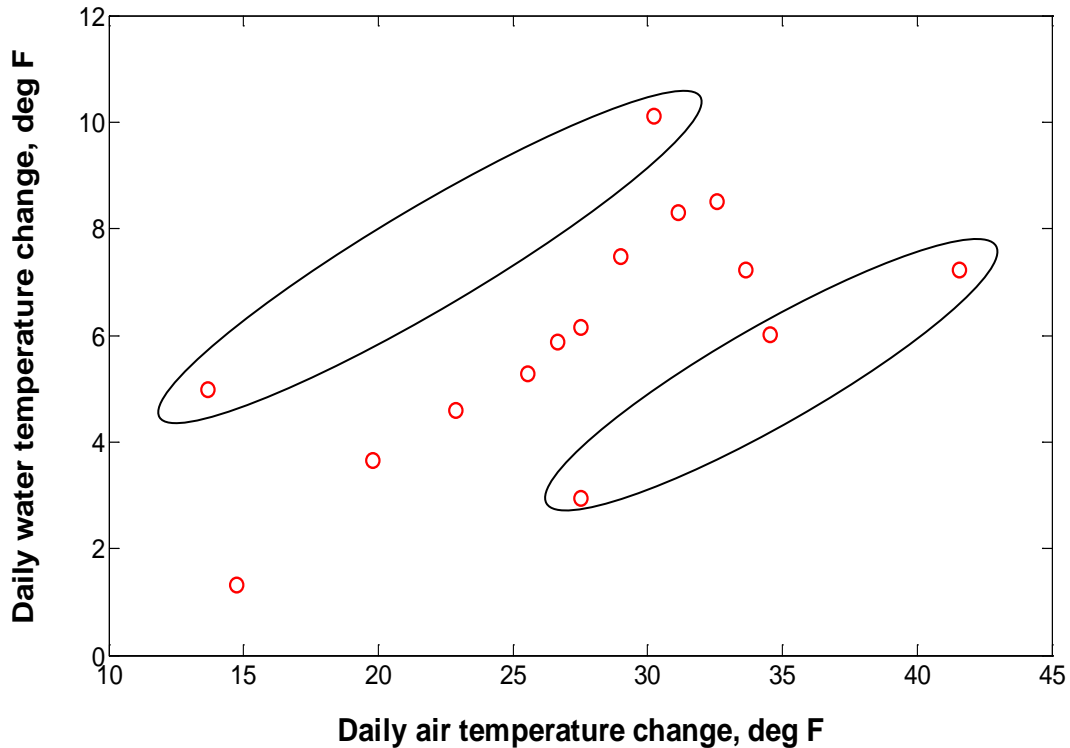


Figure 41: At SJR 204, increased scatter in the relationship between daily changes in air temperature and daily changes in maximum thermal stratification suggested local variations in pool or meteorological conditions effected the correlation between air and water temperature.

Thermal stratification increased at two different rates with increases in regional daily air temperature variations. Thermal stratification increased more with changes in air temperature at SJR 193, SJR 204, ESB 22, and ESB 33 than at the SJR 199 and ESB 29 sites (Figure 42). Thermal stratification increased less with increases in air temperature at SJR 199 and ESB 29. While analysis did not identify parameters that correlated with the different rates of thermal stratification, subsurface water temperature trends below the two sets of pools were different. Subsurface water temperature decreased with depth below the streambed at both pools where thermal stratification increased at a lower rate with increases in air temperature. Hydraulic head at each site indicated that subsurface flow did not upwell into either pool, but spatial variations in subsurface-surface water exchange may have existed. Differences in cross-channel subsurface sediment hydraulic conductivity have created spatial variations in subsurface-surface water exchange in streams (Essaid et al, 2006; Essaid et al., 2008; Hatch et al., 2010). Further data would be needed to determine if spatial variations in subsurface-surface water exchange existed and differing trends in subsurface water temperature were responsible for the different rates of pool thermal stratification.

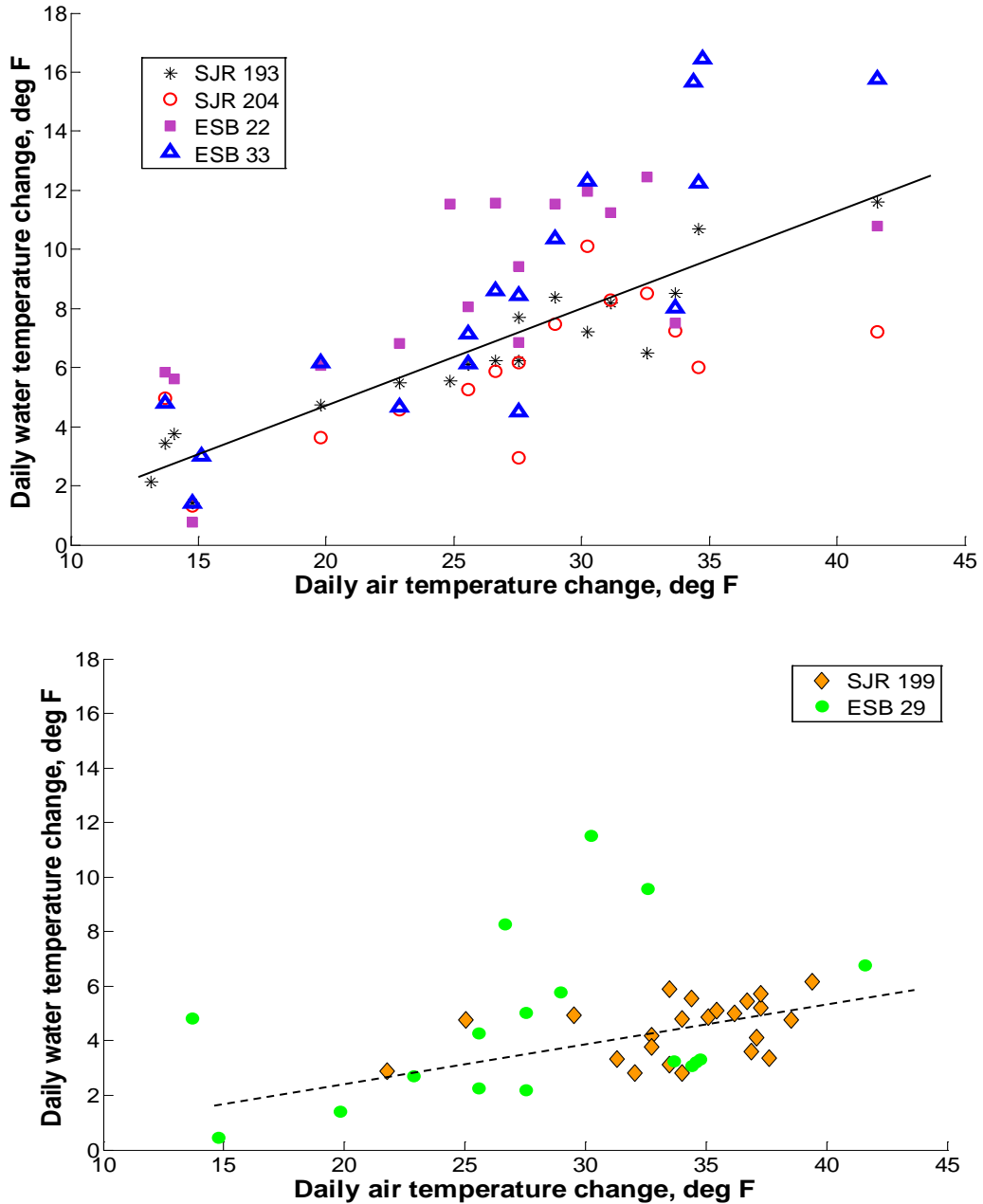


Figure 42: Instrumented pools showed two different rates of increases in thermal stratification with increases in daily air temperature variations. The two pools with a lower rate of increase in thermal stratification both had subsurface water temperature decreasing with depth.

In addition to correlations between dT_{air} and dT_{water} , the 4-day moving average daily air temperature correlated with total daily pool heat indicating air temperature was a regional influence on pool water temperature and thermal stratification (Figure 43). Total daily pool heat was calculated from water temperature measurements and pool volume estimates from the San Joaquin River digital terrain model. Daily average air temperature for a given day was averaged with the air temperature for the preceding three

days to reduce daily air temperature variability. Four days was determined to be the optimum number of days to average over to preserve weekly air temperature trends while minimizing the influence of individual daily variations. Variations in the 4-day moving average air temperature were reflected in the total pool heat. At ESB 33, as the 4-day moving average air temperature decreased, total pool heat also decreased (Figure 44).

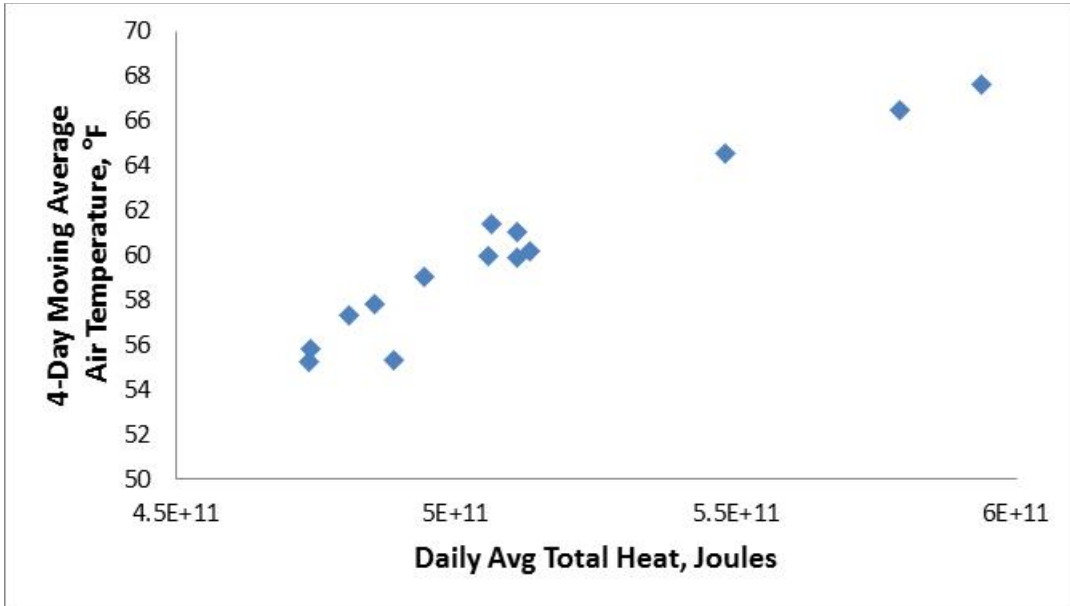


Figure 43: Daily average total pool heat calculated from water temperature measurements correlated with the 4-day moving average air temperature at ESB 33.

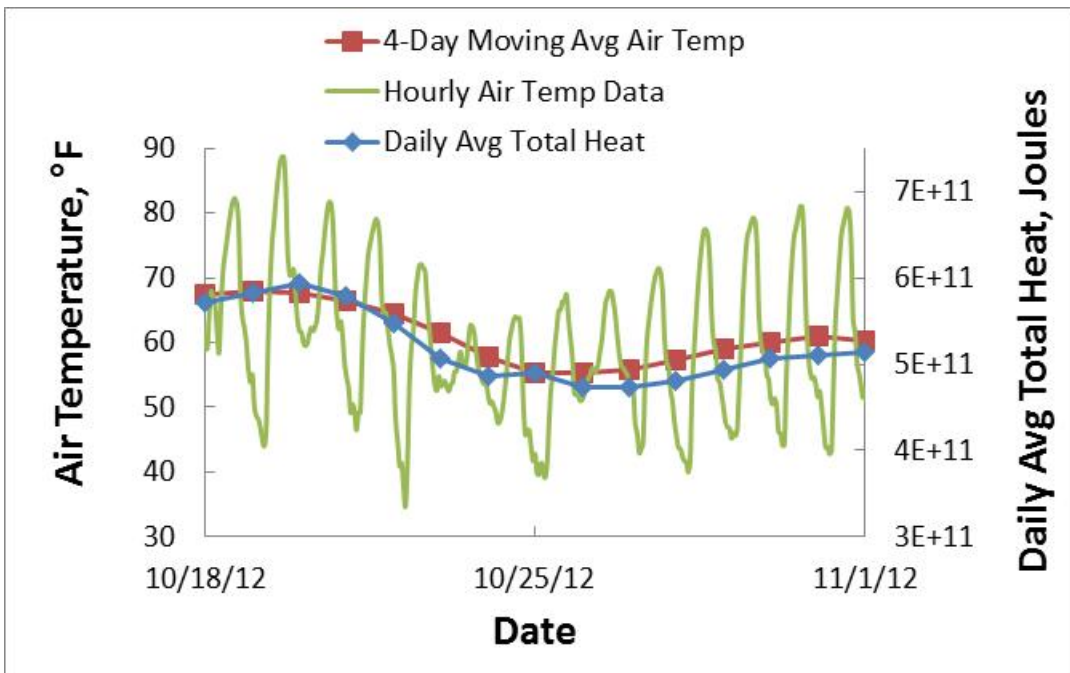


Figure 44: Trends in the daily total pool heat agreed with trends in the 4-day moving average daily air temperature at ESB 33.

Air temperature was a key influence on thermal stratification and pool heating because nightly cooling reset daily thermal stratification. Water temperature data indicated that pools in the fall began warming around 8 – 10 A.M., heated until around 3 – 5 P.M., then cooled each night until the cycle started the next day. Under equilibrium heat exchange conditions, air temperature can estimate reach scale, depth averaged stream water temperature on a weekly timescale (Mohseni and Stefan, 1999; Bogran et al., 2003; O’Driscoll and DeWalle, 2006). Heat from incoming short wave solar radiation is the primary driver of daily increases in stream temperature (Sinokrot and Stefan, 1994; Wagner et al., 2010; Herbert et al, 2011). In the San Joaquin River system, daily heating and thermal stratification at pools was dominated by heat from incoming short wave solar radiation. Heat from incoming solar radiation caused differential heating of the water column that increased surface water temperatures at the top of the pool producing daily thermal stratification. Solar radiation alone did not correlate with daily thermal stratification because it did not capture all heat exchange processes effecting pool water temperature, especially nightly cooling. Heat fluxes through the air-water interface produced convective mixing in pools when air temperature was less than water temperature. Numerical simulations and experimental results of daily convection in reservoirs highlight how cooling at the air-water interface induced convective mixing and cooler, denser water plunged down until it reached water of a similar density (Bednarz et al., 2009). When air temperature became cooler than water at the top of pool, convective mixing in pools broke down the thermal stratification that formed during the day. Convective mixing continued to cool pool water temperatures until air temperature exceeded water temperature at the air-water interface the next morning.

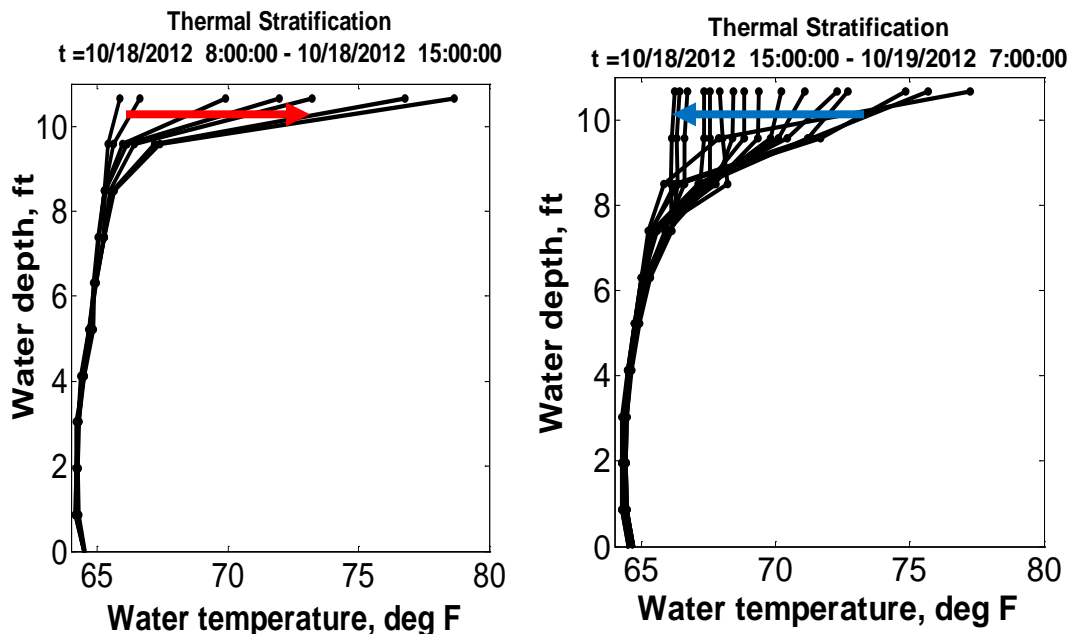


Figure 45: Daily heating and nightly cooling cycles at ESB 33. Daily heating was greater than nightly cooling for this 24 hour period so the pool began the next day thermally stratified.

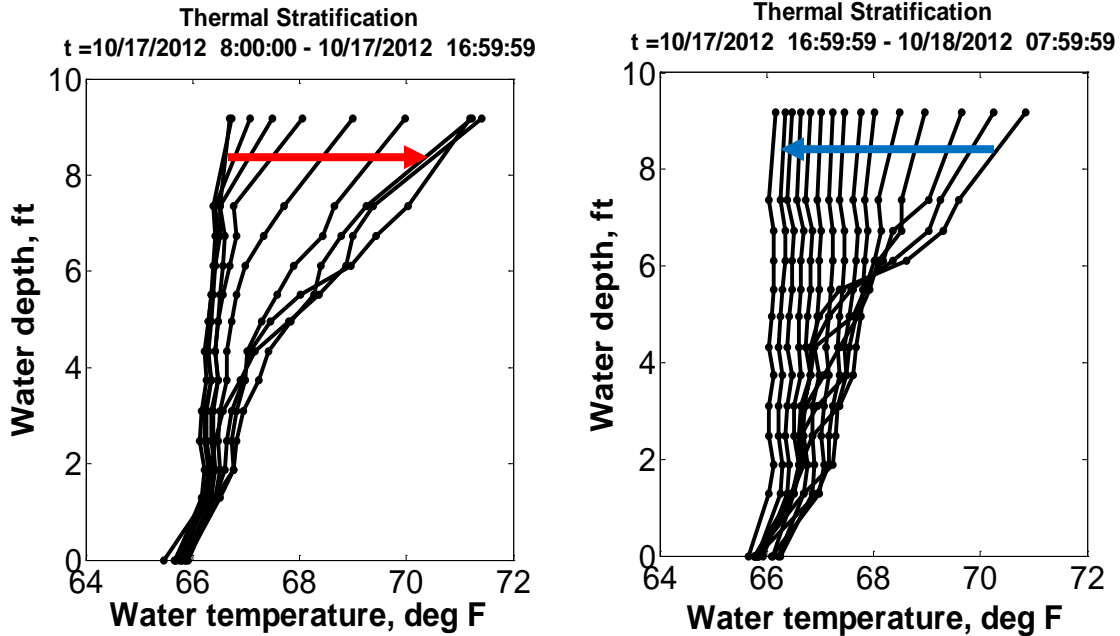


Figure 46: Daily heating and nightly cooling cycles in SJR 204. Daily heating was less than nightly cooling for this 24 hour period so the pool completely mixed and bottom water temperatures decreased.

Air temperature influenced how much pool water temperature decreased each night by causing convective mixing. When nightly cooling was less than daily heating, the pool would remain thermally stratified every day (Figure 45). When nightly cooling was greater than daily heating, convective mixing completely mixed the pool, bottom water temperature decreased, and the pool water temperature was uniform with depth at the beginning of a day (Figure 46). Nightly air temperatures at the air-water surface “reset” the thermal stratification gradient each day. On days when nightly cooling was greater than daily heating, the influence of air temperature on pool convective mixing provided a “cold water source” that lowered minimum pool water temperatures in the San Joaquin River pools during the fall.

26.4.5 Thermal Refugia in the Eastside Bypass, Reach 4B2, and Reach 5

Availability of thermal refugia suitable to migrating adult Chinook was seasonally variable in the San Joaquin River system with thermal refugia becoming more abundant as the 4-day moving average air temperature decreased. Thermal refuge was defined as water temperature below Chinook salmon temperature thresholds. While numerous temperature thresholds for Chinook exist depending on life-stage, run, food availability, and other factors, the three thresholds focused on for evaluation of thermal refuge were 59°F, 65°F, and 68°F. These three thresholds corresponded to optimal, critical, and lethal water temperature objectives for adult migrating Central Valley Chinook salmon (Moyle et al., 1995; Ward et al., 2006; Rich, 2007; SJRRP FMWG, 2010). During the summer survey in July 2012, thermal stratification was abundant in San Joaquin River system pools during the summer but thermal refugia was sparse with only 3% of surveyed pools having water temperature between 65°F and 68°F. Most pools had water temperature

above 68°F. No pools surveyed had water temperature below the critical water temperature threshold of 65°F.

During fall 2012, thermal refugia formed daily in five of the six pool sites instrumented. To compare pools with different volumes, the percentage of pool volume below Chinook temperature thresholds was calculated from the water temperature and water level data. Decreases in the percentage of pool volume below a temperature threshold indicated decreases in thermal refugia. A typical daily cycle of changes in the percentage of pool volume below Chinook temperature thresholds is shown in Figure 47. Volume below a temperature threshold decreased during the day as pool surface water temperatures peaked, then volume increased as nightly cooling reduced surface water temperature.

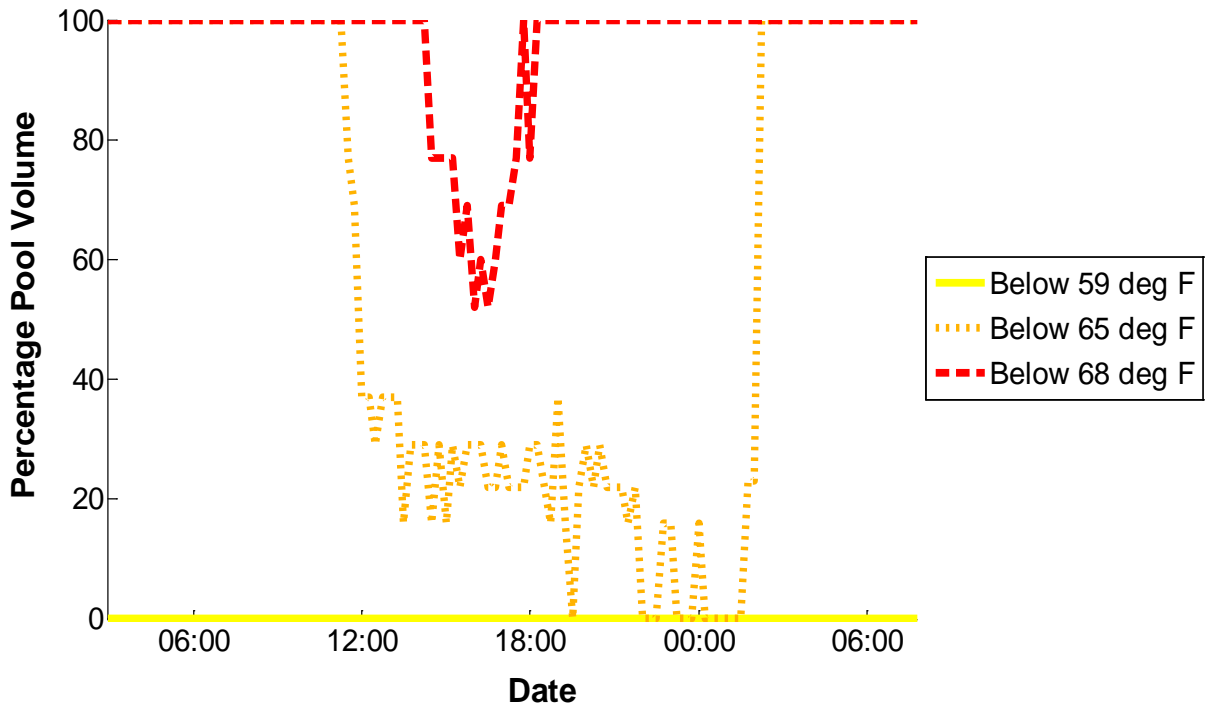


Figure 47: The volume of thermal refugia in pools varied daily with variations in surface water temperature. On 10/13 – 10/14, the percentage of the pool volume below Chinook temperature thresholds decreased as surface water temperature increased in SJR 193.

The availability of thermal refugia below 68°F was similar in the Eastside Bypass, Reach 4B2, and Reach 5, but the availability of thermal refugia below 65°F and 59°F was greater in Eastside Bypass pools. While daily pool volume with thermal refugia below 68°F ranged from 34 - 100% each day, the average daily pool volume with thermal refugia below 68°F was approximately 84% for pools all three reaches. The average daily pool volume with thermal refugia below 65°F was 66% in the Eastside Bypass, but it was 36% for Reach 4B2 and Reach 5. While the pool volume below 65°F was greater in the Eastside Bypass, the range in pool volume below 65°F was similar in both Eastside Bypass and San Joaquin River pools. In these, the percentage of Eastside Bypass pool volume below 65°F ranged from 5 - 100%, while San Joaquin River pool volume ranged

from 0 – 97%. Daily average pool volume with thermal refugia below 59°F was 6.8% in the Eastside Bypass, but it was 0% for Reach 4B2 and Reach 5. Pools in the San Joaquin River did not have thermal refugia below 59°F, so it was not possible to compare the range of pool volumes in the Eastside Bypass and the San Joaquin River. While the amount of thermal refugia varied between Eastside Bypass and San Joaquin River pools, daily variations in thermal refugia were similar in all pools (Figure 48). Decreases in thermal refugia on 10/16 occurred in all pools suggesting regional conditions dominated the fluctuations in thermal refugia. No trend between total pool volume and daily variations in the percentage of pool volume below a temperature threshold was measured.

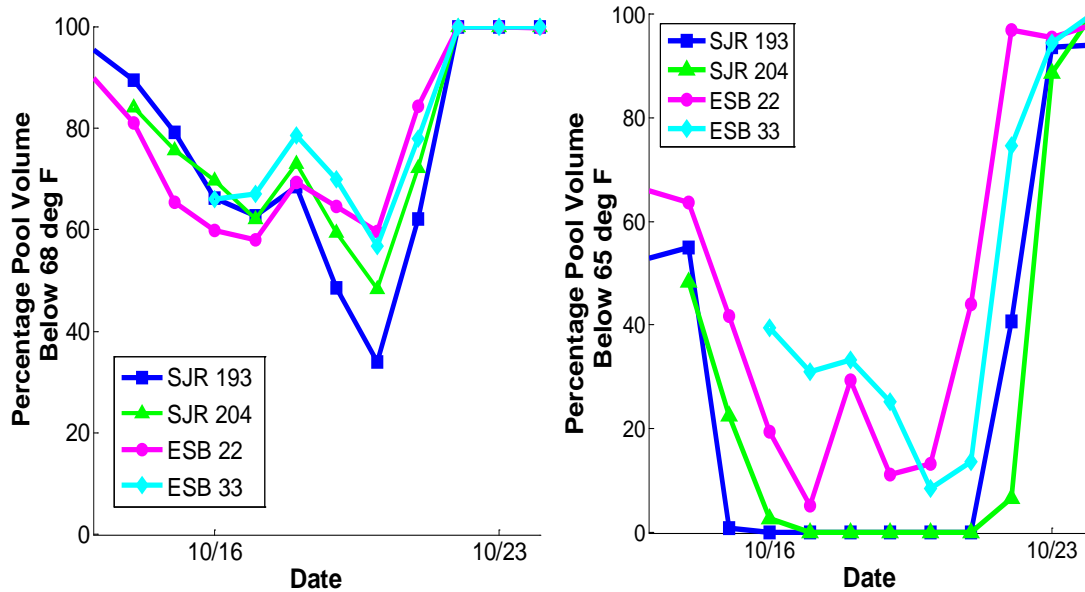


Figure 48: Daily variations in the percentage of pool volume below Chinook temperature thresholds were similar for all pools. Pools in all reaches had similar percentages of pool volume below 68°F, but Eastside Bypass pools had more thermal refugia below 65°F than San Joaquin River pools.

Variations in the availability of thermal refugia at different temperature thresholds corresponded to variations in the 4-day moving average air temperature. As previously discussed, thermal stratification and daily changes in air temperature are linked because air and water temperature are both driven by connected heat exchange processes (Mohseni and Stefan, 1999). In the San Joaquin River system, the availability of thermal refugia in San Joaquin River system pools decreased with increases in the 4-day moving average air temperature (Figure 49). As the 4-day moving average air temperature exceeded approximately 60°F, the percentage of pool volume below 68°F decreased. The volume of thermal refugia below 65°F and 59°F temperature thresholds decreased similarly with increases in the 4-day moving average air temperature. Lowering the Chinook temperature threshold lowered the 4-day moving average air temperature at which pool volume began to decrease. The percentage of pool volume below 65°F began to decrease when the 4-day average air temperature exceeded approximately 56°F (Figure 50).

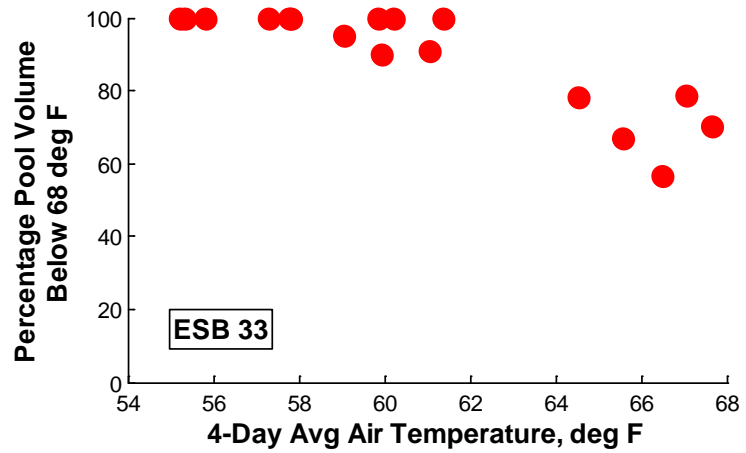
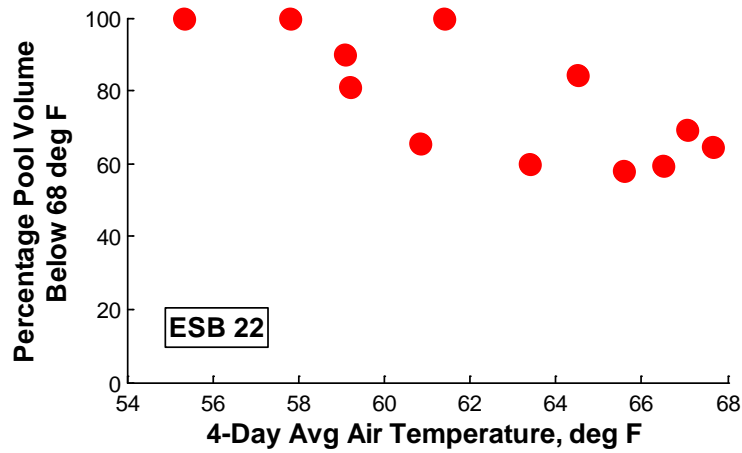
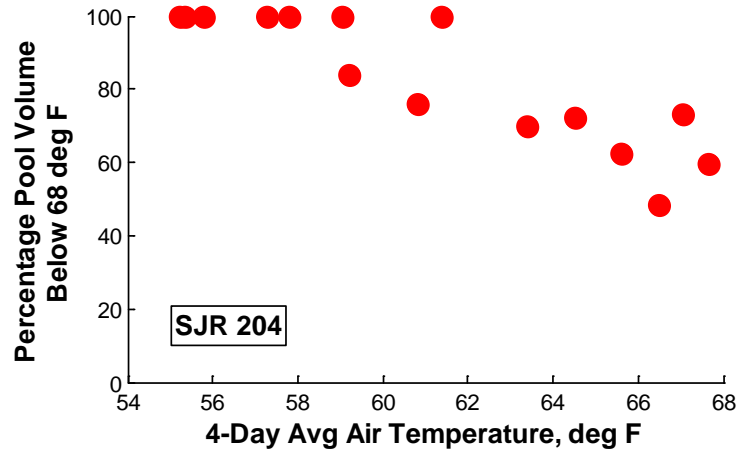
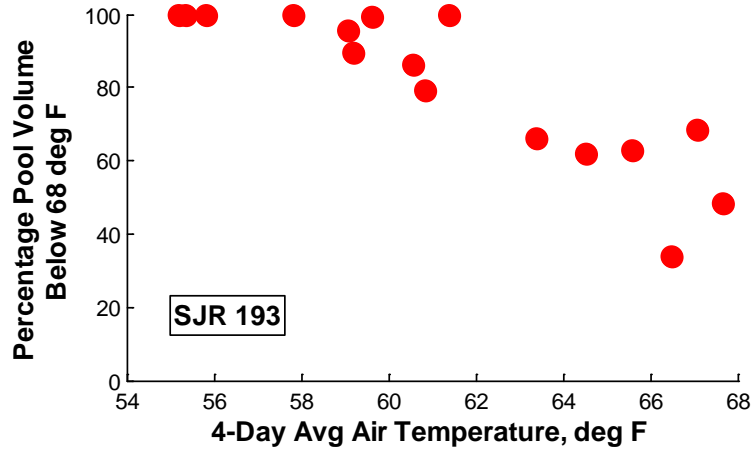


Figure 49: The percentage of pool volume with thermal refugia below 68°F decreased in San Joaquin River system pools when the 4-day moving average air temperature exceeded 60°F.

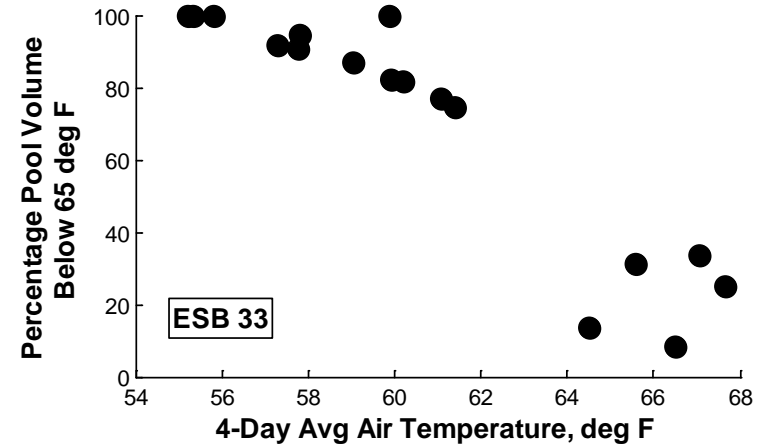
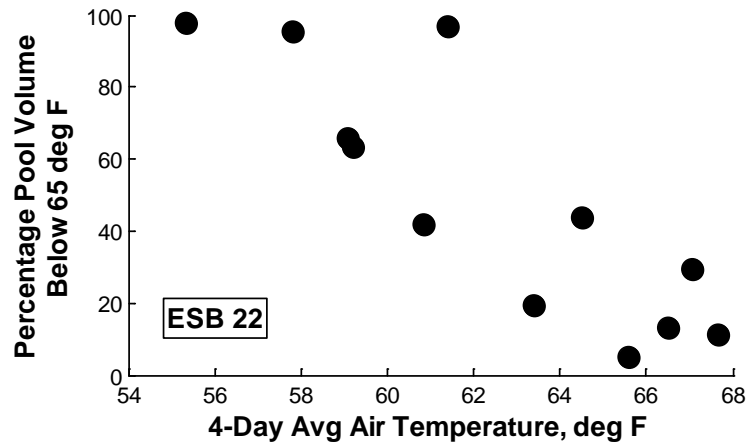
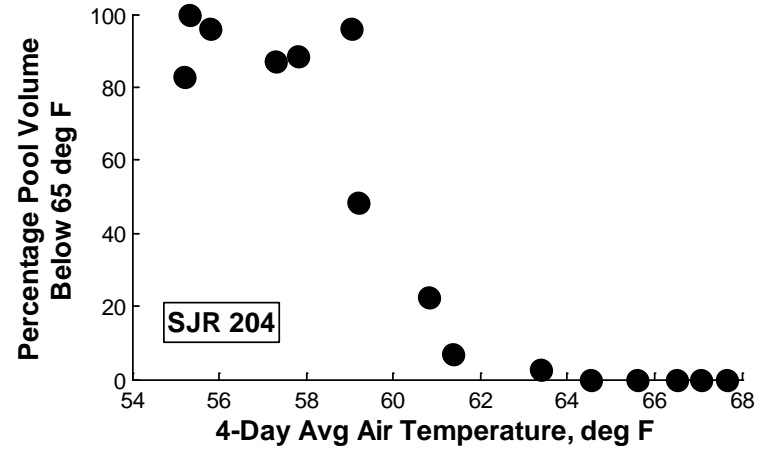
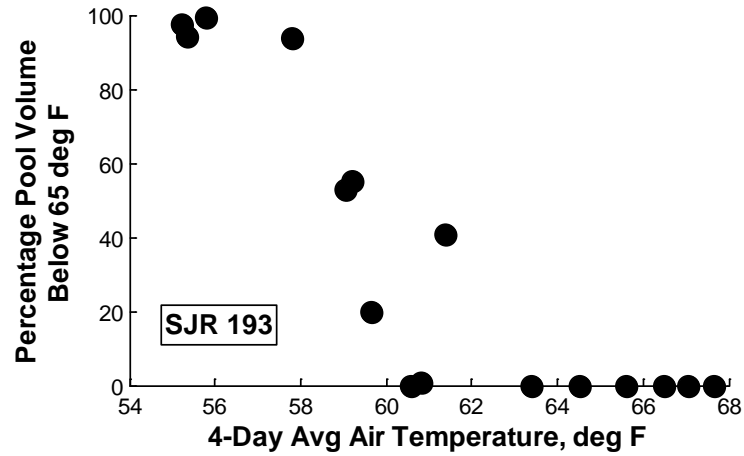


Figure 50: The percentage of pool volume with thermal refugia below 65°F decreased in San Joaquin River system pools when the 4-day moving average air temperature exceeded 56°F.

The consistency of variations in thermal refugia with variations in the 4-day moving average air temperature indicated that under current conditions the availability of thermal refugia in San Joaquin River system pools was linked to the 4-day moving average air temperature. Air temperature corresponded to the availability of thermal refugia in pools because of heat loss across the air-water interface of the pools. As discussed in Section 26.4.4, when nightly air temperature decreased below pool water temperature, heat loss from the pool air-water interface decreased pool water temperature. Variations in the air temperature caused variations in the pool heat balance with higher nightly air temperature resulting in less heat loss and more heat accumulation. Higher nightly air temperatures over multiple days increased the total pool heat until surface water temperature in pools exceeded Chinook water temperature thresholds and the volume of thermal refugia decreased. The availability of thermal refugia was linked to the 4-day moving average air temperature because the pool heat exchange correlated with the 4-day moving average air temperature. Under different flow conditions that altered the relationship between pool heat and the 4-day moving average air temperature, the availability of thermal refugia would behave differently.

26.5 Conclusions

During the summer 2012 survey, thermal stratification was common in the Eastside Bypass, Reach 4B2, and Reach 5 of the San Joaquin River system, but thermal refugia was extremely rare. Water temperature at the bottom of pools was below 68°F in only 3% of pools surveyed and no locations had water temperature below 65°F. Thermal stratification in the San Joaquin River was less than the Eastside Bypass because San Joaquin River pool minimum water temperatures were greater than those found in Eastside Bypass pools. The distribution of thermal stratification in pools was spatially variable and posed thermal and physical barriers to Chinook. Distances between pools with water temperature below 75°F exceeded 4 miles in all three reaches. Eastside Bypass pools also had physical barriers because pools disconnected upstream of Bear Creek.

During fall 2012, both thermal stratification and thermal refugia formed daily in the Eastside Bypass, Reach 4B2, and Reach 5 of the San Joaquin River system. Air temperature influenced thermal stratification and thermal refugia because nightly decreases in air temperature caused convective mixing that reset daily thermal stratification and created thermal refugia. Correlations between the daily change in air temperature and daily pool thermal stratification indicated air temperature could estimate thermal stratification in pools. Variations in the regional 4-day moving average air temperature corresponded to variations in the volume of thermal refugia. The volume of thermal refugia at different Chinook temperature thresholds decreased as the 4-day moving average air temperature increased. This suggested that the availability of thermal refugia in the San Joaquin River system can be estimated by air temperature trends.

Thermal stratification and thermal refugia were not significantly influenced by subsurface-surface water exchange. While gaining, losing, and neutral conditions were measured in all reaches and varied with changes in water surface elevation, losing

conditions were most common during fall 2012. Under losing conditions, subsurface water temperature did not promote thermal stratification. Subsurface-surface water exchange also did not promote thermal stratification because subsurface water temperature below pools increased with depth and was frequently warmer than pool bottom water temperature. Trends in subsurface water temperature were similar to regional monitoring well groundwater temperature trends.

Variations in surface flow altered thermal stratification and thermal refugia in San Joaquin River system pools. Flow variations alone did not correlate with thermal stratification, but data suggested increased surface water flow coupled with pool geometry changed the water velocity distribution and disrupted thermal stratification.

Increasing flow from approximately 10 cfs to 63 cfs collapsed thermal stratification and thermal refugia in one pool. Restoration flows would alter thermal stratification and thermal refugia conditions as increases in flow would increase water velocity and vertical mixing in pools.

26.6 Acknowledgements

Many thanks to all those that helped with the numerous demands of field work: Ted Baker, Matt Bigelow, Jessica Fontaine, Jeff Galman, Stephen Lee, David Moreno, Kristi Seabrook, and Michael Wolf. Thank you to Karl Stromayer, Bob Parris, and the staff of the San Luis National Wildlife Refuge for all their assistance working on the refuge. Thank you to all those at Friant Dam for help fabricating the piezometers, providing space for all my equipment, and providing equipment and personnel for much of the field work. Thank you to Christine Hatch, Jim Hunt, and Matt Kondolf for their advice on experiment design. Thanks are also due to Brian Heywood, Craig Moyle, and Don Portz and his team for the various ways they assisted me in this research. Thank you to Tom Heinzer and Diane Williams for all their work using the digital terrain model to calculate the pool volume and heat. Thank you to Katrina Harrison, Erin Rice, and Celia Zamora for reviewing an early draft of this report. Finally, thank you to the entire San Joaquin River Restoration Program for the support, funding, and opportunity to conduct this study.

26.7 References

- Acuña, V., and K. Tockner. 2009. Surface-subsurface water exchange rates along alluvial river reaches control the thermal patterns in an Alpine river network. *Freshwater Biology* 54: 306 – 320. doi:10.1111/j.1365-2427.2008.02109.x.
- Arrigoni, A.S., G.C. Poole, L.A.K. Mertes, S.J. O’Daniel, W.W. Woessner, and S.A. Thomas. 2008. Buffered, lagged, or cooled? Disentangling hyporheic influences on temperature cycles in stream channels. *Water Resources Research* 44: W09418. doi:10.1029/2007WR006480.
- Bednarz, T.P., C. Lei, and J.C. Patterson. 2009. Unsteady natural convection induced by diurnal temperature changes in a reservoir with slowly varying bottom topography. *International Journal of Thermal Sciences* 48: 1932 – 1942.
- Bilby, R.E. 1984. Characteristics and frequency of cool-water areas in a western Washington stream. *Journal of Freshwater Ecology* 2: 593 – 602.
- Bogan, T., O. Mohseni, and H.G. Stefan. 2003. Stream temperature – equilibrium temperature relationship. *Water Resources Research* 39(9): 1245 – 1256.
- Burkholder, B.K., G.E. Grant, R. Haggerty, T. Khangaonkar, and P.J. Wampler. 2008. Influence of hyporheic flow and geomorphology on temperature of a large, gravel-bed river, Clackamas River, Oregon, USA. *Hydrological Processes* 22: 941 – 953. doi: 10.1002/hyp.6984.
- CFC (California State Board of Fish Commissioners). 1875. Fourth biennial report of the Commissioners of Fisheries of the State of California for the years 1874 and 1875. CFC, Sacramento, California.
- CFC (California State Board of Fish Commissioners). 1877. Fourth biennial report of the Commissioners of Fisheries of the State of California for the years 1876 and 1877. CFC, Sacramento, California.
- Conant, B.J. 2004. Delineating and quantifying ground water discharge zones using streambed temperature. *Ground Water* 42(2): 243 – 257.
- Constantz, J. 2008. Heat as a tracer to determine streambed water exchanges. *Water Resources Research* 44: W00D10. doi: 10.1029/2008WR006996.
- Ebersole, J.L., W.J. Liss, and C.A. Frissell. 2001. Relationship between stream temperature, thermal refugia and rainbow trout *Oncorhynchus mykiss* abundance in arid-land streams in the northwestern United States. *Ecology of Freshwater Fish* 10: 1-10.
- Ebersole, J.L., W.J. Liss, and C.A. Frissell. 2003. Cold water patches in warm streams: Physicochemical characteristics and the influence of shading. *Journal of the American Water Resources Association* 39: 355 – 368.

- Essaid, H.I., J.T. Wilson, and N.T. Baker. 2006. Spatial and temporal variability in streambed fluxes, Leary Weber Ditch, Indiana. *Paper presented at Joint 8th Federal Interagency Sedimentation and 3rd Federal Interagency Hydrologic Modeling Conference*. U.S. Dept. of Agriculture, Reno, NV: 2 – 6 April.
- Essaid, H., C.M. Zamora, K.A. McCarthy, J.R. Vogel, and J.R. Wilson. 2008. Using heat to characterize streambed water flux variability in four stream reaches. *Journal of Environmental Quality* 36; 1010 – 1023. doi: 10.2134/jeq2006.0448.
- Frissell, C.A., J.L. Ebersole, W.J. Liss, B.J. Cavallo, G.C. Poole, and J.A. Stanford. 1996. Potential effects of climate change on thermal complexity and biotic integrity of streams: seasonal intrusion of non-native fishes. Environmental Protection Agency Final Report CR-822019-01-0. Duluth, Minnesota.
- Fry, F.E.J. 1971. The effects of environmental factors on the physiology of fish. Pages 1-98 in W.S. Hoar and D.J. Randall, editors. *Fish Physiology*. Academic Press, New York.
- Gartrell, G. Jr. 1979. Studies on the mixing in a density-stratified shear flow. Ph.D. thesis, 478 pp., California Institute of Technology, Pasadena, California.
- Gibson, R.J. 1966. Some factors influencing the distribution of brook trout and young Atlantic salmon. *Journal of the Fisheries Research Board of Canada* 23: 1977 – 1980.
- Hannah, D.M., I.A. Malcolm, and C. Bradley. 2009. Seasonal hyporheic temperature dynamics over riffle bedforms. *Hydrological Processes* 23: 2178 – 2194. doi: 10.1002/hyp.7256.
- Harvey, J. W. and K.E. Bencala. 1993. The effect of streambed topography on surface-subsurface water exchange in mountain catchments. *Water Resources Research* 29: 89 – 98.
- Harvey, J.W., B.J. Wagner, and K.E. Bencala. 1996. Evaluating the reliability of the stream tracer approach to characterize stream-subsurface water exchange. *Water Resources Research* 32(8): 2441 – 2451.
- Hatch, C.E., A.T. Fisher, J.S. Revenaugh, J. Constantz, and C. Ruehl. 2006. Quantifying surface water-groundwater interactions using time series analysis of streambed thermal records: method development. *Water Resources Research* 42(10): W10410. doi: 10.1029/2005WR004787.
- Hatch C.E., A.T. Fisher, C.R. Ruehl, and G. Stemler. 2010. Spatial and temporal variation in streambed hydraulic conductivity quantified with time-series thermal methods. *Journal of Hydrology* 389: 276 – 288. doi: 10.1016/j.jhydrol.2010.05.046.

- Herbert, C., D. Caissie, M.G. Satish, and N. El-Jabi. 2011. Study of stream temperature dynamics and corresponding heat fluxes within Miramichi River catchments (New Brunswick, Canada). *Hydrological Processes* 25: 2439 – 2455. doi: 10.1002/hyp.8021.
- Johnson, S.L. 2004. Factors influencing stream temperature in small streams: substrate effects and a shading experiment. *Canadian Journal of Fisheries and Aquatic Sciences* 61: 913 – 923. doi: 10.1139/F04-040.
- Keller E.A. and T.D. Hofstra. 1983. Summer cold pools in Redwood Creek near Orick, California, and their importance as habitat for anadromous salmonids. Pages 221– 224 *in* Proceedings of first biennial conference of research in California national parks. U.S. National Park Service, Cooperative Park Studies Unit, Davis, California.
- Keller, E.A., T.D. Hofstra, and C. Moses. 1995. Summer “cold pools” in Redwood Creek near Orick, California. Chapter U. *In* Geomorphic processes and aquatic habitat in the Redwood Creek Basin, Northwestern California. *Edited by* K.M. Nolan, H.M. Kelsey, and D.C. Marron. U.S. Geological Survey Professional Paper No. 1454: U1 – U9.
- Li, H.W., T.N. Pearsons, C.K. Tait, J.L. Li, and R. Gaither. 1993. Approaches to evaluate habitat improvement programs in streams of the John Day Basin. Completion Report, Oregon Cooperative Fishery Research Unit, Oregon State University, Corvallis, Oregon.
- MacVicar, B.J. and C.D. Rennie. 2012. Flow and turbulence redistribution in a straight artificial pool. *Water Resources Research* 48: W02503. doi: 10.1029/2010WR009374.
- Malcolm, I.A., C. Soulsby, A.F. Youngson, and D.M. Hannah. 2005. Catchment scale controls on groundwater – surface water interactions in the hyporheic zone: implications for salmon embryo survival. *River Research and Applications* 21: 977 – 989.
- Matthews, K.R., and N.H. Berg. 1997. Rainbow trout responses to water temperature and dissolved oxygen stress in two southern California stream pools. *Journal of Fish Biology* 50: 50 – 67.
- Matthews, W.J., and E.G. Zimmerman. 1990. Potential effects of global warming on native fishes of the southern Great Plains and the Southwest. *Fisheries* 15: 26 – 32.
- Meisner, J.D. 1990. Potential loss of thermal habitat for brook trout, due to climatic warming, in two southern Ontario streams. *Transactions of the American Fisheries Society* 119: 282 – 291.

- Madej, M.A., C. Currens, V. Ozaki, J. Yee, and D.G. Anderson. 2006. Assessing possible thermal rearing restrictions for juvenile Coho salmon (*Oncorhynchus kisutch*) through thermal infrared imaging and in-stream monitoring. Redwood Creek, California. *Canadian Journal of Fisheries and Aquatic Sciences* 63: 1384 – 1396. doi:10.1139/F06-043.
- McBain and Trush, Inc. (eds.). 2002. San Joaquin River Restoration Study Background Report, prepared for the Friant Water Users Authority, Lindsay, California, and Natural Resources Defense Council, San Francisco, CA.
- Mohseni, O., and H.G. Stefan. 1999. Stream temperature/air temperature relationship: a physical interpretation. *Journal of Hydrology* 218: 128 – 141.
- Moyle, P.B., R.M. Yoshiyama, J.E. Williams, and E.D. Wikramanayake. 1995. Fish species of special concern in California. Final Report. Prepared by Department of Wildlife and Fisheries Biology, University of California, Davis for California Department of Fish and Game, Inland Fisheries Division, Rancho Cordova, California.
- Nelson, S.M. and G.K. Reed. 2012. Observations on the hyporheic environment along the San Joaquin River below Friant Dam. Bureau of Reclamation Technical Service Center, Technical Memorandum No. 86-68220-11-03. San Joaquin River Restoration Program Annual Technical Report 2011. U.S. Bureau of Reclamation, San Joaquin River Restoration Program, Sacramento, California.
- Nielsen, J. L., T.E. Lisle, and V. Ozaki. 1994. Thermally stratified pools and their use by steelhead in northern California streams. *Transactions of the American Fisheries Society* 123: 613 – 626.
- O'Driscoll, M.A. and D.R. DeWalle. 2006. Stream-air temperature relations to classify stream-ground water interactions in a karst setting, central Pennsylvania, USA. *Journal of Hydrology* 329: 140 – 153. doi:10.1016/j.jhydrol.2006.02.010.
- Ozaki, V.L. 1988. Geomorphic and hydrologic conditions for cold pool formation on Redwood Creek, California. Redwood National Park, Research and Development Technical Report 24, Arcata, California.
- Packman, A.I., M. Salehin, and M. Zaramella. 2004. Hyporheic exchange with gravel beds: basic hydrodynamic interactions and bedform-induced advective flows. *Journal of Hydraulic Engineering* 130(7): 647 – 656. doi: 10.1061/(ASCE)0733-9429(2004)130:7(647).
- Poole, G.C. and C.H. Berman. 2001. An ecological perspective on in-stream temperature: natural heat dynamics and mechanisms of human-caused thermal degradation. *Environmental Management* 27(6): 787 – 802. doi: 10.1007/s002670010188.

- Poole, G.C., S.J. O'Daniel, K.L. Jones, W.W. Woessner, E.S. Bernhardt, A.M. Helton, J.A. Stanford, B.R. Boer, and T.J. Beechie. 2008. Hydrologic spiralling: the role of multiple interactive flow paths in stream ecosystems. *River Research and Applications* 24: 1018 – 1031. doi: 10.1002/rra.1099.
- Reinfelds, I., and S. Williams. 2011. Threshold flows for the breakdown of seasonally persistent thermal stratification: Shoalhaven River below Tallow Dam, New South Wales, Australia. *River Research and Applications*. doi: 10.1002/rra.1485.
- Rich, A.A., and Associates. 2007. Impacts of water temperature on fall-run Chinook salmon, *Oncorhynchus tshawytscha*, and Steelhead, *O. mykiss*, in the San Joaquin River System. San Anselmo, California.
- Sawyer, A.M., G.B. Pasternack, H.J. Moir, and A.A. Fulton. 2010. Riffle-pool maintenance and flow convergence routing observed on a large gravel-bed river. *Geomorphology* 114(3): 143 – 160.
- San Joaquin River Restoration Program (SJRRP). 2010. April 2010 Bathymetric Surveys of the San Joaquin River. Annual Technical Report. U.S. Bureau of Reclamation, San Joaquin River Restoration Program, Sacramento, California.
- Reclamation. *See* U.S. Bureau of Reclamation.
- SJRRP Fisheries Management Work Group (FMWG). 2009. Fisheries Management Plan. U.S. Bureau of Reclamation, San Joaquin River Restoration Program, Sacramento, California.
- SJRRP FMWG. 2010. Conceptual Models of Stressors and Limiting Factors for San Joaquin River Chinook Salmon. U.S. Bureau of Reclamation, San Joaquin River Restoration Program, Sacramento, California.
- SJRRP Water Management Work Group (WMWG). 2008a. Temperature Model Sensitivity Analyses Sets 1 and 2. Draft Technical Memorandum. U.S. Bureau of Reclamation, San Joaquin River Restoration Program, Sacramento, California.
- SJRRP WMWG. 2008b. Temperature Model Sensitivity Analyses Set 3. Draft Technical Memorandum. U.S. Bureau of Reclamation, San Joaquin River Restoration Program, Sacramento, California.
- SJRRP WMWG. 2008c. Temperature Model Sensitivity Analyses Sets 4 and 5. Draft Technical Memorandum. U.S. Bureau of Reclamation, San Joaquin River Restoration Program, Sacramento, California.
- Sinokrot, B.A. and H.G. Stefan. 1994. Stream water-temperature sensitivity to weather and bed parameters. *Journal of Hydraulic Engineering* 120(6): 722 – 736.
- Soulsby, C., D. Tetzlaff, N. van den Bedem, I.A. Malcolm, P.J. Bacon, and A.F. Youngson. 2007. Inferring groundwater influences on surface water in montane

- catchments from hydrochemical surveys of springs and streamwaters. *Journal of Hydrology* 333: 199 – 213.
- Stillwater Sciences. 2003. Restoration Strategies for the San Joaquin River. Prepared by Stillwater Sciences, Berkeley, CA, for the Natural Resources Defense Council, San Francisco, California, and Friant Water Users Authority, Lindsay, California.
- Sullivan, K., D.J. Martin, R.D. Cardwell, J.E. Toll, and S. Duke. 2000. An analysis of the effects of temperature on salmonids of the Pacific Northwest with implications for selecting temperature criteria, Sustainable Ecosystems Institute, Portland, Oregon.
- Tate, K.W., D.L. Lancaster, D.F. Lile. 2007. Assessment of thermal stratification within stream pools as a mechanism to provide refugia for native trout in hot, arid rangelands. *Environmental Monitoring and Assessment* 124: 289 – 300. doi: 10.1007/s10661-006-9226-5.
- Thompson, D.M., C.R. McCarrick. 2010. A flume experiment on the effect of constriction shape on the formation of forced pools. *Hydrology and Earth System Sciences* 14: 1321 – 1330. doi: 10.5194/hess-14-1321-2010.
- Thompson, D.M., J.M. Nelson, and E.E. Wohl. 1998. Interactions between pool geometry and hydraulics. *Water Resources Research* 34(12): 3673 – 3681.
- Tompkins, M.R. 2006. Floodplain connectivity and river corridor complexity: Implications for river restoration and planning for floodplain management, Ph.D. dissertation, 392 pp., University of California, Berkeley, Berkeley, California.
- Tonina, D. and J.M. Buffington. 2007. Hyporheic exchange in gravel bed rivers with pool-riffle morphology: Laboratory experiments and three-dimensional modeling. *Water Resources Research* 42: W01421. doi: 10.1029/2005WR004328.
- Torgersen, C.E., D.M. Price, H.W. Li, and B.A. McIntosh. 1999. Multiscale thermal refugia and stream habitat associations of Chinook salmon in Northeastern Oregon. *Ecological Applications* 9(1): 301-319.
- U.S. Bureau of Reclamation (Reclamation). 2007a. San Joaquin Basin Water Temperature Modeling and Analysis. Prepared by Resource Management Associates, Inc., and Bureau of Reclamation, Mid-Pacific Region. April.
- Wagner, R.W., M. Stacey, L.R. Brown, and M. Dettinger. 2010. Statistical models of temperature in the Sacramento-San Joaquin Delta under climate-change scenarios and ecological implications. *Estuaries and Coasts*. doi: 10.1007/s12237-010-9369-z.
- Ward, P.D., T.R. McReynolds, and C.E. Garman. 2006. Butte Creek spring-run Chinook salmon, *Oncorhynchus tshawytscha* pre-spawn mortality evaluation. California

- Department of Fish and Game, Inland Fisheries Administrative Report No. 2006-1.
- White, D. S. 1993. Perspectives on defining and delineating hyporheic zones. *Journal of North American Benthological Society* 12(1): 61 – 69.
- Woessner, W.W. 2000. Stream and fluvial plain ground water interactions: rescaling hydrogeologic thought. *Ground Water* 38(3): 423 – 429.
- Yoshiyama, R. M., E. R. Gerstung, F. W. Fisher, and P. B. Moyle. 1996. Historical and present distribution of Chinook salmon in the Central Valley drainage of California. Pages 309-362 *in* Sierra Nevada Ecosystem Project: final report to congress. Volume III: Assessments, commissioned reports, and background information. University of California, Center for Water and Wildland Resources, Davis, California.

26.8 Appendix

26.8.1 Fall Instrumentation Individual Site Analysis

San Joaquin River 193 Sensor Array Site (SJR 193)

The furthest upstream San Joaquin River sensor array site was located in Reach 4B2 at approximately river mile 193 (SJR 193) downstream of the Mariposa Bypass (Figure A-1). Four sensor arrays were deployed at SJR 193 from October 11, 2012 until October 29, 2012. To measure the shallow and deep subsurface water conditions, two sensor arrays were installed at the upstream pool location, while the other two sensor arrays were installed in the downstream pool location. Onset Hobo U22-001, Solinst Levellogger Gold, and Levellogger Edge sensors were used to measure water temperature and level at both locations. At SJR 193.24(2), water temperature sensors were placed at the streambed (0 cm), below the streambed (-10 cm), in the shallow subsurface (-63 cm), and in the deep subsurface (-126 cm). The downstream sensor arrays at SJR 193.29 placed ten water temperature sensors spaced vertically every 14 cm through surface water of the pool in addition to water temperature sensors at the streambed (0 cm), below the streambed (-10 cm), in the shallow subsurface (-61 cm), and in the deep subsurface (-130 cm).



Figure A-1: Aerial view of the San Joaquin River sensor array site SJR 193.

San Joaquin River Restoration Program 2012 Thermal Refugia Study

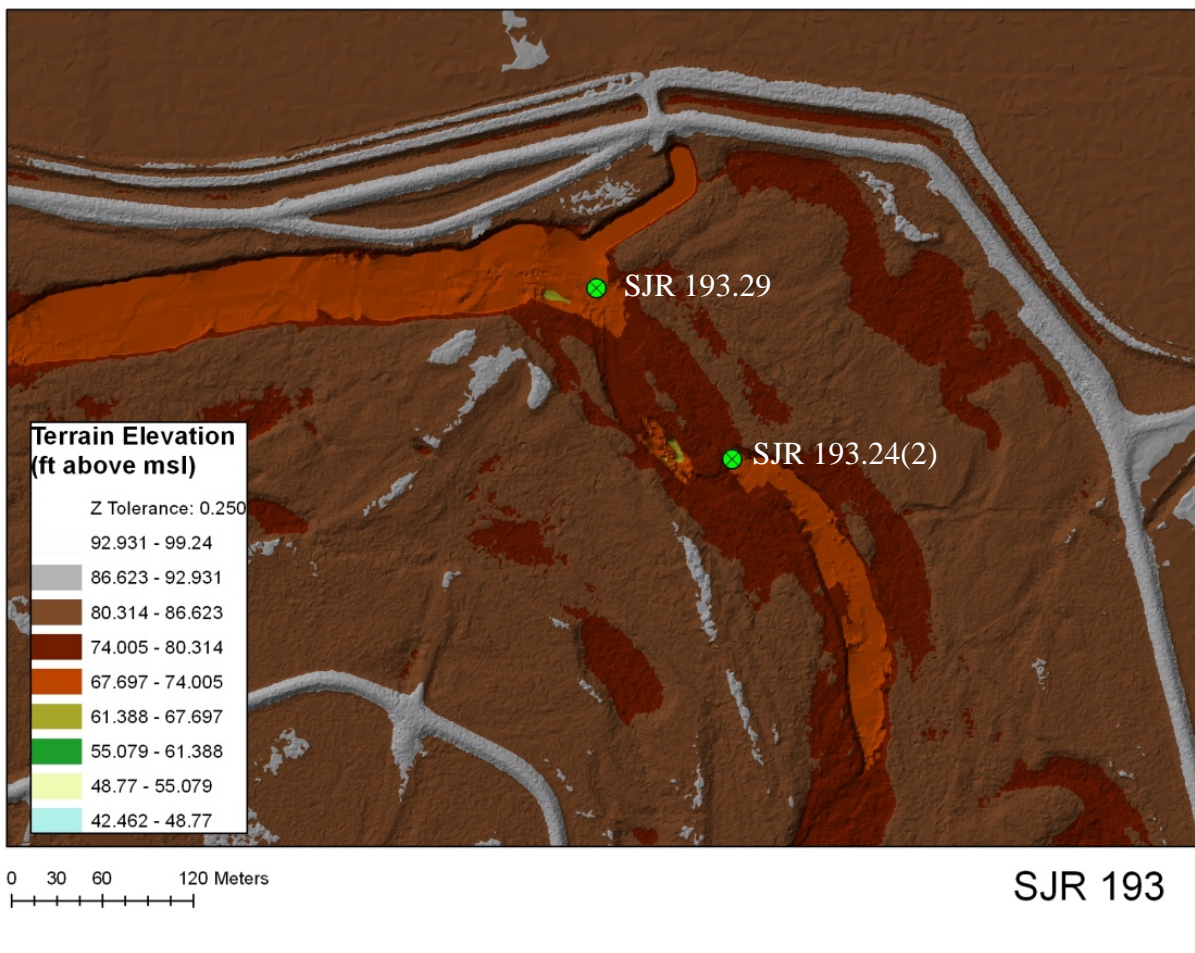


Figure A-2: San Joaquin River System digital terrain model plan view of the San Joaquin River sensor array site SJR 193.

SJR 193.24(2) Upstream Location



Figure A-3: View of sensor array installation as SJR 193.24(2) looking upstream.



Figure A-4: View of sensor array installation in SJR 193.24(2) looking downstream.

Subsurface water temperature at SJR 193.24 increased with depth into the streambed and showed a strong diurnal variation at all depths measured (Figure A-5). The amplitude of the diurnal variation in water temperature decreased with depth below the streambed. The average daily change in temperature ($dT_{\text{avg daily}}$) was 0.71°C for the streambed, while $dT_{\text{avg daily}}$ was 0.46°C for the deepest sensor at -126 cm .

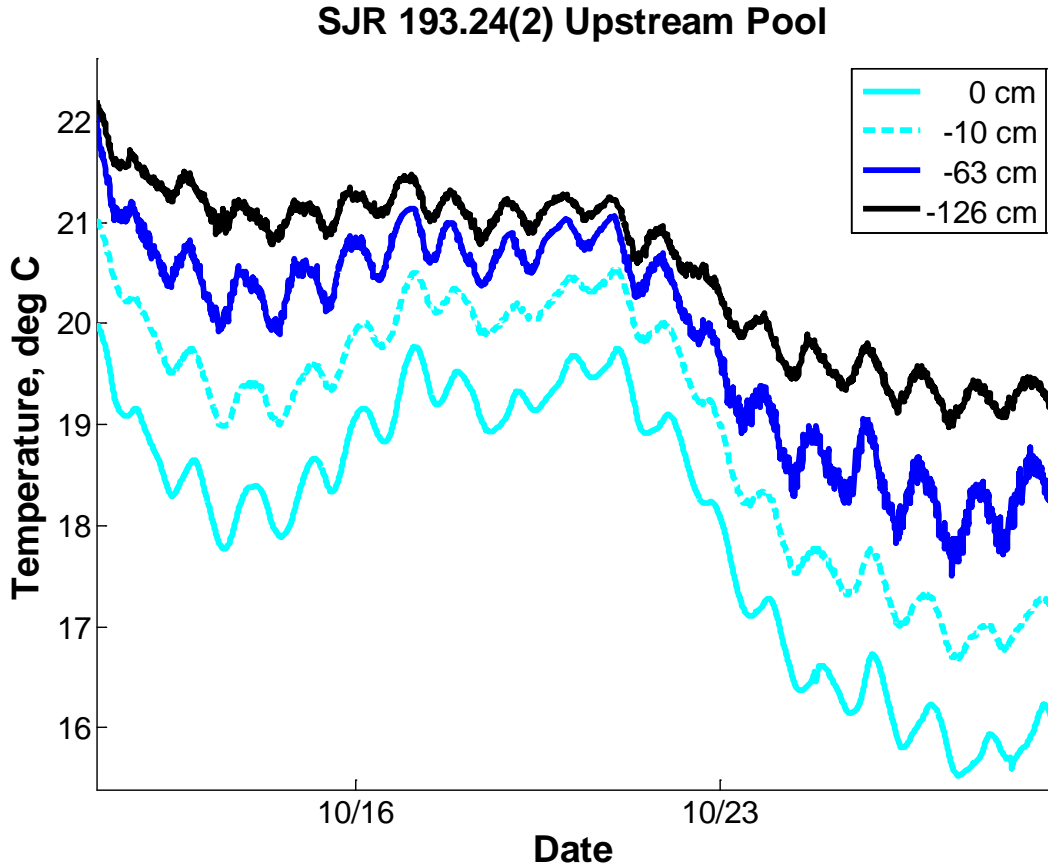


Figure A-5: At the upstream SJR 193.24(2) location, water temperature had a diurnal variation from the streambed level to 126 cm below the streambed.

Hydraulic head data indicated the direction of subsurface flow varied during the instrumentation period with an overall neutral trend (Figure A-6). Initially, hydraulic head at the streambed was greater than the hydraulic head at -63 cm and -126 cm so pool water was downwelling through the streambed into the subsurface. From 10/17 to 10/19, streambed hydraulic head was less than the hydraulic head at -63 cm so subsurface water upwelled through the streambed into the pool surface water. Between 10/19 until 10/22, hydraulic head at the streambed and -63 cm was the same within the $\pm 0.5\text{ cm}$ accuracy of the water level sensors. Streambed hydraulic head then increased from 10/22 until 10/26 where it once again became the same as the hydraulic head at -63 cm . Hydraulic head decreased with depth indicating subsurface flow moved downward between -63 cm and -126 cm .

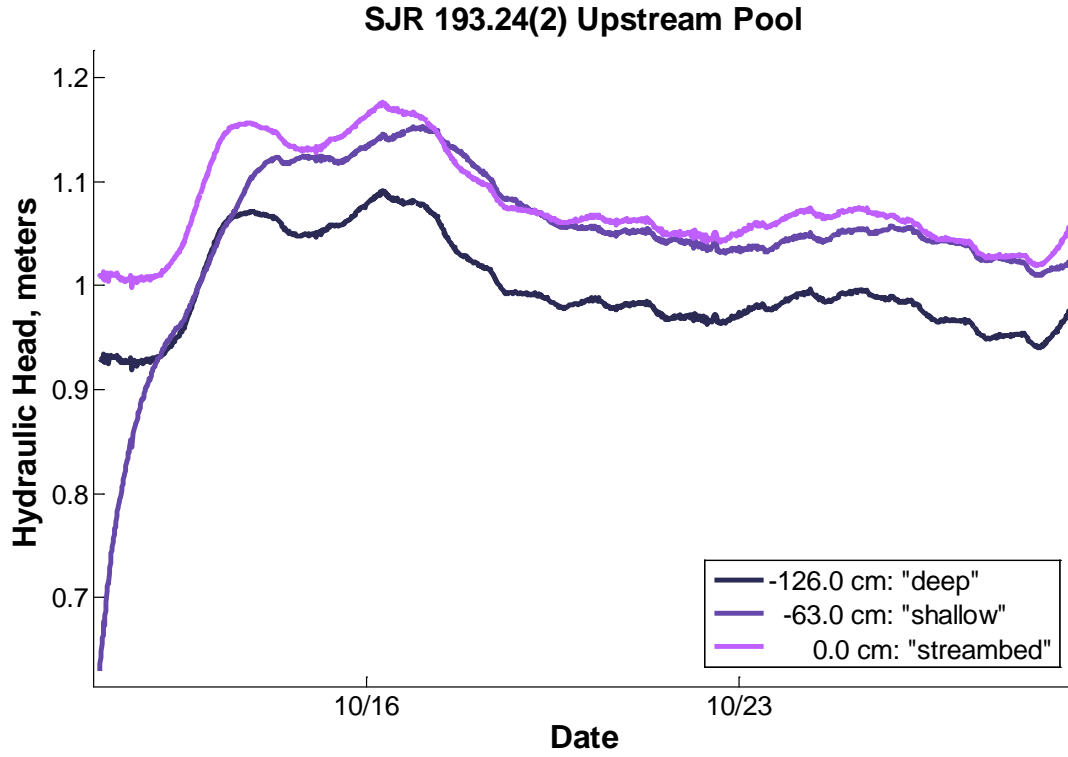


Figure A-6: Variation in hydraulic head with depth into the subsurface at SJR 193.24(2) upstream pool.

SJR 193.29 Downstream Location

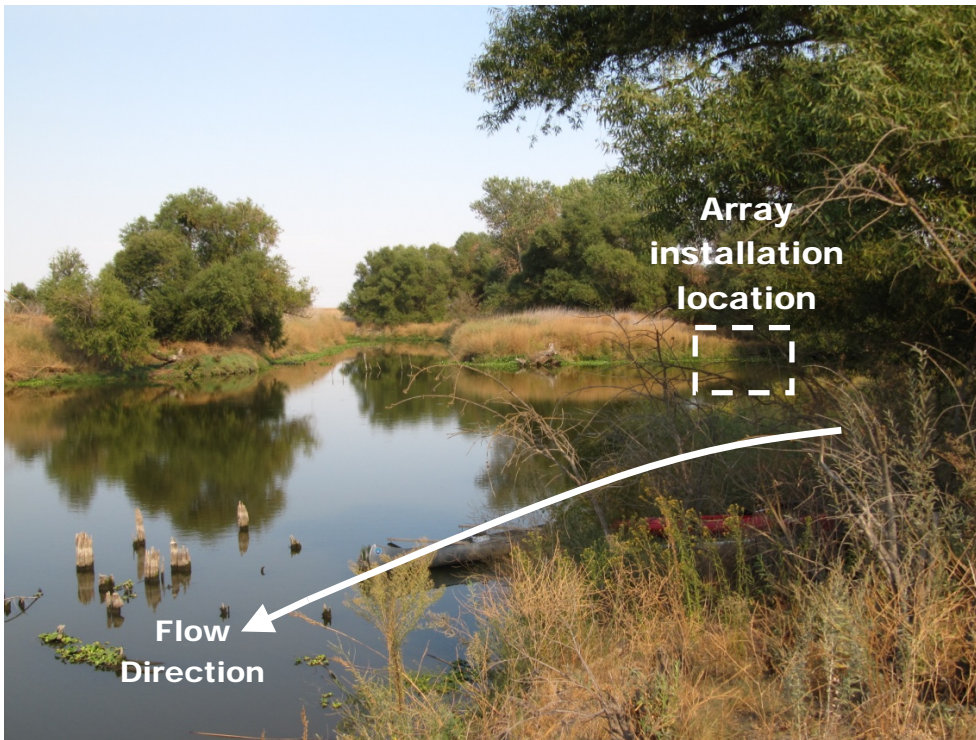


Figure A-7: View of SJR 193.29 pool looking upstream.



Figure A-8: View of SJR 193.29 pool looking downstream.



Figure A-9: SJR 193.29 sensor arrays looking northwest towards the right bank.

Water temperature data at SJR 193.29 is plotted in Figure A-10. Water temperature sensors are labeled based on their depth in centimeters above or below the streambed with the streambed level being zero. Depths greater than zero indicate sensors measuring

surface water temperatures, while depths less than zero are sensors measuring subsurface water temperatures.

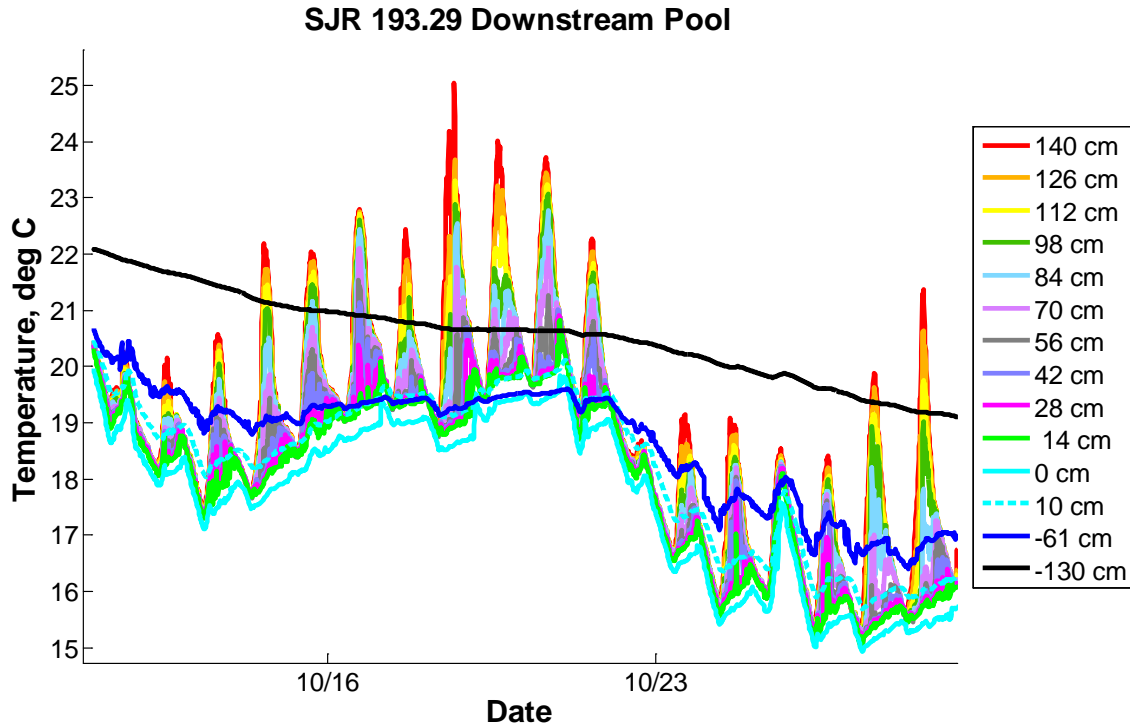


Figure A-10: Variation in surface and subsurface water temperature showing daily thermal stratification from 10/11/2012 to 10/29/2012 at SJR 193.29.

Daily thermal stratification in the pool surface waters occurred during the entire instrumentation period at SJR 193.29. The maximum daily thermal stratification between the top sensor (SJR 193.29 Sensor 140) closest to the air-water interface and the streambed sensor varied daily and ranged from as little as 0.78°C to as much as 6.4°C with an average daily thermal stratification of 3.5°C . Most of the thermal stratification was the result of the water temperature near the air-water interface increasing more than the water temperature near the streambed. Water temperature at SJR 193.29 Sensor 140 ranged from 1.6°C to 6.2°C while water temperature near the streambed (SJR 193.29 Sensor 0) ranged from 0.28°C to 1.9°C .

Water temperature increased with depth below the streambed at SJR 193.29 (Figure A-11). Subsurface water temperature at -10 cm and -60 cm followed daily cycles of water temperature similar to those found at the streambed (0 cm), but with a reduced amplitude of temperature variation. Subsurface water temperature at all depths had a decreasing trend during the instrumentation. Subsurface water temperature at -130 cm showed a decreasing trend in average daily water temperature from 21.9°C to 19.2°C and an average daily temperature variation of 0.08°C . Daily variation in water temperature at -130 cm was most pronounced on days with a large variation in streambed temperature. Subsurface water temperature at -130 cm was greater than the maximum surface water

temperature in the pool from 10/11 until 10/14 and 10/22 to 10/27 even though surface water temperature varied by as much as 3.4°C during those periods.

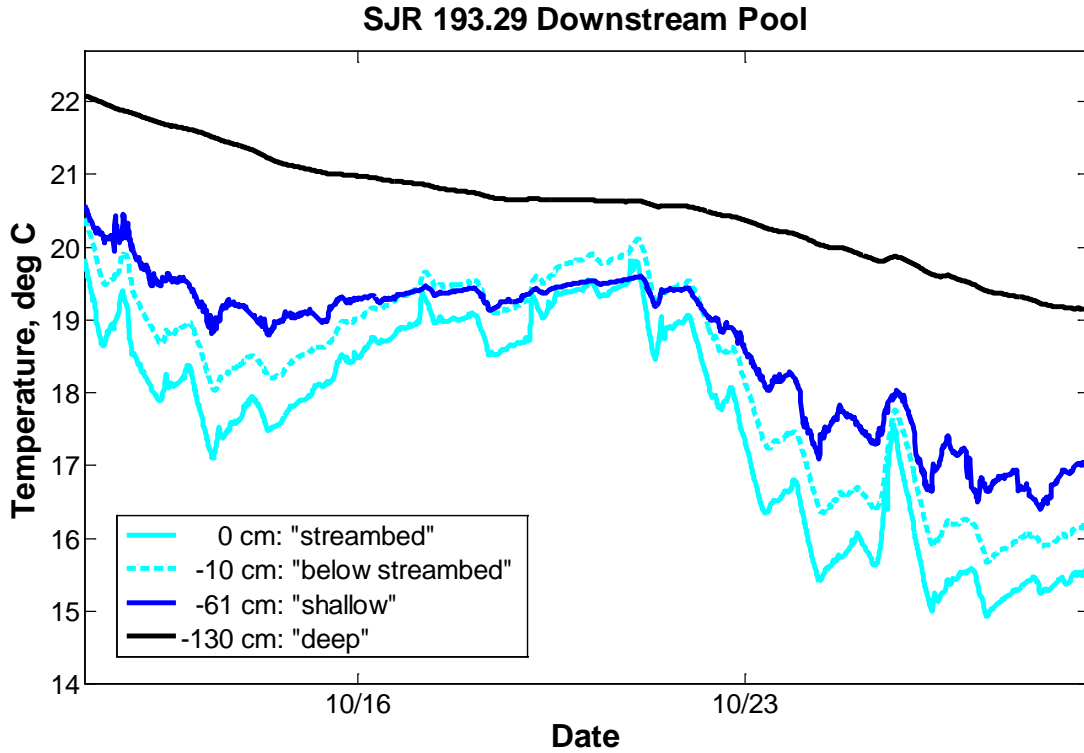


Figure A-11: Variation of subsurface water temperature at SJR 193.29.

Hydraulic head decreased with depth at SJR 193.29 indicating that pool surface water flowed down through the streambed into the subsurface (Figure A-12). Hydraulic head gradient consistently decreased with depth so water only downwelled into the subsurface at SJR 193.29 during the instrumentation period.

N

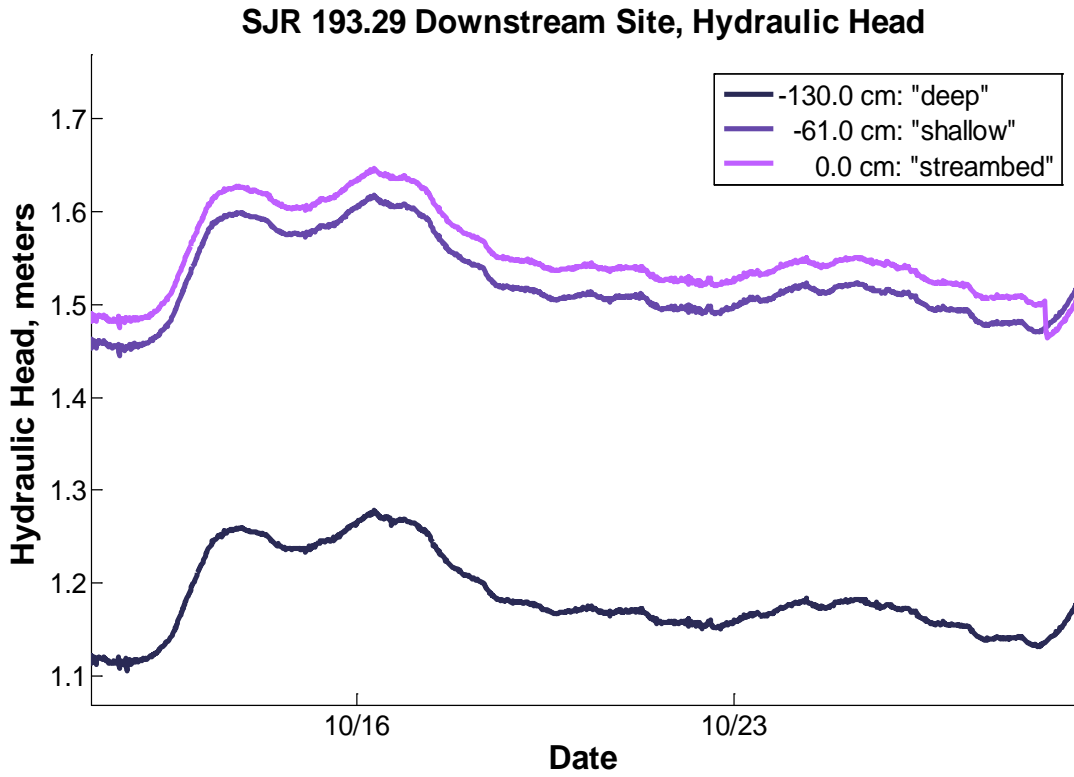


Figure A-12: Variation in hydraulic head with depth into the subsurface at SJR 193.29.

San Joaquin River 199 Sensor Array Site (SJR 199)

The middle San Joaquin River sensor array site was located in Reach 4B2 at approximately river mile 199 (SJR 199) (Figure A-13). SJR 199 was above the confluence of the San Joaquin River with the Eastside Bypass. Four sensor arrays were deployed at SJR 199 from September 13, 2012 until October 6, 2012. To measure the shallow and deep subsurface water conditions, two sensor arrays were installed at the upstream pool location, while the other two sensor arrays were installed in the downstream pool location.

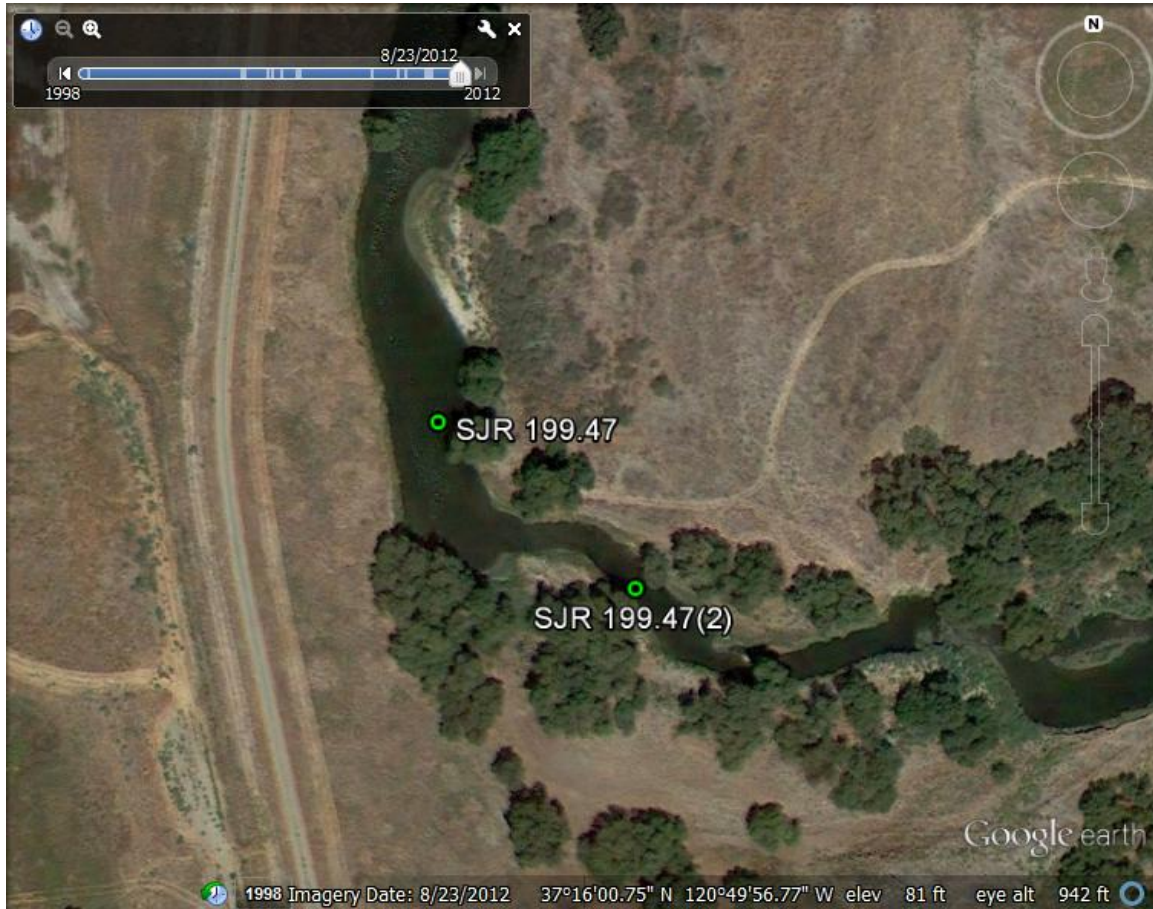
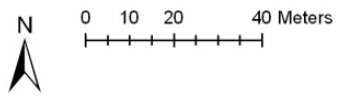
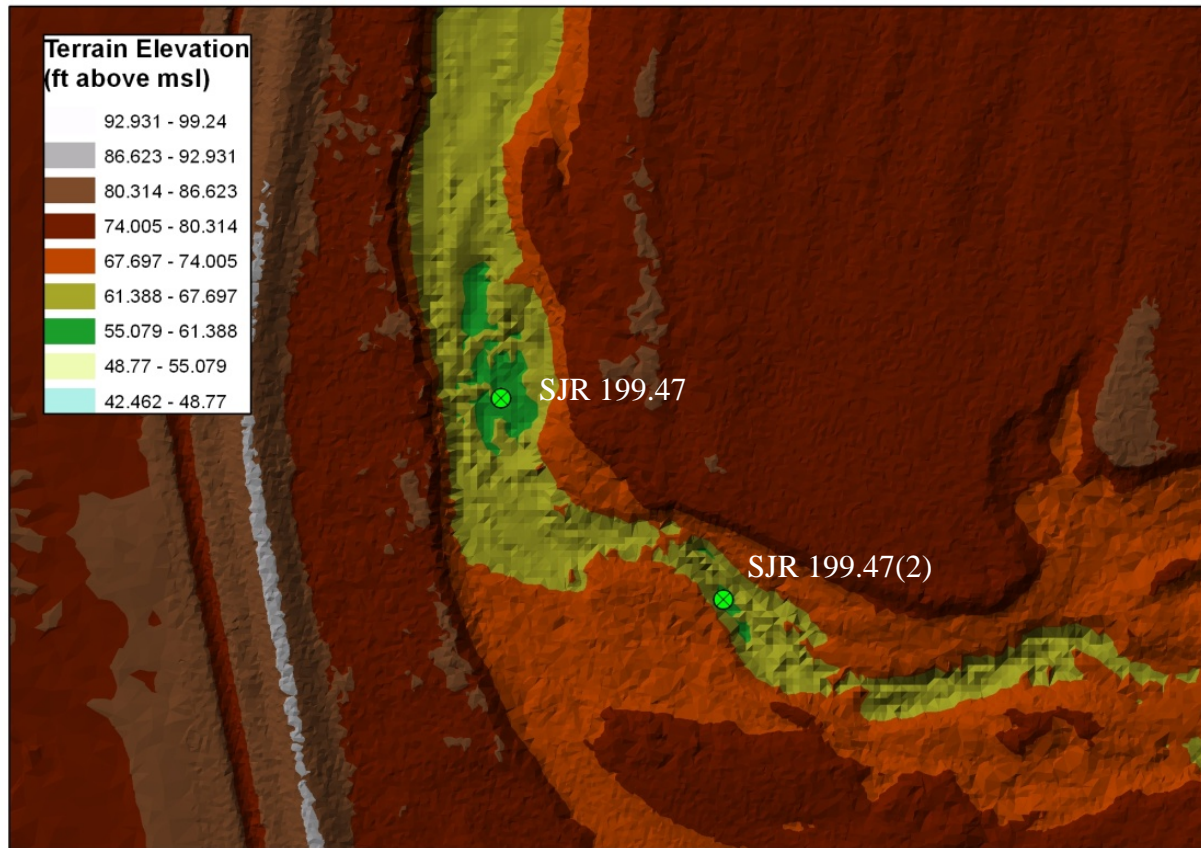


Figure A-13: Aerial view of the San Joaquin River sensor array site SJR 199.

San Joaquin River Restoration Program 2012 Thermal Refugia Study



SJR 199

Figure A-14: San Joaquin River System digital terrain model plan view of the San Joaquin River sensor array site SJR 199.

SJR 199.47(2) Upstream Location



Figure A-15: SJR 199 upstream pool sensor arrays looking upstream.

Water temperature data from all sensors at the upstream SJR 199 site was plotted in Figure A-16. Water temperature sensors were labeled based on their depth in centimeters above or below the streambed with the streambed level being zero. Depths greater than zero indicated sensors measuring surface water temperatures, while depths less than zero were sensors measuring subsurface water temperatures.

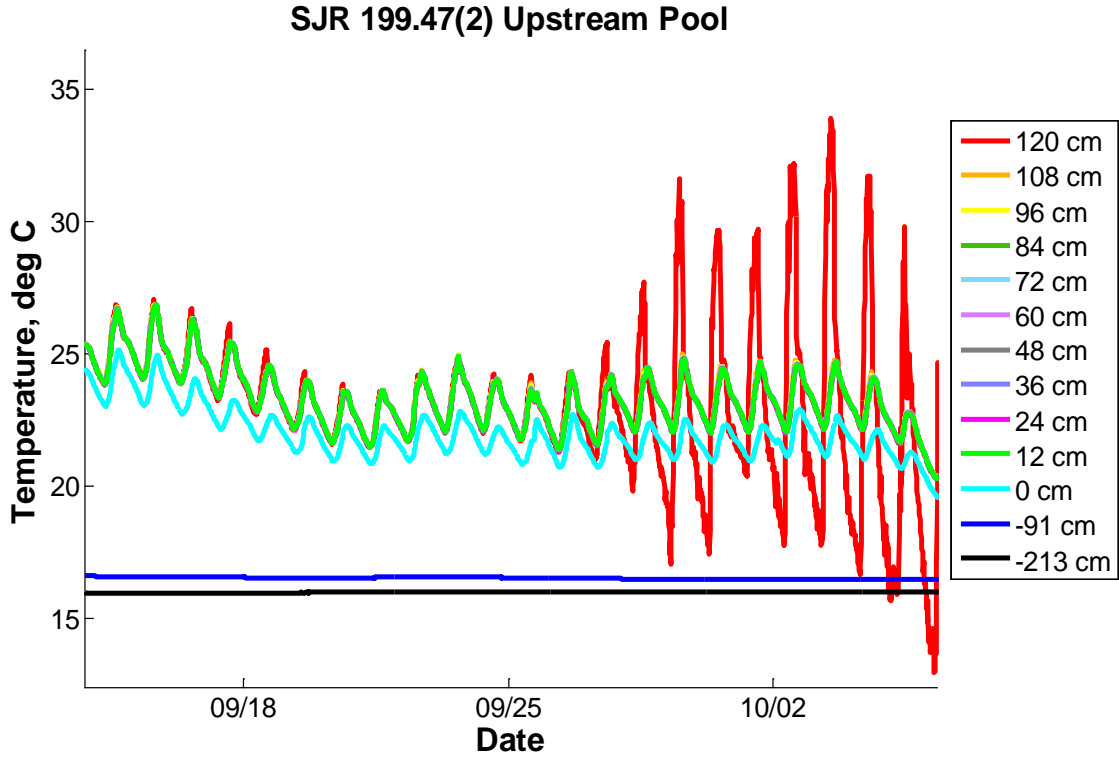


Figure A-16: Surface and subsurface water temperature variation from 9/13 to 10/6 at the upstream location SJR 199.47(2) for the SJR 199 site.

No thermal stratification occurred in the surface water at the SJR 199.47(2) upstream location during the instrumentation period. Surface water temperature differences at SJR 199.47(2) Sensor 0 and Sensor 120 occurred, but these water temperature variations are not due to surface water temperature variations. Water temperature variations at SJR 199.47(2) Sensor 0 occurred because the sensor sank into the streambed sediments and measured the saturated sediments temperature at the streambed-surface water interface rather than surface water temperature. From 9/27 to 10/6, the temperature at 120 cm differed from the temperature recorded by other surface water sensors because SJR 199.47(2) Sensor 120 recorded air temperature during this period. On 9/27 the water level in the pool dropped below 120 cm or the height SJR 199.47(2) Sensor 120 was in the surface water column (Figure A-17). When sensors were recovered from the pool on 10/6/2012, SJR 199.47(2) Sensor 120 was seen in the air directly above the pool air-water interface.

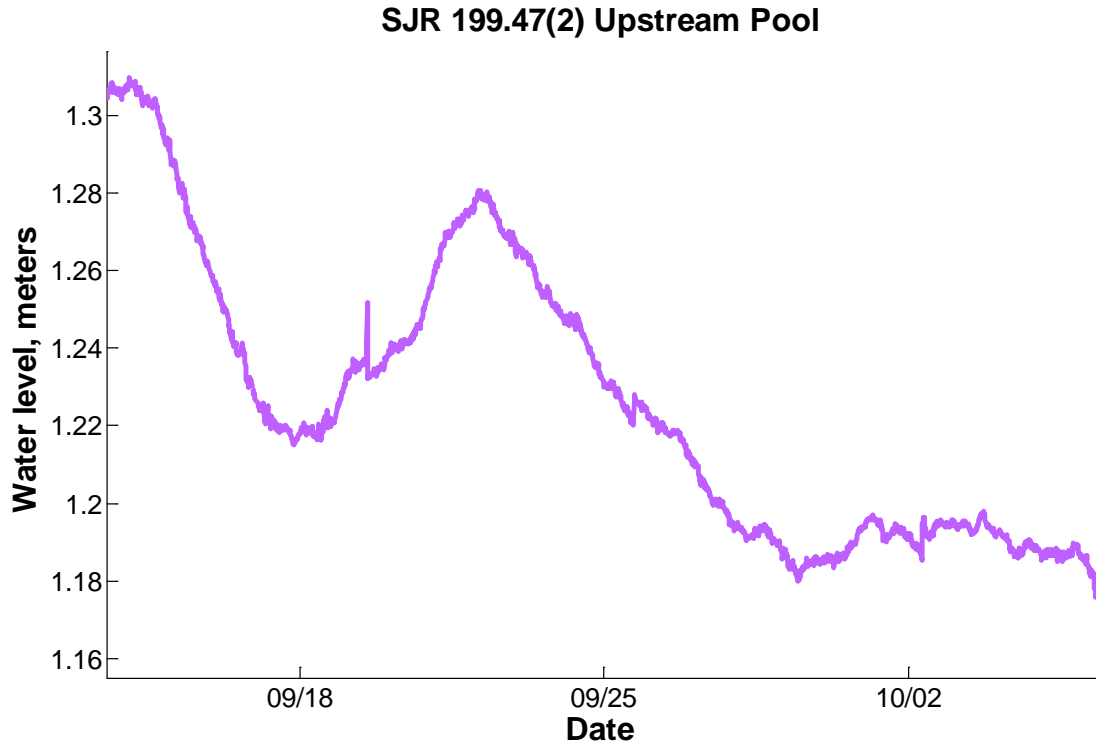


Figure A-17: Variation of water level in SJR 199.47(2). After 9/27/2012, the water level dropped below 1.20 m so SJR 199.47(2) Sensor 120 recorded air temperature instead of water temperature.

Subsurface water temperatures decreased with depth, but showed no daily variation in water temperature. SJR 199.47(2) Sensor -91 showed a weekly trend in subsurface water temperature variation that matched the weekly surface water temperature trend (Figure A-18). SJR 199.47(2) Sensor -213 showed an increasing trend with subsurface water temperature increasing 0.05°C over the measurement period.

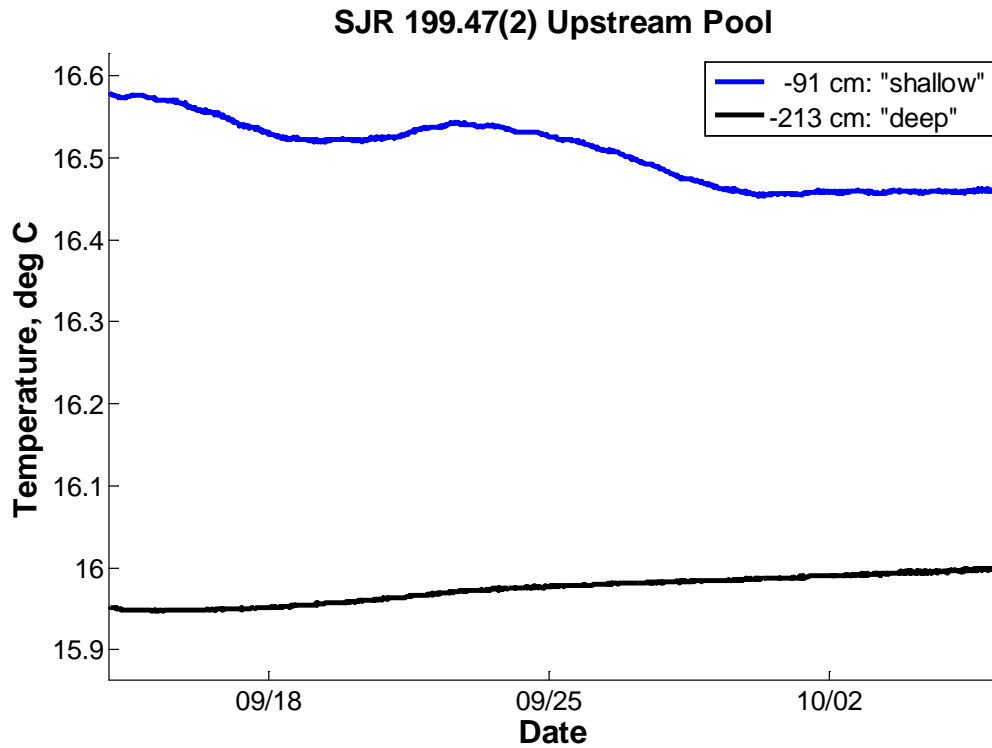


Figure A-18: Variation in subsurface water temperature indicated that shallow subsurface water temperature followed weekly surface water trends, but deep subsurface water temperature was increasing over time.

Hydraulic head data indicated that subsurface water was not upwelling into the pool. At SJR 199.47(2) hydraulic head at 0 cm and -91 cm was approximately same within the accuracy of the water level sensors indicating the subsurface-surface water exchange was neutral (Figure A-19). Hydraulic head decreased between -91 cm and -213 cm so it was hypothesized that either the stream was overall losing surface water at SJR 199.47(2) or a low hydraulic conductivity layer existed between the two depths. No sediment cores were taken at the location so the hypothesis could not be tested.

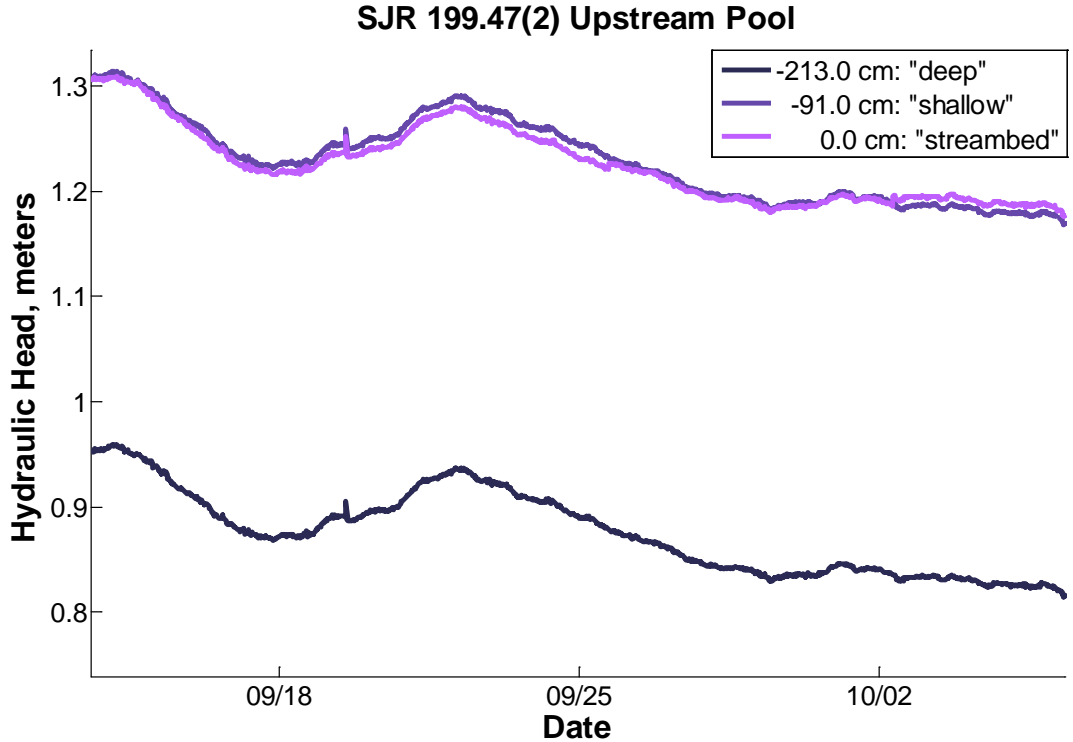


Figure A-19: Hydraulic head at SJR 199.47(2) between 0cm and -91cm was the same indicating neutral subsurface-surface water exchange conditions. An overall losing trend is suggested by the decreasing hydraulic head with greater depth at -213cm.

SJR 199: Downstream Location



Figure A-20: SJR 199 downstream pool sensor arrays looking downstream.



Figure A-21: SJR 199 downstream pool sensor arrays looking upstream.

Water temperature data from all sensors at the downstream SJR 199.47 location is plotted in Figure A-22. Water temperature sensors are labeled based on their depth in centimeters above or below the streambed with the streambed level being zero. Depths greater than zero indicate sensors measuring surface water temperatures, while depths less than zero are sensors measuring subsurface water temperatures.

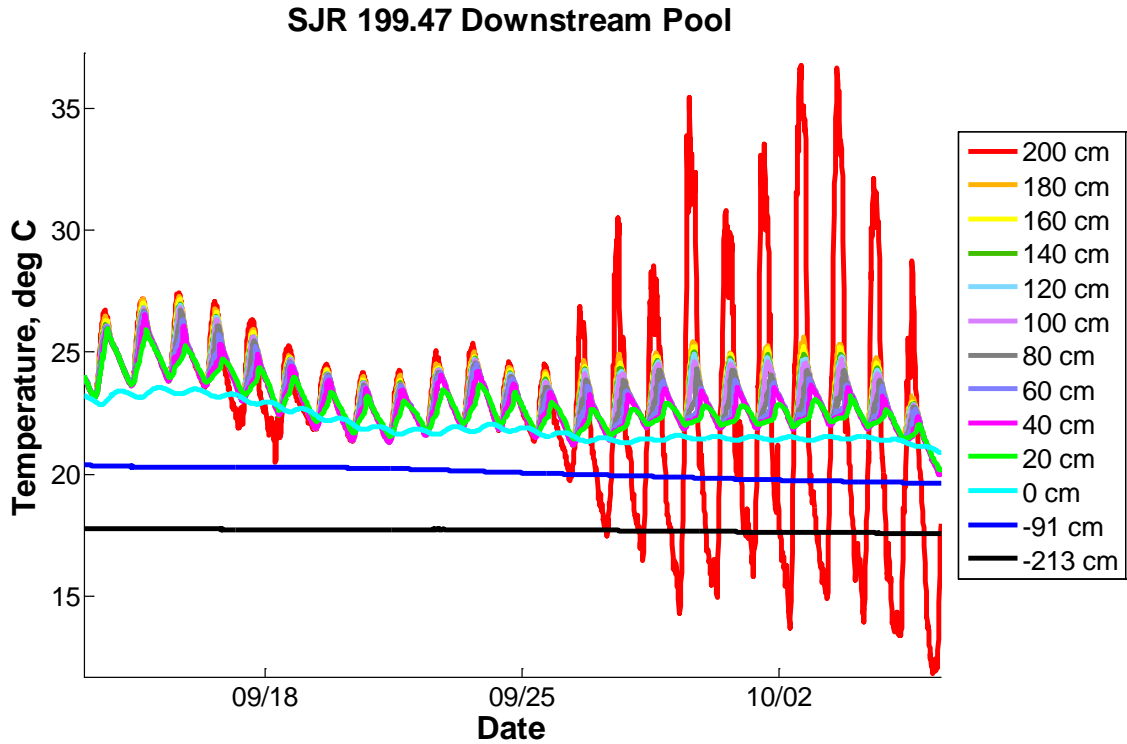


Figure A-22: Surface and subsurface water temperature variation from 9/13 to 10/6 at the downstream pool SJR 199.47.

Surface water temperature data indicates thermal stratification occurred in the surface water for the SJR 199.47 downstream location during the instrumentation period. Similar to the upstream location, a soft, muddy streambed resulted in the streambed water temperature sensor (0 cm) measuring the temperature of the streambed sediment. Pool water level varied during the instrumentation period resulting in the topmost sensor, SJR 199.47 Sensor 200, recording air temperature from 9/27 to 10/6. (Figure A-23). The depth of water in the pool dropped below 200 cm on 9/27 exposing Sensor 200 to the air. Increased variation in the amplitude of temperature indicated when the sensor was no longer reading water temperature.

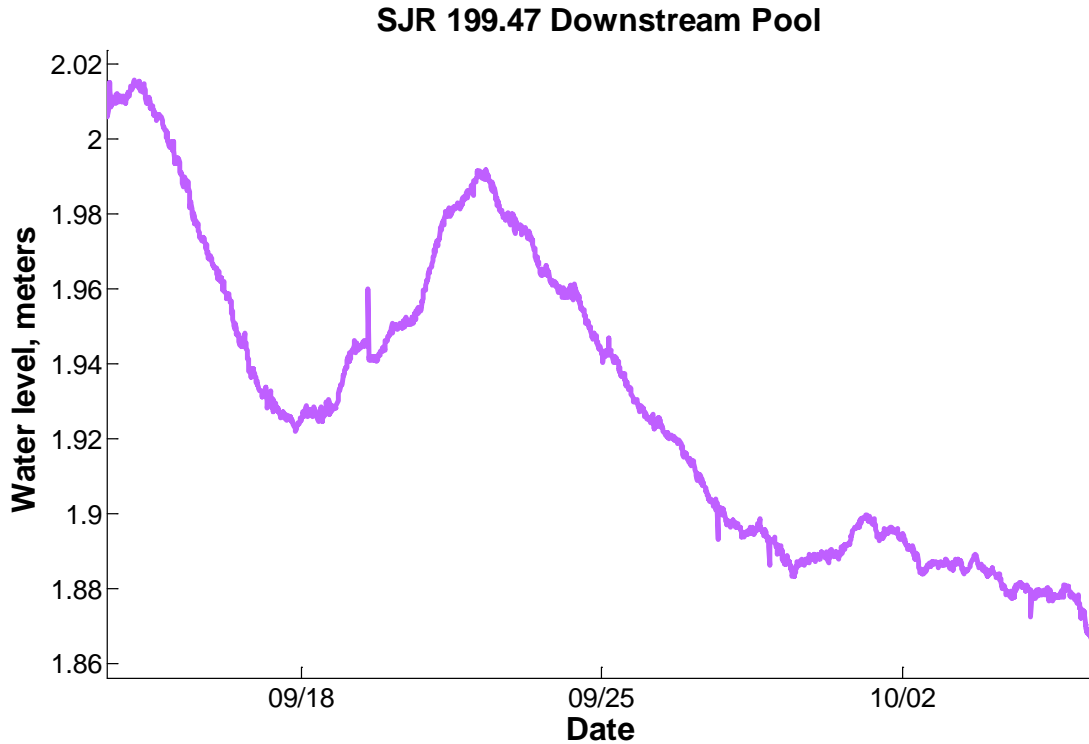


Figure A-23: Variation in pool depth at downstream SJR 199.47 location.

Thermal stratification was calculated as the temperature difference between the top surface water sensor (either Sensor 200 or Sensor 180) and Sensor 20, the sensor closest to the streambed. The maximum daily thermal stratification varied daily and ranged from 1.56°C to 3.42°C with an average daily thermal stratification of 2.47°C. Much of the thermal stratification was due to water temperature increasing more near the air-water interface than near the pool bottom. Water temperature ranged from 3.66°C to 2.38°C for the sensor nearest the air-surface water interface while Sensor 20 ranged from 2.80°C to 0.81°C.

Similar to the upstream location, subsurface water temperature at SJR 199.47 decreased with depth and showed no daily variation in water temperature. Both subsurface temperature sensors recorded the subsurface water temperature decreasing with time and showing a small weekly variation in water temperature (Figure A-24).

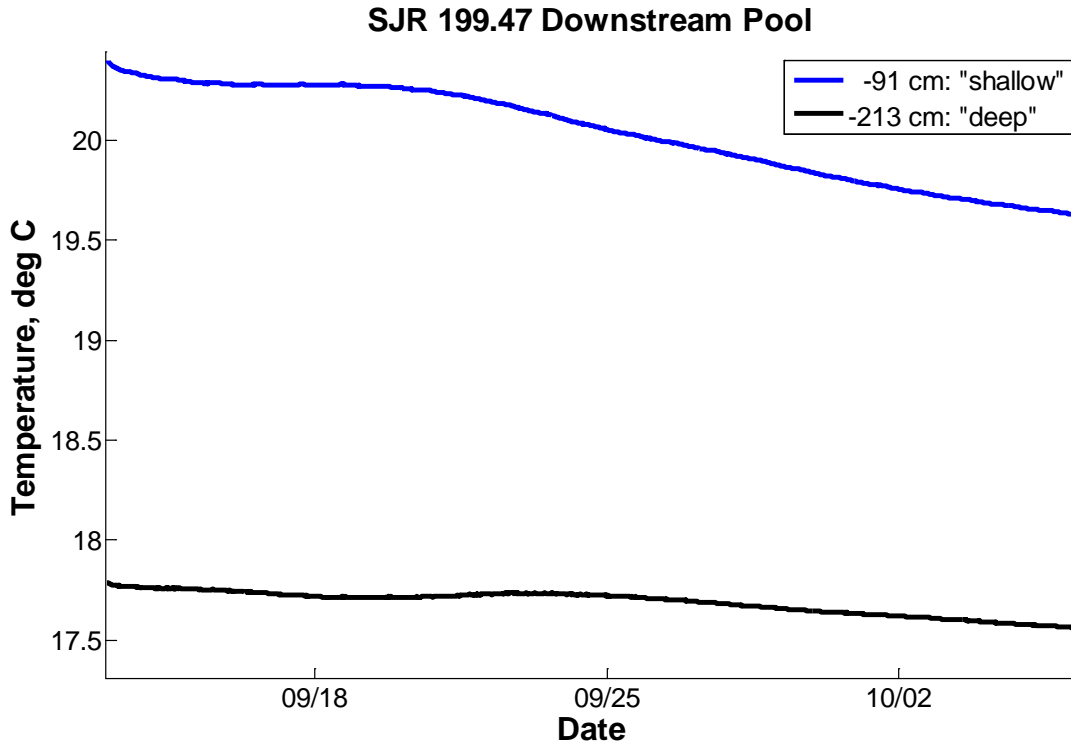


Figure A-24: Variation in subsurface water temperature at SJR 199.47 location.

Subsurface water temperature was not influencing the surface water temperature in the downstream pool SJR 199.47. Hydraulic head at the streambed was greater than hydraulic head in the shallow or deep piezometer indicating flow was down through the streambed and into the subsurface (Figure A-25). Hydraulic head at SJR 199.47 Sensor - 91 cm increased during the entire instrumentation period, but it increased at a progressively slower rate. The increasing hydraulic head was the response curve as the hydraulic head approached but never reached its quasi-equilibrium state.

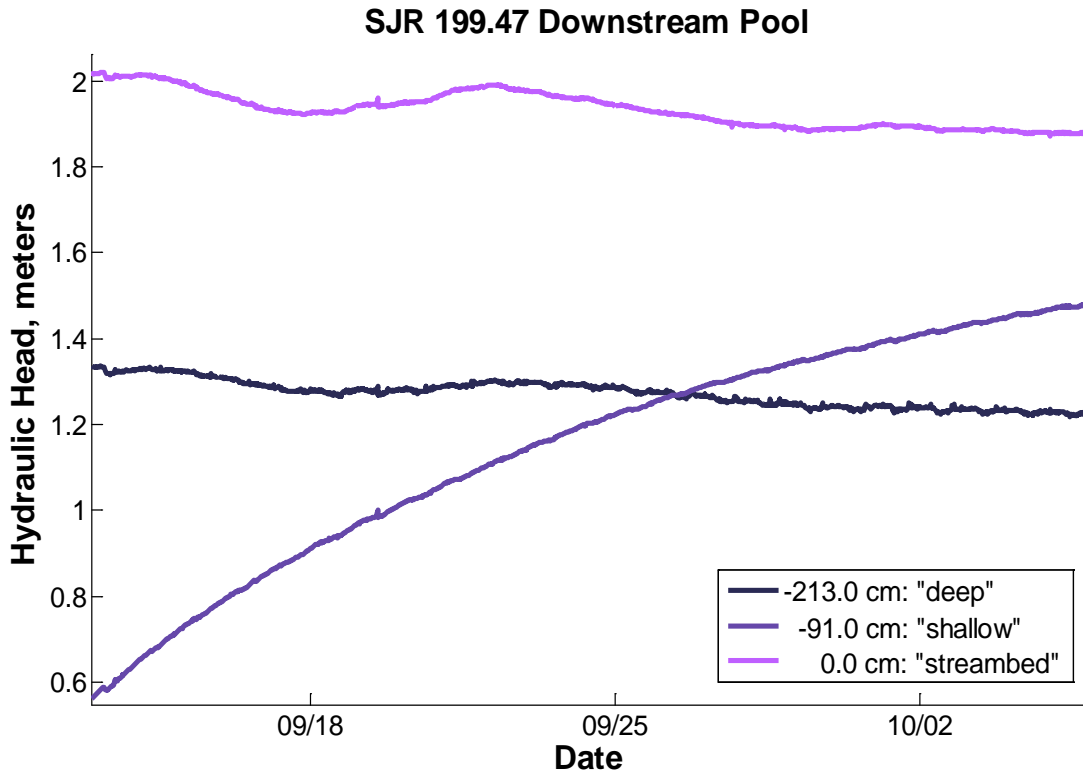


Figure A-25: Variation in hydraulic head at SJR 199.47.

San Joaquin River 204 Sensor Array Site (SJR 204)

The furthest downstream San Joaquin River sensor array site was located in Reach 5 at approximately river mile 204.6 (SJR 204). It was downstream of the San Joaquin River's confluence with the Eastside Bypass and immediately downstream of the CA Highway 140 bridge (Figure A-26).

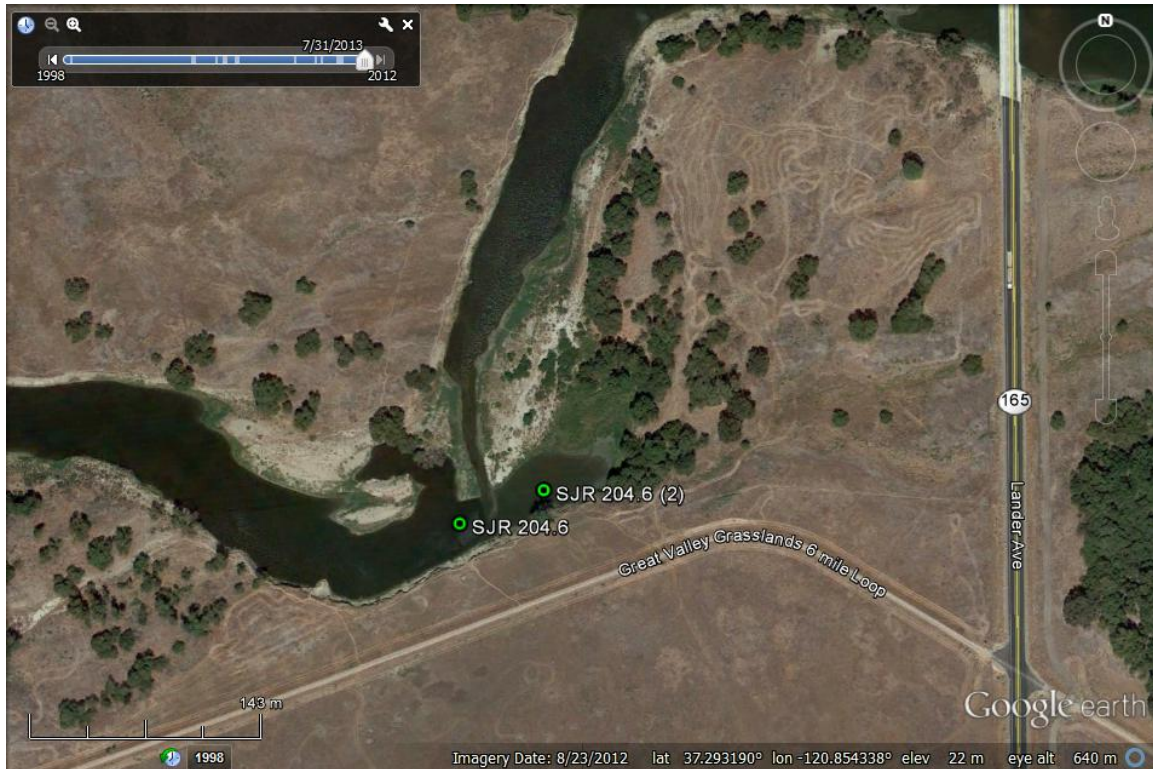


Figure A-26: Aerial view of the San Joaquin River site SJR 204 taken on 8/23/2012.

Four sensor arrays were deployed at SJR 204 from October 13, 2012 until October 30, 2012. To measure the shallow and deep subsurface water conditions, two sensor arrays were installed at the upstream backwater pool location, while the other two sensor arrays were installed in the downstream pool (Figure A-27). A combination of Onset Hobo U22-001, Solinst Levellogger Gold, and Levellogger Edge sensors were used to measure water temperature and level. The upstream sensor arrays in the backwater pool at SJR 204.6(2) placed water temperature sensors at the streambed (0 cm), below the streambed (-12 cm), in the shallow subsurface (-59 cm), and in the deep subsurface (-130 cm). The downstream sensor arrays in SJR 204.6 had twelve water temperature sensors placed vertically through the surface water of the pool in addition to water temperature sensors at the streambed (0 cm), in the shallow subsurface (-36 cm), and in the deep subsurface (-122 cm).

San Joaquin River Restoration Program 2012 Thermal Refugia Study

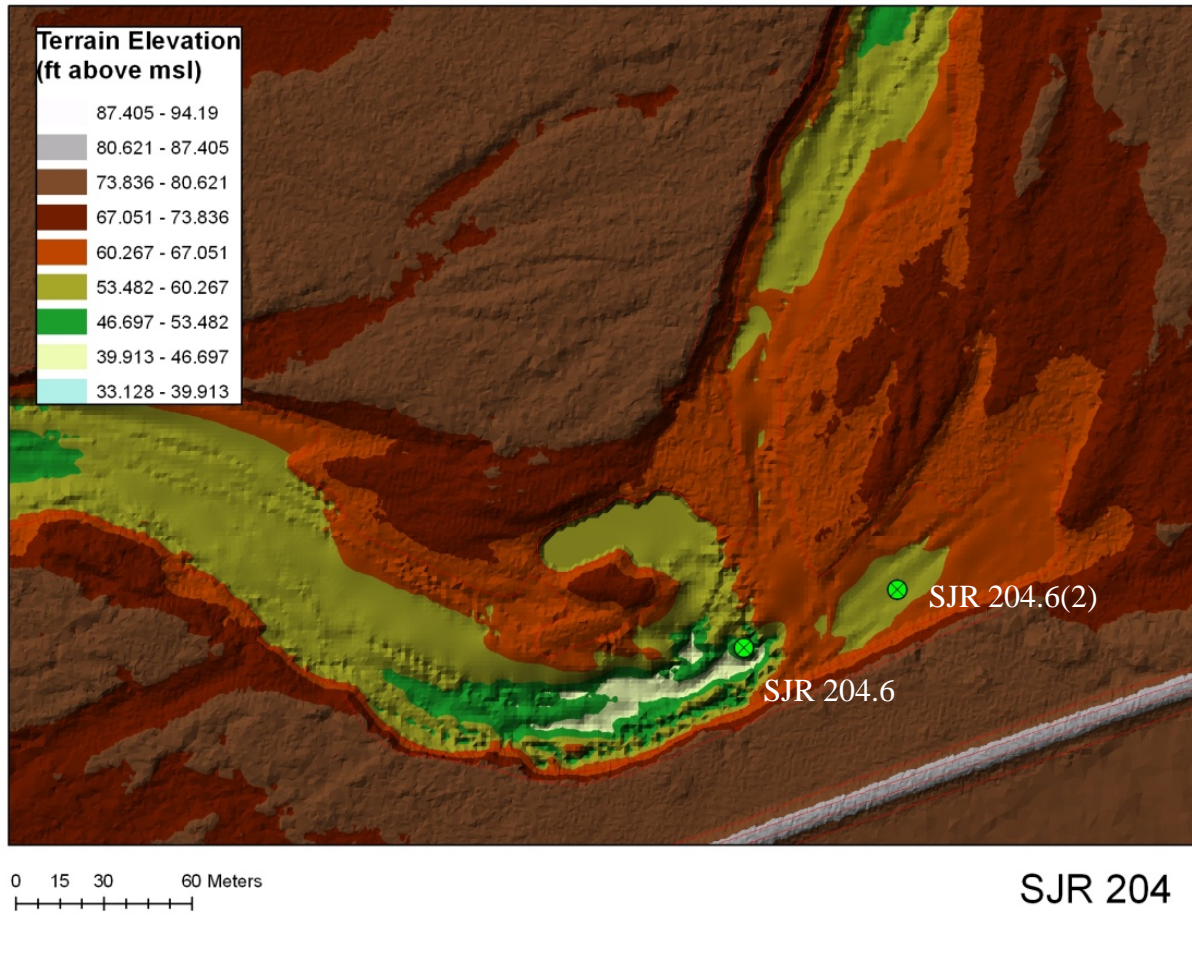


Figure A-27: San Joaquin River System digital terrain model plan view of the San Joaquin River sensor array site SJR 204.

SJR 204.6(2) Upstream Location

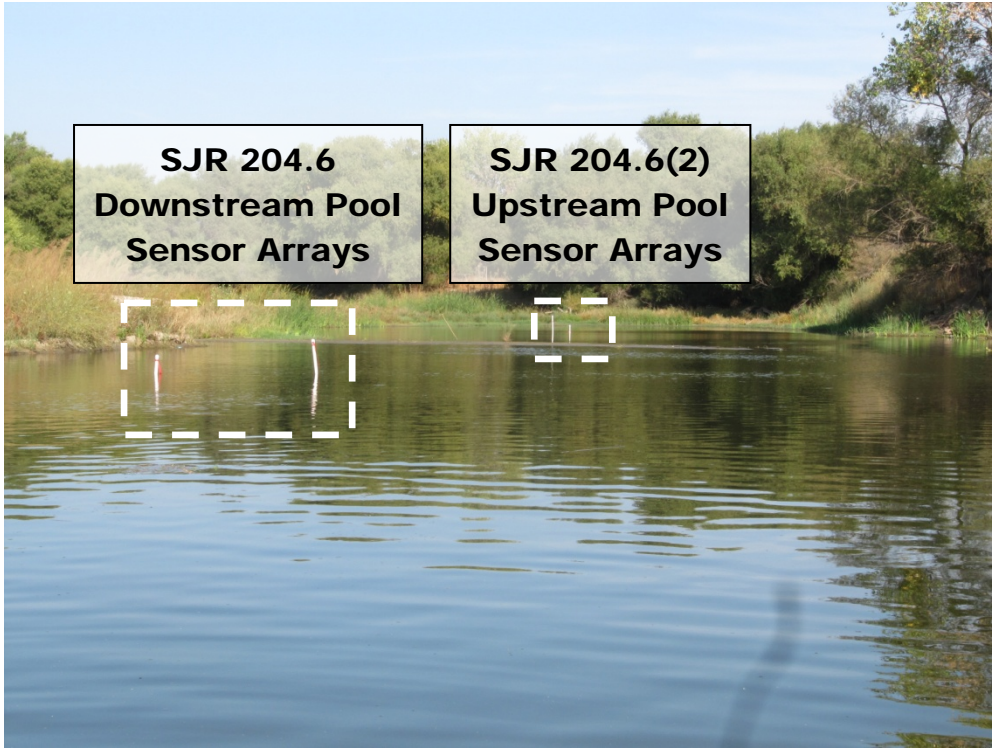


Figure A-28: SJR 204.6 pool sensor arrays looking upstream.

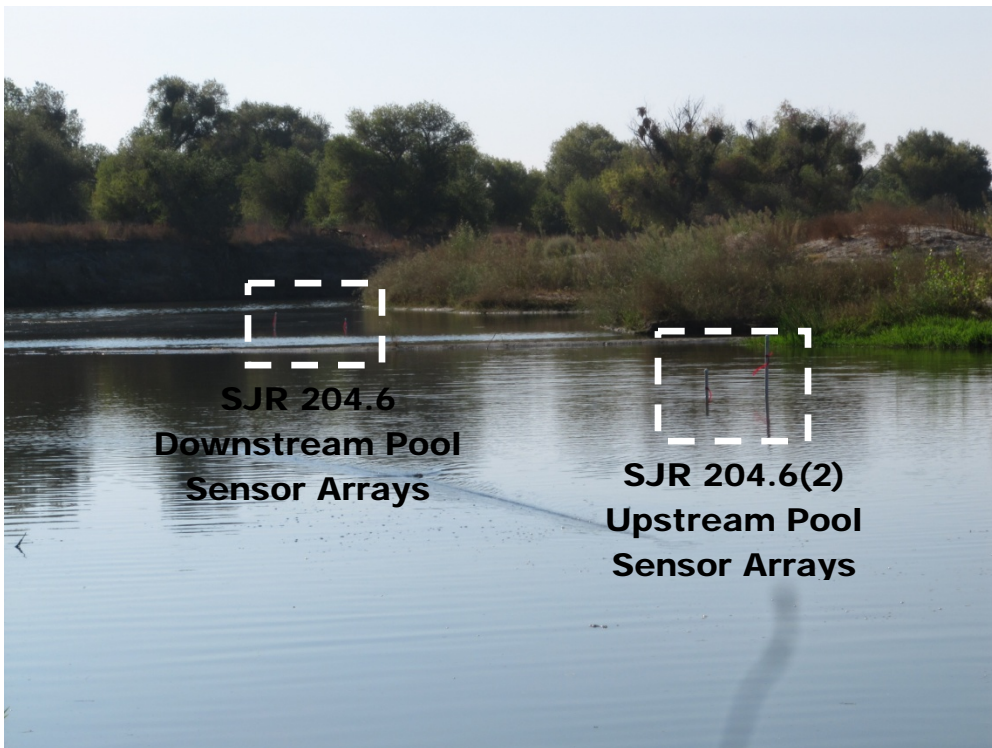


Figure A-29: SJR 204.6 pool sensor arrays looking downstream.

Subsurface water temperature at SJR 204.6(2) increased with depth into the streambed during most of the instrumentation period, but water temperature trends with depth were not constant during the entire time (Figure A-30). Between 10/15 and 10/22, the water temperature trends with depth changed with the streambed water temperature (0 cm) becoming greater than subsurface water temperature. Subsurface water temperature also exhibited two key changes during this period suggesting a change in subsurface flow conditions. First, near streambed water temperature (-12 cm) increased until it was greater than shallow (-59 cm) and deep (-130 cm) subsurface water temperature. Second, the average daily change in water temperature ($dT_{\text{avg daily}}$) at -59 cm and -130 cm decreased between 10/15 and 10/22. Initially, $dT_{\text{avg daily}}$ was 0.59°C at -59 cm and 0.27°C at -130 cm, but during that one week period, $dT_{\text{avg daily}}$ was 0.29°C at -59 cm and 0.22°C at -130 cm. After 10/22, $dT_{\text{avg daily}}$ was 0.58°C at -59 cm and 0.40°C at -130 cm suggesting again subsurface flow had changed.

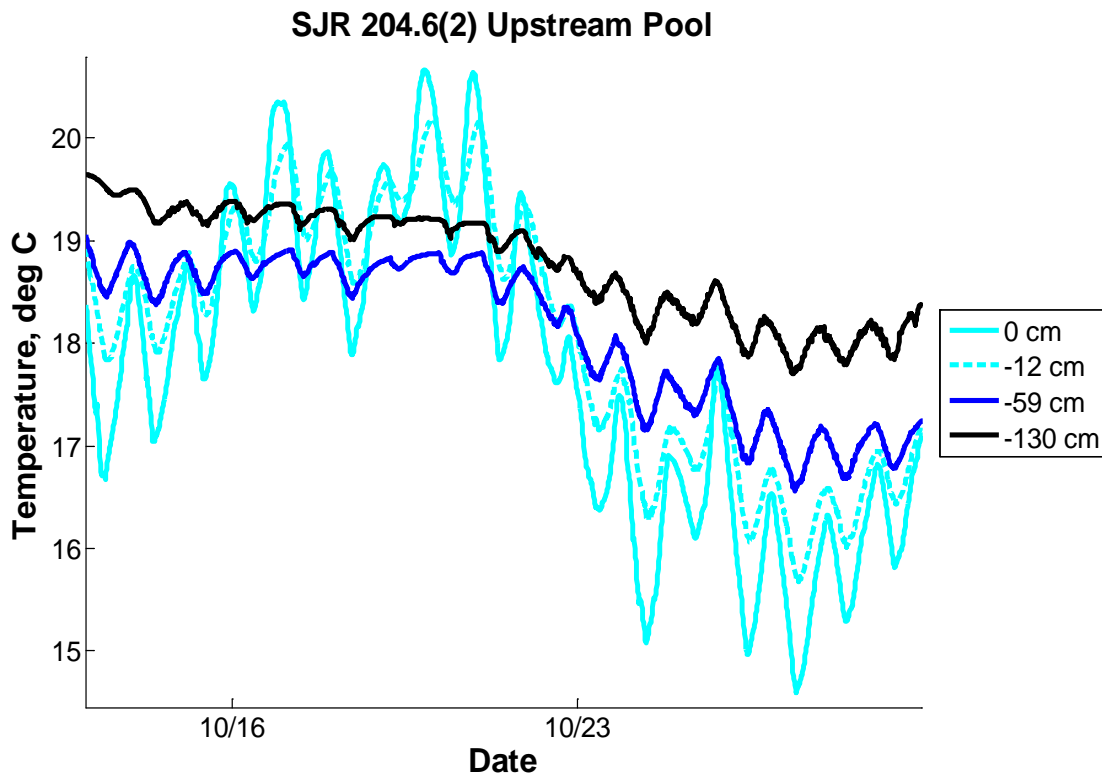


Figure A-30: Water temperature data showed a diurnal variation from the streambed level to 130 cm below the streambed at the SJR 204.6(2) upstream backwater pool location.

During the one week period when the pool thermal environment behaved differently, the water level in the backwater pool rose above 0.83 m (Figure A-31). The water level dropped below 0.83 m again on 10/22 corresponding to the day the subsurface thermal environment reverted back to its previous behavior. Water level remained below 0.83 m during the rest of the instrumentation period.

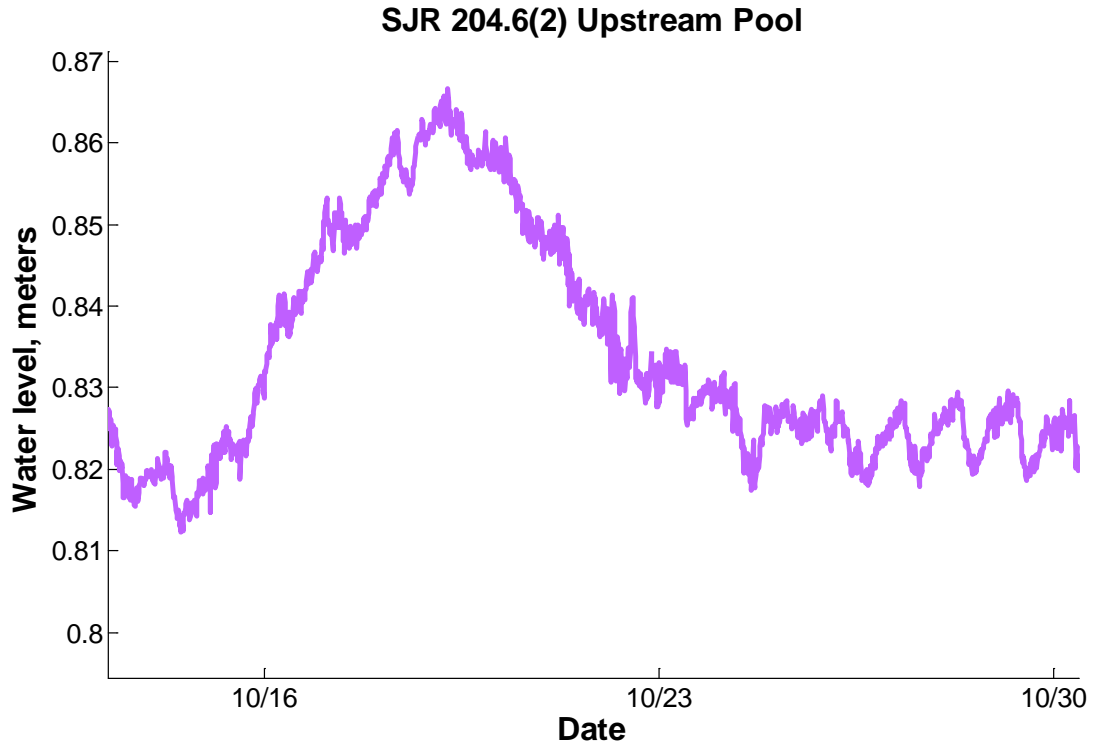


Figure A-31: Water level in SJR 204.6(2) peaked between 10/15 and 10/22 corresponding with the time the subsurface thermal environment changed.

Hydraulic head data indicated the backwater pool at SJR204.6(2) was gaining with hydraulic head increasing with depth near the streambed (Figure A-32). Hydraulic head between 0 cm and -59 cm indicated subsurface flow was upwelling, but hydraulic head between -59 cm and -130 cm indicated subsurface flow was downwelling. It is unclear from the data why this inconsistency existed, but it was hypothesized that a low hydraulic conductivity sediment layer existed between -59 cm and -130 cm that formed a perched higher hydraulic head region near the streambed. Differences in the response time of the shallow and deep piezometers indicated hydraulic conductivity was different between -59 cm and -130 cm. The deep (-130 cm) piezometer had a response time of approximate 9 days until the hydraulic head reached a quasi-steady state equilibrium. The shallow (-59 cm) piezometer also exhibited a response time for the hydraulic head, but it was only 6 hours.

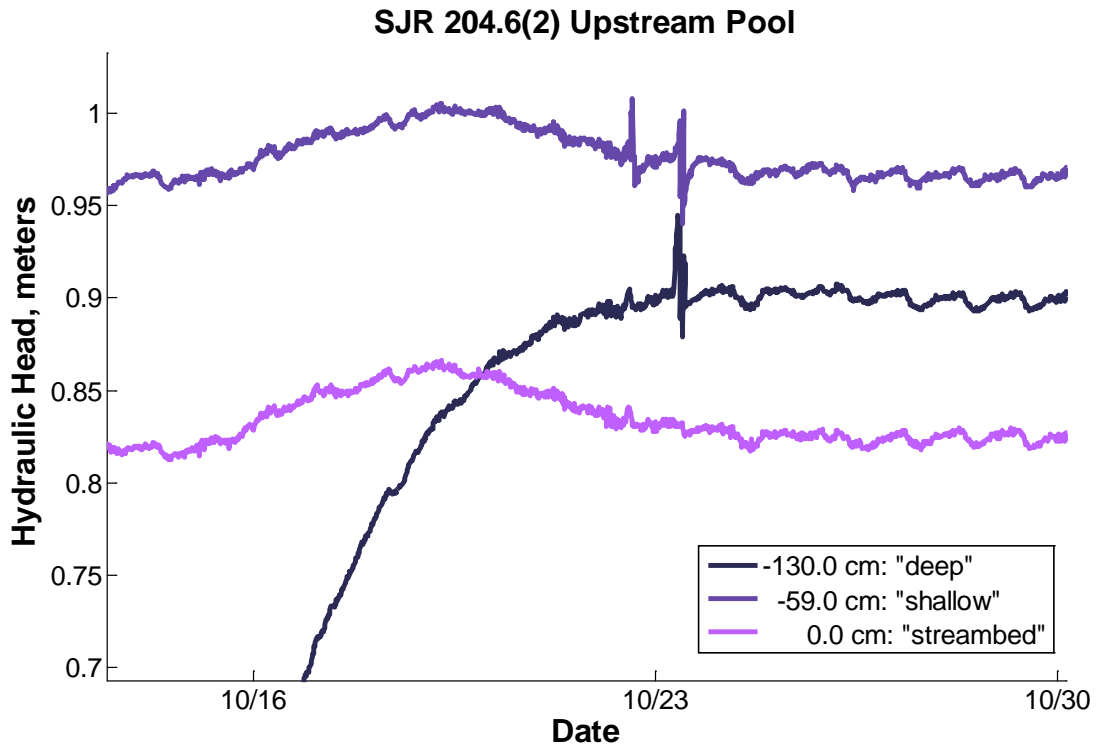


Figure A-32: Variation in hydraulic head with depth into the subsurface at SJR 204.6(2) upstream backwater pool location.

Hydraulic head data at 0 cm and -59 cm showed a peak during the one week when the subsurface thermal conditions changed. Changes in hydraulic head at SJR 204.6(2) Sensor -59 cm tracked the changes in hydraulic head at SJR 204.6(2) Sensor 0 cm suggesting the change in surface water level in the pool influenced the near streambed hydraulic head, subsurface flow, and hence the thermal conditions with depth.

SJR 204.6 Downstream Location

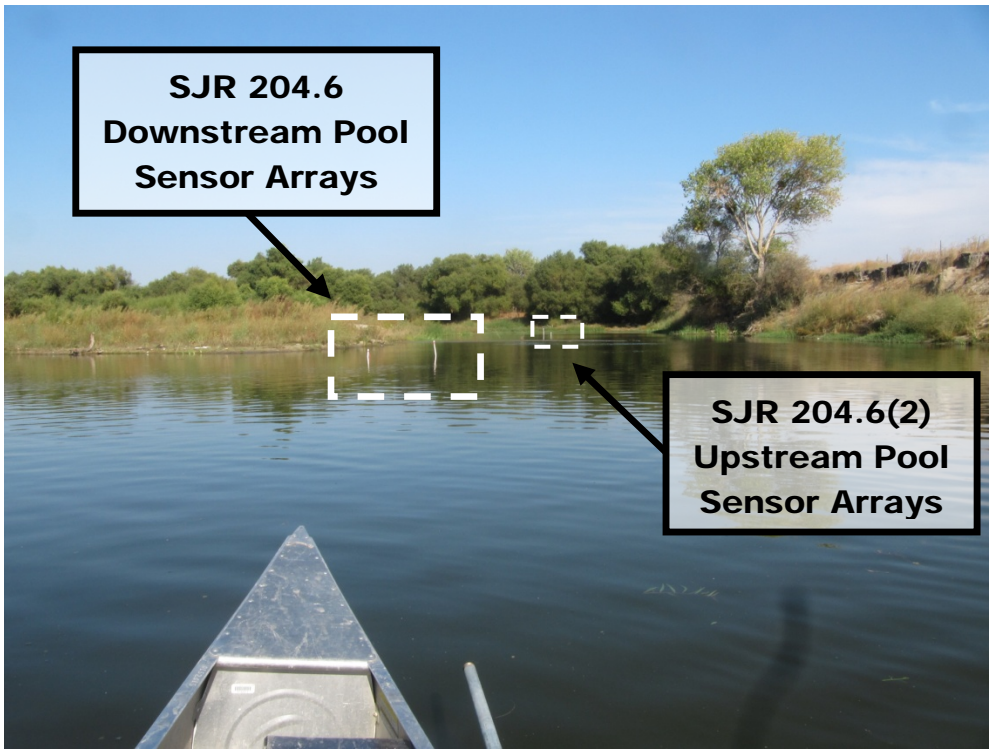


Figure A-33: SJR 204.6 pool sensor arrays looking upstream.

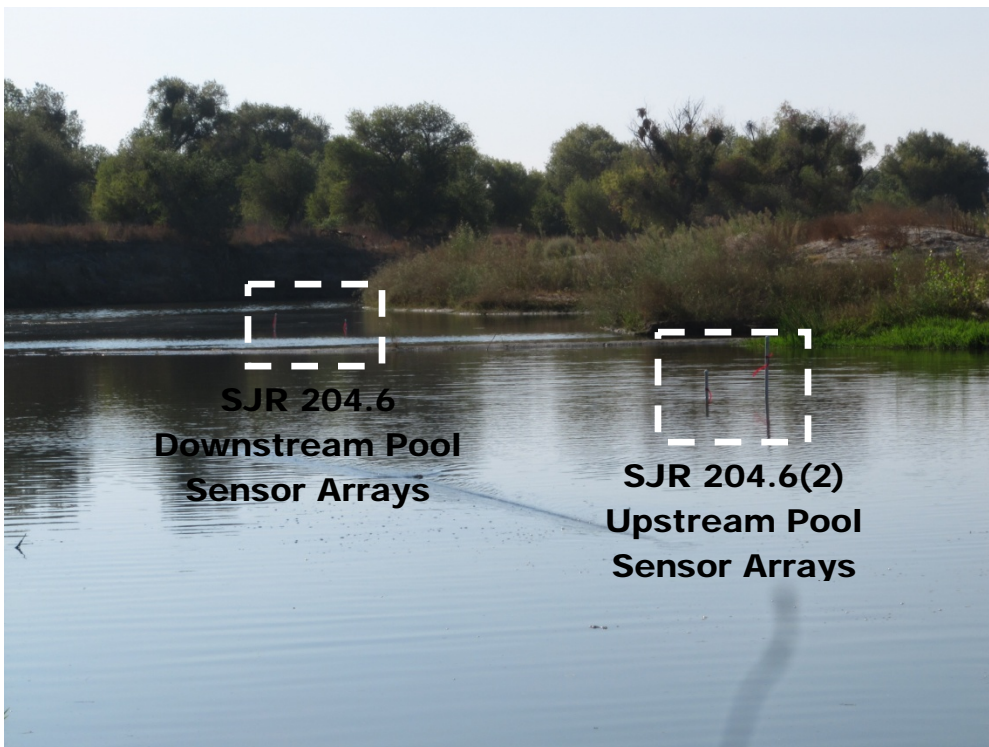


Figure A-34: SJR 204.6 pool sensor arrays looking downstream.

Water temperature data from all sensors at SJR 204.6 are plotted in Figure A-35. Water temperature sensors are labeled based on their depth in centimeters above or below the streambed with the streambed level being zero. Depths greater than zero measured surface water temperatures, while depths less than zero were sensors that measured subsurface water temperatures. Surface water temperature data indicated that daily thermal stratification occurred in the pool at SJR 204.6 during the entire instrumentation period. The maximum daily thermal stratification between the top sensor closest to the air-water interface (SJR 204.6 Sensor 447) and the streambed sensor (SJR 204.6 Sensor 0) varied daily and ranged from 0.73°C to 5.62°C with an average daily thermal stratification of 3.42°C. Thermal stratification was primarily the result of the water temperature near the air-water interface increasing during the day more than the water temperature near the streambed. Daily water temperature variation at SJR 204.6 Sensor 447 ranged from 1.26°C to 5.02°C while the daily water temperature variation at SJR 204.6 Sensor 0 ranged from 0.14°C to 1.02°C.

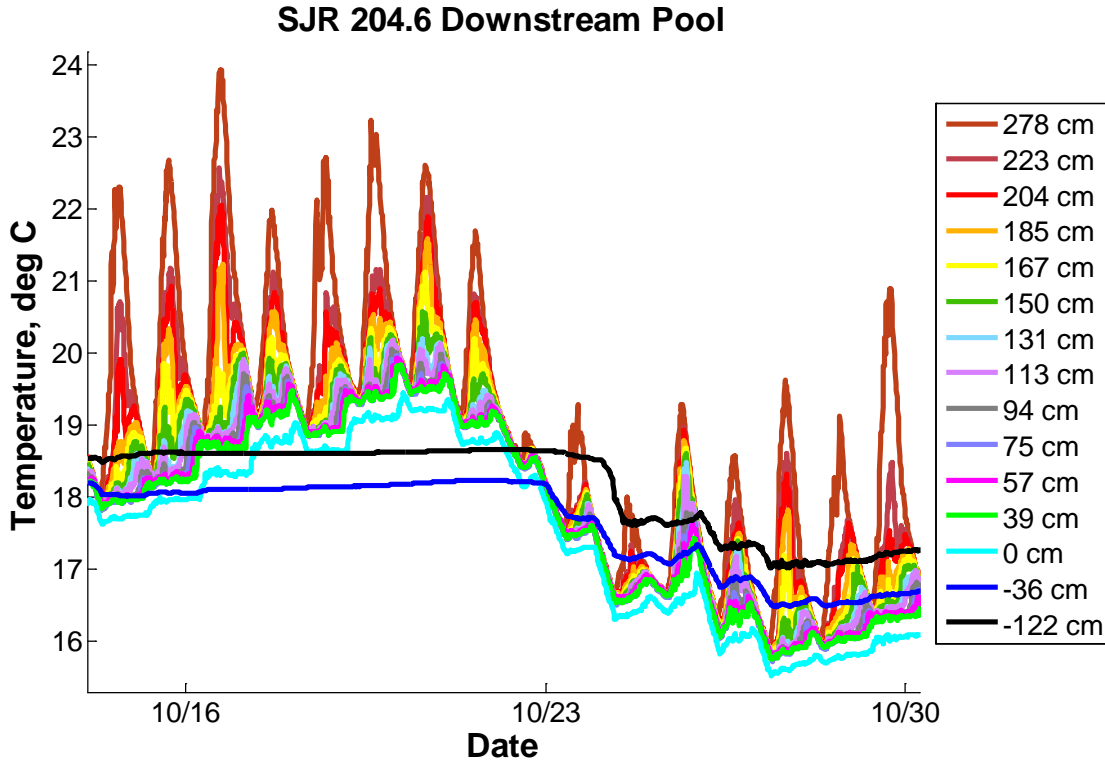


Figure A-35: Variation in surface and subsurface water temperature showed daily thermal stratification from 10/14 to 10/30 at SJR 204.6.

Water temperature in the subsurface was increasing with depth though it varied whether the streambed (SJR 204.6 Sensor 0) water temperature was greater or less than the subsurface water temperature. When surface water temperature peaked between 10/16 and 10/23, the streambed water temperature was greater than subsurface water temperatures. During the rest of the instrumentation period, streambed temperature was less than subsurface water temperature so upwelling subsurface water flow would not have provided any cooling to the pool.

Subsurface water temperature trends at -36 cm and -122 cm were similar, but water temperature variations at -122 cm tended to have a smaller amplitude and peak later than water temperature variations at -36 cm. Changes in subsurface water temperature variations corresponded to changes in pool depth suggesting surface water level was an important control on subsurface thermal conditions (Figure A-36 and Figure A-37). Between 10/16 and 10/23 when the subsurface water temperature showed no daily water temperature variations, the pool depth was greater than 3.01 m. After 10/23, the pool depth decreased below 3.01 m and subsurface water temperature began showing daily variations again with the average daily variation in subsurface water temperature at -36 cm being 0.32 °C.

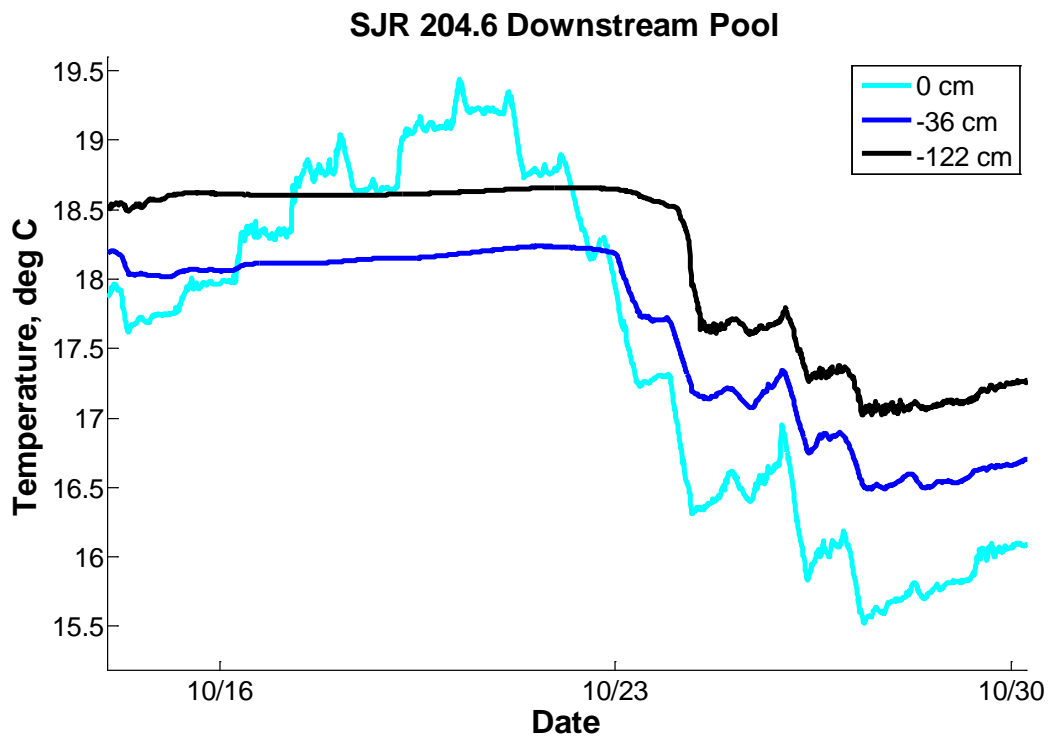


Figure A-36: Reduced subsurface water temperature variations between 10/16/2012 and 10/23/2012 corresponded to changes in surface water level at SJR 204.6.

SJR 204.6 Downstream Pool

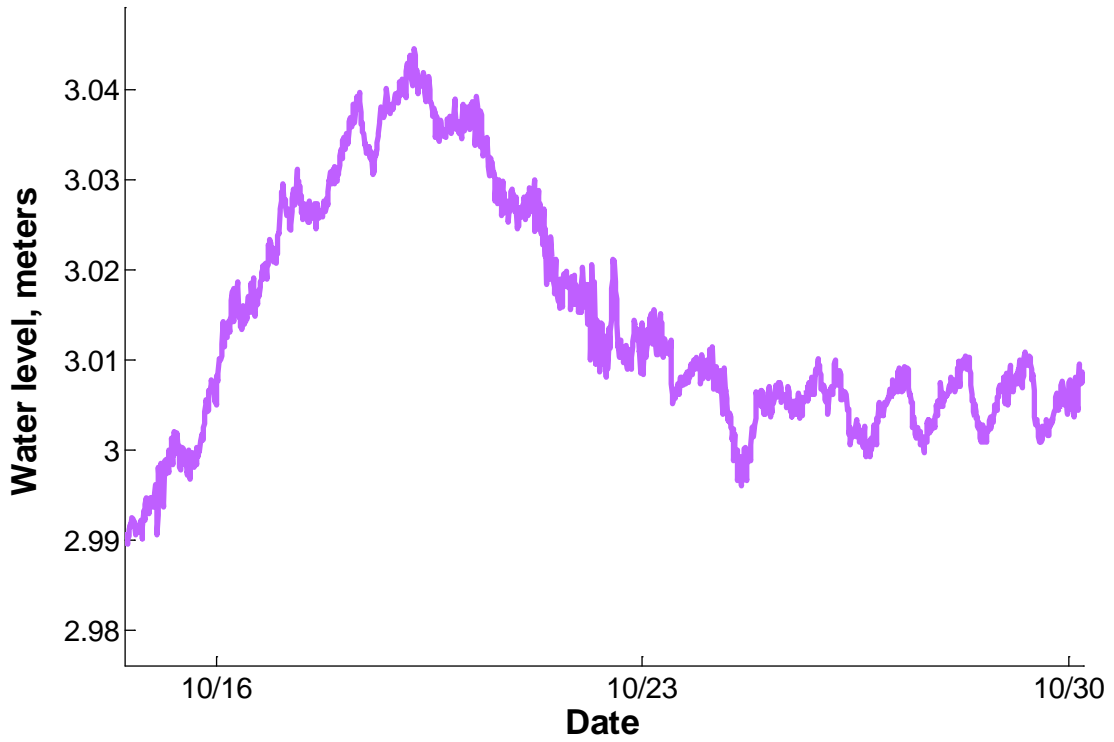


Figure A-37: SJR 204.6 water level increased above 3.01 m between 10/16/2012 and 10/23/2012 and corresponded to decreased subsurface water temperature variations.

Hydraulic head decreased towards the streambed indicating the subsurface flow was consistently upwelling during the instrumentation period (Figure A-38). Hydraulic head at all depths below the streambed peaked when the surface water level increased above 3.01 m.

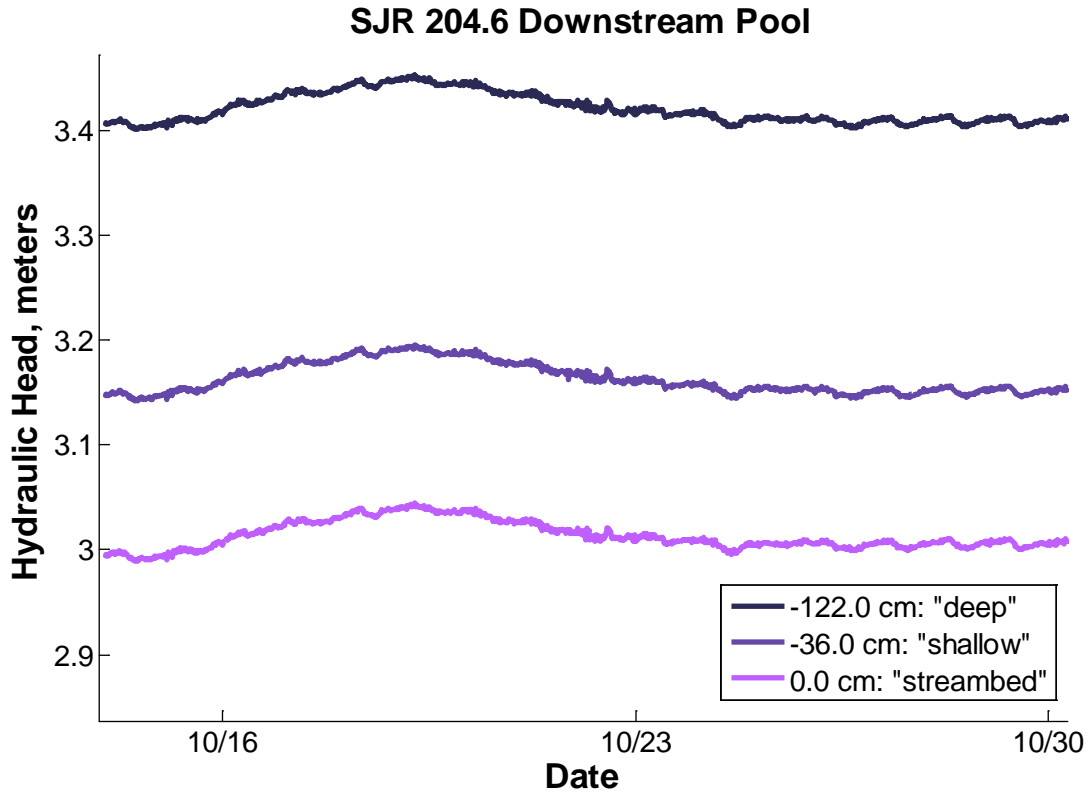


Figure A-38: Variation in hydraulic head with depth into the subsurface at SJR 204.6 downstream pool.

Eastside Bypass 22.4 Sensor Array Site (ESB 22)

The furthest upstream Eastside Bypass sensor array site was located in the Merced National Wildlife Refuge upstream of the intersection of Dan McNamara Road and West Sandy Mush Road. ESB 22 is approximately 22.4 miles downstream of the confluence of the Chowchilla Bypass with the Fresno River (Figure A-39).

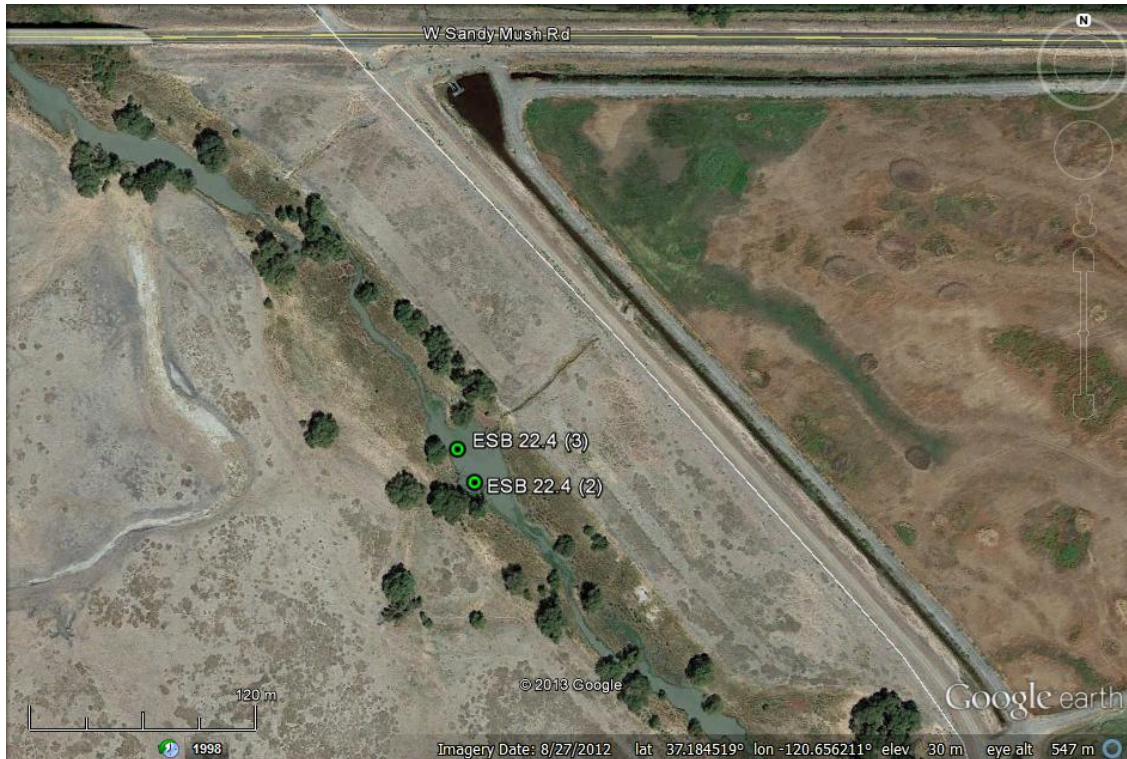
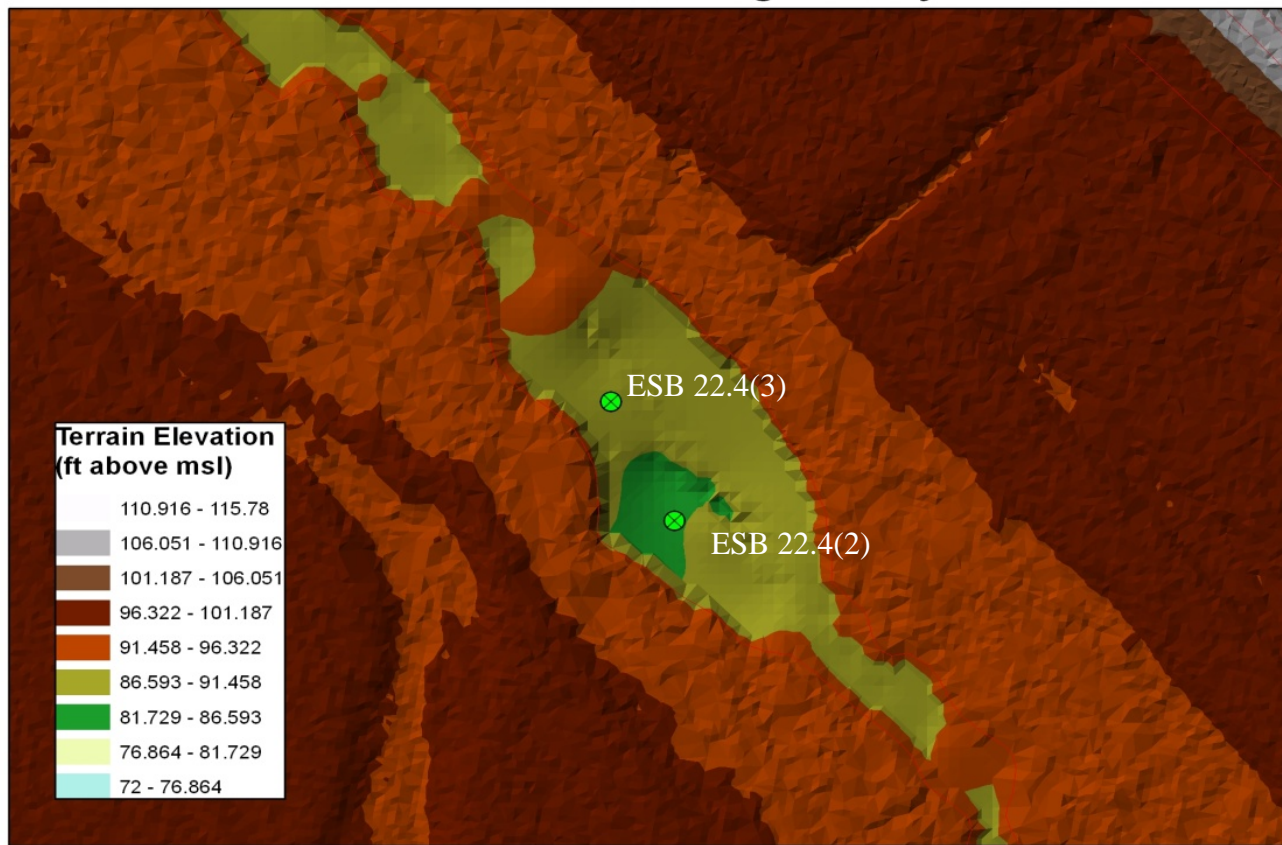


Figure A-39: Aerial view of the Eastside Bypass taken on 8/23/2012 showing sensor array site ESB 22.

Four sensor arrays were deployed at ESB 22 from October 12, 2012 until October 29, 2012. ESB 22 was a single pool with shallow, vegetated glides upstream and downstream. Sensor arrays were installed in upstream and downstream locations of the single pool. Two sensor arrays were installed in the deepest middle section of the ESB 22 pool while the other two sensor arrays were installed at the downstream tail of the pool (Figure A-40). Onset Hobo U22-001, Solinst Levellogger Gold, and Levellogger Edge sensors were used to measure water temperature and level. The upstream sensor arrays at ESB 22.4(2) had ten water temperature sensors placed vertically in the surface water of the pool in addition to water temperature and level sensors at the streambed (0 cm), in the shallow subsurface (-23 cm), and in the deep subsurface (-67 cm). The downstream sensor arrays towards the pool tail at ESB 22.4(3) had water temperature and level sensors at the streambed (0 cm), in the shallow subsurface (-32 cm), and in the deep subsurface (-52 cm). It was not possible to install piezometers completely vertically at ESB 22 because the streambed sediments were extremely resistant to driving. The angles of the piezometers from vertical were measured after being driven into the streambed and correction factors were applied to sensor depth.

San Joaquin River Restoration Program 2012 Thermal Refugia Study



ESB 22

Figure A-40: San Joaquin River System digital terrain model plan view of the Eastside Bypass sensor array site ESB 22.

ESB 22.4(2) Upstream Location



Figure A-41: ESB 22.4 pool looking upstream from the right bank.



Figure A-42: ESB 22.4 pool viewed from the right bank.



Figure A-43: ESB 22.4 pool looking downstream from the right bank.

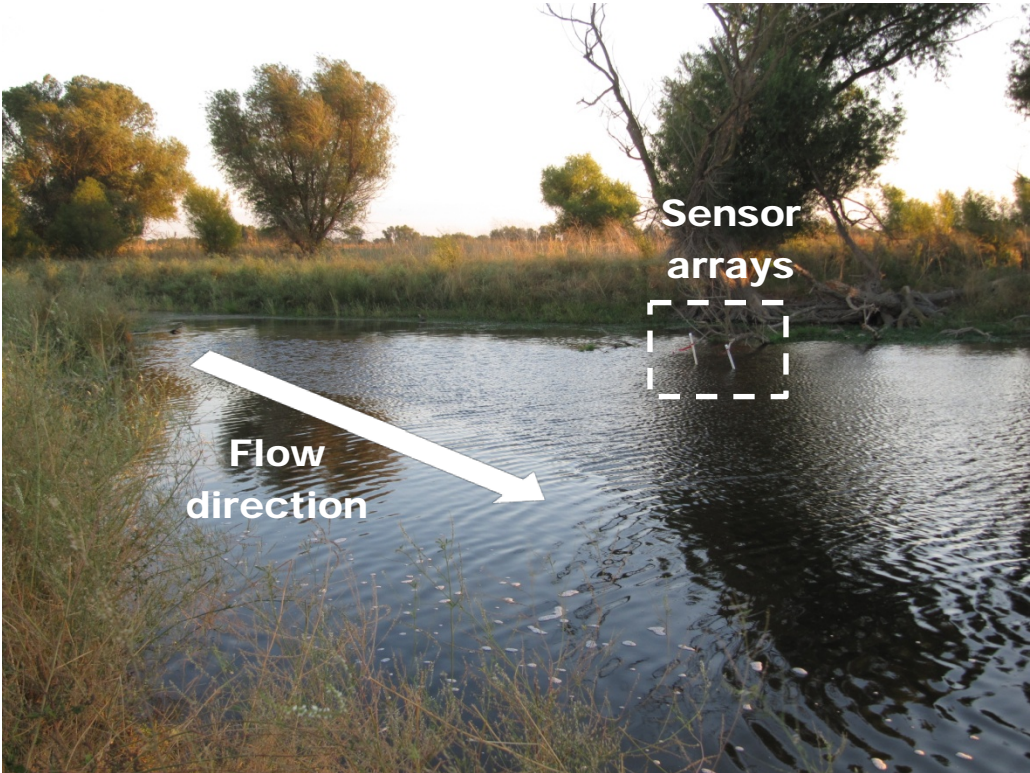


Figure A-44: ESB 22.42(2) pool upstream sensor arrays looking upstream from the right bank.

Water temperature data from all sensors at ESB 22.4(2) are plotted in Figure A-45. Water temperature sensors are labeled based on their approximate depth in centimeters above or below the streambed with the streambed level being zero. Depths greater than zero indicate sensors measuring surface water temperatures, while depths less than zero are sensors measuring subsurface water temperatures.

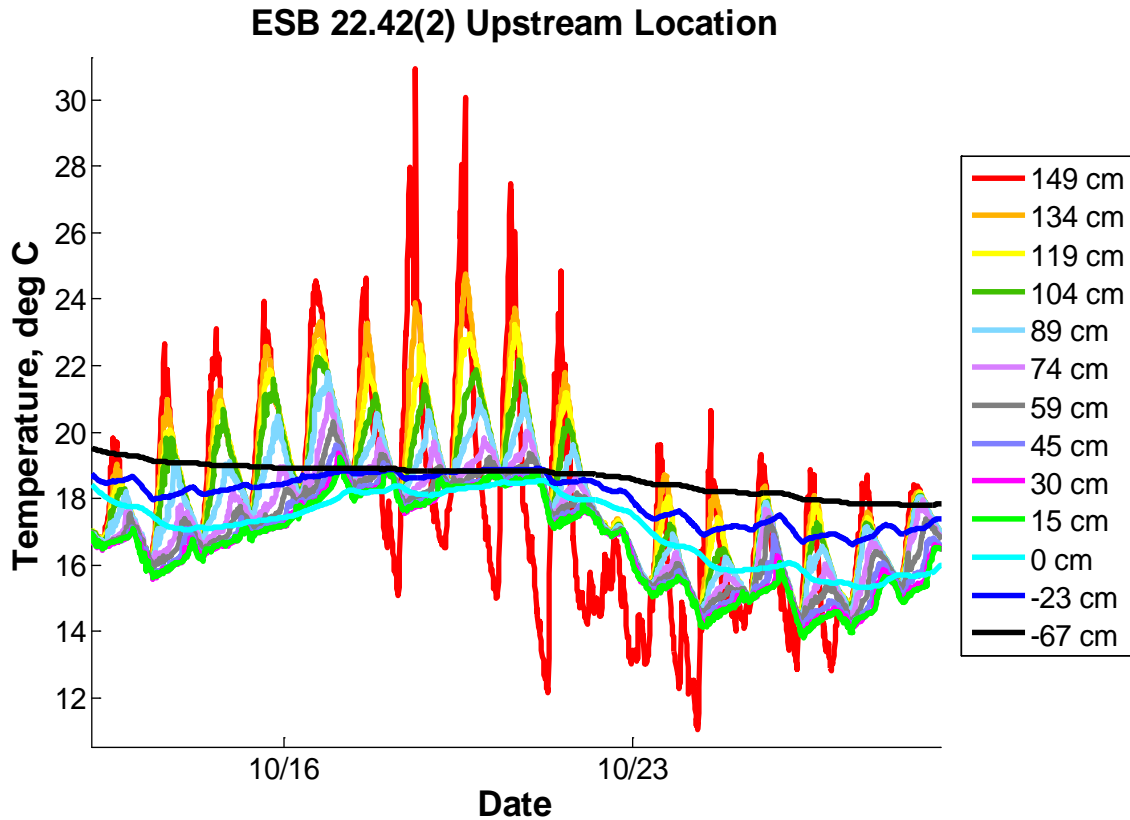


Figure A-45: Variation in surface and subsurface water temperature showed daily thermal stratification from 10/12 to 10/29 at the upstream sensor array location ESB 22.4(2).

Daily thermal stratification occurred at the upstream location of the ESB 22.4 pool during the entire instrumentation period. ESB 22.4 (2) Sensor 149 was identified as being out of the water between 10/17 and 10/27. During this period, the amplitude of the temperature variation in Sensor 149 increased and the cooler temperature measured by Sensor 149 would have been an unstable condition. Cool water is denser than warm water and would have mixed quickly so Sensor 149 had to have measured air temperature rather than water temperature. The period the sensor was out of water also corresponded directly with the period water level in the pool was less than 1.6 m (Figure A-46)

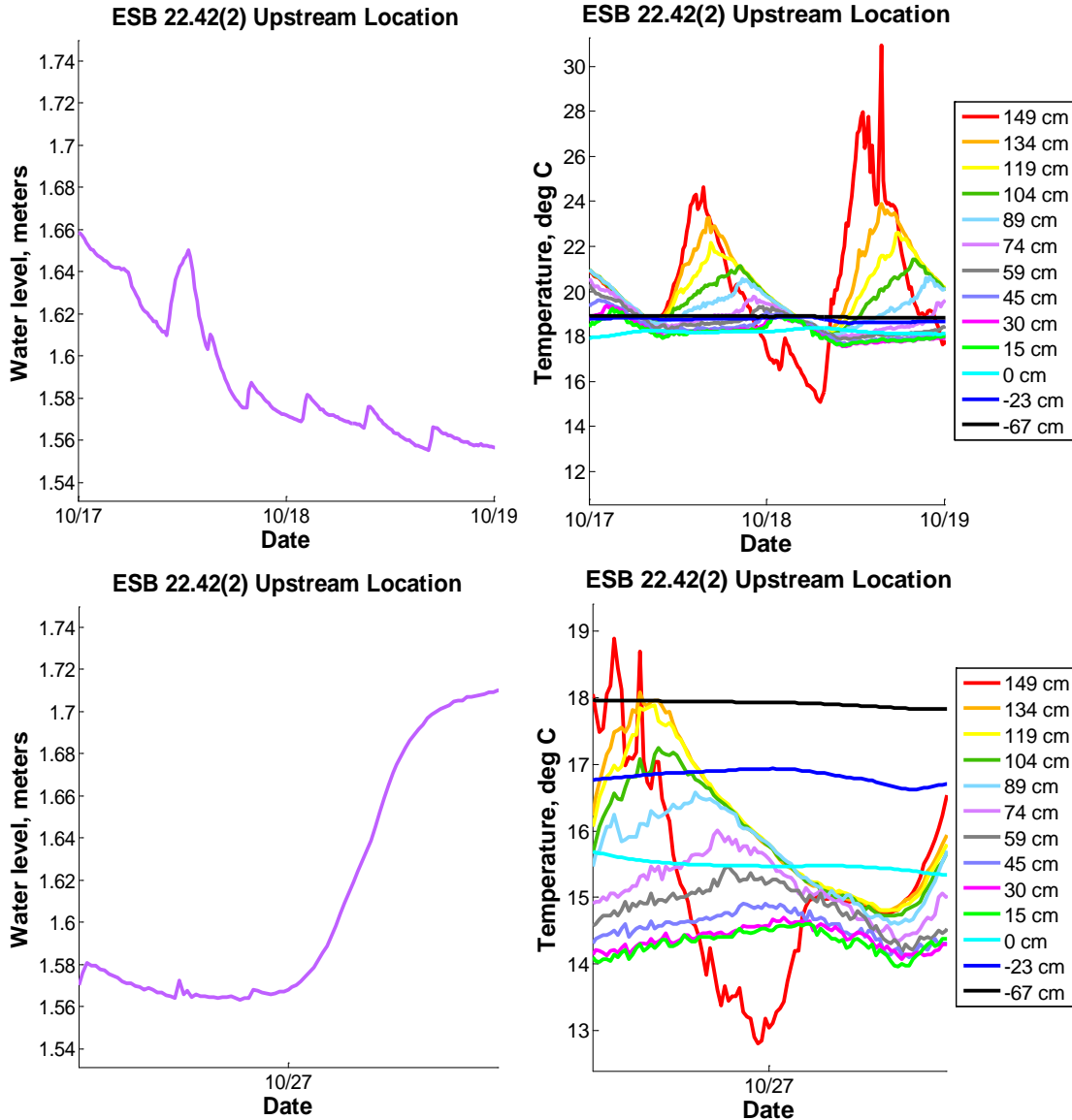


Figure A-46: Correlation between changes in pool depth and temperature recorded by ESB 22.4 (2) Sensor 149cm at ESB 22.4(2).

The maximum daily thermal stratification between the top sensor closest to the air-water interface (ESB 22.4(2) Sensor 149 or ESB 22.4(2) Sensor 134) and the streambed sensor (ESB 22.4(2) Sensor 15) varied daily and ranged from 0.81°C to 6.92°C with an average daily thermal stratification of 4.86°C. Similar to sites on the San Joaquin River, thermal stratification primarily occurred because water temperature near the air-water interface increased more than the water temperature near the streambed. Daily water temperature variation at the top sensor closest to the air-water interface (ESB 22.4(2) Sensor 149 or ESB 22.4(2) Sensor 134) ranged from 2.28°C to 6.50°C while the daily water temperature variation at ESB 22.4(2) Sensor 15 ranged from 0.48°C to 1.96°C.

Water temperature in the subsurface generally increased with depth though subsurface water temperature at -23 cm was warmer than at -67 cm from 10/19 to 10/21 (Figure A-

47). Subsurface water temperature at -23 cm and -67 cm showed daily cycles of water temperature variation similar to those found at the streambed (0 cm), but with different amplitudes of temperature variation. The average amplitude of the variation in daily subsurface water temperature was greater at -23 cm than at either 0 cm or -67 cm suggesting subsurface flow was multidimensional. Daily variation in water temperature at -67 cm was most pronounced on days with a large variation in streambed temperature like 10/25. Subsurface water temperature at -23 cm and -67 cm both showed a decreasing trend in average daily water temperature similar to the weekly water temperature trend at the streambed. Streambed water temperature was cooler than subsurface water temperature during the entire instrumentation period so upwelling subsurface water flow would not have provided a cold water source to promote thermal stratification in the pool.

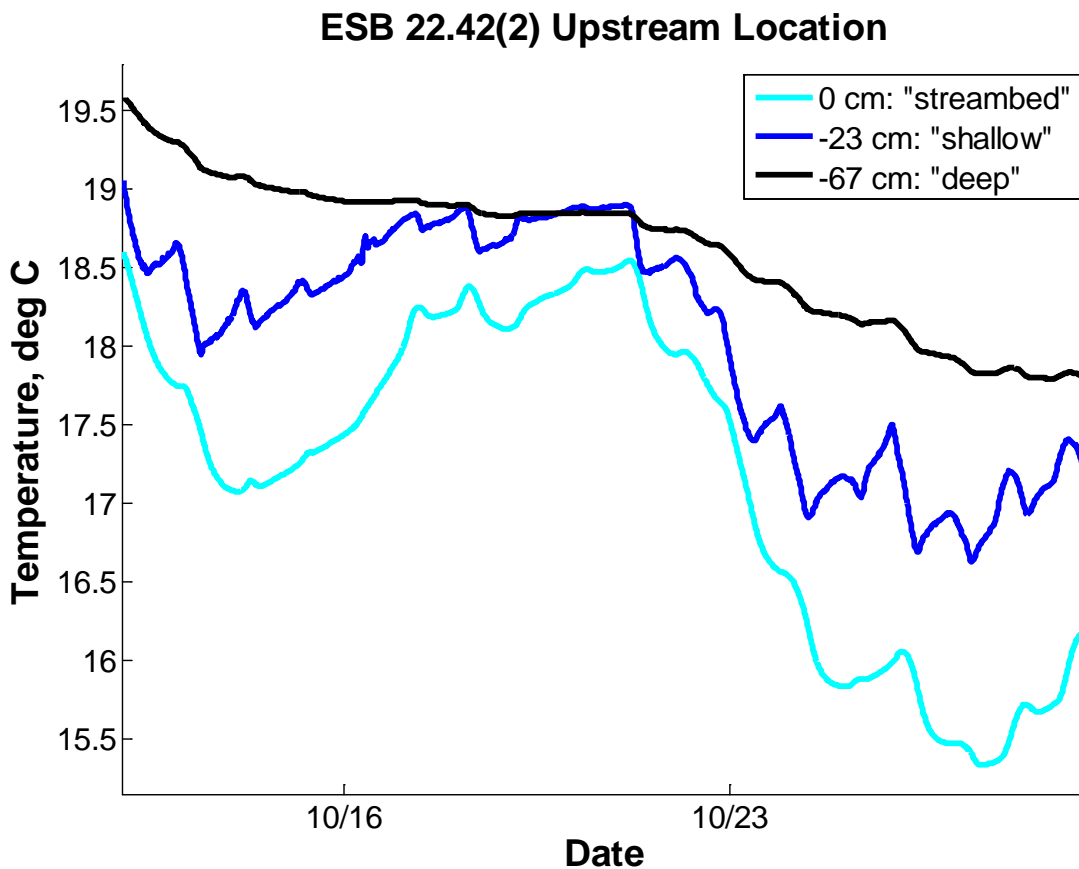


Figure A-47: Variation in subsurface water temperature from 10/12 to 10/29 at ESB 22.4(2).

Hydraulic head at ESB 22.4(2) suggested subsurface flow was multi-dimensional and potentially upwelled into the pool. Hydraulic head at the streambed was less than hydraulic head at both -23 cm and -67 cm (Figure A-48). However, hydraulic head at -23 cm was greater than hydraulic head at -67 cm implying subsurface flow was multi-dimensional and variable with depth. It was hypothesized that a low hydraulic conductivity confining layer existed between ESB 22.4(2) Sensor -23 and ESB22.4(2)

Sensor -67. The low hydraulic conductivity layer between -23 cm and -67 cm formed a perched higher hydraulic head region that resulted in hydraulic head being greater at -23 cm than -67 cm. Hydraulic head at -67 cm had a longer response time to variations in surface water level than the hydraulic head at -23 cm suggesting a lower hydraulic conductivity between -23 cm and -67 cm. When the surface water level increased on 10/27/2012 over the course of approximately 14 hours, the response time of the hydraulic head at -67 cm was 31 hours, while the response time of the hydraulic head at -23 cm was approximately 21 hours. No sediment cores were taken at the site so changes in hydraulic conductivity with depth under the streambed was not be verified. Further measurements of subsurface sediment hydraulic conductivity would be needed to test the hypothesis.

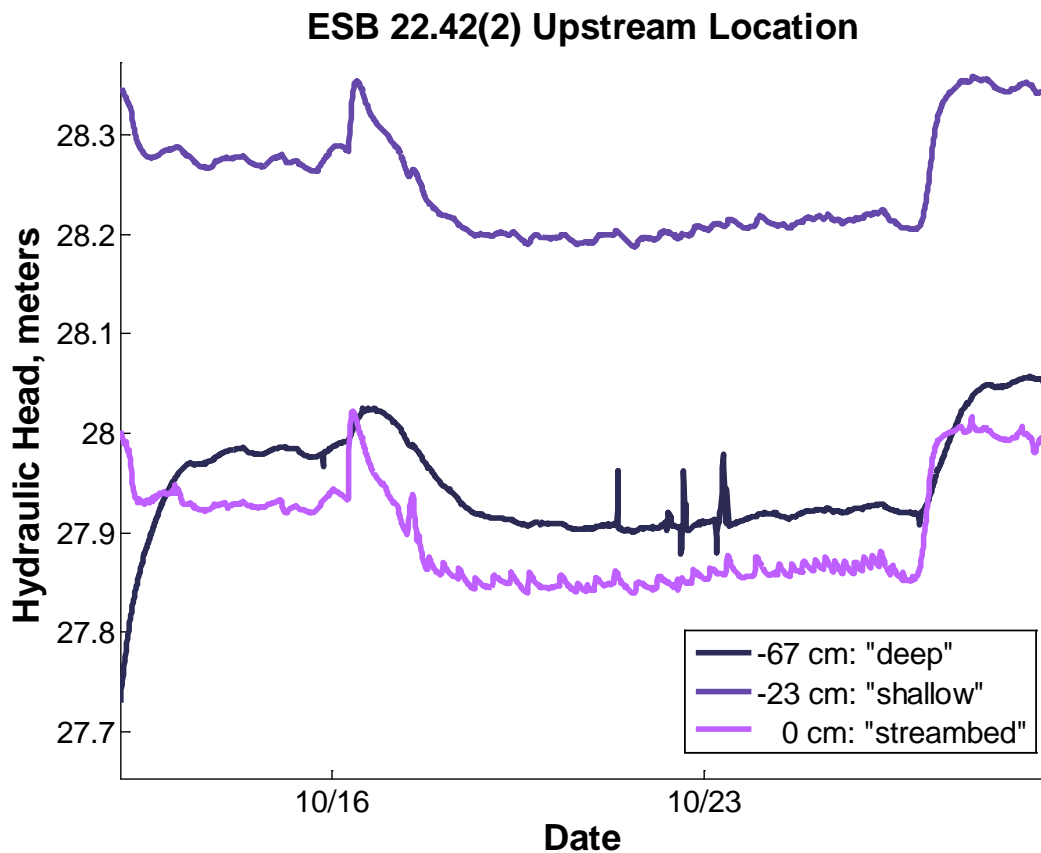


Figure A-48: Variation in hydraulic head with depth into the subsurface at the ESB 22.4(2) upstream pool location.

ESB 22.4(3) Downstream Location



Figure A-49: ESB 22.4 pool looking upstream from the right bank.



Figure A-50: ESB 22.4 pool viewed from the right bank.



Figure A-51: ESB 22.4 pool looking downstream from the right bank.

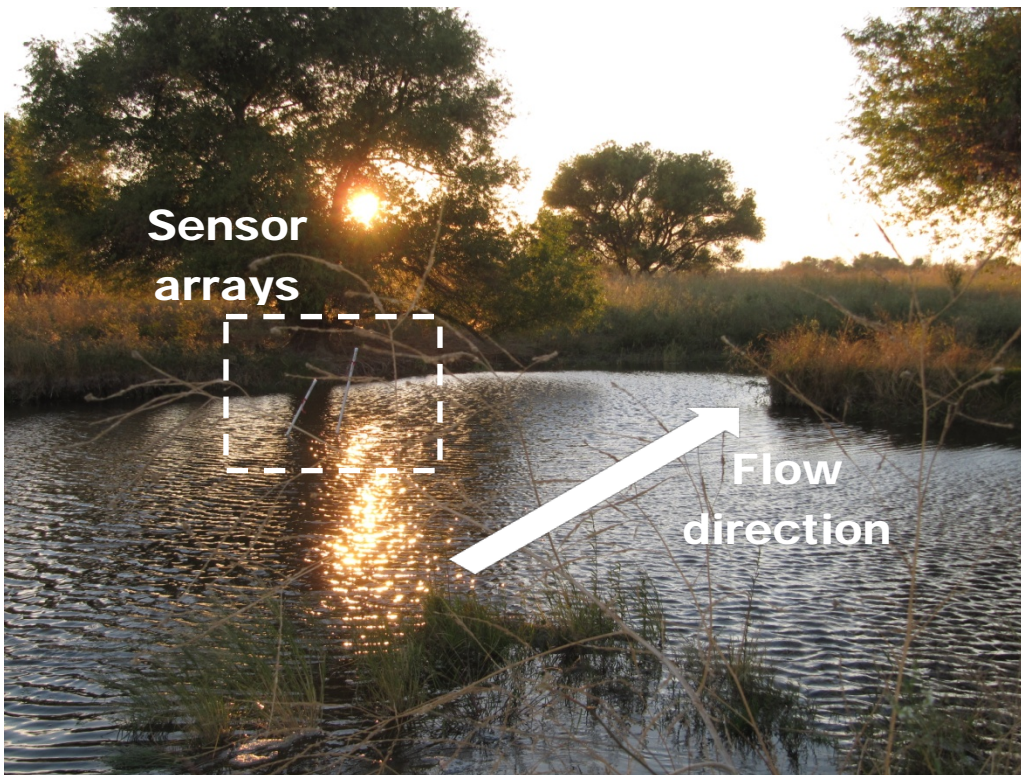


Figure A-52: ESB 22.42(3) pool downstream sensor arrays looking downstream from the right bank.

ESB 22.42(3) Downstream Location

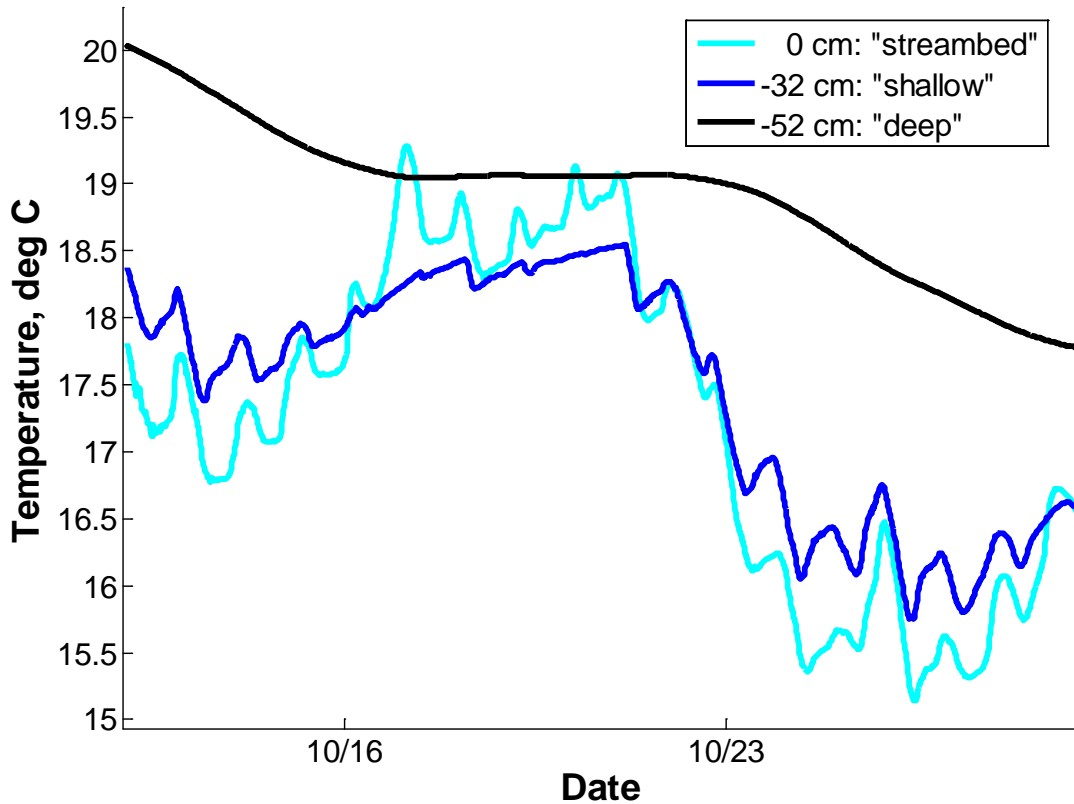


Figure A-53: Variation in subsurface water temperature at the downstream sensory array site ESB 22.4(3) from 10/12 to 10/29.

Water temperature in the subsurface at the downstream site ESB 22.4(3) is plotted in Figure A-53. Water temperature generally increased with depth into the subsurface though Sensor 0 was warmer than Sensor -32 from 10/16 to 10/21. Water temperature at all depths had a weekly decreasing trend in average water temperature. Variation in water temperature at 0 cm and -32 cm was greater than at -52 cm. Water temperature at -52 cm showed no daily variations. Weekly downstream and upstream subsurface water temperature variations were similar, but there was not a consistent change in water temperature with depth (Figure A-54). Downstream shallow (-32 cm) subsurface water temperature was cooler than upstream shallow (-23 cm) subsurface water temperature. Downstream deep (-52 cm) subsurface water temperature was warmer than upstream deep (-67 cm) subsurface water temperature. With the exception of 10/16 to 10/21, subsurface water temperature was warmer than streambed water temperature, so upwelling subsurface flow into the pool would not have provided any cooling to the pool.

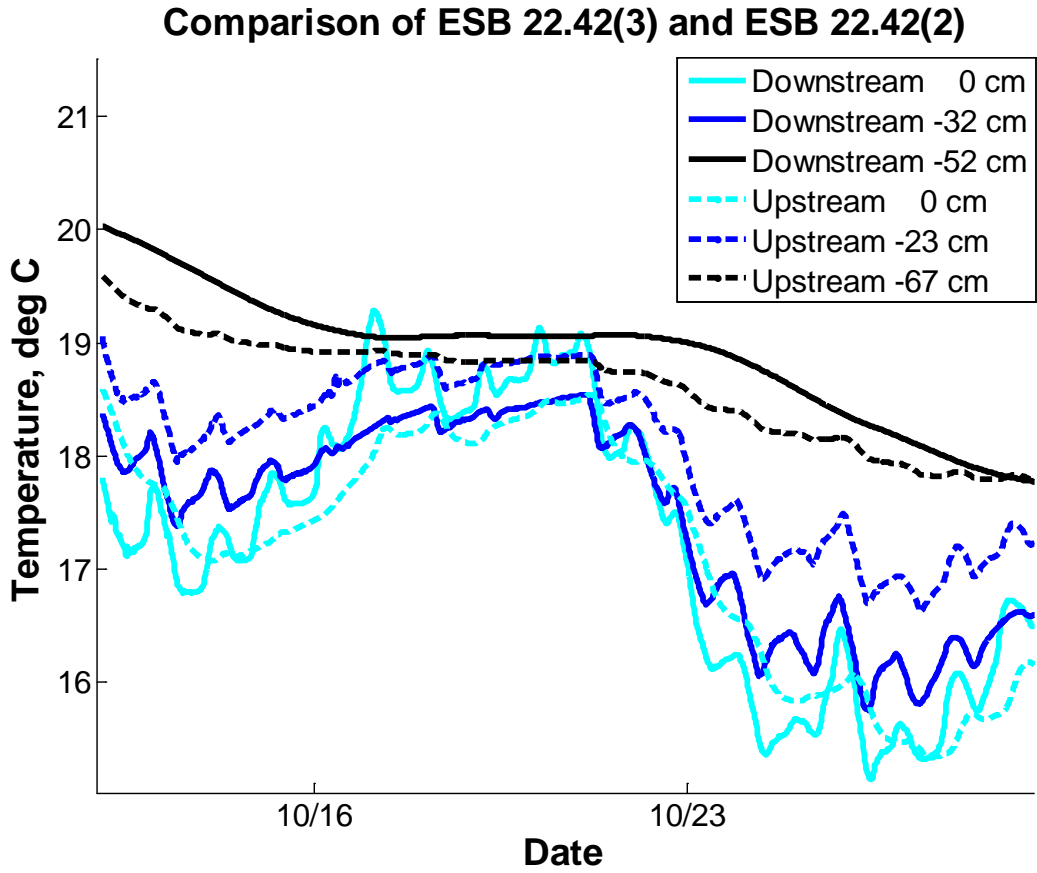


Figure A-54: Comparison of subsurface water temperature at the upstream and downstream sensor array locations.

Hydraulic head at the downstream ESB 22.4(3) location consistently increased with depth below the streambed indicating subsurface flow upwelled into the pool (Figure A-55). After the hydraulic head in the deep (-52 cm) piezometer reached quasi-steady equilibrium, hydraulic head at both -32 cm and -52 cm was greater than streambed hydraulic head. Streambed hydraulic head was briefly greater than hydraulic head at -32 cm when surface water levels increased on 10/27 because the shallow (-32 cm) piezometer response time to variations in water level was approximately 24 hours.

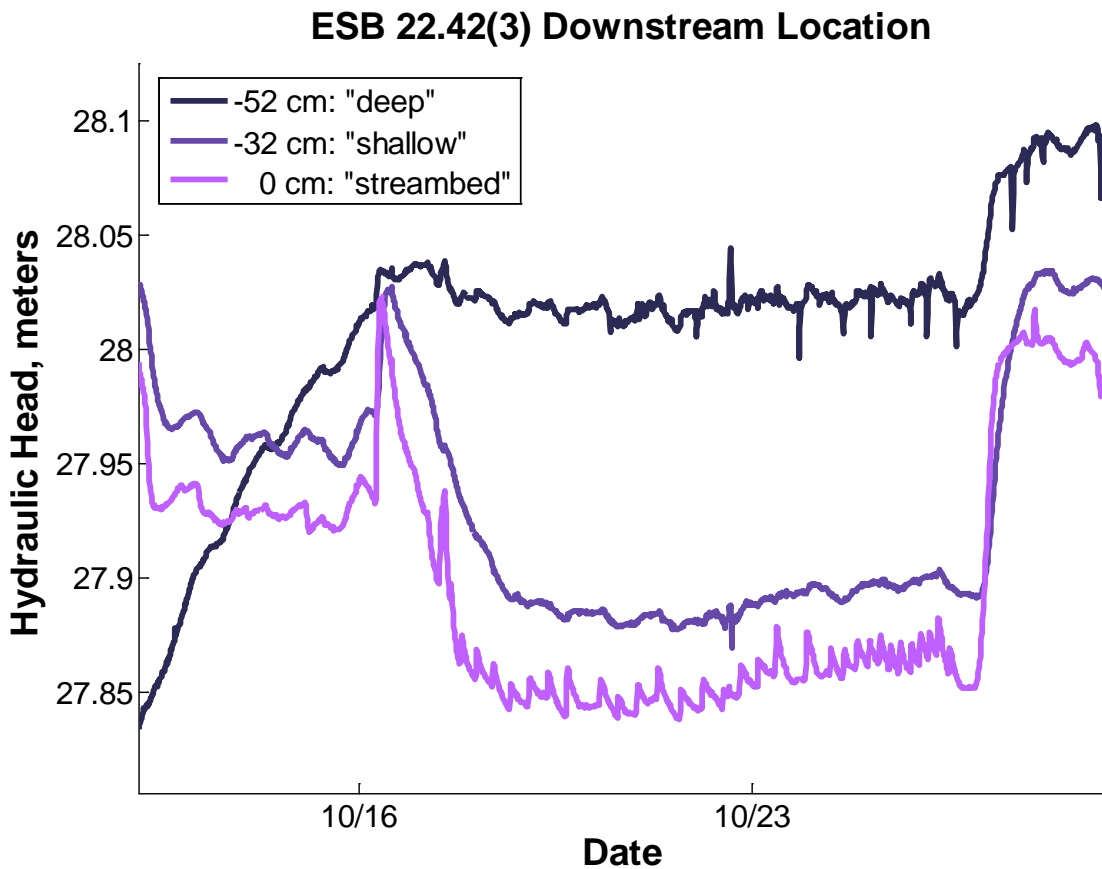


Figure A-55: Variation in hydraulic head with depth into the subsurface at the downstream ESB 22.4(3) pool location.

Eastside Bypass 29.25 Sensor Array Site (ESB 29)

The middle Eastside Bypass sensor array site was located downstream of the Merced National Wildlife Refuge near the San Luis Wildlife Refuge's western boundary with Greenhouse Road. ESB 29 is approximately 29.25 miles downstream of the confluence of the Chowchilla Bypass with the Fresno River (Figure A-56).



Figure A-56: Aerial view of the Eastside Bypass showing sensor array site ESB 29.

Four sensor arrays were deployed at ESB 29 from October 15, 2012 until November 1, 2012. ESB 29 was a deeply incised pool-riffle-pool sequence with no incoming surface flow entering the upstream pool when sensors were installed on 10/15. Surface water levels in the pools were so low the upstream and downstream pools were disconnected on 10/15. The downstream pool was connected to pools further downstream. During the instrumentation, surface water levels in the pools rose and reconnected the pools. Sensor arrays were installed in the deepest parts of the upstream and downstream pools (Figure A-57). Onset HOBO U22-001, Solinst Levelogger Gold, and Levelogger Edge sensors were used to measure water temperature and level at both locations in the ESB 29 pool. The upstream sensor arrays at ESB 29.25(3) had ten water temperature sensors placed vertically through the surface water of the pool in addition to water temperature and level sensors at the streambed (0 cm), in the shallow subsurface (-62 cm), and in the deep subsurface (-122 cm). The downstream sensor arrays at ESB 29.25(2) had water temperature sensors placed above the streambed (25 cm) and near the air-water interface (277 cm) along with water temperature and level sensors installed at the streambed (0

cm), in the shallow subsurface (-35 cm), and in the deep subsurface (-62 cm). At ESB 29.25(3), seven of the surface water temperature sensors attached to the array and the streambed sensor could not be recovered due to fluctuations in the surface water level.

San Joaquin River Restoration Program 2012 Thermal Refugia Study

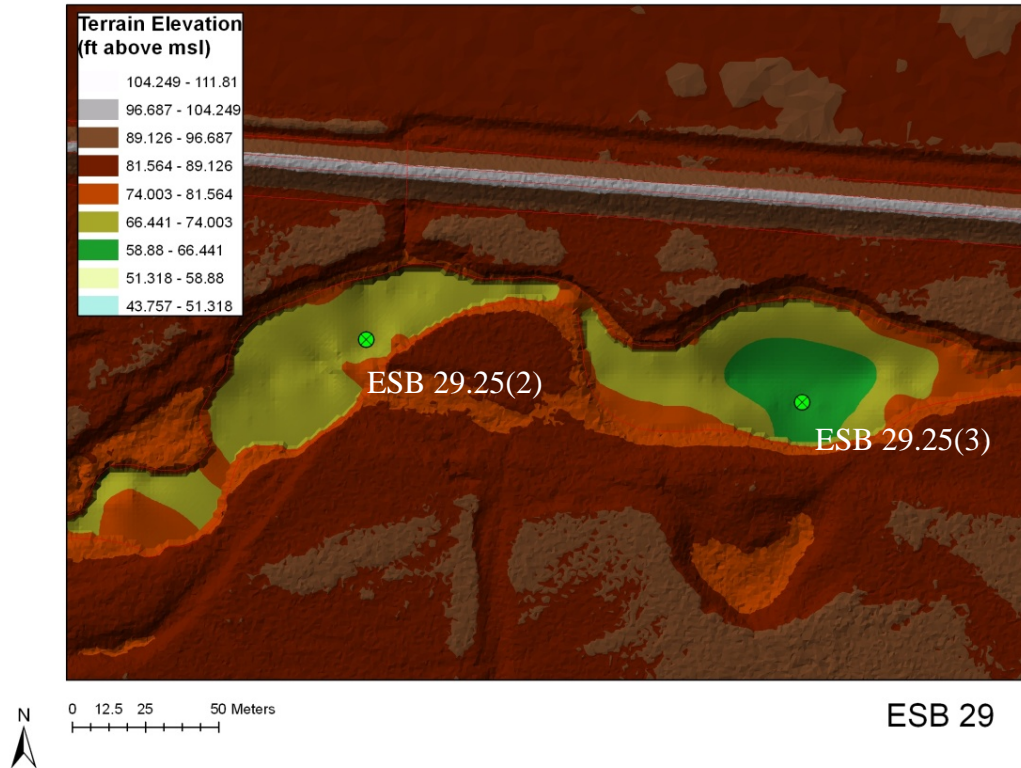


Figure A-57: San Joaquin River System digital terrain model plan view of the Eastside Bypass sensor array site ESB 29.

ESB 29.25(3) Upstream Location

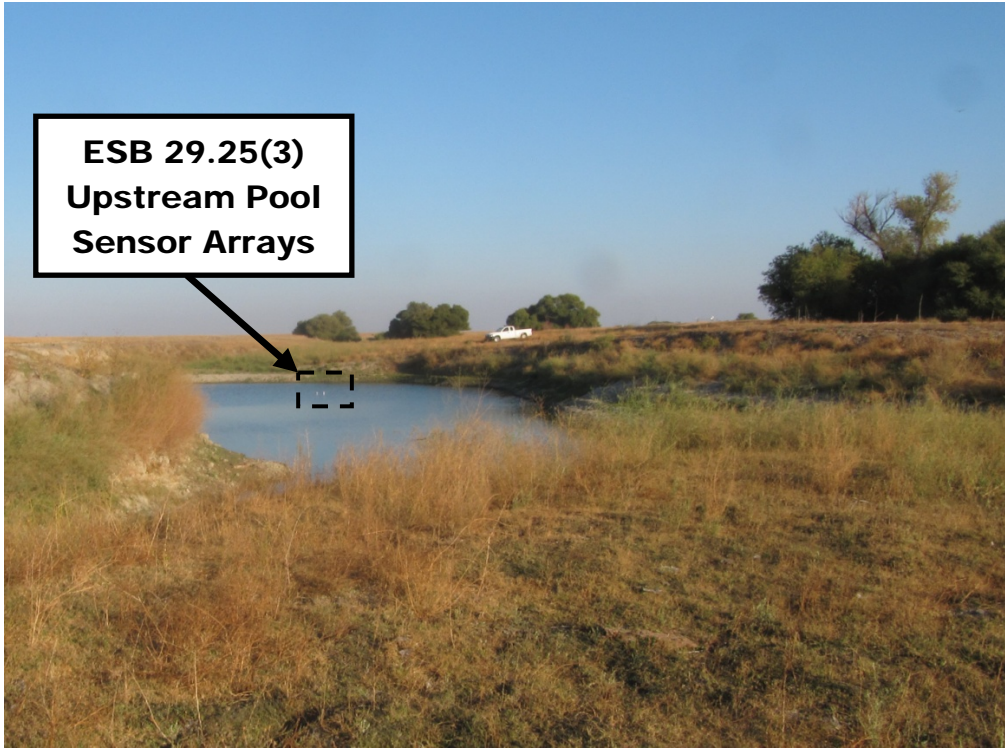


Figure A-58: ESB 29.25(3) pool sensor arrays looking upstream.

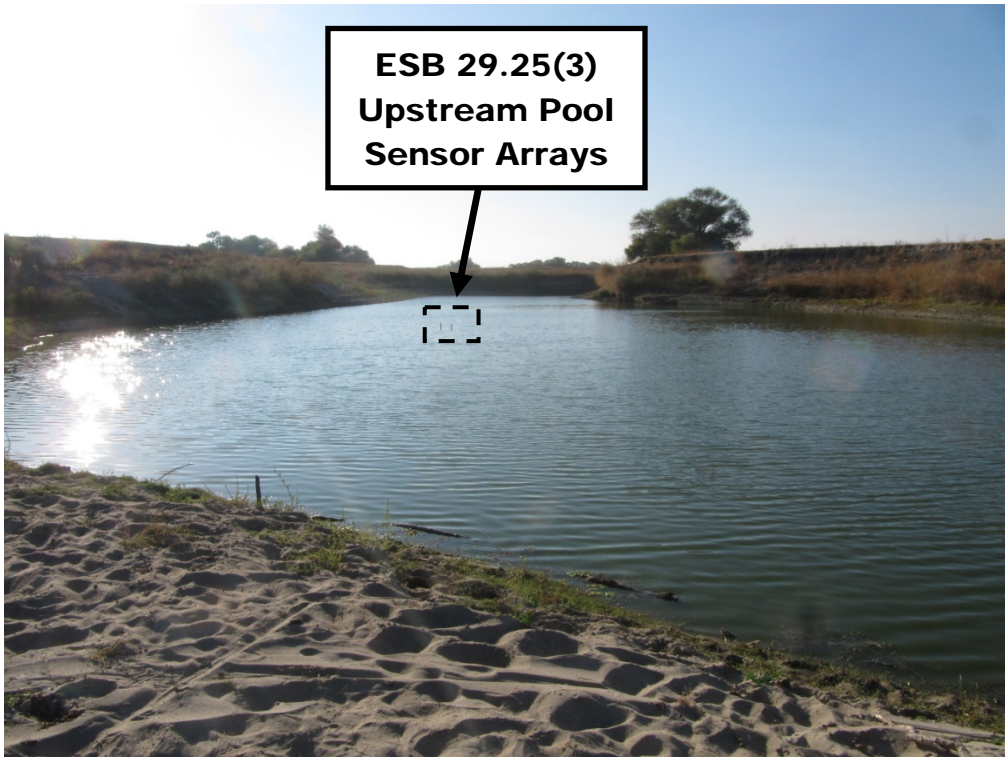


Figure A-59: ESB 29.25(3) pool looking downstream from dry streambed.

Water temperature from all sensors at the upstream pool ESB 29.25(3) is plotted in Figure A-60. Water temperature sensors are labeled based on their depth in centimeters above or below the streambed with the streambed level being zero. Depths greater than zero indicate sensors measuring surface water temperatures, while depths less than zero are sensors measuring subsurface water temperatures.

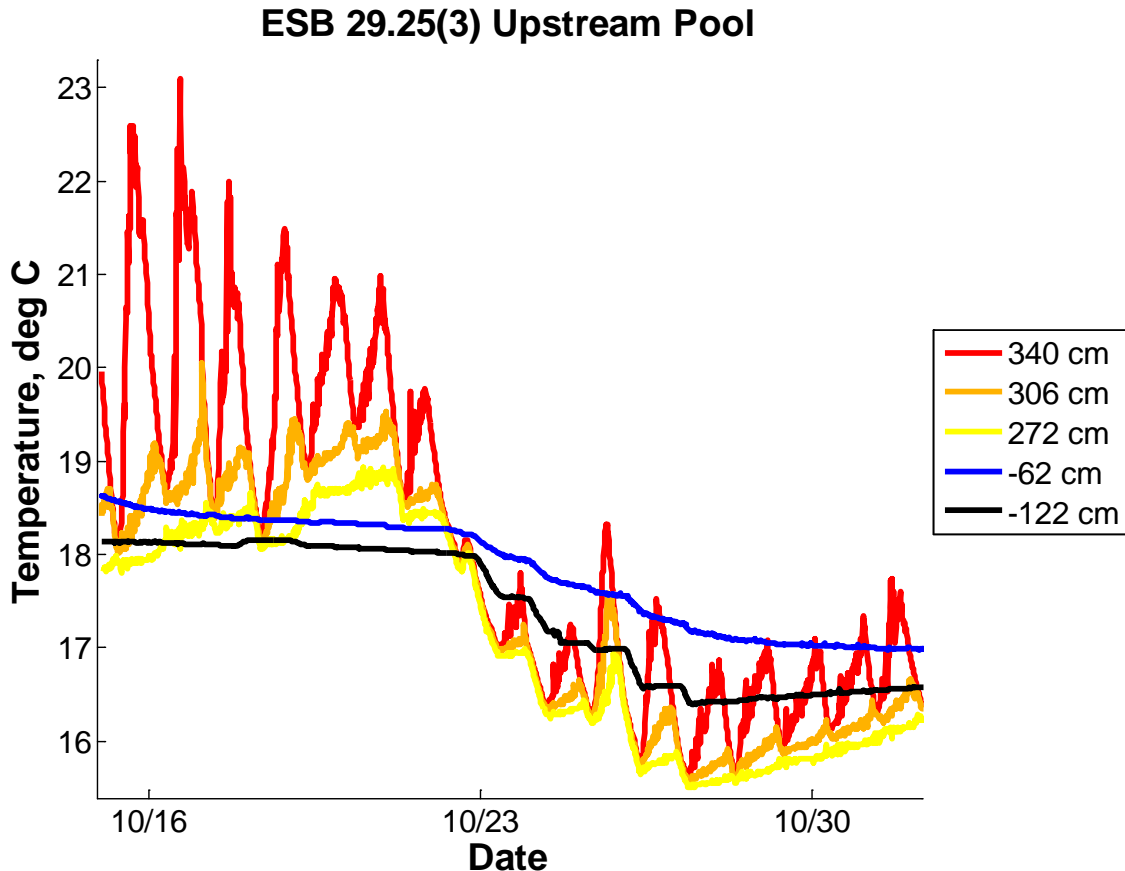


Figure A-60: Variation in surface and subsurface water temperature showed daily thermal stratification from 10/15/2012 to 11/01/2012 at the upstream sensor array site ESB 29.25(3).

Daily thermal stratification occurred at ESB 29.25(3) based on the available water temperature data. Further detailed analysis of thermal stratification was not possible since the sensors in the middle of the water column and the pool bottom water temperature sensor could not be recovered.

Subsurface water temperature at ESB 29.25(3) decreased between -62 cm and -122 cm, but was warmer than surface water temperature during at least half of the instrumentation period. It is uncertain if subsurface water temperature was warmer than surface water temperature during the other half because the middle and pool bottom water temperature sensors could not be recovered.

Hydraulic head decreased with depth suggesting that subsurface flow downwelled into ESB 29.25(3). Hydraulic head at -62 cm was greater than hydraulic head at -122 cm so subsurface flow was flowing downward between those two depths. Further analysis was not possible since the streambed sensor was not recovered.

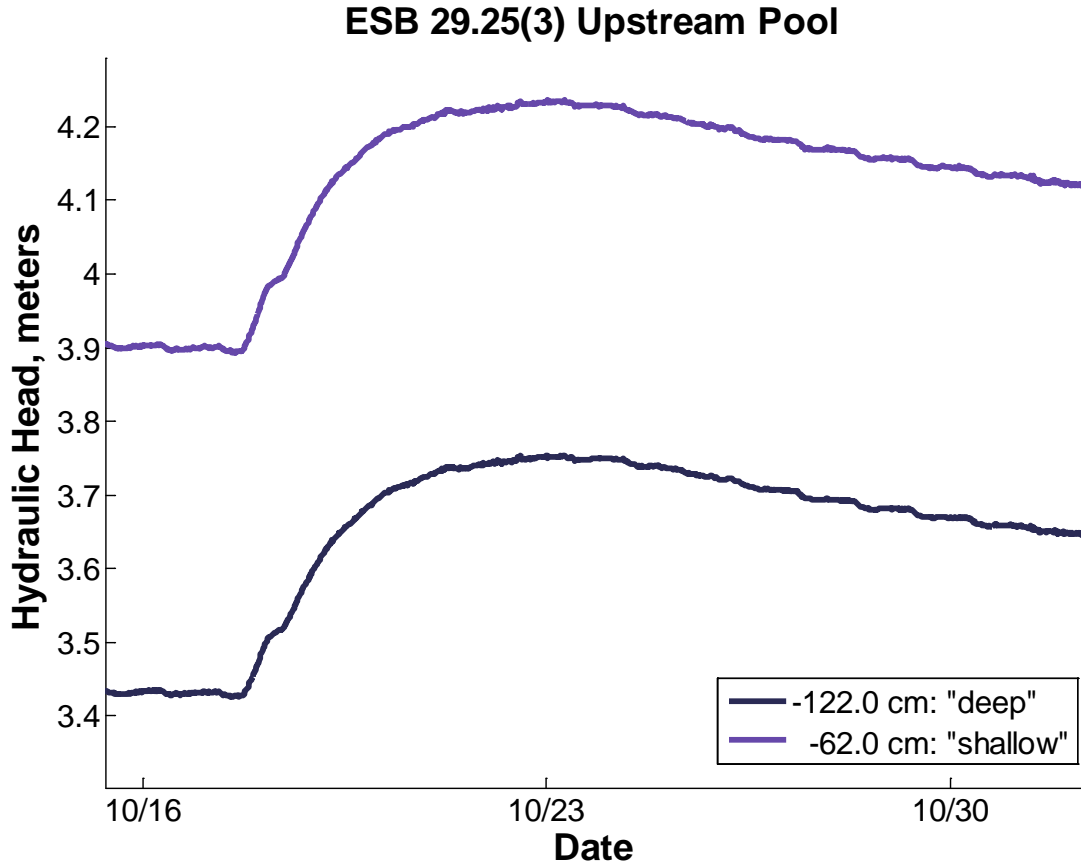


Figure A-61: Variation in hydraulic head with depth into the subsurface at the ESB 29.25(3) upstream pool location.

ESB 29.25(2) Downstream Location



Figure A-62: ESB 29.25(2) pool sensor arrays looking upstream.



Figure A-63: ESB 29.25(2) pool sensor arrays looking downstream.

Water temperature from all sensors at the upstream pool ESB 29.25(2) is plotted in Figure A-64. Water temperature sensors are labeled based on their depth in centimeters above or below the streambed with the streambed level being zero. Depths greater than zero indicate sensors measuring surface water temperatures, while depths less than zero are sensors measuring subsurface water temperatures.

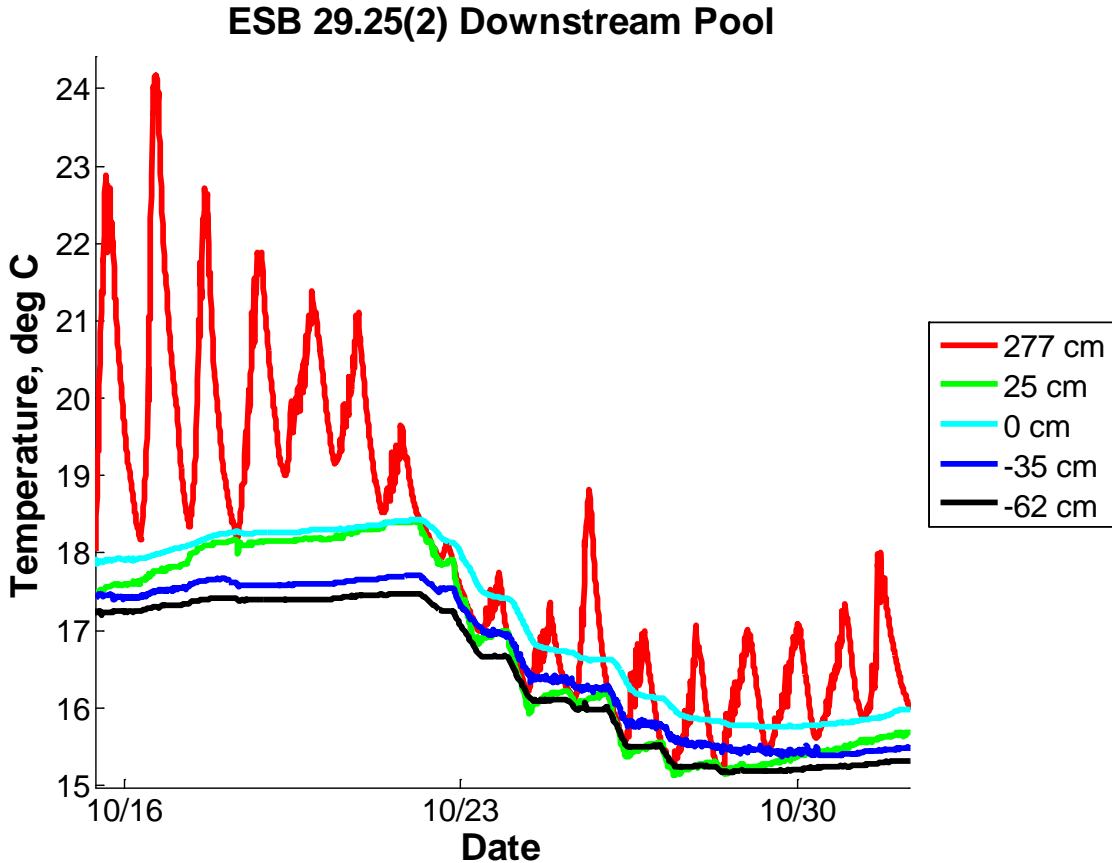


Figure A-64: Variation in surface and subsurface water temperature showed daily thermal stratification from 10/15/2012 to 11/01/2012 at the ESB 29.25(2) downstream pool.

Daily thermal stratification occurred at ESB 29.25(2) during the entire instrumentation period. The maximum daily thermal stratification ranged from 6.4°C to less than 0.3°C with an average of 2.6°C. Thermal stratification was greatest at the beginning of the instrumentation when the average maximum daily thermal stratification was 5.4°C. Average maximum daily thermal stratification decreased on 10/18 to 3.2°C and corresponded to an increase in surface water level. Other sites did not show a decrease in thermal stratification between 10/18 and 10/21 during the week long warming trend suggesting the decrease in thermal stratification at ESB 29.25(2) was due to local conditions. It could not be verified if the increase in water level was linked to the decrease in average maximum daily thermal stratification.

Subsurface water temperature decreased with depth below the streambed, but was only cooler than surface water temperature during the first half of the instrumentation. During the second half of the instrumentation, subsurface water temperature was greater than or equal to the surface water temperature indicating subsurface water would not consistently have provided a cold water source.

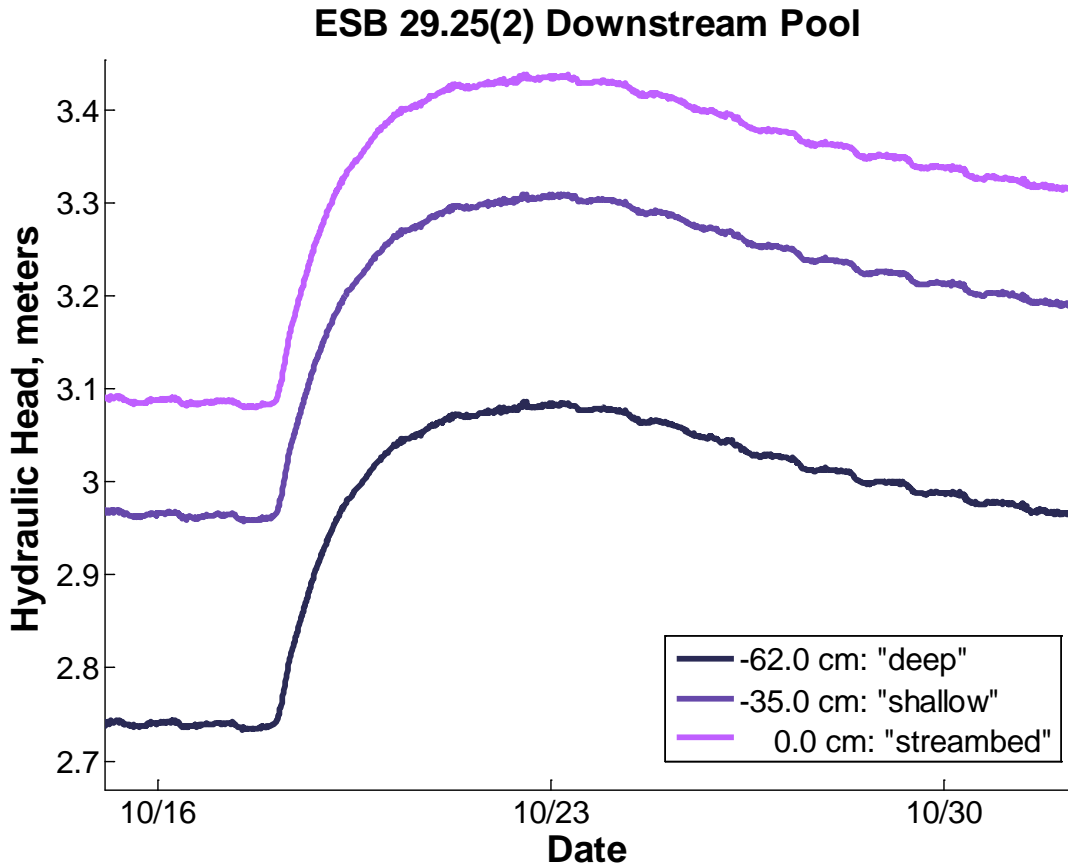


Figure A-65: Variation in hydraulic head with depth into the subsurface at the ESB 29.25 (2) downstream pool location.

Hydraulic head decreased with depth below the streambed indicating subsurface flow downwelled (Figure A-65). Subsurface water temperature would not have influenced surface water temperature at ESB 29.25(2) since subsurface water flowed downward.

Eastside Bypass 33.8 Sensor Array Site (ESB 33)

The furthest downstream Eastside Bypass sensor array site was located at ESB 33 approximately 33.8 miles downstream of the confluence of the Chowchilla Bypass with the Fresno River (Figure A-66). ESB 33 was located approximately 2.3 miles downstream of the Eastside Bypass's confluence with Bear Creek and 1.6 miles upstream of its confluence with the San Joaquin River.

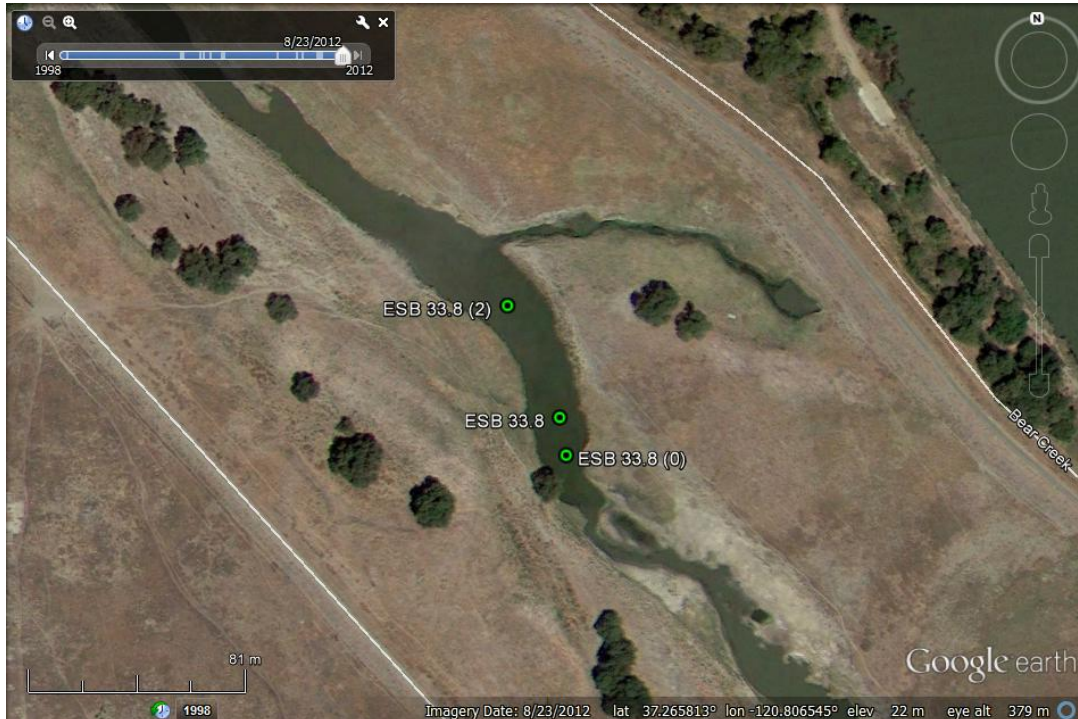


Figure A-66: Aerial view of the Eastside Bypass taken on 8/23/2012 showing sensor array site ESB 33.

ESB 33 was a single pool with shallow glides upstream and downstream and a pond drain entering from the right bank side at ESB 33's downstream end. Sensor arrays were installed longitudinally in the pool at three locations: the upstream pool entrance slope, the deepest middle point, and downstream exit slope (Figure A-67). At the upstream location ESB 33.8(0) and the downstream location ESB 33.8(2), four sensor arrays were deployed from October 17, 2012 until November 5, 2012. At the middle location ESB 33.8, two sensor arrays were deployed from October 16, 2012 until November 5, 2012. Onset Hobo U22-001, Solinst Levellogger Gold, and Levellogger Edge sensors were used to measure water temperature, level, and electro-conductivity at all three locations in the ESB 33 pool. The upstream sensor arrays at ESB 33.8(0) had six water temperature sensors placed vertically in the surface water of the pool in addition to water temperature, level, and conductivity sensors at the streambed (0 cm), in the shallow subsurface (-62 cm), and in the deep subsurface (-122 cm). The middle sensor arrays at ESB 33.8 had ten water temperature sensors placed vertically through the surface water of the pool. Subsurface water conditions at ESB 33.8 were measured by water temperature, level, and conductivity sensors at the streambed (-7 cm), in the shallow subsurface (-68 cm), in the

deep subsurface (-104 cm) and one water temperature sensor placed in the mud below the streambed (-17 cm). The downstream sensor arrays at ESB 33.8(2) had nine water temperature sensors placed vertically through the surface water of the pool. Subsurface water conditions at ESB 33.8(2) were measured by water temperature, level, and conductivity sensors at the streambed (-9 cm), and in the shallow subsurface (-70 cm) and one water temperature sensor placed in the mud below the streambed (-19 cm). A deep subsurface sensor was installed at ESB 33.8(2), but it was lost during the instrumentation period. All streambed sensors sunk between 0 cm and 9 cm below the streambed into the clay-mud pool bottom sediments, hence measured water temperature in the streambed sediment not surface water temperatures.

San Joaquin River Restoration Program 2012 Thermal Refugia Study

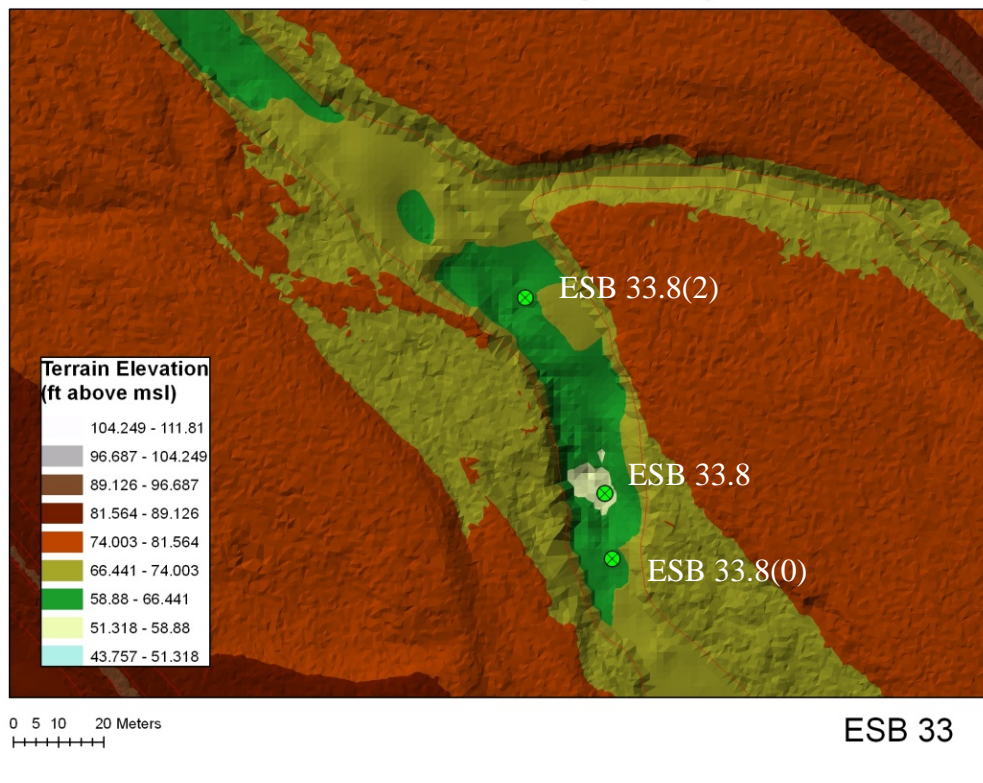


Figure A-67: San Joaquin River System digital terrain model plan view of the Eastside Bypass sensor array site ESB 33.

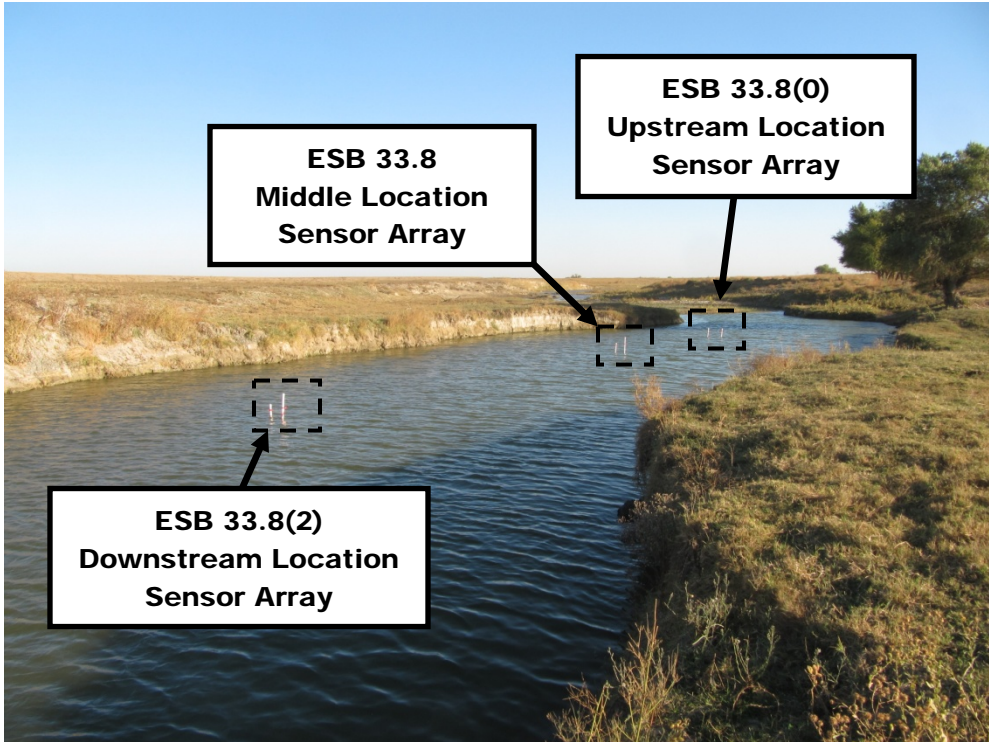


Figure A-68: ESB 33.8 pool looking upstream

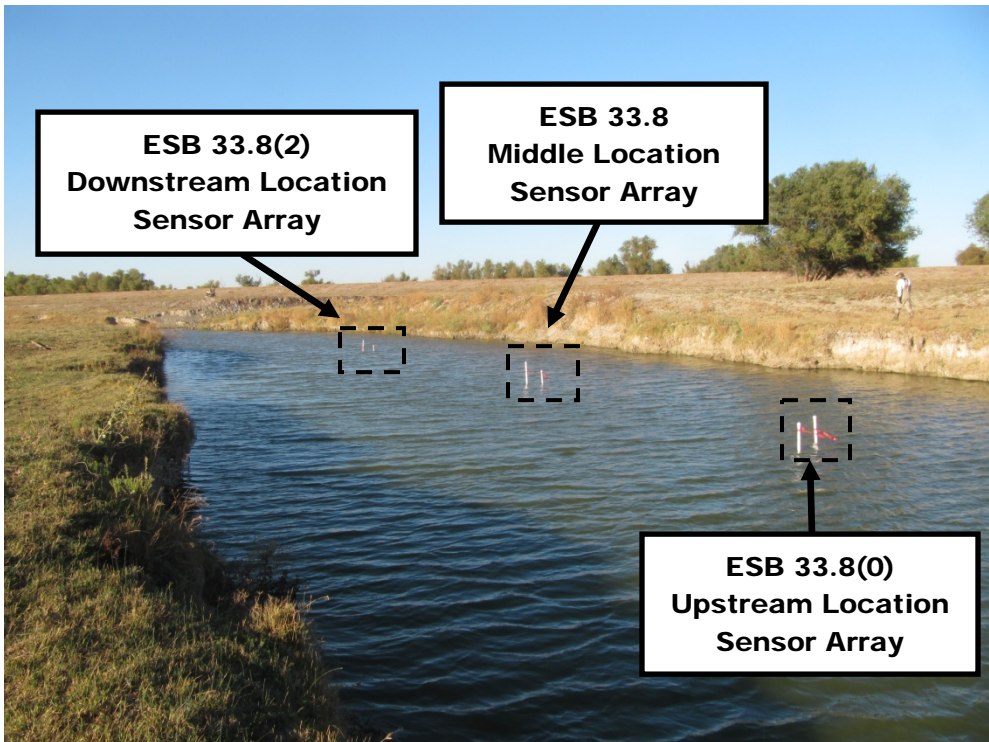


Figure A-69: ESB 33.8 pool looking downstream

ESB 33.8(0) Upstream Location

Thermal conditions at the upstream pool location ESB33.8(0) varied with daily thermal stratification occurring between 10/17 to 11/02 followed by a period of no thermal stratification from 11/02 until the sensors were removed on 11/05 (Figure A-70). During the thermal stratification period, the maximum daily thermal stratification between the top sensor closest to the air-water interface (ESB 33.8(0) Sensor 200) the sensor nearest the streambed measuring water temperature (ESB 33.8(0) Sensor 40) varied daily and ranged from 1.0°C to 5.5°C with an average daily thermal stratification of 3.4°C. Thermal stratification occurred as water temperature near the air-water interface increased more than the water temperature near the streambed. Daily water temperature variation at ESB 33.8(0) Sensor 200 ranged from 1.0°C to 4.5°C while the daily water temperature variation at ESB 33.8(0) Sensor 40 ranged from 0.31°C to 1.6°C.

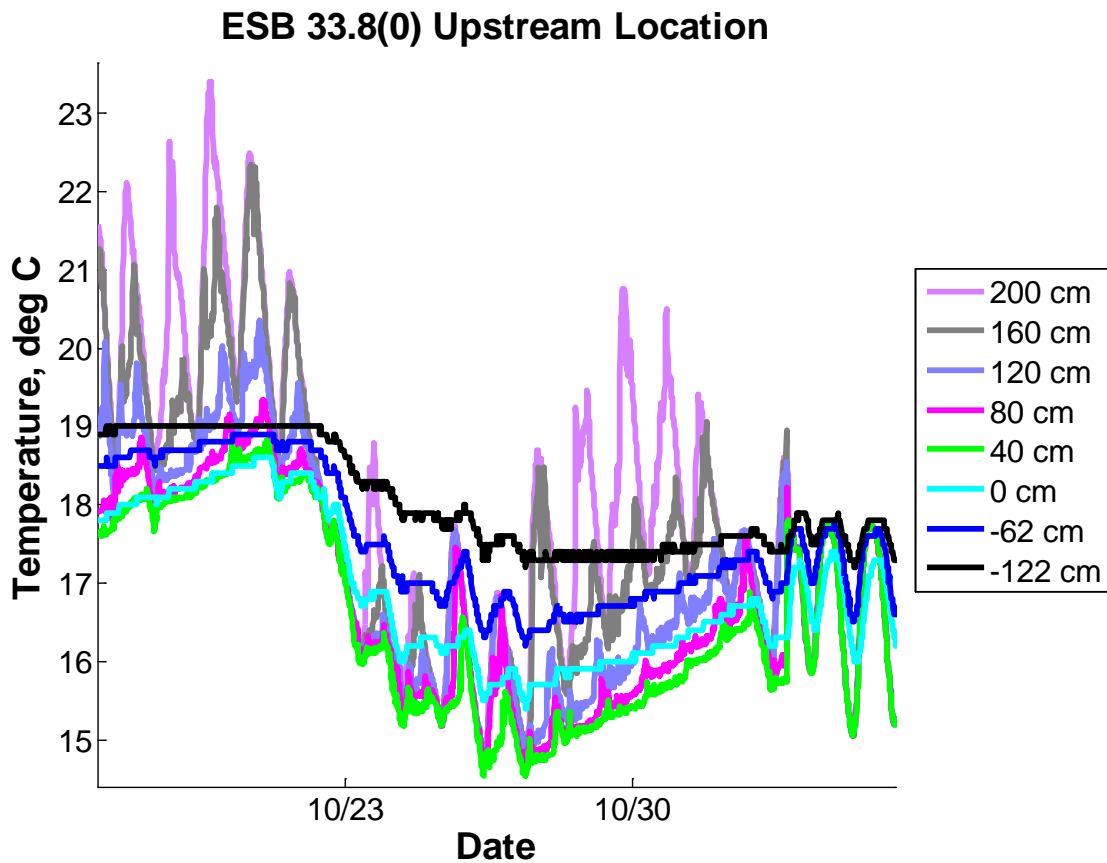


Figure A-70: Variation in surface and subsurface water temperature showed daily thermal stratification from 10/17/2012 to 11/05/2012 at the upstream sensor array site ESB 33.8(0).

Thermal stratification at ESB 33.8(0) changed on 11/02 when surface flow into ESB 33.8 increased from less than 0.3 m³/s to approximately 1.4 m³/s. Water flow in ESB 33.8 was observed to be less than 0.3 m³/s when sensor arrays were installed on 10/17, but was greater during sensor removal on 11/05. Correlations between surface water flow and

water level at the Department of Water Resources Stevinson gauge indicated that increases in pool water level corresponded to increased flow in the Eastside Bypass. Water level in ESB 33.8 increased on 11/02 when thermal stratification collapsed (Figure A-71).

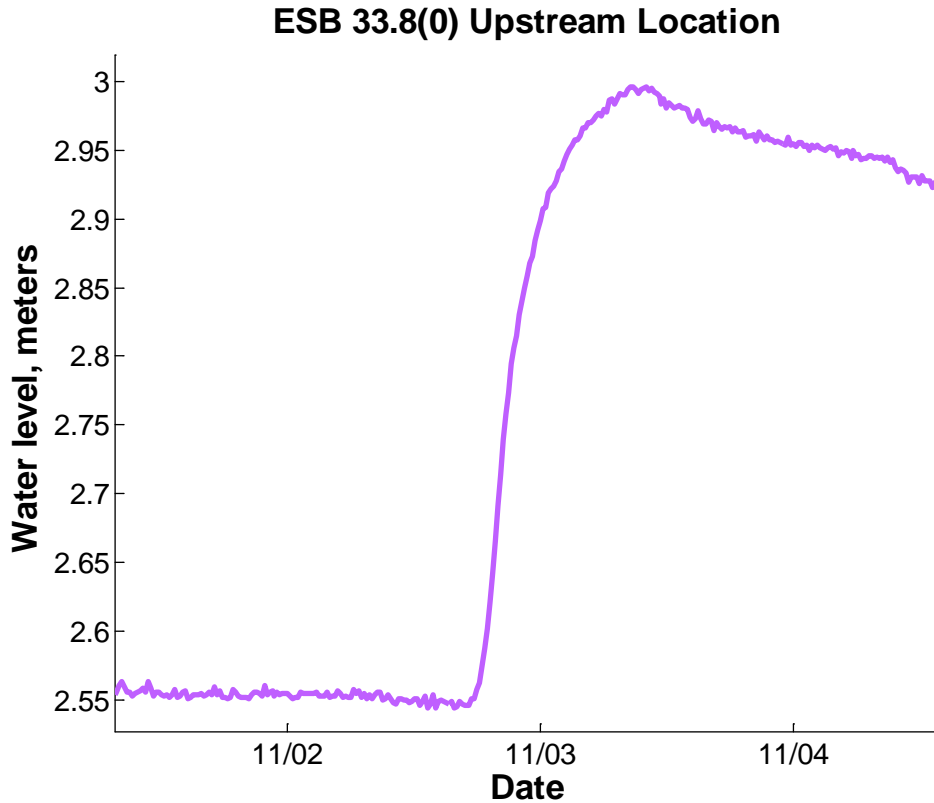


Figure A-71: Surface water level at ESB 33.8(0) increased on 11/02/2012 as surface water flow increased in the Eastside Bypass.

Between 6PM and 8PM on 11/02, the surface water temperature at all depths converged eliminating thermal stratification (Figure A-72). Daily variations in the surface water temperature occurred after 8PM 11/02 with the pool warming during the day and cooling during the night, but the vertical water temperature was uniform with depth. The daily average vertical water temperature difference between 200 cm and 40 cm ranged from 0.00 °C to 0.04 °C during the no stratification period.

ESB 33.8(0) Upstream Location

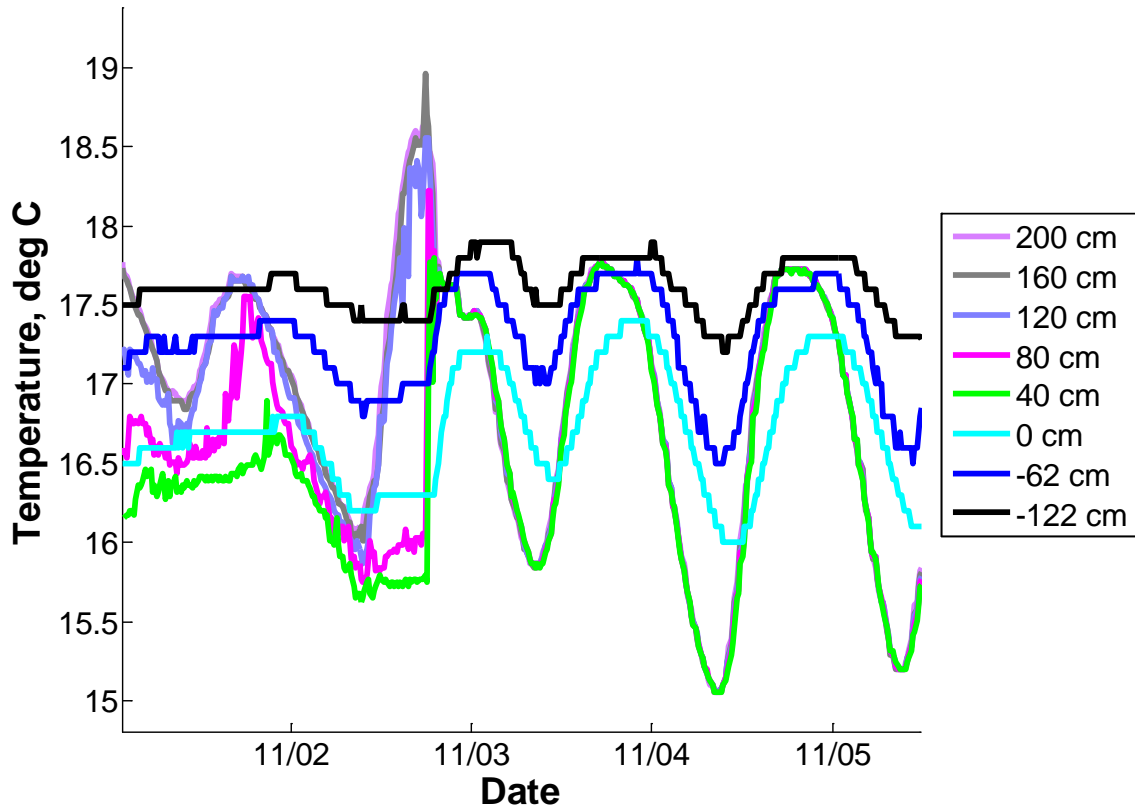


Figure A-72: Thermal stratification in the surface water at ESB 33.8(0) ceased on 11/02/2012 when water level in the Eastside Bypass increased.

Subsurface water temperature increased with depth into the subsurface at the upstream site ESB 33.8(0) throughout the instrumentation period (Figure A-73). Water temperature at the streambed was consistently warmer than subsurface water indicating that subsurface water temperature was not providing any cooling to the upstream site ESB 33.8(0). Water temperature at all depths followed similar weekly trends, yet the amplitude of daily variation in water temperature generally decreased with depth. Increased flow in the surface water corresponded to increased daily variation in subsurface water temperature, but did not change patterns of water temperature with depth below the streambed.

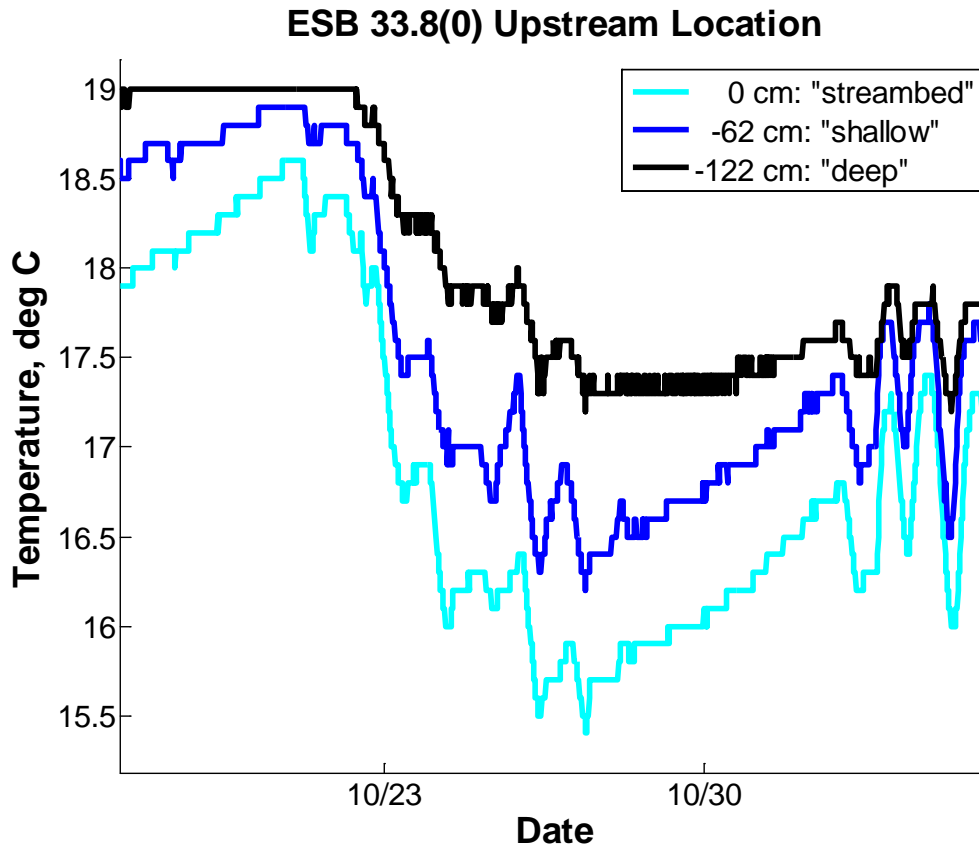


Figure A-73: Subsurface water temperature at ESB 33.8(0) increased with depth below the streambed. Daily variation in subsurface water temperature increased when surface flow increased between 11/02/2012 to 11/05/2012.

Hydraulic head decreased with depth below the streambed indicating the subsurface flow was downwelling during the instrumentation period and not influencing surface water temperature conditions (Figure A-74). The hydraulic head gradient between 0 cm and -62 cm was small suggesting downwelling was also small at the upstream location ESB 33.8(0). Hydraulic head increased on 11/02 corresponding to the time surface flow increased, but trends in hydraulic head with depth remained the same.

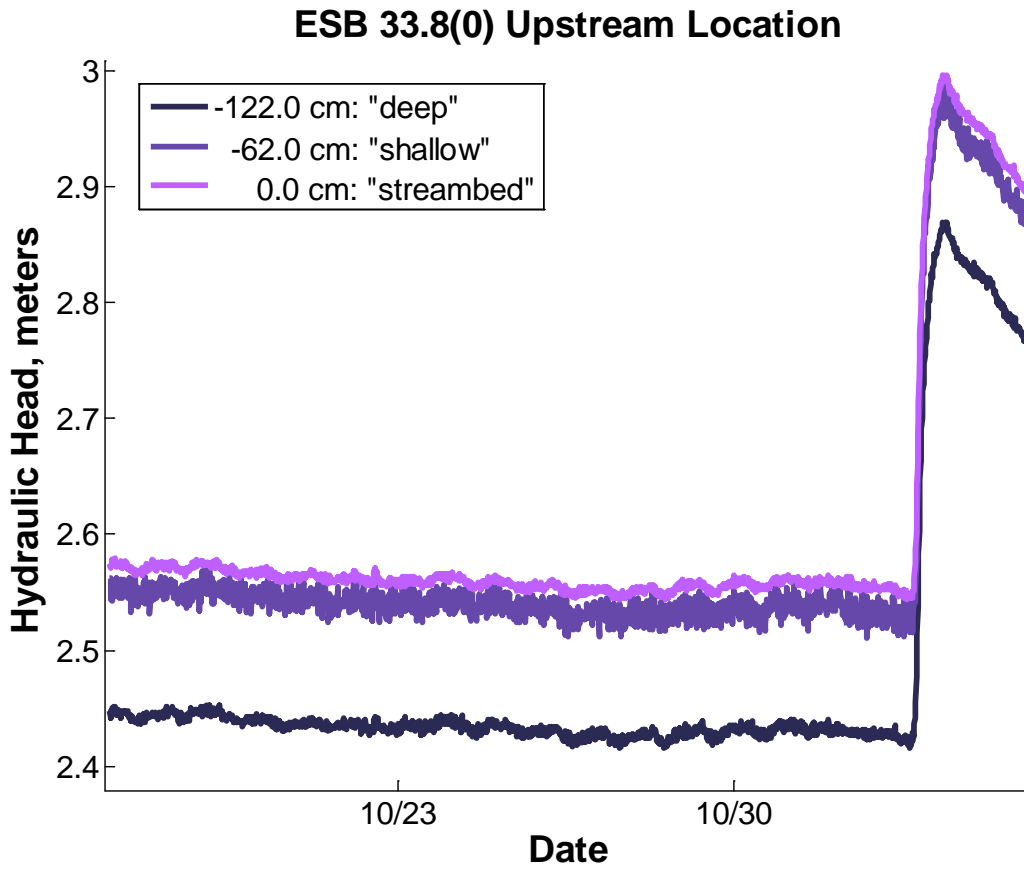


Figure A-74: Variation in hydraulic head with depth into the subsurface at the ESB 33.8(0) upstream pool location

Water specific conductance (SC) measurements at ESB 33.8(0) indicated SC increased with depth into the subsurface (Figure A-75). Specific conductance at the streambed ranged between 0.33 mS/cm and 0.3 mS/cm during the instrumentation period, while SC at -62cm was between 1.8 mS/cm and 1.6 mS/cm and SC at -122 cm ranged from 2.29 to 2.19 mS/cm.

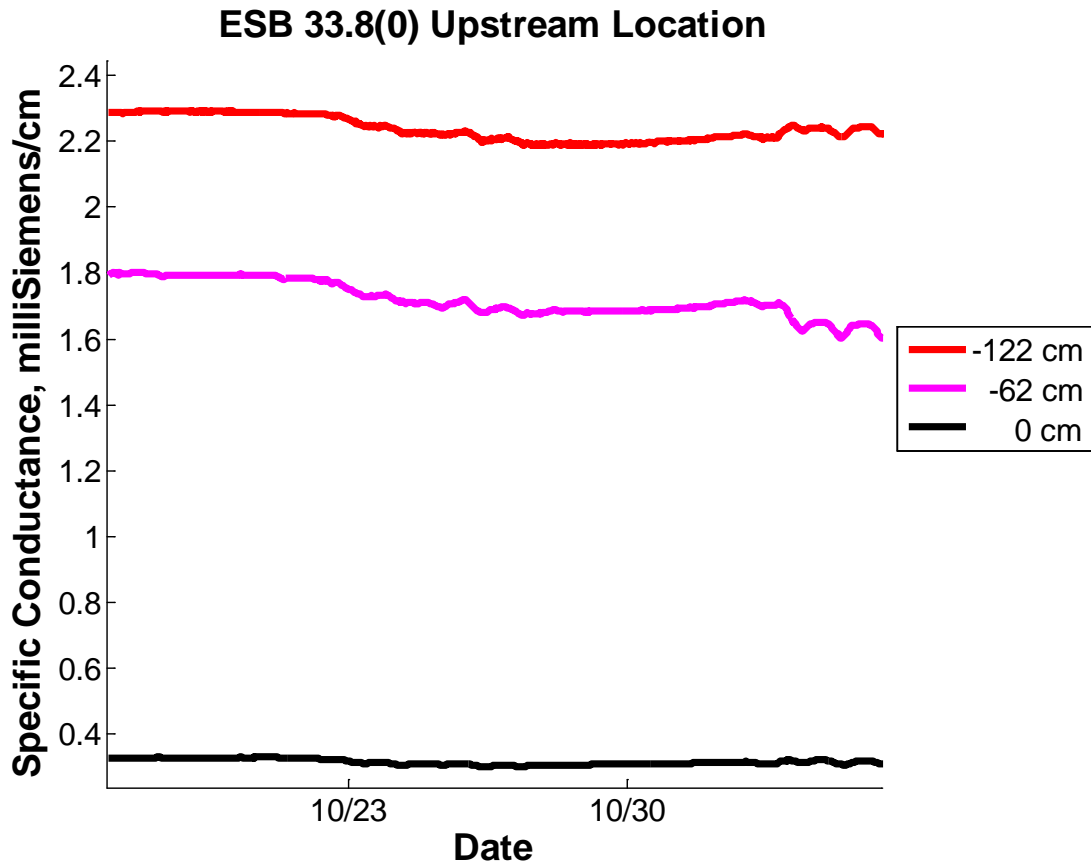


Figure A-75: Variation in water specific conductance with depth into the subsurface at the ESB 33.8(0) upstream pool location

Water specific conductance at ESB 33.8(0) also exhibited weekly trends (Figure A-76). Weekly variations in SC occurred at all depths and followed patterns similar to subsurface water temperature trends. After surface flow increased on 11/02, SC developed a diurnal cycle. Specific conductance peaked around midnight and reached its minimum around noon each day.

ESB 33.8(0) Upstream Location

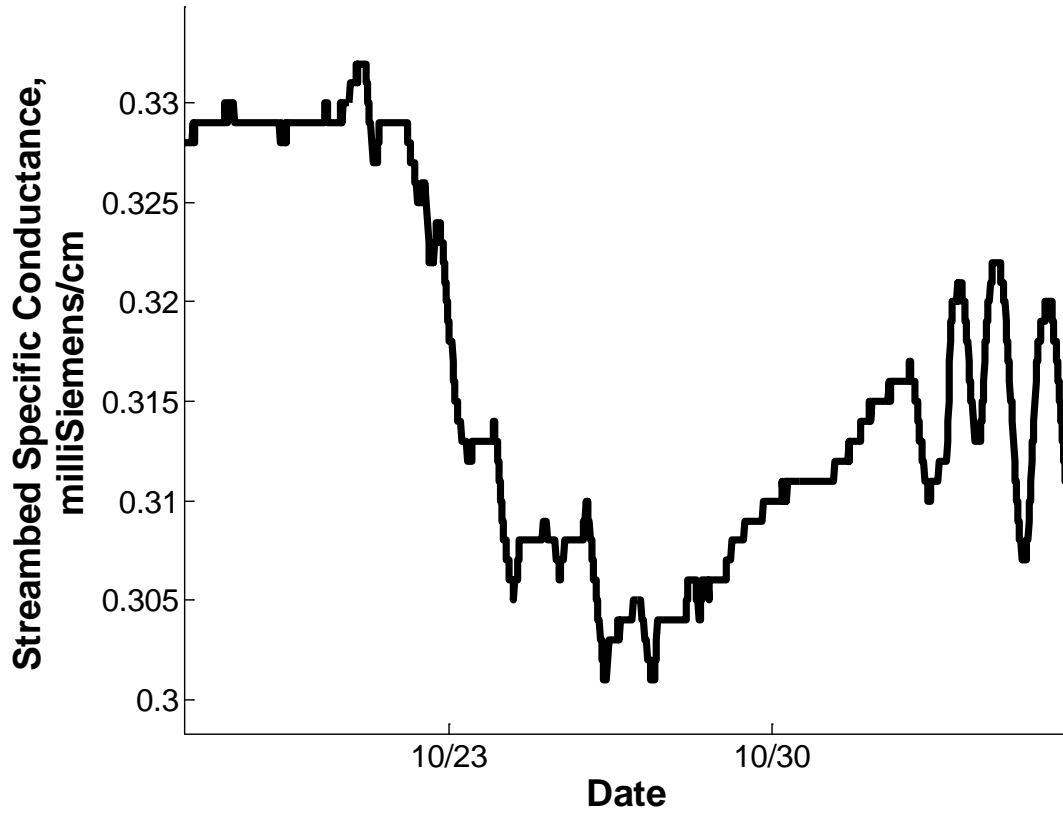


Figure A-76: Hourly variations specific conductance along the streambed at the ESB 33.8(0) upstream pool location

ESB 33.8 Middle Location

Thermal conditions at the middle pool location ESB 33.8 varied with daily thermal stratification occurring between 10/16 to 11/02 followed by a period of no thermal stratification from 11/02 until the sensors were removed on 11/05 (Figure A-77). During the thermal stratification period, the maximum daily thermal stratification varied daily and ranged from 1.1°C to 9.1°C with an average maximum daily thermal stratification of 4.7°C. Daily water temperature variation at the top sensor ESB 33.8 Sensor 323 ranged from 1.0 °C to 8.0 °C. Daily water temperature variation at the pool bottom sensor, ESB 33.8(0) Sensor 26, ranged from 0.1°C to 1.4°C. Consistent with the upstream location ESB 33.8(0), thermal stratification at the middle location ESB 33.8 changed on 11/02 when surface flow into ESB 33.8 increased. Between 6PM and 8PM on 11/02, the surface water temperature at all depths became uniform. Diurnal heating and cooling occurred after 8PM 11/02 in surface water temperature, but surface water temperature was uniform with depth. The daily average vertical water temperature difference between 323 cm and 26 cm ranged from 0.05 °C to 0.08 °C during the no stratification period from 11/02 to 11/05.

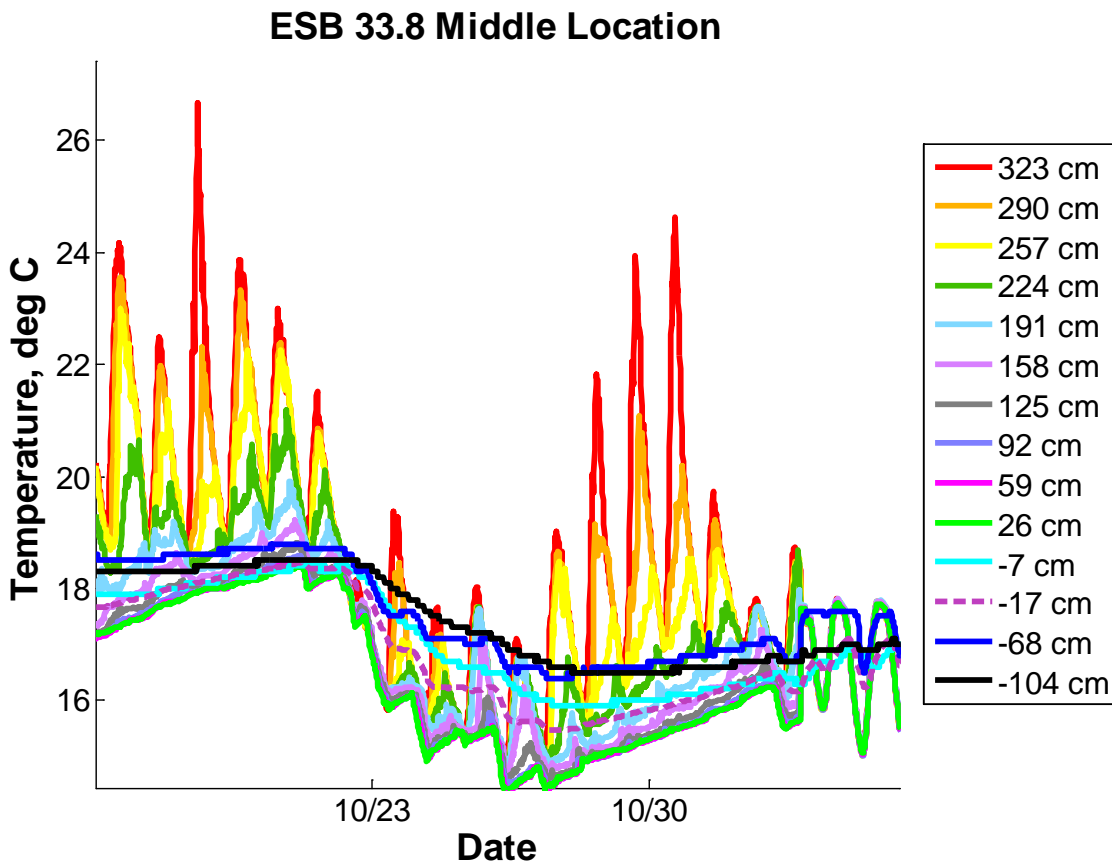


Figure A-77: Upstream sensor array site ESB 33.8 surface and subsurface water temperature from 10/16 to 11/05 showing daily thermal stratification from 10/16 until 11/02.

Subsurface water temperature generally increased with depth at the middle location ESB 33.8 though most of the variation in temperature was within the sensor accuracy (Figure A-78). The square wave variation in subsurface water temperature resulted from the temperature resolution and accuracy of 0.1 °C for Solinst LTC Levelogger Junior sensors used at -7cm, -68cm, and -104cm. Water temperature at -17cm was measured by an Onset Hobo U22-001 sensor with a temperature resolution of 0.02 °C and accuracy of 0.21 °C. Post experiment cross comparison of the sensors' behavior under known temperature conditions indicated that Sensor -17 and Sensor -104 were frequently biased cooler than Sensor -7 and Sensor -68 when measuring decreasing temperature trends. There was not a consistent bias between sensors so no correction factor could be applied.

Even with sensor error considered, subsurface water temperature increased with depth between the near subsurface sensors (-7 cm and -17 cm) and shallow/deep subsurface (-68 cm and -104 cm). Increasing water temperature with depth into the subsurface indicated that subsurface water did not provide any cooling influence to pool surface water temperatures during the instrumentation period. Subsurface water temperature developed more pronounced daily variations when surface water flow increased on 11/02, but water temperature still increased with depth.

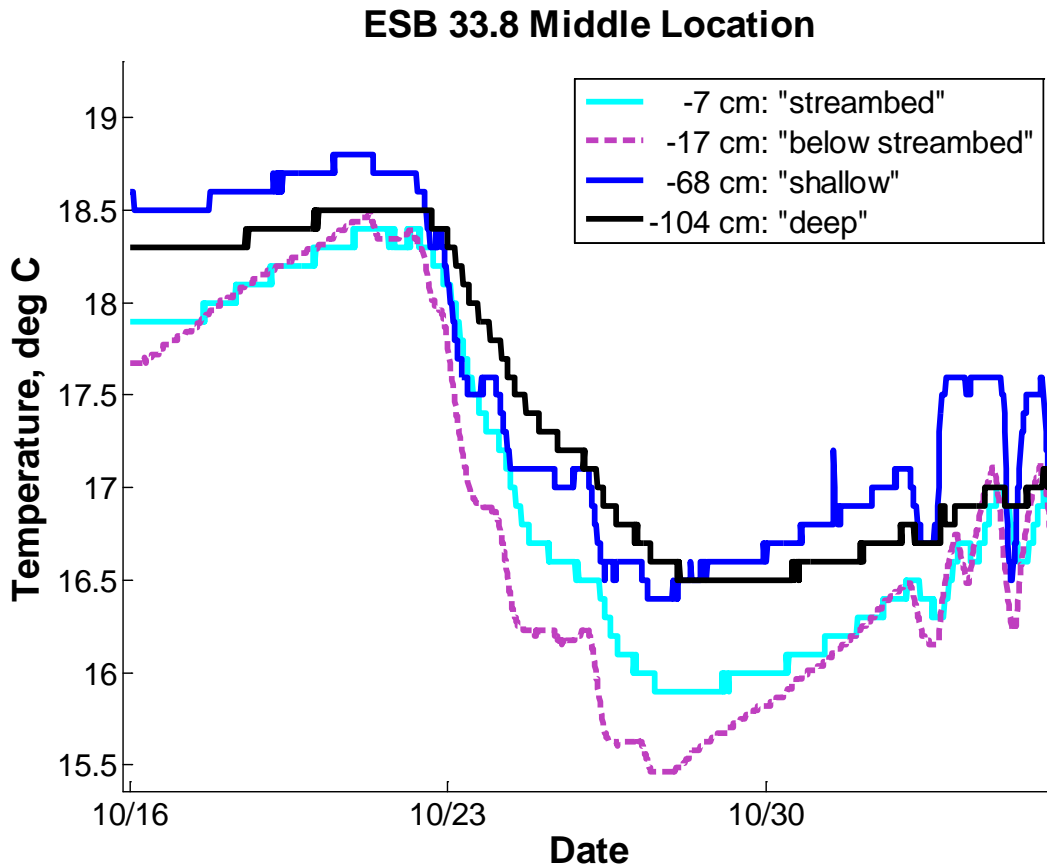


Figure A-78: Middle sensor array site ESB 33.8 subsurface water temperature from 10/16/2012 to 11/05/2012.

Hydraulic head at ESB 33.8 decreased with depth below the streambed indicating the subsurface flow was consistently downwelling during the instrumentation period and not influencing surface water temperature conditions (Figure A-79). On 11/02, hydraulic head increased corresponding to the time surface flow increased, but trends in hydraulic head with depth remained consistent.

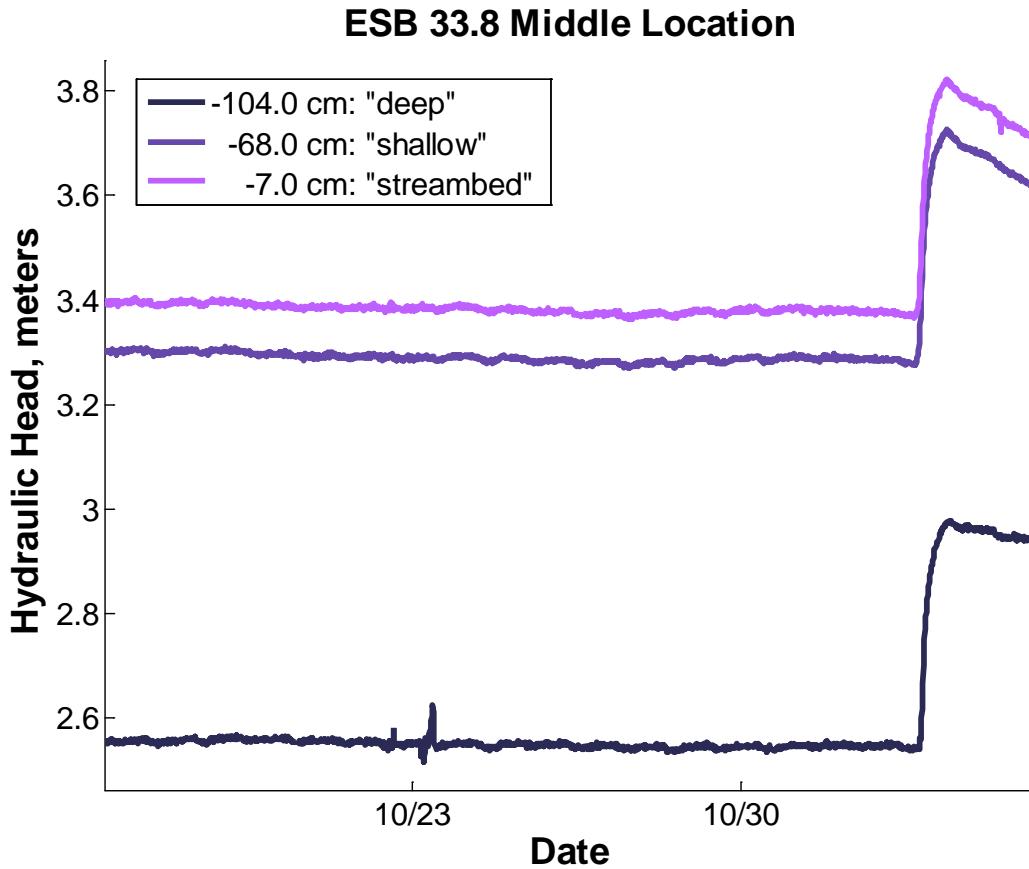


Figure A-79: Variation in hydraulic head with depth into the subsurface at the ESB 33.8 middle pool location.

Specific conductance at the ESB 33.8 middle location indicated specific conductance decreased with depth into the subsurface (Figure A-80). Specific conductance trends with depth completely reversed between the upstream location ESB 33.8(0) and the middle location ESB 33.8 with the maximum specific conductance occurring at -7cm for ESB 33.8. Specific conductance did not share the same trends at all depths at ESB 33.8. Specific conductance at -7cm initially increased, became near constant, then increased again slightly when surface flow increased on 11/02. Specific conductance at -68 cm followed trends similar to the upstream location ESB 33.8. Specific conductance at -104 cm increased until the 11/02 when surface flow in the pool increased. Between 6PM 11/02 and 6PM 11/03, specific conductance at -104 cm decreased 0.16 mS/cm, then it began to rise again. Unlike the upstream location ESB 33.8(0), specific conductance did not show any diurnal variations at the ESB 33.8 middle location.

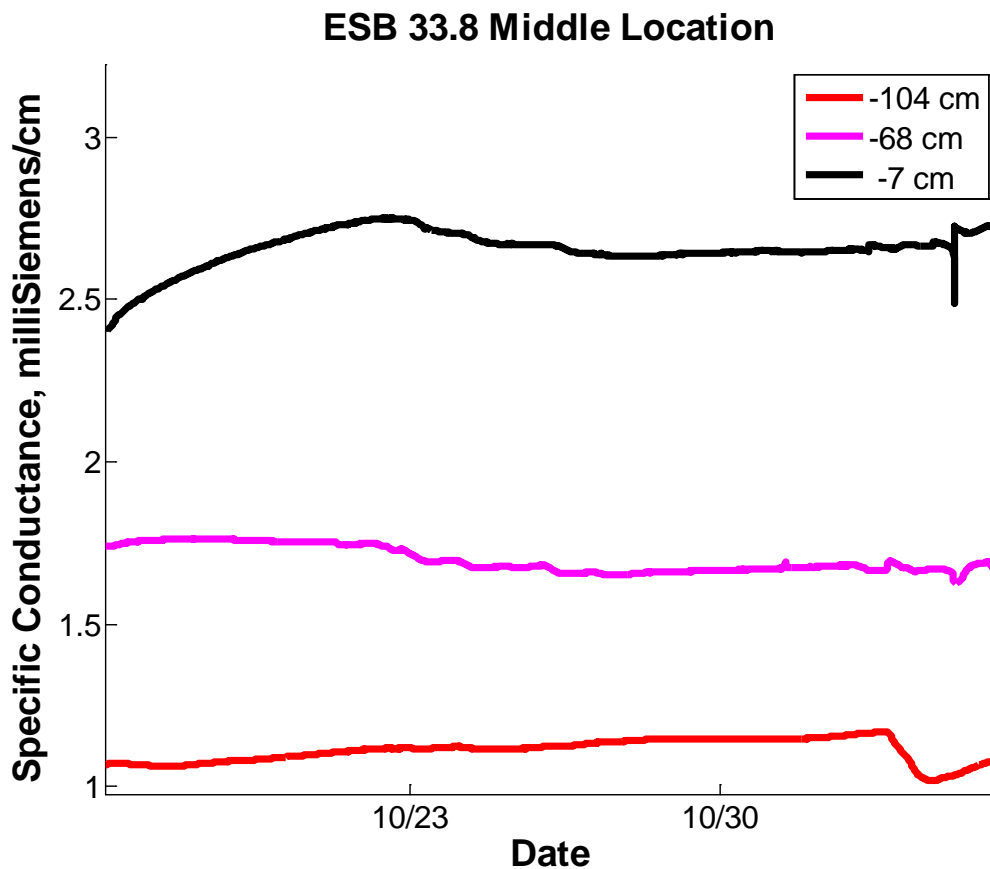


Figure A-80: Variation in water specific conductance with depth into the subsurface at the ESB 33.8 middle pool location.

ESB 33.8(2) Downstream Location

Thermal conditions at the downstream pool location ESB 33.8(2) varied with daily thermal stratification occurring between 10/17 to 11/02 followed by a period of no thermal stratification from 11/02 until the sensors were removed on 11/05 (Figure A-81). Similar to the middle pool site, the sensor near the streambed sank -9cm below the streambed and measured water temperature in the streambed sediment rather than the pool surface water temperature. During the thermal stratification period, the maximum daily thermal stratification varied daily and ranged from 1.1°C to 7.2°C with an average daily thermal stratification of 3.8°C. Daily water temperature variation at the top sensor ESB 33.8(2) Sensor 243 ranged from 0.9°C to 6.2°C while the daily water temperature variation at the pool bottom sensor ESB 33.8(2) Sensor 19 ranged from 0.2°C to 1.4°C. Consistent with the upstream and middle pool locations, thermal stratification at the downstream location ESB 33.8(2) changed on 11/02 when surface flow into ESB 33.8 increased. Surface water temperature at all depths converged between 6PM and 8PM on 11/02 and surface water temperature was uniform with depth after 8PM 11/02. The daily average vertical water temperature difference between 243 cm and 19 cm ranged from 0.08°C to 0.10°C during the no stratification period after 11/02.

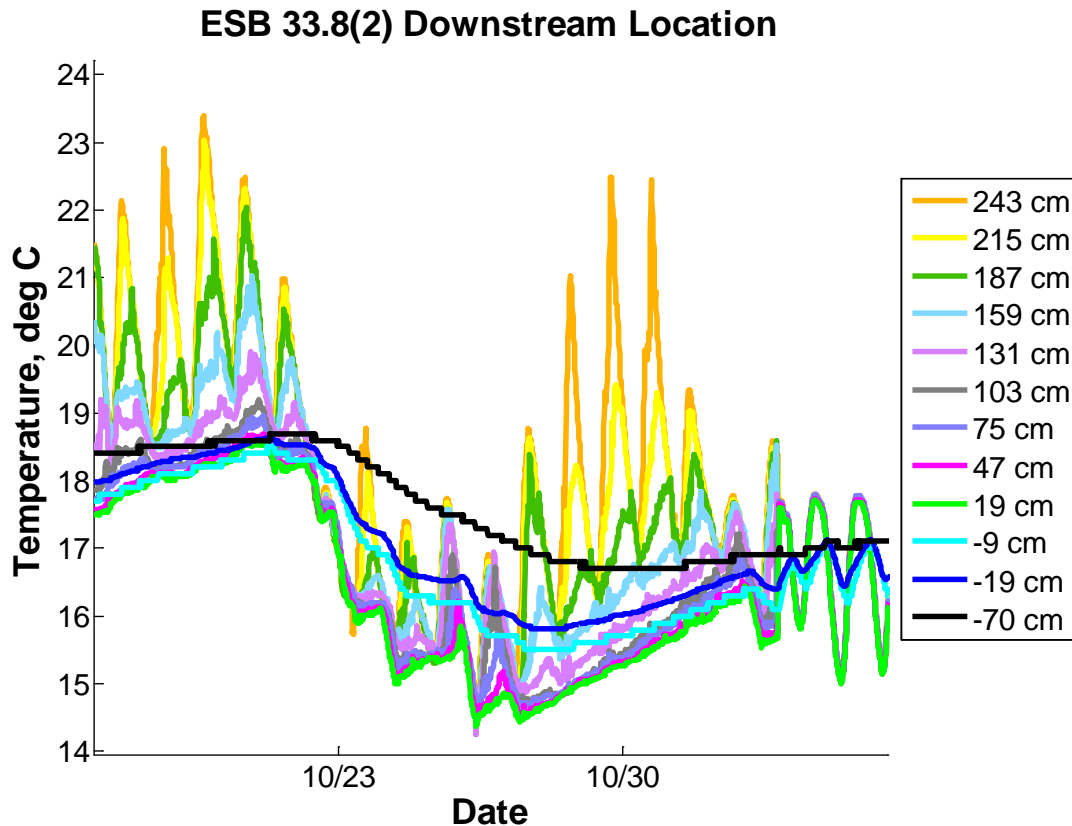


Figure A-81: Downstream sensor array location ESB 33.8(2) surface and subsurface water temperature from 10/17 to 11/05 showed daily thermal stratification from 10/17 until 11/02.

Subsurface water temperature increased with depth at the downstream location ESB 33.8(2) indicating subsurface water did not provide cooling to pool surface water (Figure A-82). While the temperature resolution of the sensors at -9 cm and -70 cm created a square wave signal in subsurface water temperature data, measurement bias between sensors did not impact data at ESB 33.8(2). Subsurface water temperature developed more pronounced daily variations when surface water flow increased on 11/02, but water temperature remains consistent with depth.

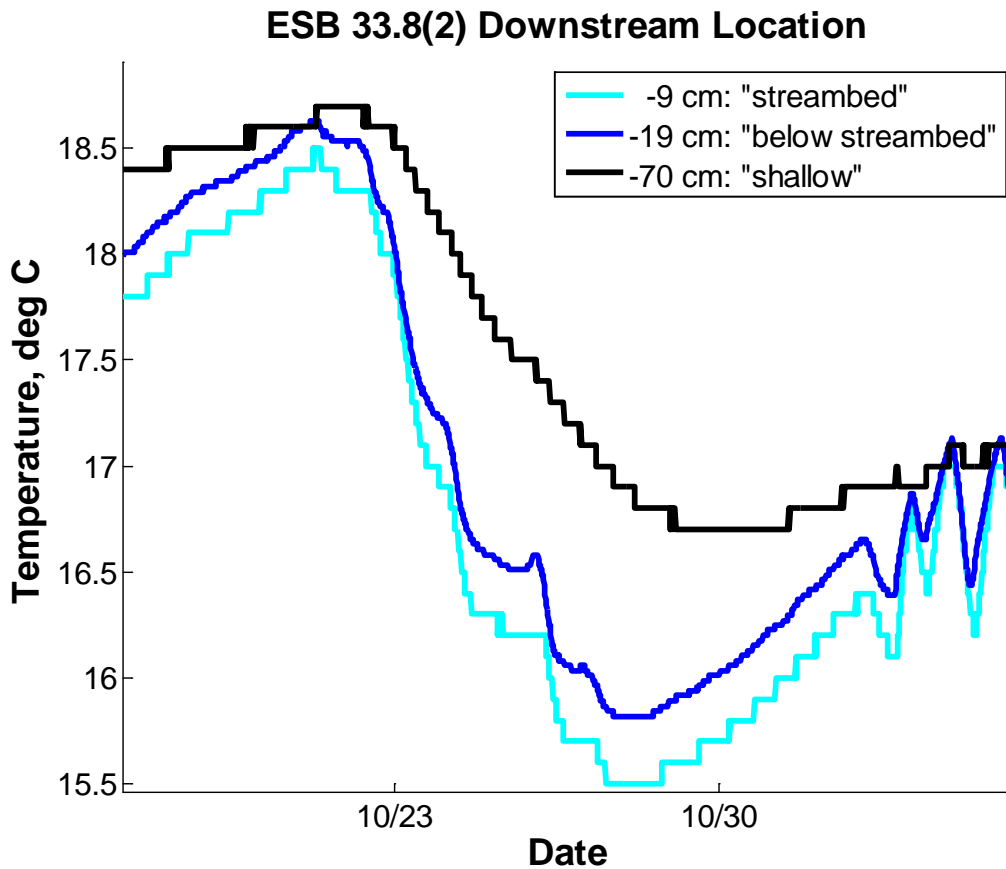


Figure A-82: Downstream sensor array site ESB 33.8(2) subsurface water temperature from 10/17/2012 to 11/05/2012.

Hydraulic head at ESB 33.8(2) decreased with depth below the streambed so subsurface flow downwelled during the instrumentation period and did not influence surface water temperature conditions (Figure A-83). Similar to both the upstream and middle measurement location, hydraulic head increased on 11/02 corresponding to the time surface flow increased, but trends in hydraulic head with depth remained consistent.

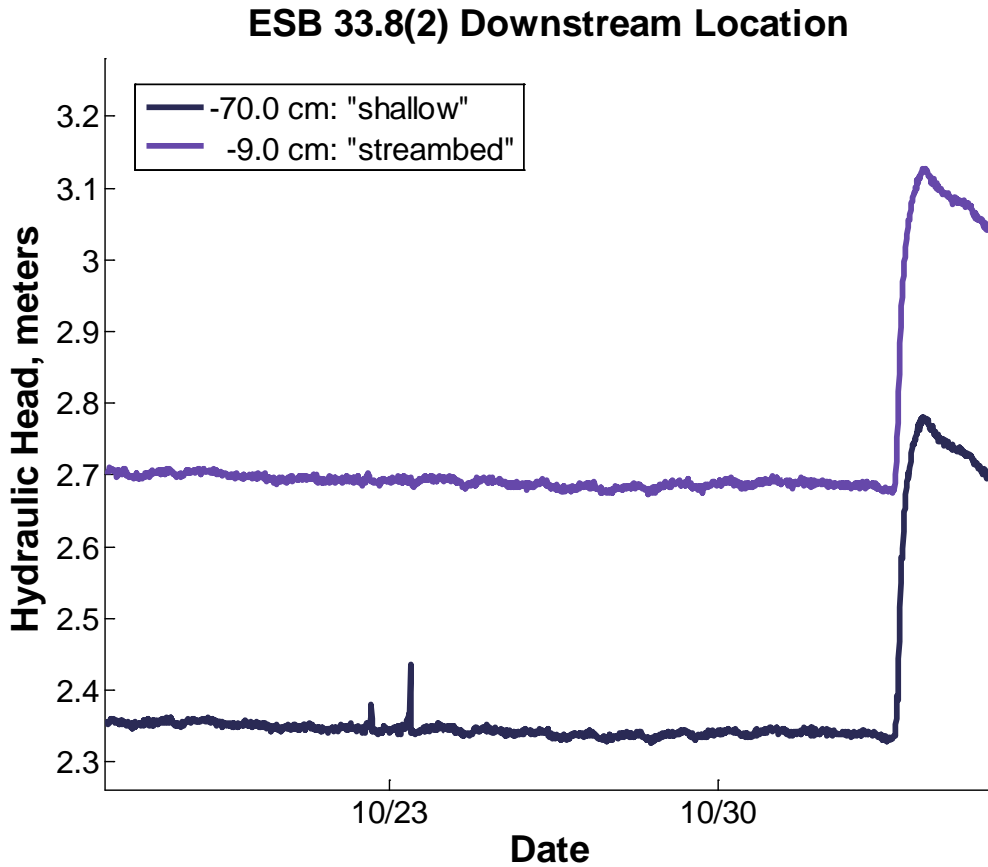


Figure A-83: Variation in hydraulic head with depth into the subsurface at the ESB 33.8(2) downstream pool location.

Water specific conductance at ESB 33.8(2) decreased with depth into the subsurface (Figure A-84). Specific conductance trends with depth at the downstream location ESB 33.8(2) were similar to those at the middle location ESB 33.8 with specific conductance near the streambed greater than 2 mS/cm. Near streambed sensors at the upstream, middle, and downstream location in ESB 33.8 all experienced increased specific conductance when surface flow increased. The magnitude of the specific conductance increase varied between locations. Specific conductance at -70 cm in ESB 33.8(2) decreased when surface flow increased on 11/02 similar to the specific conductance at -104 cm at the middle location ESB 33.8.

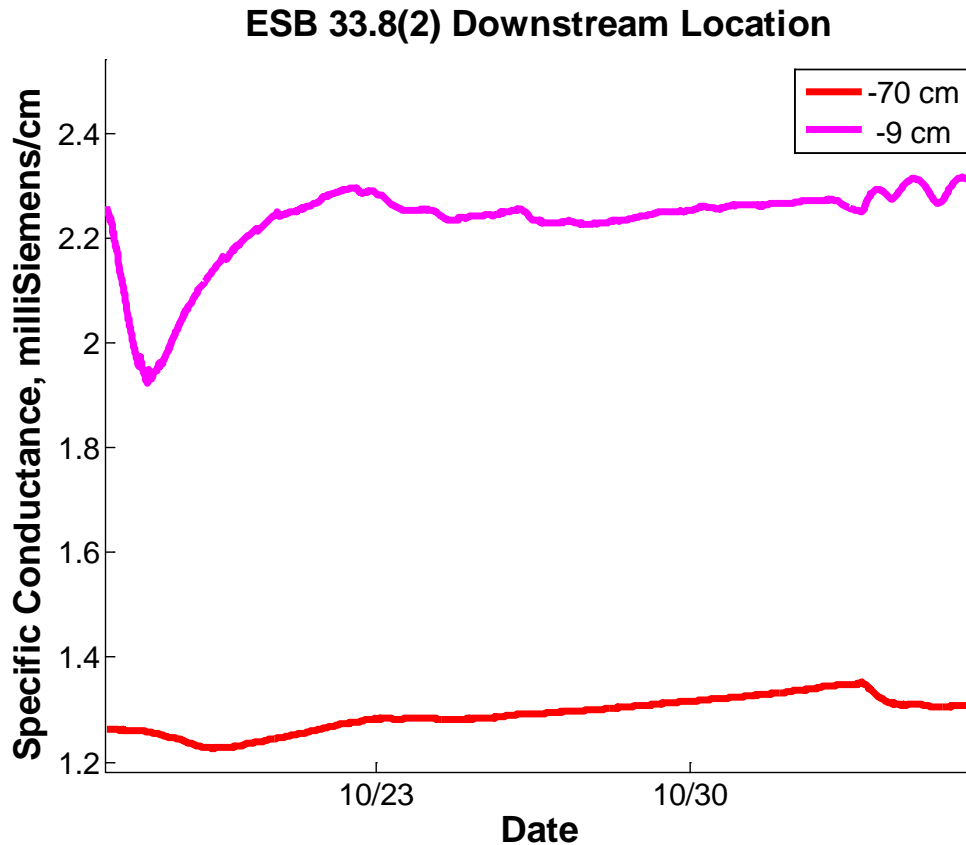


Figure A-84: Variation in water specific conductance with depth into the subsurface at the ESB 33.8(2) downstream pool location.

This page left blank intentionally